IntechOpen

Updates in Volcanology
Linking Active Volcanism and the Geological Record

Edited by Károly Németh

Updates in Volcanology - Linking Active Volcanism and the Geological Record

Edited by Károly Németh

Published in London, United Kingdom

Updates in Volcanology - Linking Active Volcanism and the Geological Record
http://dx.doi.org/10.5772/intechopen.104012
Edited by Károly Németh

Contributors
Károly Németh, Bo'xin Li, Vladislav Zakharovskyi, Julie Palmer, Alan Palmer, Ilmars Gravis, Ekaterina V. Lebedeva, Luigina Vezzoli, Claudia Principe, Daniele Giordano, Sonia La Felice, Patrizia Landi, Mohamed A. Abu El-Rus, Ali A. Khudier, Sadiq Hamid, Hassan Sayed Abbas, Joan Martí

First published in London, United Kingdom, 2023 by IntechOpen
IntechOpen is the global imprint of INTECHOPEN LIMITED, registered in England and Wales, registration number: 11086078, 5 Princes Gate Court, London, SW7 2QJ, United Kingdom

British Library Cataloguing-in-Publication Data
A catalogue record for this book is available from the British Library

Additional hard and PDF copies can be obtained from orders@intechopen.com

Updates in Volcanology - Linking Active Volcanism and the Geological Record
Edited by Károly Németh
p. cm.
Print ISBN 978-1-83768-104-4
Online ISBN 978-1-83768-105-1
eBook (PDF) ISBN 978-1-83768-106-8

Meet the editor

Károly Németh is an expert at the Saudi Geological Survey working on volcanic geology, volcanic hazard, geoheritage, and geodiversity of monogenetic volcanic fields (harrats) of the Arabian Peninsula. He is also a Senior Researcher at the Institute of Earth Physics and Space Science, Hungary, an Adjunct Professor of Volcanic Risk Solutions, at Massey University, New Zealand, and a Research Affiliate at the National Institute of Geophysics and Volcanology, Italy. He was an elected member of the Executive Committee of the International Association of Volcanology and Chemistry of Earth Interior and leads its Volcaniclastic Sediments, Monogenetic Volcanism and Volcanic Geoheritage commissions. Currently, he is a Vice President of the International Association of Sedimentologists.

Contents

Preface

Updates in Volcanology - Linking Active Volcanism and the Geological Record provides an exciting snapshot of research around the hot topic of volcanic geology. Volcanic geology is a fast-growing research arena within volcanology in which the basic aspects of volcano science are revisited based on direct geological observations from the field. As field geology is the fundamental data provider for any geological research, such work examines the basic elements of how volcanoes work. In addition, the volcanic geology approach to understanding volcanic systems can provide a strong evidence-based approach to design analogue and numerical modeling of various volcanic processes ranging from the eruption-fed aspects to the more secondary elements governed by the background environment within which the volcanism takes place. In proximal settings, primary volcaniclastic successions are more abundant and complex (**Figure 1**), while in distal regions, volcanic eruptive products tend to form clear stratigraphy marker horizons. As volcanic rocks or rocks that formed under volcanic influence form vital elements of the geological record, tracing the transition from modern pyroclastic and volcaniclastic successions to rocks formed from such is key to providing valid and realistic reconstructions from preserved rocks in any geoenvironment. Naturally, this subject is too broad to be covered in a single book, but it is also a subject that can be evaluated through various locations, volcanic systems, and

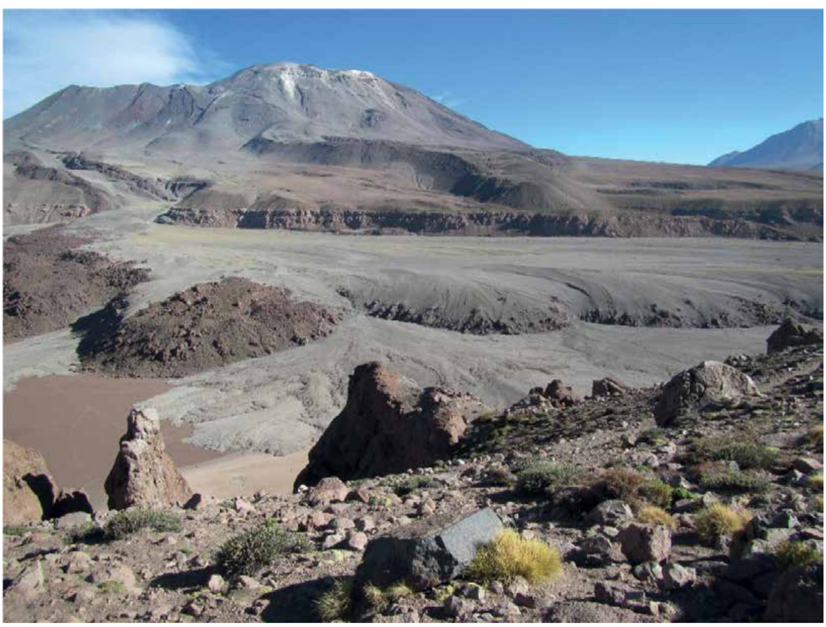

Figure 1.
Proximal region of the Lascar Volcano (northern Chile) complex primary pyroclastic successions and lava flows filling the landscape. Pyroclastic flows tend to fill the valleys such as the deposits of the 1993 eruption (light-colored zone in the middle of the view).

geological times through specific research topics. This book discusses a wide range of volcanic systems and describes their volcanic geology.

The link between active volcanic processes, their eruptive products, and what is preserved in the geological record is fundamental to understanding the growth and erosion processes of volcanoes. Volcanic systems and volcanic rocks differ from other geological processes and rock types because they act and form during extremely short time scales and can also be voluminous (**Figure 2**). As such, volcanic rocks are commonly viewed as excellent chronostratigraphy markers that can present across large sedimentary basins but on a very large spatial scale, such as thin tephra layers in marine or terrestrial settings. On the contrary, massive landscape-forming successions can completely alter the sedimentation of entire regions and thus their impact on the geological record is huge. There is no other geosystem where such a dramatic range of time and space needs to be considered within a single volcanic system and commonly in repeated fashion over longer time scales. It is critical to acknowledge this issue in the geological mapping of volcanic terrains or regions influenced by volcanism in the past. The impact of volcanism on sedimentary basins far from an active volcano might just be an accumulation of thin volcanic ash layers that can be preserved in the geological record as sharp chronostratigraphic horizons. Information from these thin layers however is vital to identify and define the nature of volcanism interacting with the normal sedimentary environment. To be able to trace these gradual changes to obtain the maximum potential information volcanic rocks can provide in the context of sedimentary basin evolution, it is important to be able to assign the correct time and space scales of volcanism recorded in the rock successions.

Figure 2.
Enormous spatial-scale variations of volcanism and their products in one photo in northern Chile. In the foreground, Cerro Overo maar represents a fast and small-volume eruption that cut through a landscape-forming ignimbrite succession (pink). Group of complex andesite stratovolcanoes are a magnitude less in edifice and eruptive volume than those exceptionally large ignimbrite sheets.

Chapter 1 introduces and summarizes the subject matter. Chapter 2 provides a summary of the role of paleovolcanology within the context of volcanic geology based on past research. The chapter is a useful guide to identifying the correct scale of volcanism and linking it to the volcanic rock record. Chapter 3 discusses one of the largest volumes and potentially the most complex type of volcanism associated with convergent plate margins. It outlines some models that link the active subduction processes and what we can see in the geological record. Chapter 4 focuses on dispersed volcanic systems such as mafic monogenetic volcanic fields whose eruptions can span over millions of years despite the individual volcanoes being very short-lived in the geological time scale. The chapter provides an overview of using the geological record to define the most likely eruptive scenarios in future eruptions in long-lived volcanic fields. While mafic volcanism is the most common manifestation of volcanism on Earth, large silicic systems can be the most explosive or produce unusually effusive products, as outlined in Chapter 5. Volcanic systems act as part of the normal sedimentary environment; hence volcanism can alter, modify, or completely switch the nature of sedimentation. Chapter 6 describes this process, which can be traced well along fluvial systems evolving in volcanic terrains.

Overall, this book provides a representative overview of the problem geologists face when geological reconstruction involves volcanic successions in various time and space scales. This book is a useful reference for approaching and solving this problem.

Károly Németh
Saudi Geological Survey,
Jeddah, Kingdom of Saudi Arabia

Institute of Earth Physics and Space Science,
Sopron, Hungary

Massey University,
Volcanic Risk Solutions,
Palmerston North, New Zealand

National Institute of Geophysics and Volcanology,
Bologna, Italy

Chapter 1

Introductory Chapter: Linking Modern and Ancient Volcanic Successions

Károly Németh

1. Introduction

Understanding volcanic rocks plays a crucial role in reconstructing the environment in various scales within volcanic rocks formations. Volcanic processes can act in a short time scale and still produce large volumes of eruptive products that commonly can misbalance the sedimentary budget of a sedimentary basin, regardless of their geoenvironmental position (e.g., marine, or terrestrial). Distal ash, on the other hand, can travel hundreds of kilometers away from their source and fall into the background sedimentary environment and can produce a very characteristic and sharp time marker across the entire region. This makes volcanic deposits excellent chronostratigraphy markers [1]. Volcanic processes are also diverse not only by the way coherent and fragmented source materials get generated (e.g., fragmentation style variations, eruption intensity diversity) but also by the way those materials get transported and accumulated. Large volumes of volcanic material can accumulate quickly (hours to days) and alter the entire drainage pattern of large regions. The same accumulated volcaniclastic deposits later can gradually get redeposited and altered by normal surface processes but can provide volcanic detritus over prolonged time along the transportation arteries that eventually lead to marine basins [2, 3]. While this process seems to be a slow and gradual way effectively remove large volume of volcanic deposits from source regions and disperse it over large territories, such processes can also take place in a dramatic and abrupt fashion. Massive breakout lahars can mobilize large volumes of water and damp their sediments suddenly over large areas. On many occasions, like in the Taupo Volcanic Zone in New Zealand, large volumes of caldera-forming silicic eruptions had modified the landscape dramatically and promoted the formation of large lake systems, which, from time to time, initiated breakout lahars moving large volumes of volcaniclasts to other sedimentary basins [4]. Over time, major sedimentary basins from terrestrial to marine produce massive successions of complex multisource volcaniclastic aprons, fans, and basin fills. In ancient settings, such basins and their complex volcaniclastic successions can be the only "messengers" of former high-intensity volcanism, especially if the preserved volcaniclastic rocks are preserved as part of tectonically dissected terrains.

Volcaniclastic sedimentology has evolved in recent years dramatically. Primary eruption-fed processes considered to produce fragmented volcanic materials generate pyroclasts that can start their journey through initial primary volcanic processes that later interact with the normal sedimentary environment, making it increasingly

IntechOpen

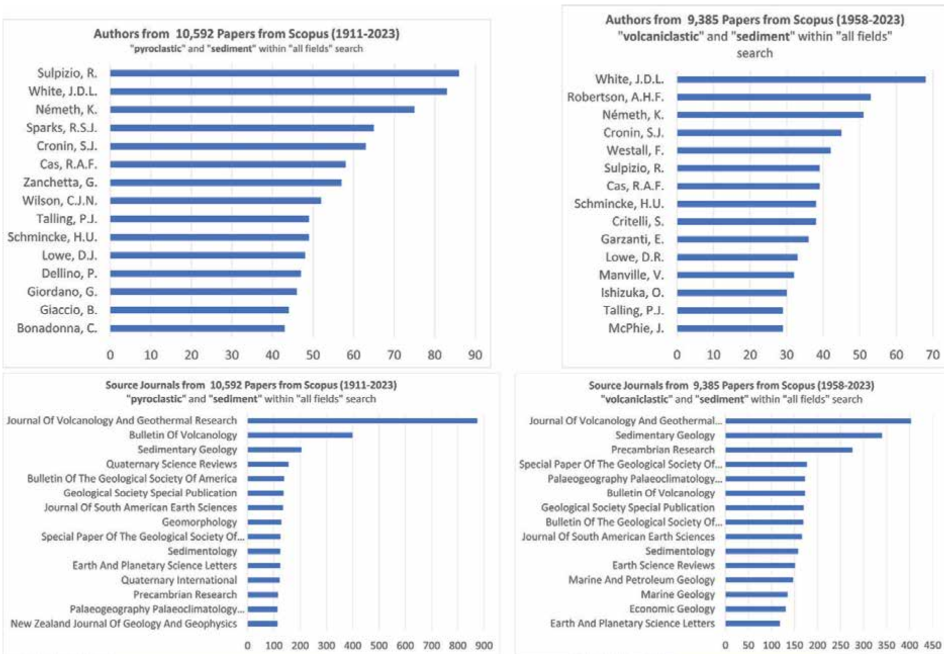

Figure 1.
Bibliometric surveys based on Scopus data for search terms of "volcaniclastic" and "sediment" as well as "pyroclastic" and "sediment" within keyword, title, and abstract documents.

difficult to distinguish the effect of the primary volcanic and the background sedimentary processes. This difficulty manifests in the way how we describe and interpret the preserved volcanic material in the geological record. In the past decades, various terminologies have appeared with an aim to provide a clear method to document objectively volcanic rocks, keeping the descriptive and interpretative aspects of the nomenclature separated [5]. It is apparent that over time, such terminologies have become more and more process related, expressing the strength of the link between primary (eruption-fed) and secondary (background sedimentation-dominated) processes [6–8]. In the past decades, entire volcaniclastic sedimentology schools have formed with key research groups (**Figure 1**) with diverse geological backgrounds, demonstrating the vitality of volcaniclastic sedimentology. Moreover, in recent years, the geology-based approach has reemerged, and new research has applied basic geological rules to look at volcanoes through volcano geology perspective [9, 10].

2. Polygenetic vs. monogenetic systems

Volcano types are commonly distinguished along their appearance, volume, and the time required for their formation. Polygenetic volcanic systems are characteristically long-lived volcanoes with a stable melt source and conduit system. Individual eruptions occur in diverse eruption styles, but they activate many times over the total lifespan of the volcano. As a result, a large volcanic edifice will build up that is surrounded by a broad ring plain where mostly valley-filling pyroclastic density currents, hot and cold reworked equivalent of them, accumulate alongside with landscape-draping ash fall beds. Further away we are from the source volcano, the higher the

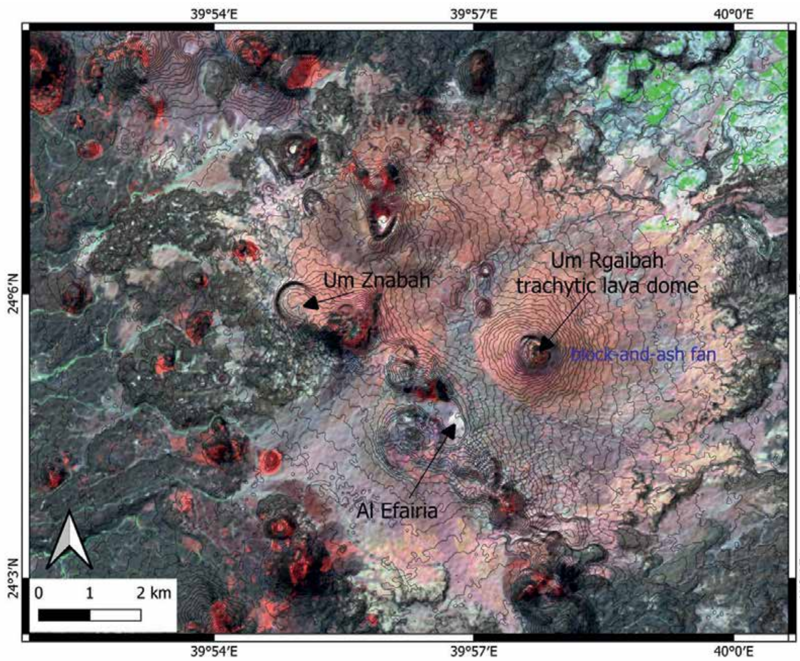

Figure 2.
Harat Rahat in Saudi Arabia is a typical mature monogenetic volcanic field with several silicic eruptive centers forming maars, small calderas, and lava domes such as the Holocene Um Rgaibah. The trachytic block-and-ash fan is clearly distinct on a Sentinel Highlight Optimized satellite image.

influence of the background sedimentation, resulting in developing extensive volcaniclastic sedimentary basins. On the contrary, small-volume and short-lived, so called "one shot," eruptions are commonly defined as monogenetic volcanoes [11]. They mostly form complex groups of volcanoes, a volcanic field where the primary volcanic deposits (e.g., directly fed by an eruption) are dispersed over large (100 s km^2) areas (**Figure 2**). While each volcano erupts only once, their eruption record could show great variation of eruption styles as a function of the interaction between the magmatic and external (mostly water) impacts on the individual explosive eruptions. Overall, if the volcanic field is long lived (million years scale), significant volumes of inter-volcano volcaniclastic deposits can accumulate. Over time, volcanic fields can reach mature stages when they can feed from magmas that have evolved over time and produce simple silicic explosive volcanoes such as known from many volcanic fields from the Arabian Peninsula (**Figure 2**).

3. Role of type of volcanism, environment, and volcano instability

Large volumes of silicic magma-dominated volcanism commonly culminate in caldera formation that is associated with large volumes of ignimbrite accumulation. Such processes can be landscape forming as they change not only the hydrology of a large area but also the orography of a large area. Caldera-forming eruptions are common in the geological record, and their volcanic facies architecture can stay relatively intact over millions of years. Their most important characteristic is that an entirely distinct sedimentary system can form within the caldera that is different from the extra-caldera-depositional systems. In a volcanic terrain where a large number of volcanoes can form in a relatively small region, volcanic products can accumulate from different sources. In addition, such closely spaced composite volcanoes can interact with the background sedimentary environment, especially if that is complex and exhibits a multitude of small sedimentary systems across the composite volcanoes (**Figure 3**). Large stratovolcanoes are commonly associated with convergent plate margins and subduction processes. Along old and long-lived volcanic arcs, volcanoes spaced in a regular fashion result in aligned volcanic fronts that can spread across many climatic zones. Individual volcanoes can provide steady intermediate pyroclast input through medium but occasional high-intensity explosive volcanic eruptions. The sudden input of pyroclasts to the terrestrial environment can behave differently if that occurs in arid or humid climatic conditions. In arid conditions, the preservation potential of primary pyroclastic successions can be good, keeping near-original deposit characteristics intact over longer time; however, occasional high-intensity rainfall events can rapidly modify those features as soil formation is limited, and exposed deposits can be remobilized quickly. On the contrary, in humid climatic conditions, remobilization of pyroclasts due to meteorological and/or volcanic events can trigger massive volcanic mass flows commonly named as lahars (volcanic mud and debris flows).

Major lahars can follow the normal fluvial system, and deposition can interact with fluvio-lacustrine elements. Such systems can form confined long valleys such as observed in the aftermath of the Pinatubo 1991 [12] (**Figure 4**) eruptions.

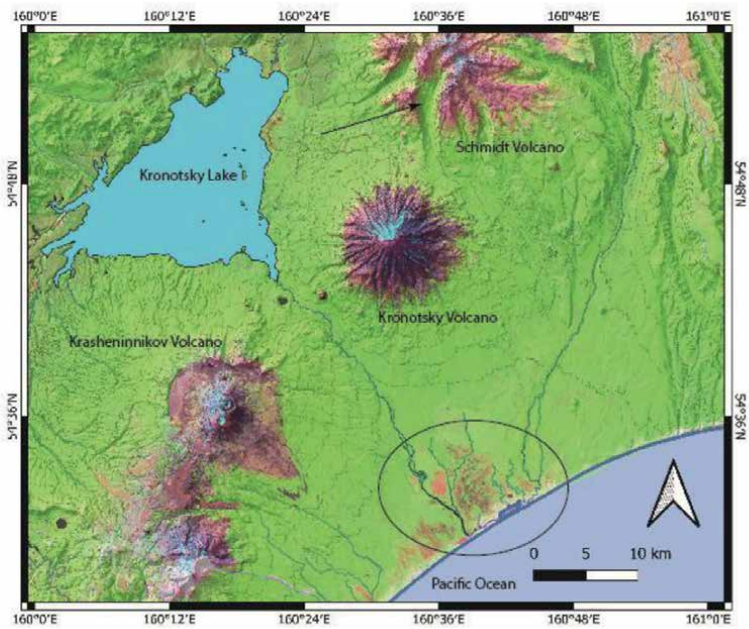

Figure 3.
Complex terrestrial–marine sedimentary system around the Kronotsky volcano in central eastern Kamchatka, Russia on a Sentinel Short Wave Infra-Red satellite image sensitive for wet zones (green or blue). Note the large lake (Kronotsky Lake), the complex fluvial systems "sampling" volcanic sources of various ages and compositions. Note the deep erosional gullies on the Pleistocene Schmidt Volcano that functions as the main sediment delivery channel. Also, note the complex coastal plain to shallow marine sedimentary system that likely collects volcaniclastic material from a complex, multi-source volcanic terrain (circle).

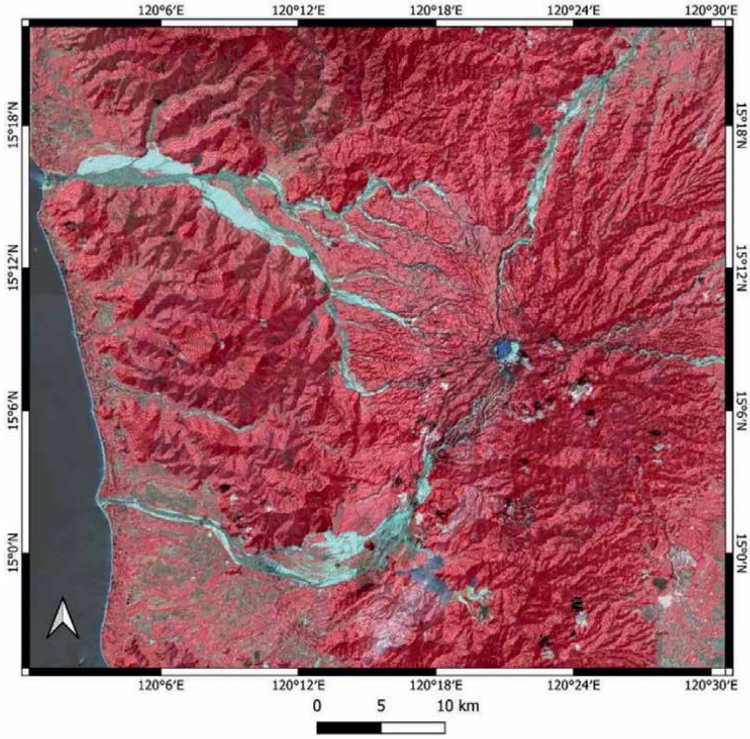

Figure 4.
Pinatubo Volcano (Philippines) on a Sentinel False Color satellite image. On the image, fresh sediment-dominated fluvial channels are shown in various gray colors. These fluvial channels functioned as major lahar channels following the Pinatubo 1991 Plinian/ultra-Plinian Volcanic Explosivity Index (VEI) 6 eruption.

Recognition of volcanic instability is dated back to the advent of remote sensing in the late 80s, when peculiar patterns over tens of km^2 areas recognized along Andean volcanoes were associated with horseshoe-shaped central cone morphology [13]. Volcanic instability is either directly linked to an explosive eruption and/or triggered by the gravitational spreading of the volcano. This means that the type of explosive volcanic activity, the steady degassing of the volcanic system that generate structurally controlled hydrothermal alterations to weaken the growing volcanic edifice, and the environment where the volcano activates together will put the volcanic edifice to a specific course to collapse over time. Large-volume volcanic collapses are known in every geometrical scale across volcanic arcs. Especially in those in arid climate where salt formation is intense such as around the Atacama Basin in Chile, volcanic instability is even accelerated as salt provides good lubrication for the volcanic edifice to slide apart catastrophically [14].

Explosive eruption-triggered volcano collapses are also more frequent than previously thought as the 1980 eruption of Mount St. Helens shed light on the scale of such events (**Figure 5**). Volcanic collapses, especially those that occur in temperate or tropical climate (e.g., humid conditions) where vegetation cover quickly develops (decadal scale), can initiate new sedimentary regimes as they open large surface areas where unconsolidated volcanoclasts can be remobilized and fed into fluvio-lacustrine sedimentation arteries. Such a process is clearly demonstrated from the Taranaki Volcano in New Zealand and followed dup at Mount St. Helens since the eruption

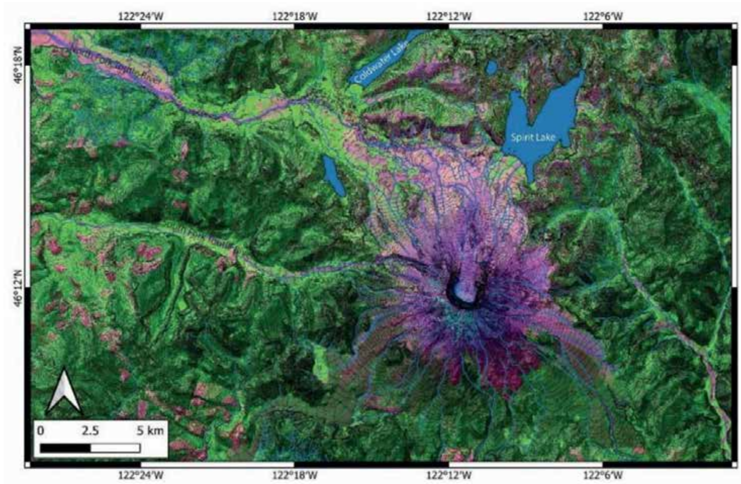

Figure 5.
Mount St. Helens (Washington State) on a Sentinel Short Wave Infra-Red satellite image. Note the horseshoe-shaped scar on the edifice and the connected fluvial system along volcaniclastic material transported away.

occurred. In some stratovolcanoes such as Taranaki, even the cyclicity of such volcano collapses and their sedimentary responses have been recognized [15]. Individual volcanic particles preserved in ancient rock units carry vital information about the style and type of volcanic eruptions that created those particles, while sedimentary features and the overall facies characteristics can provide information on the transportation and deposition of those individual particles. In arc settings, especially under temperate to tropical, humid climates complex sedimentary environments can form where the volcanism and the background sedimentation together can create complex volcano-influenced sedimentary aprons.

Author details

Károly Németh[1,2,3]

1 Saudi Geological Survey, Jeddah, Kingdom of Saudi Arabia

2 Institute of Earth Physics and Space Science, Sopron, Hungary

3 Volcanic Risk Solutions, Massey University, Palmerston North, New Zealand

*Address all correspondence to: nemeth.k@sgs.gov.sa; nemeth.karoly@epss.hu; k.nemeth@massey.ac.nz

References

[1] Martí J, Groppelli G, Brum da Silveira A. Volcanic stratigraphy: A review. Journal of Volcanology and Geothermal Research. 2018;**357**:68-91

[2] Kósik S, Rees C, Palmer AS, Todd M, Tost M, McKay W. From sink to source: Late quaternary landscape evolution and fluvial dynamics of the Hautapu River catchment, New Zealand. Geomorphology. 2022;**412**. Article id: 108319

[3] Procter J, Zernack A, Mead S, Morgan M, Cronin S. A review of lahars; past deposits, historic events and present-day simulations from Mt. Ruapehu and Mt. Taranaki, New Zealand. New Zealand Journal of Geology and Geophysics. 2021;**64**(2-3):479-503

[4] Manville V. An overview of break-out floods from Intracaldera lakes. Global and Planetary Change. 2010;**70**(1-4):14-23

[5] Fisher RV, Schmincke H-U. Pyroclastic Rocks. Heidelberg: Springer; 1984. p. 474

[6] Cas R, Wright J. Volcanic Successions Modern and Ancient - A geological approach to processes, products and successions. Dordrecht: Springer; 1988. p. 528. DOI: 10.1007/978-94-009-3167-1

[7] McPhie J, Doyle M, Allen R. Volcanic textures. In: A Guide to the Interpretation of Textures in Volcanic Rocks. Tasmania: Tasmanian Government Printing Office; 1993. p. 19

[8] Németh K, Martin U. Practical Volcanology - Lectures Notes for Understanding Volcanic Rocks from Field Based Studies. Budapest, Hungary: Magyar Allami Foldtani Intezet; 2007. p. 221

[9] Németh K, Palmer J. Geological mapping of volcanic terrains: Discussion on concepts, facies models, scales, and resolutions from New Zealand perspective. Journal of Volcanology and Geothermal Research. 2019;**385**:27-45

[10] Di Capua A, De Rosa R, Kereszturi G, Le Pera E, Rosi M, Watt Sebastian FL. Volcanically-derived deposits and sequences: a unified terminological scheme for application in modern and ancient environments. Geological Society, London, Special Publications. 2023;**520**(1):SP520-2021-201

[11] Smith IEM, Németh K. Source to surface model of monogenetic volcanism: A critical review. In: Németh K, Carrasco-Nuñez G, Aranda-Gomez JJ, IEM S, editors. Monogenetic Volcanism. Geological Society of London Special Publications. Bath, UK: The Geological Society Publishing House; 2017. pp. 1-28

[12] Umbal JV, Rodolfo KS. The 1991 Lahars of Southwestern Mount Pinatubo and evolution of the Lahar-Dammed Mapanuepe Lake. In: Christopher NG, Punongbayan RS, editors. Fire and Mud: Eruptions and Lahars of Mount Pinatubo, Philippines. Seattle, WA: University of Washington Press; 1996. pp. 951-970. ISBN 9780295975856

[13] Francis PW, Gardeweg M, Ramirez CF, Rothery DA. Catastrophic debris avalanche deposit of Socompa volcano, Northern Chile. Geology. 1985;**13**(9):600-603

[14] Clavero J, Polanco E, Godoy E, Aguilar G, Sparks RSJ, van Wyk de Vries B, et al. Substrata influence in the transport and emplacement mechanism of the Ollague debris avalanche (northern Chile). Acta Vulcanologica. 2004;**16**:59-76

[15] Zernack AV, Procter JN. Cyclic growth and destruction of volcanoes. In: Roverato M, Dufresne A, Procter J, editors. Volcanic Debris Avalanches: From Collapse to Hazard. Cham: Springer International Publishing; 2021. pp. 311-355

Chapter 2

Volcano Geology Applications to Ancient Volcanism-Influenced Terrains: Paleovolcanism

Joan Martí

Abstract

This chapter discusses how to apply the most significant aspects and concepts of modern volcanology to the study the ancient volcanic terrains, where volcanic successions appear exposed in discontinuous outcrops, with various degrees of deformation, which are often manifested in the presence of metamorphosed and hydrothermally altered volcanic rock assemblages. The way to understand paleovolcanism is through the identification and interpretation of the products of past volcanic activity in terms that is equivalent to what is done in modern terrains, despite the difficulty of having to characterize and recompose all those subsequent geological processes that have been superimposed upon them. This chapter summarizes the most fundamental aspects of the study of ancient volcanic terrains, paying special attention to the definition of facies associations, the characterization of their spatial and genetic relationships, and their paleoenvironmental and paleogeographic significance, as well as to the possible causes of the original facies modification. The implications for the presence of volcanism in the dynamics of sedimentary basins and its relationship with different geodynamic environments are also analyzed.

Keywords: volcanic processes, volcano-stratigraphy, volcano-tectonics, volcanogenic sediments, alteration processes, paleoenvironmental reconstruction

1. Introduction

Volcanic deposits are present since the very beginning of the geological record, thus confirming that volcanism has been a main component of Earth's evolution. Active volcanism has important implications for our society. There is of course the constant threat that volcanic activity represents for the immediate areas around active volcanoes, but there are also risks at greater distances, even globally, depending on the intensity of this activity. On the other hand, volcanic systems represent an important source of natural resources (e.g., geothermal energy, mineral deposits) (**Figure 1a**). In addition, volcanism provides relevant information to understand the dynamics of the Earth's mantle and crust, which is essential to understand the evolution our planet, in addition to other planetary bodies with similar characteristics. For these reasons, characterizing past volcanic events in the same way that we characterize active volcanism is essential to decipher the meaning of these past volcanic episodes

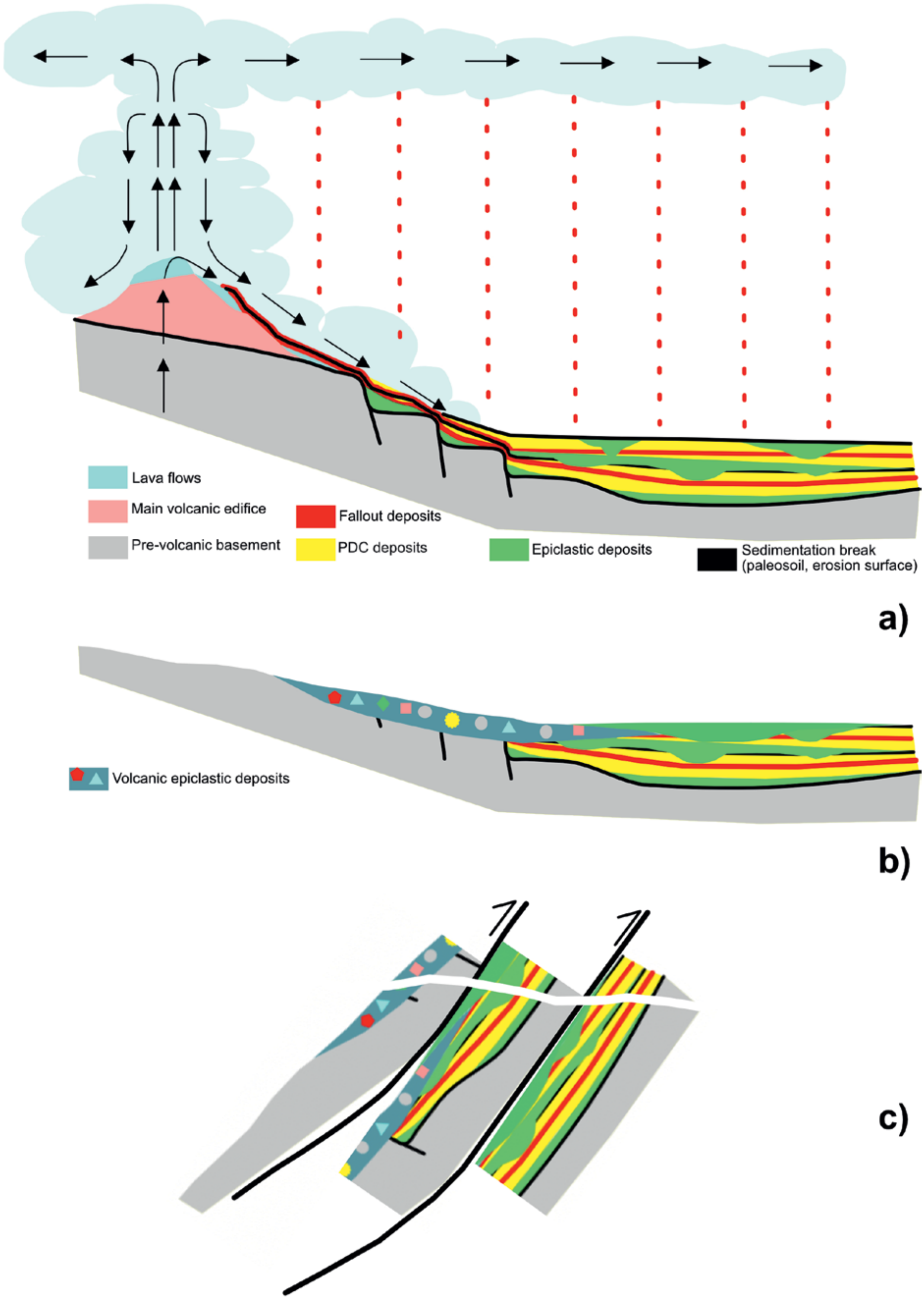

Figure 1.
Sketch illustrating the main concepts of modern and paleovolcanism and their main observational differences. a) Current state of an active central volcano and sedimentation in and adjacent basin. Primary volcanic deposits (lava flows, pyroclastic (air fall, PDC, lahars, etc.)) deposits contribute to the infill of the basin together with deposits resulting from their erosion and redeposition (reworking) by external (epiclastic) processes. Black arrows indicate the sense of movement of magma inside the volcanic edifice, lava flows, eruption column, and PDC. b) State of the same depositional environment after volcanic activity has ceased and the volcanic edifice has been partially dismantled, producing volcanic epiclastic deposits that will mostly contain fragments from the primary volcanic deposits. c) Same scenario after hypothetical compressional tectonics and further erosion (white line).

in a local, regional, or even global context. Unfortunately, the degree of preservation of ancient volcanic deposits, which may have suffered important transformations due to erosion, diagenesis, hydrothermal alteration, tectonic deformation, etc., may not always be conclusive to recognizing their nature and significance, hence complicating their comparison with modern deposits (**Figure 1b**). However, the study of ancient volcanic successions, even if this represents an additional handicap, should employ the same concepts and methods (e.g., stratigraphic correlations, facies analysis, textural characterization, componentry analysis) that are used in the characterization and interpretation of historical eruption products (e.g., [1]).

The same transformation that volcanology has undergone regarding the study of active or recent volcanic areas—from a basically descriptive to a more interpretative and quantitative science—should also affect the study of ancient volcanic terrains. The presence of volcanic episodes in the geological record should not be regarded as an isolated or sporadic event that does not necessarily need to be relevant to interpret the remainder of rocks found at a particular site [2]. On the contrary, we should try to deduce the tectonic controls that conditioned the rise and accumulation of magmas and their geodynamic significance, the mechanisms responsible for their eruptions, or to determine the influence that volcanic activity had had on sedimentation in the basin. In this sense, the invariance over time of the physical parameters that control the ascent and eruption of magmas allows ancient and modern volcanic products to be compared and interpreted in the same terms.

In this chapter, I will revise the main concepts that should be considered in the study of ancient volcanic succession to achieve the same degree of accuracy and information as in the study of recent volcanism.

2. Definitions

Before starting with the identification criteria for paleovolcanic rocks, it is necessary to review some definitions referring to the processes and products of paleovolcanism. The first aspect that requires our attention is the proper definition of paleovolcanism.

There is no specific age from which the limit between ancient volcanism (or paleovolcanism) and modern volcanism can be distinguished, since we can find relatively recent terrains that have been strongly altered and eroded (e.g., some volcanic islands or active calderas hosting geothermal fields), and ancient terrains that preserve a large part of the original characteristics of their volcanic materials (e.g., Permo-Carboniferous volcanism in some areas). For this reason, and although there is no specific definition for the term paleovolcanism, we will consider it as the volcanism recorded in the stratigraphic record of regions that have undergone erosion, diagenesis, tectonics, hydrothermal, and/or metamorphic processes, thus causing significant changes in the original volcanic facies.

The second aspect that needs our attention is the difference between processes and products (**Figure 2**). Processes refer to those aspects concerning the origin as well as the transport and emplacement mechanisms of volcanic materials, while the term products should be understood as the result of these processes. While this is not particularly problematic when referring to a lava flow—and in this case, both the process and the product will receive the same name, *lava flow*—the situation is much more complex when we refer to any type of clastic volcanic deposits (e.g., covering the full spectrum of primary, eruption-fed products to secondary, epiclastic successions). For

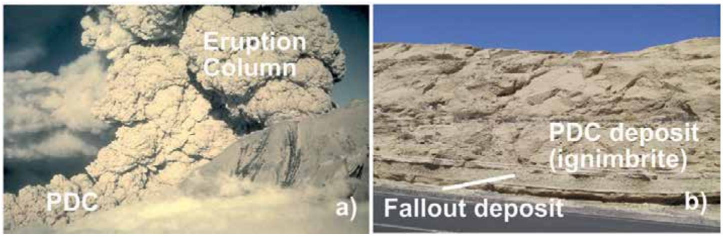

Figure 2.
Difference between processes and products in volcano-sedimentary environments: a) formation of an eruption column that will rise into the atmosphere and will disperse horizontally controlled by the predominant winds and initiation of a PDC that will run away from the vent on the volcano slopes controlled by gravity (Mount Saint Helens 1980 eruption, (photo by H. Glicken-U.S. Forrest Service. Credit: USGS). b) Fallout deposit formed by the deposition of pumice fragments from the eruption column and of an ignimbrite deposited from a PDC (Tenerife, Canary Islands) (credit: Joan Martí).

this reason, it is necessary to distinguish here between process and product and to use an appropriate nomenclature that allows them to be differentiated. As an example, we can use the term pyroclastic density current (PDC), which refers to the flow processes of transport and deposition of primary pyroclastic material (e.g., [3, 4]). It is therefore incorrect to use this term as a particular type of fragmentary volcanic deposit. The term PDC deposit, as a general term to refer to an indeterminate type of deposit produced by such a process, or the terms ignimbrite, block-and-ash flow, dilute PDC deposit, dense PDC, deposit, etc., applied to specific deposits derived from PDCs with different characteristics, are appropriate to refer to the products of this process.

This complexity increases when referring to paleovolcanic materials where the discrimination between primary and secondary products (derived from the weathering and erosion of the former) is not always straightforward (e.g., [1, 5]). Likewise, terms such as ignimbrite, block-and-ash, Plinian fall deposit, although they refer to a deposit, imply a specific type of process in each case. In paleovolcanism, it is not always straightforward to identify the genetic characteristics of a deposit based on its lithological features, hence I recommend using purely descriptive terms (see below), even though this description may fit for the products of different processes, and there will be time to apply more precise terms if the information obtained eventually allows it.

To clarify the nomenclature of clastic volcanic materials, Fisher [6, 7] established two groups of definitions, the first group is non-genetic, based on the lithological characteristics of volcanic materials in order to differentiate the different products, and the second group comprises definitions focused on differentiating between their genetic mechanisms. Some of these definitions were reviewed by Fisher and Schmincke [8] and Fisher and Smith [9]. According to Fisher's definitions, the term volcaniclastic includes the entire spectrum of clastic materials composed in part or entirely of volcanic fragments originating from any particle formation mechanism (i.e., pyroclastic, hydroclastic, epiclastic, autoclastic), transported by any mechanism, deposited in any physiographic environment, or mixed with any other volcaniclastic type, or with any type of non-volcanic fragments in any proportion whatsoever. This non-genetic term allows products to be identified without the need to attribute origins or processes to them.

The main fragmentation processes that generate volcaniclastic deposits are pyroclastic, hydroclastic, autoclastic, and epiclastic (**Figure 3**) [7, 9]. Pyroclasts are formed by direct fragmentation of magma due to the rapid exsolution and explosive expansion of the gases it contains. Hydroclasts are formed by explosive or non-explosive water-magma interactions that result in frozen glass particles. Autoclastic

Figure 3.
Examples of products originated by different fragmentation processes. a) Pumice-rich ignimbrite resulting from pyroclastic fragmentation of the erupting magma at the conduit (Cerro Galán ignimbrite, Central Andes, Argentina, 2 Ma). b) Hyaloclastites originated by hydrofragmentation of a subglacial basaltic lava flow (precaldera deposits, Deception Island, Antarctica, unknown age). c) Autobrecciated sub-aerial andesitic lava flow (Coll de Vanses andesites, Catalan Pyrenees, NE Spain, 300 Ma). d) Epiclastic deposit (ep) formed by water erosion and redeposition of a previous ignimbrite (ig). (Castellar de N'Hug Permian red beds, Catalan Pyrenees, NE Spain, 285 Ma) (credits: Joan Martí).

fragmentation is caused by the mechanical friction of lava flows that are being emplaced or by the gravitational collapse of domes or spines. Finally, epiclastic fragments are lithic fragments and crystals derived from any type of preexisting rock by weathering and erosion—in this case, volcanic or volcaniclastic. Fisher and Smith [9] suggested that to understand volcanic facies and sedimentation differences between volcanic and non-volcanic areas, fragmentation processes must be clearly separated from particle transport processes (e.g., wind, pyroclastic flows, flowing water, ice, avalanches), since these terms refer to the processes that create the particles and that cannot change from one type of particle to another simply by changing the transport agent.

In this chapter, I follow Fisher's conceptual recommendations, and therefore, an attempt is made to clearly differentiate between processes (fragmentation, transport, and deposition mechanisms) and their products (rocks and deposits), bearing in mind that before deducing the process, we must describe and correctly interpret the products, which is not always possible.

3. Volcanic deposits

In general terms, a volcanic deposit can be defined as a stratigraphic unit that is generated directly or indirectly by a volcanic process. This includes lavas, any type of primary volcaniclastic deposits, in addition to any epiclastic deposits that are directly derived from the erosion, reworking, and redeposition of primary volcanic deposits. Unlike with non-volcanic sedimentary deposits, which tend to preserve their characteristics and appearance over long distances and wide extensions, volcanic deposits may change drastically over very short distances, which makes it difficult to determine their lateral and spatial correlations when the outcrops are non-continuous. For this reason, facies—defined as a body or fraction of rock or sediment that has a unique defining character that allows it to be differentiated from other facies or fractions of rock or sediment [10, 11]—are widely used in the reconstruction of volcanic environments [1, 8, 9, 12]. When describing volcanic deposits or volcanic facies, there will be always a set of factors (e.g., physical, chemical, and biological) that will help to define their origin (e.g., eruption, transport, and depositional mechanisms), source area, and depositional environment [13]. An important aspect to be considered here is that eruption processes are very rapid, much more so than the geological timescale. Thus, volcanic deposits, in particular those that present a very wide spatial extent, will represent very valuable isochrones in the geological record, which will be crucial to stratigraphic corrections. Therefore, the correct identification and interpretation of volcanic deposits are so important. In each case, the degree of details used in the stratigraphic division will depend on the type of study we want to do, the degree of exposure of the selected materials, and the level of knowledge we have.

The genesis or mode of formation of volcanic deposits is not always evident, so initially, as Cas and Wright [1] propose, it is better to use descriptive terms (e.g., lava flow, intraformational breccias, deposit of supported matrix, rhyolitic) rather than terms that imply a certain genesis (e.g., ignimbrite, co-ignimbritic breccia). For this reason, both during field work and while writing it once the data have been prepared, it is always advisable to first adequately describe the materials and, at the end of the process, to propose an interpretation of them, since a well-done description, in addition to being more impartial, will always remain and can be useful for later work, while interpretations and genetic models always depend on each particular author and on the trends (writing style) of the moment.

3.1 Lithological characteristics of ancient volcanic deposits

3.1.1 Lava flows

Lava flows are the products of effusive volcanism and may form stratigraphic units of variable extents and thicknesses depending on the composition of the erupting magma and the size of the eruption. The internal characteristics of lava flows are mostly preserved in ancient volcanic terrains (**Figure 4**), but their superficial aspects may have been partially or totally obliterated by further erosion or burial by younger sediments. In fact, on many occasions when we will only observe a cross section of the lava flow, and like so, we will be able to distinguish aspects such as macroscopic texture, autobrecciation, columnar jointing, the presence of scoriae at the base and/or top of the deposit, but rarely we will see the original surface or base of the lava flow. On some occasions, it will be difficult to distinguish between true lava flows and younger sills that have intruded into previous sediments along a stratigraphic plane. This may be relevant when trying to interpret the cores extracted from boreholes drilled in volcanic successions, as they may have a very similar aspect. Another important aspect of paleo lava flows is the different degree of alteration that they may have experienced, as this may severely affect their original texture and mineralogy.

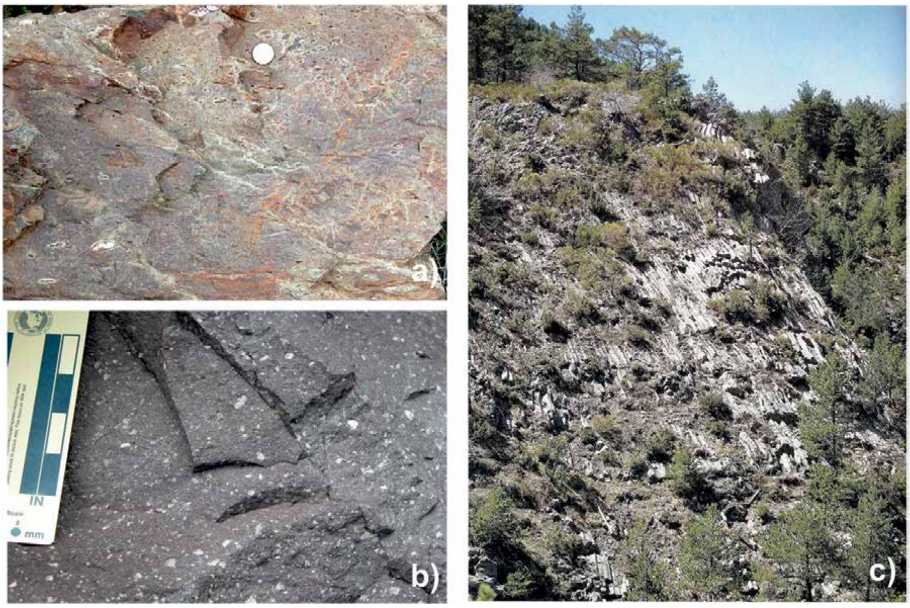

Figure 4.
Field photographs of a) a vesicular andesitic lava flow (upper Ordovician, Catalan Pyrenees, NE Spain, 450 ma); vesicles are now filled with secondary minerals, b) classical porphyritic texture in dacitic lavas (Camprodon, Catalan Pyrenees, 300 ma) and (c) of a dacitic dome with well-developed columnar jointing (El Querforadat, Catalan Pyrenees, 300 ma) (credits: Joan Martí).

3.1.2 Volcaniclastic deposits

The main lithological criteria to consider in the study and characterization of volcaniclastic deposits are the nature of the clastic components, namely the morphology of the grains and the resulting texture of the deposit, in addition to the petrological and geochemical characteristics of the volcanic components and the identification of the alteration products [1, 9, 14]. First, we must analyze the nature of the grains. It is necessary to identify whether it is a primary volcaniclastic deposit or, on the contrary, it has been formed by weathering and erosion of preexisting materials. Although the lithological characterization of the deposit may not be sufficient to make this discrimination, such that other criteria may be also necessary, it helps to obtain essential information when trying to characterize the deposit and identify its origin [12].

The aspects that must be analyzed to define the texture of a deposit are grain size distribution, the degree of sorting of the different fragment populations, their shape, their degree of rounding, and the fabric (**Figure 5**) [1, 8, 15, 16]. The characteristics of paleovolcanic deposits, which are generally compacted, altered, and sometimes deformed and metamorphosed, complicate their study compared with recent deposits. Although there are few difficulties in identifying the nature of the different components—for example, it is almost impossible to obtain an absolute grain-size distribution of these deposits—nonetheless, the relative size comparison of the fragments at a macroscopic level, in addition to the point count, can give us a first-order approximation on the size distribution.

Also, due to the consolidation of most ancient deposits, it is not possible to carry out a three-dimensional grain morphology study. Furthermore, alteration processes tend to modify pyroclastic morphologies (e.g., [17]). However, a detailed petrographic study can reveal some primary morphological characteristics of the volcanic grains and, consequently, reveal their fragmentation mechanism. Likewise, the degree of rounding can be examined without difficulty at macroscopic and microscopic levels, which also gives us information about the transport mechanisms of the deposits.

Other textural aspects, such as the orientation of crystals and fragments, the presence of lineations, geometry of the spaces between the clasts, etc., can provide information on the nature of the deposit and the transport and deposition mechanisms. For example, the products derived from the explosive activity of siliceous magmas almost always contain pumice fragments. Due to its vitreous nature and its high content of vesicles, this component is easily altered by post-depositional processes. However, the texture of pumice fragments can remain relatively preserved (**Figure 5**); this occurs in those cases where the vesicle content of the original fragments was relatively low due to the stretching they underwent when emplaced at high temperature (ignimbrites and welded pumice deposits), now appearing as clayey aggregates with a frayed appearance, while being preferentially oriented. However, this texture is not exclusive to welded rocks, but can also appear in deformed rocks that contained stretched or unstretched pumice fragments (**Figure 6**), or simply by compaction of devitrified pumice fragments at edaphic levels [17]. The interpretation in each case should be based not only on the textural aspect, which will be similar in all of them, but also on the relationships with the other deposits of the same sequence.

Another lithological criterion that must be taken into account is the petrological and geochemical composition of the rocks, although this is only feasible in the case of lava or other massive volcanic rocks, or in some particular cases of primary pyroclastic deposits formed almost entirely of juvenile material. In most cases, volcaniclastic rocks, whether primary or derived from the reworking of preexisting rocks, contain a variable number of lithic fragments of diverse compositions and origins. In consolidated rocks, such as most ancient volcaniclastic rocks, the impossibility of separating the different components of the deposit makes chemical analysis of the rock unfeasible, since the presence of lithic fragments contaminates the true composition of the eruptive magma. Likewise, the existence of alteration (hydrothermal, diagenetic, and/or meteoric), a common characteristic of paleovolcanic rocks, also makes it difficult to identify the chemical composition of juvenile volcanic components. However, the mineralogical composition of volcanic fragments can be established in most cases by petrographic analysis, although when alteration processes have been important, the original mineralogical composition can also be obliterated.

Figure 5.
Field photographs of two ignimbrites with eutaxitic texture, a) from the upper Miocene (6 ma) (Central Andes, Argentina), and b) from the upper Ordovician (450 ma) (eastern Pyrenees, Spain). Despite the difference in age between the two rocks they show a very similar appearance (credits: Joan Martí).

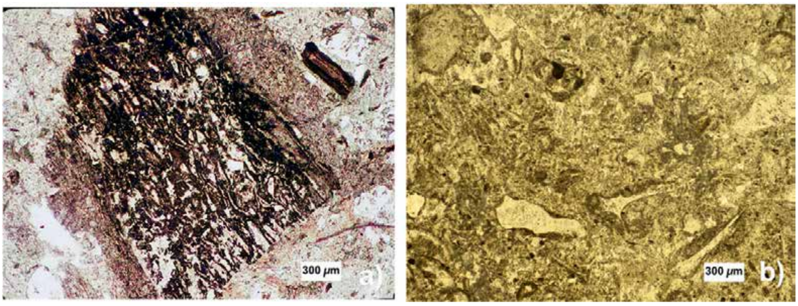

Figure 6.
Microphotographs of a) a vesicular pumice texture in a fallout deposit, with vesicles now filled with secondary minerals (Gréixer rhyolitic succession, Catalan Pyrenees, NE of Spain, 300 ma), and b) elongated pumice fragments (fiamme) in a) strongly welded ignimbrite (upper carboniferous, Campelles, Catalan Pyrenees, 450 ma). In both cases, pumice fragments are now devitrified and transformed into clay aggregates. (credits: Joan Martí).

3.2 Geometry of paleovolcanic deposits

Geometry defines the three-dimensional shape of the deposit and will be controlled by the topography of the terrain, the volume of deposit, the transport and deposition mechanisms of volcanic materials, the existence of non- and post-depositional erosive processes, and the existence of subsequent deformations [1, 8, 12].

Three-dimensional deposit geometries are difficult to observe in ancient volcanic terrains. The paleovolcanic successions correspond to parts of complex volcanic edifices that are very rarely well preserved, such that the resulting successions and their geometry will depend on the relationship between deposition, erosion, and deformation. In general, volcanic materials are easily altered and eroded, so that a large part of them will disappear, partially forming the epiclastic volcaniclastic deposits. Moreover, paleovolcanic terrains may have been affected by further tectonic movements, so they may have been incorporated into different tectonics units that may have hidden them or have altered their original lateral continuity. This implies that the lateral extension of paleovolcanic deposits and, consequently, their relative age cannot be always established. Only in cases of rapid accumulation of large volumes of pyroclastic materials—as is the case of intra-caldera deposits in collapse calderas (e.g., [18])—can most of the original materials be preserved (**Figure 7**).

On the other hand, the presence of discontinuities in volcanic terrains is frequent and may have a relatively local significance, with the corresponding erosive episodes generally being the result of an eruptive event rather than a tectonic uplift (**Figures 7** and **8**) [2]. Likewise, the presence of strong dips in this type of terrain does not necessarily imply the existence of tectonic pulses. On the contrary, the volcanic edifices may initially have steep slopes that will determine the geometry of subsequent deposits. Thus, the interpretation of the geometry of paleovolcanic deposits must be done with great care, since otherwise the existence of phenomena may be assumed that had never really occurred [2]. A good recommendation when interpreting the geometry of ancient volcanic deposits is to compare it with current analogs in which its three-dimensional representation at the regional level can be deduced.

3.3 Sedimentological characteristics

Sedimentary structures occur before deposition (i.e., erosional features), during deposition (stream-generated structures), and after deposition (bioturbations,

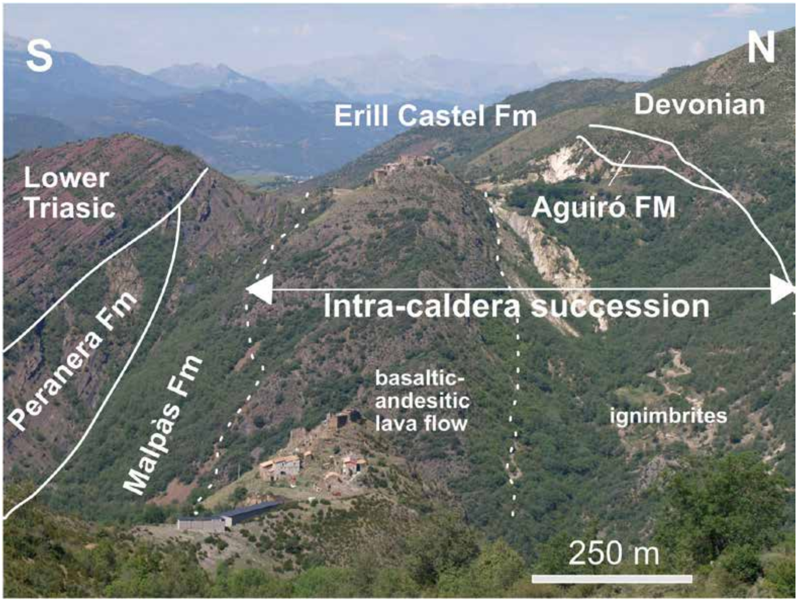

Figure 7.
Panorama of the post-Variscan Permo-carboniferous volcano-sedimentary formations at Erillcastell (Catalan Pyrenees, NE Spain, 300–270 ma), where an entire intra-caldera succession (Erillcastell Fm.) is preserved [16]. Also observe the discontinuities between some of the formations, which indicate the existence of inter-formational tectonic movements. (credit: Joan Martí).

deformations in soft sediments) of sedimentary aggregates. Together with the textural aspects, they inform us about the characteristics of the emplacement and deposition processes. Sediments can basically be transported in two ways, particle by particle or en masse, resulting in different structures in both cases, although not always exclusive, such that each sediment must be analyzed in detail and evaluated on its own merits [1].

These types of transport mechanisms can occur both in primary pyroclastic materials and in other types of sediments, although the transport medium is usually gas in the former, while in the latter it is frequently water. This implies differences in the morphological and textural characteristics of the sediment components, which will allow us to identify the genetic character of the deposit.

Volcaniclastic deposits tend to present elements (either textural or sedimentary structures) that allow us to reconstruct the directions of the paleocurrents. In epiclastic materials, the existence of ripples, dunes, cross-stratification, imbrications, angle of repose, etc., constitute the basic elements for this task. Pyroclastic materials can also exhibit unidirectional sedimentary structures, especially in the case of dilute PDC (i.e., pyroclastic surge) deposits (**Figure 8**). Massive deposits, such as dense PDC deposits or lahars, may present other types of structures such as imbrications, lineations of elongated elements (crystals, stretched pumice fragments, plant remains, etc.) that also allow the direction of flow to be identified.

3.4 Fossils

The use of fossils as paleoenvironmental indicators is essential not only for non-volcanic successions, but also for volcanic ones. In paleovolcanic successions, the

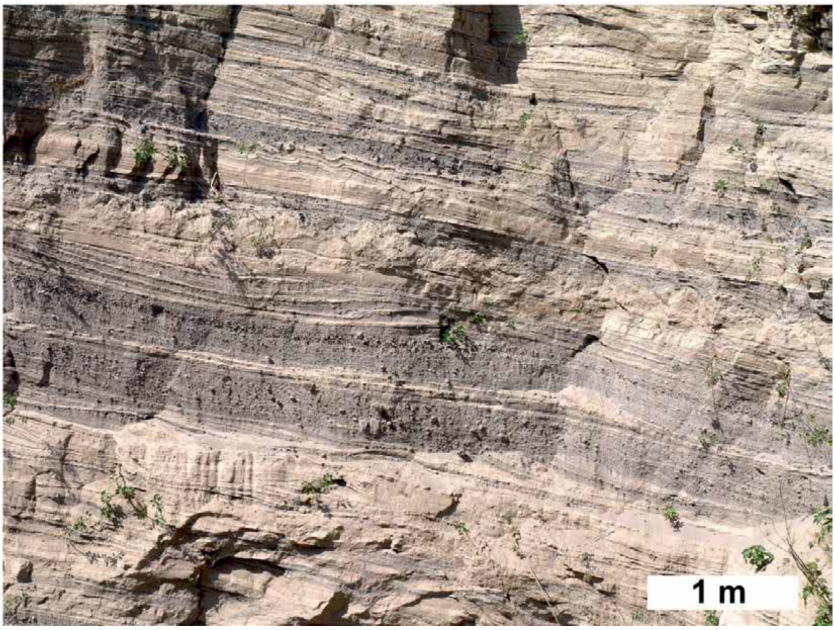

Figure 8.
Succession composed of primary phreatomagmatic pyroclastic deposits mostly emplaced by dilute PDCs, showing a wide diversity of sedimentary structures (middle Miocene, México) (credit: Joan Martí).

presence of fossils in the interbedded epiclastic, but also in the pyroclastic deposits, can provide information about the age of the rocks and their depositional environment, although it is not always easy to know whether the fossils were deposited *in situ* or were transported and redeposited. The presence of fossils (vertebrate, invertebrate and plants) within pyroclastic deposits (e.g., [19]) and lavas (e.g., [20]) is common. In addition to the stratigraphic, paleoenvironmental, and paleoclimatological information that this represents (e.g., [21, 22]), we can also obtain information on the emplacement temperature of the deposit and the direction and sense in which it was emplaced (e.g., [23, 24]). Also significant is the presence of fossils in the post-eruptive successions of maars (e.g., [25]), or the presence of vertebrate tracks on volcanic and associated deposits [26], which helps to decipher their paleoenvironmental evolution.

3.5 Factors that alter the original characteristics of volcanic deposits

Volcanic materials may undergo, including from the stages immediately after their emplacement, a series of transformations that can imply significant changes in their texture, mineralogy, and chemistry. The metastable nature of volcanic glass, the main component in this type of rocks, favors these changes. In paleovolcanic terrains, there is also the superposition of large-scale erosive and re-sedimentation processes, such as sediment gravity flows or debris avalanches, diagenesis, tectonic deformations, and even metamorphism. For all these reasons, the lithological characteristics that we can identify in modern deposits are not always comparable or identifiable with the same clarity in ancient materials.

One of the conflicting points in the interpretation of the alteration processes experienced by volcanic materials is the distinction between the results produced by processes such as weathering, hydrothermal alteration, or diagenesis. In all cases, the result of the transformations of the affected rocks is the devitrification of the glass and the formation of secondary minerals replacing the original glass, filling the pores of the rock, and/or partially or totally replacing the primary minerals. Consequently, there will be a change in the chemical composition of the original volcanic components, although the intensity of this change will depend on the intensity of the alteration processes and the original composition and texture of the rock (**Figure 9**).

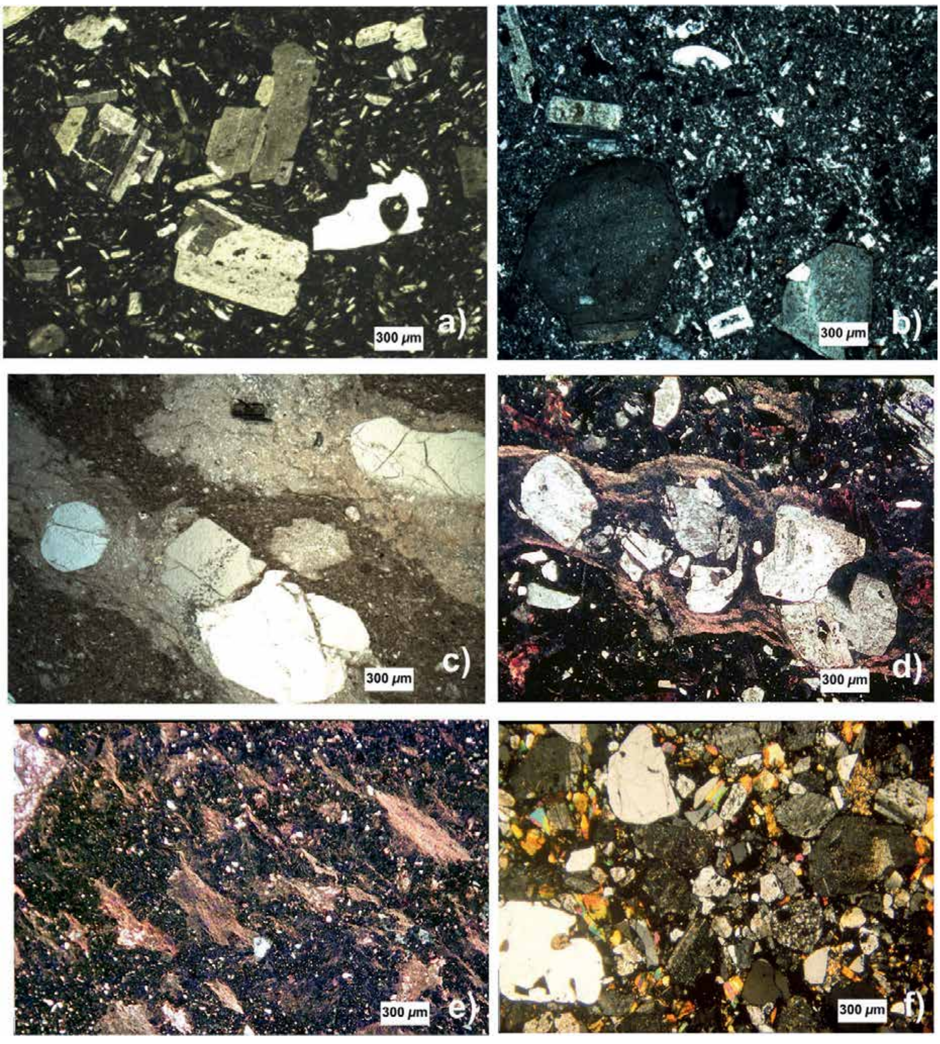

Figure 9.
Examples of microphotographs of volcanic and subvolcanic rocks from the Permo-carboniferous terrains (305–285 ma) of the Catalan Pyrenees (NE Spain) showing different degrees of alteration. a) Dacitic lava flow, showing a porphyritic texture with phenocrysts of quartz and plagioclase. b) Granodioritic dyke, showing a porphyritic texture with phenocrysts of quartz and partially altered plagioclase. c) Crystal-rich (phenocrysts of quartz, plagioclase, and biotite), totally devitrified (to microcrystalline quartz aggregates) pumices, in a partially welded ignimbrite. d) Crystal-rich (phenocrysts of quartz, plagioclase, and biotite), totally devitrified (to microcrystalline clay aggregates) fiamme pumice fragments, in a very crystal-rich ignimbrite matrix. e) Eutaxitic texture in an ignimbrite matrix with devitrified fiamme transformed into clay aggregates. f) Crystal-rich dilute PDC deposits. (credits: Joan Martí).

Weathering includes a set of processes, such as the chemical action of the atmospheric air and rainwater and of plants and bacteria, as well as the mechanical action associated with temperature changes, by means of which the rocks exposed on the Earth's surface alter until they become soils [27, 28]. Weathering depends on the climatic conditions prevailing in the deposition area and on the composition of the rocks. The changes produced by weathering tend to cause a compositional zonation in the rock, in most times grading vertically in intensity but also from an unaltered zone in the interior to zones with variable alteration in the external part. In the altered parts, weathering can imply a loss of original porosity in the rock, although sometimes this can also increase due to the dissolution of the original glass components (e.g., [29, 30]).

Hydrothermal alteration includes the chemical, mineralogical, and textural changes that occur in rocks due to thermal and chemical changes in the environment in the presence of hot water, steam, or gas [31, 32]. Hydrothermal alteration involves ion exchange reactions, mineral phase transformations, mineral dissolution, and the precipitation of new mineral phases [1]. In most volcanic zones, hydrothermal alteration is associated with the proximal zones, which are characterized by the presence of fluids secreted directly from the residual magma chamber, or *via* the percolation of meteoric water that is heated at depth by this magmatic heat source. These hydrothermal fluids experience a convective-type permanent circulation that allows an almost continuous transformation of the host rocks. However, in distal areas of pyroclastic and lava deposits, a particular type of hydrothermal (or autohydrothermal) alteration can also occur, caused by the magmatic gases themselves that have been trapped in the deposit ("vapor phase alteration"), producing rapid devitrification of its vitreous components and precipitation of secondary mineral phases in the vesicles and pores of the rock [33–37].

Hydrothermal alteration can produce quartz aggregates, amorphous silica, potassium feldspar, albite, calcite, montmorillonite, illite, kaolinite, alunite, chlorite, zeolites, and low-grade metamorphic minerals, depending largely on the composition of the rock and the origin and composition of the hydrothermal fluids. Likewise, hydrothermal alteration is responsible for the presence of important epithermal mineralizations of precious metals and metallic sulfides that are associated with many volcanic zones, especially in paleovolcanic terrains (e.g., [38]). Sometimes hydrothermal alteration is also responsible for the existence of pseudo-eutaxitic or clastic textures, since it tends to give patching-type structures (e.g., [1, 39, 40]), which can confuse massive lava flows for volcaniclastic deposits. This implies that extreme care must be taken when examining the textures of paleovolcanic rocks and using other criteria such as their relationship with other deposits, their geometries, lateral variations, before making a final diagnosis of their nature. Special attention should be given to rocks that have undergone subsequent deformation and therefore present penetrative schistosity, since the recrystallization of clay minerals, micas, and chlorites is more important and can enhance the presence of pseudo-clastic textures.

Diagenetic changes group all those that can take place within sediment following its deposition and burial, except those that are due to metamorphism or weathering on the Earth's surface. There has been an ongoing discussion among researchers about the exact demarcation limits under which diagenesis occurs. In our case, we consider as such the chemical, mineralogical, and textural changes that occur slowly and at low temperatures (between 20 and 300°C), which occur in the sediment (volcanic rocks) after its burial, although being relatively close to the surface to be able to withstand pressures less than 1 kbar (~ 3 km deep).

Diagenesis is a process associated with the lithification of sediments, which includes compaction, cementation, recrystallization, authigenic mineralization, and the growth of concretions or nodules [41]. Diagenetic processes occur in the early stages of burial of deposits and are associated with the circulation of interstitial fluids, these being mostly meteoric water. Unlike what happens with weathering or hydrothermal alteration, diagenesis affects the entire rock more homogeneously, especially in terms of changes in texture, although there may be zoning in the appearance of sequences of secondary minerals. The diagenesis of volcaniclastic rocks is of great importance in the exploration of hydrocarbons, since it produces a modification of the original porosity of the rock, generating a secondary porosity and favoring the maturation of hydrocarbons (see [42]).

In rocks that contain abundant primary volcanic components (pyroclastic rocks), diagenesis can be favored by the existence of previous compositional and textural changes in the glass produced during their transport and initial weathering. However, in the case of intra-caldera succession (e.g., [43, 44]), the rapid emplacement of thick ignimbritic successions prevents weathering and favors the vapor phase and a very early diagenesis (or hydrothermal alteration) but at a much higher temperature than it would be in a normal burial process.

Metamorphic transformations, whether due to regional or contact metamorphism, constitute a higher degree extension of diagenesis, although they should not be confused with hydrothermal alteration, which generally has a much more localized effect [1]. Metamorphism produces significant mineralogical and textural changes and, if accompanied by deformation, can completely obliterate the initial texture of the rock, especially when there are intermediate to high-grade transformations. In low-grade metamorphic transformations (green schist facies), it is possible, however, to still recognize some primary textural aspects such as welding textures, vitroclasts, or perlite fractures (**Figure 10**).

In all these alteration processes, the fundamental factor is the metastable character of the volcanic glass, the resulting products reflecting its original composition. The devitrification of basaltic or silicic glasses can give rise to totally different products even when they have been generated under very similar conditions. Palagonitization is a typical alteration of basaltic glass in both subaqueous and subaerial conditions, characterized by its transformation first into an apparently amorphous substance (palagonite), due to the initial hydration process, and later into smectites and zeolites. Palagonitization is explained as the result of hydrothermal or diagenetic alteration [8, 45–50], especially in submarine environments, although it can also be explained because of hydrovolcanic processes (e.g., [51]). Unlike basaltic composition glasses, the devitrification of silica glasses gives rise to the formation of perlite textures in the initial stages of hydration (without emplacement) and the majority formation of zeolites, clay minerals, and potassium feldspar in the more advanced stages. A singular case is the formation of tonsteins (e.g., [52]) and bentonites (e.g., [53]) that correspond, respectively, to layers rich in kaolinite (illite and smectites) interbedded between deposits of marl, slates, and especially coal layers and to layers that are dominated by smectites. In both cases, it is the product of the alteration of layers of silicic ashfall deposits.

In addition to the alterations described above, it should be noted that volcanic terrains are places where contemporaneous crustal movements take place and because many of them are associated with orogenic belts, where subsequent penetrative deformation may take place. Deformation can significantly change the original stratigraphic relationships and deposit geometry. Likewise, deformation can also

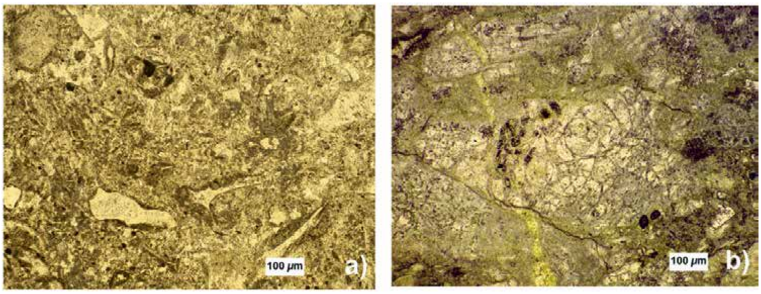

Figure 10.
a) Microphotographs of vitroclasts in an ignimbrite matrix b), perlite fractures in a highly welded, rheomorphic pyroclastic deposit (Gréixer-Coll de pi rhyolitic succession, Catalan Pyrenees, NE Spain, 300 ma) (credits: Joan Martí).

produce important changes at macroscopic and microscopic scales, causing important problems for the identification of primary textures. For this reason, in paleovolcanic terrains that have undergone tectonic transformations, it is important to carefully study the textures of the volcaniclastic rocks, in order to not confuse aspects superimposed by the deformation of the original elements of the rocks. In the same way, at a regional and outcrop level, it is necessary to know how tectonic deformation has affected the original structure of the area and, if possible, to conduct a palinspastic restoration of the terrain to its original position (e.g., [54]).

4. Stratigraphy of paleovolcanic successions

An important aspect in the characterization of paleovolcanic terrains is the correct description and interpretation of their stratigraphy. We have already highlighted some of the most relevant difficulties in merely identifying ancient volcanic deposits, not to mention the challenges to establish their lateral relationships and the relative ages. The development of a detailed stratigraphy can help alleviate these difficulties and correctly interpret the succession of events that make up a given succession of deposits. Likewise, the completion of such a stratigraphy is essential to be able to interpret such successions in terms of eruptive sequences.

The stratigraphic divisions to be established, as well as their geological mapping, will depend on the type of study to be carried out. However, there must be some general criteria that allow us to establish a stratigraphy that can be compared with other similar examples and, therefore, can always be interpreted in the same way. When investigating a given area, the first step must always be the objective description of the local stratigraphic succession in terms of lithostratigraphic units able to be mapped and correlated. Lithostratigraphy consists of the description, identification, and interpretation of rock units (see [55]). Individual units must be described and defined based on their general lithological characteristics and their interrelationships with adjacent units. Stratigraphy of volcanic terrains, both modern and ancient, should try to identify the stratigraphic and chronological order in which the products of an eruption, a series of eruptions, or of an interruptive period (epiclastic deposits or reworked volcanics) appear in the geological record (**Figure 11**) [2]. Therefore, the most logical way to describe the stratigraphy of volcanic terrains is by using the same principles as classical stratigraphy (e.g., [56]), that is, to identify and group the different existing units based on a hierarchy that allows for the identification of a temporal succession of events or units of eruptive activity [2, 8]. In recent volcanism, the identification of the different lithostratigraphic units can be done without too much difficulty since the products of the different eruptions can nearly always be easily distinguished. Likewise, the variations in the compositional trend of the magmas, eruptive styles, or other characteristics that allow the deposits from different eruptions to be grouped in cycles of volcanic activity are equally identifiable. However, in older terranes, due to the complications discussed above, establishing the correct lithostratigraphy is not always possible. Despite this, attempts should be made to use the same lithostratigraphic subdivisions, since an accurate interpretation of a paleo-volcanic zone must include (or at least attempt) the identification and interpretation of the different volcanic episodes recorded in the succession of deposits. Martí et al. [2] have provided a detailed review of the principles of volcanic stratigraphy and how they should be applied in field studies of volcanic terrains. I direct the reader to this contribution to be informed about the methods used in volcanic stratigraphy.

As we have seen previously, the different deposits can be identified based on their lithology (mineralogy, petrology, alteration, color, degree of welding, grain-size distribution), geometry, and relative stratigraphic position. Within a volcano-sedimentary succession, the existence of different deposits corresponding to the same eruption (i.e., Member) and of different members constituting a formation can be established based on the presence of first-order discontinuities such as paleosoils, erosional surfaces, or interbedded epiclastic deposits. However, the presence of erosional surfaces or interbedded epiclastic deposits does not always indicate a significant interruption in eruptive activity. This can be especially important when trying to reconstruct an eruptive sequence from a poorly exposed succession of deposits. Recall that some pyroclastic deposits are emplaced in a highly turbulent regime (e.g., [57]), so

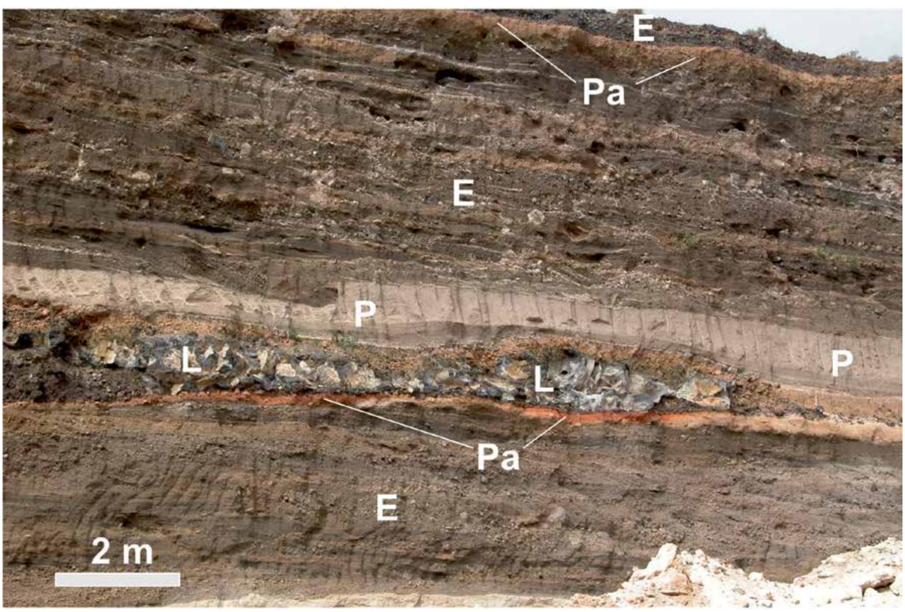

Figure 11.
Example of a volcano-sedimentary succession in which different volcanic units (lava flows (L), primary pyroclastic deposits (P), and epiclastic deposits (E)) all having originated by reworking of volcanic material (Tenerife, Canary Islands). The presence of paleosoils (Pa) separating some of the deposits is also visible. (credit: Joan Martí).

they can erode previously formed deposits without indicating a change of eruption. In the same way, the existence of rainfall, sometimes torrential, associated with volcanic eruptions is a common fact, and this may cause some primary pyroclastic deposits to be partially reworked during the eruption itself (e.g., [58]). In this case, the maturity of the epiclastic deposit (degree of reworking) will be a criterion to consider in its identification.

Establishing the age of the deposits forming a particular stratigraphic succession is crucial to determine the eruptive history of a particular volcanic system. This will permit distinguishing between several eruptions and also establishing the existence of possible cycles of activity. However, knowing the "absolute" (radiogenic) age is not always possible, since it will depend on the quality (degree of alteration) of the samples, their mineralogy, and the limitations of the method itself. The same restrictions or uncertainties apply with dating based on flora found in ancient pyroclastic or associated deposits. Therefore, what is essential is to establish at least the relative chronology of the set of deposits studied.

The importance of establishing a correct stratigraphy for correlation purposes relies on the fact that pyroclastic materials can be deposited over wide extensions, sometimes exceeding the limits of the basin itself, which means that these volcaniclastic horizons occasionally constitute excellent correlation levels. As previously mentioned, we should also consider that a volcanic eruption represents a very short period of time (generally hours or a few days), which, when translated to the geological scale, means an instant; in this way they can be considered as a physical representation of an isochron.

In recent years, magnetostratigraphy, which uses variations within the stratigraphic sequence of the magnetic properties of rocks (magnetic susceptibility and direction of remanent magnetism), has emerged as an excellent method for geological correlations (see [59]) and particularly in old volcanic terranes (see e.g., [60]). In this sense, we must consider that magnetostratigraphy, together with radiometric or fossil dating, allows us to obtain not only relative ages but also an absolute timescale of the volcanic succession.

In any case, it must be kept in mind that when going backward (toward older terrains) in the examination of paleovolcanic terrains, the geological timescale is progressively less well defined, so we may find that simple stratigraphic unit levels are representing very important periods of time, even several million years long, as the degree of preservation of volcanic materials becomes worse proportional to the age of the terrain. However, in fact, a volcanic level—and especially those of pyroclastic origins—represents an instant not only on the geological timescale, but also on the human timescale. For this reason, we must be very careful in interpreting the chronostratigraphic value of volcanic units in ancient terrains since each deposit by itself represents a single event in geological time but corresponds to the culmination of long geodynamic and magmatic processes that may extend significantly longer than the observed stratigraphic succession.

Volcanic deposits may show significant lateral variations from the vicinity to the vent to the areas away from it (e.g., [61]). In this sense, it is worth mentioning that proximal to distal definition is far not as fixed as in normal sedimentary environment. In volcanic systems, these can be in a very broad range, even with similar eruption styles but different eruption intensity, eruption rate, etc. This is particularly important in paleovolcanic systems where we have limited spatial knowledge about them system. So what we see in the cross sections offered by most outcrops needs to be scale up to 3D to be able to provide an "intelligent guess" for the location's position relevant to the source.

Figure 12.
Example of a) proximal (co-ignimbrite lag breccias), b) intermediate (units of ignimbrites showing a characteristic planar basal contact), and c) distal (distal, > 100 km away from the vent, strongly indurated (silicified) ash fallout deposits), deposits from the Permo-carboniferous volcanism of the Catalan Pyrenees (NE Spain) (credits: Joan Martí).

Depending on the distance to the vent, volcanic deposits can be proximal, intermediate, or distal. For example, fall deposits will progressively decrease in thickness and grain size with the distance from the vent. For ballistically emplaced deposits, a more or less radial distribution can be observed around the vent, but the deposits associated with the horizontal dispersion of the eruptive column will present a distribution that will depend on the orientation of the prevailing winds, although the proximal to distal distribution will be as mentioned before. The deposits generated by PDCs may also present significant lateral variation with distance from the vent. In the case of deposits emplaced from dense PDCs, they may correspond to thick units (intra-formational breccias) in the proximal zones (**Figure 12a**), massive ignimbrites in the intermediate zones (**Figure 12b**), and co-ignimbritic ash layers in the most distal areas (**Figure 12c**). Deposits emplaced from dilute PDCs, especially those associated with tuff ring or cone-type edifices, present a very characteristic distribution from the vent to the distal zones, with significant changes in their internal sedimentary structures. However, in ancient volcanic terrains, especially for those in which later tectonic processes have been important, it is possible that only parts of the geological record corresponding to volcanic activity have been preserved, so that these variations from proximal to distal will probably only be assumed on the basis of variations in the deposit's thickness, grain size, or rock type [61–63].

Within this ideal model of proximal-distal (referred to the vent area) variations in volcanic terrains (**Figure 1a** and **12**), proximal areas are mainly represented by lava flows, domes, and coarse-grained primary pyroclastic deposits or epiclastic volcaniclastic materials generated by erosion and gravitational processes, which act on the steep slopes of the volcanic edifice. In deeply eroded terrains, proximal areas may also include different groups of subvolcanic intrusive rocks (stocks, sills, and dykes). The presence of a significant fumarolic alteration is also a good guide to identify proximal zones in paleovolcanic terrains. The intermediate areas are mostly represented by the terminal parts of lava flows and thick successions of PDC, as well as some fallout deposits and their reworked products. Increasing the distance from the vent also increases the amount of re-sedimented pyroclastic material and epiclastic deposits. Finally, the distal areas will be formed by fine-grained fallout deposits interbedded with abundant non-volcanic sedimentary material.

5. Depositional environment

An important aspect in the study of ancient volcanic terrains is to identify the corresponding depositional environments. These include all the physical, chemical, biological, and geological aspects that affect sedimentation within a specific area, being possible to distinguish between local environments (e.g., marine and non-marine, fluvial, lacustrine, wind, deep, shallow), defined in geomorphological terms, and tectonic environments with a much broader regional implication [13].

The explosive character of some volcanic activity is widely recognized in subaerial environments, and the distinctive characteristics of the products of this type of volcanic activity are well established. However, in relatively shallow subaquatic environments, explosive volcanic activity with characteristics similar to subaerial ones and with nearly identical products can also occur [64–70]. Likewise, this may be the case for PDC deposits originating in a subaerial environment, but that were ultimately emplaced in a subaqueous environment. In this case, there are no particular characteristics that allow them to be distinguished from purely subaerial or subaquatic deposits of the same type [71–75]. Furthermore, it will be necessary to identify the existing lateral variations within the volcanic deposits and the characteristics of the interbedded epiclastic deposits in order to accurately determine the depositional environment. In deep submarine environments, the hydrostatic pressure of the water column inhibits the vesiculation of magmas (e.g., [76, 77]), such that the volcanic activity will be predominantly effusive, regardless of the type of magma, until the volcanic edifice grows enough for the magma column to reach sufficiently superficial levels where it can experience explosive vesiculation, thus beginning to generate the first pyroclastic products [70, 77].

Depositional environments will also depend strongly on the tectonic setting where they develop, as this will control the geometry of sedimentary basins, rate of subsidence, location of volcanic vents, types of volcanism, local tectonics, and the general sedimentation rate.

Finally, it is worth mentioning that in paleovolcanic terrains in which the mixture of pyroclastic material with sedimentary material (with different proportions of each) is frequent, subsequent transformations experienced by volcanic deposits can cause significant changes with respect to the primary composition and texture of these rocks. However, both the composition and the secondary texture resulting from these transformations can serve to establish groups of deposits based on compositional and textural characteristics that may help their spatial and temporal correlation (**Figure 13**).

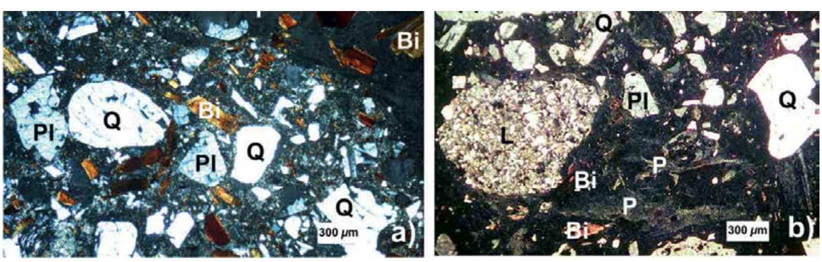

Figure 13.
Comparison between two microphotographs of crystal-rich, pumice rich ignimbrites from a) Cerro Galan, Argentine (2 ma) and b) Prats d'Aguiló, Catalan Pyrenees, NE Spain (300 ma). Both show a very similar texture, with a similar content of phenocrysts of the same composition (quartz, Q; plagioclase, Pl; biotite, Bi), pumice fragments (P), vitric in the Gerro Galán ignimbrite and devitrified (clay aggregates) in the Prats d'Aguiló ignimbrite, and lithic fragments (L). (credits: Joan Martí).

6. Volcanism, basin dynamics, and sedimentation

The presence of volcanic deposits is frequent in many sedimentary basins. The existence of volcanic episodes in the sedimentary record represents an important source of information to understanding the geological evolution of that particular time frame. Specifically, the presence of volcanism responds to geodynamic conditions that favor the genesis and rise of magmas and that, on the other hand, can translate into suitable tectonic conditions for the development of a subsidence structure [78]. In paleovolcanic terrains, where erosion and tectonics may have obliterated their original characteristics, the location of vent zones or proximal areas will help to infer the position of the main fault zones that controlled volcanism and that occasionally may also be associated with basin subsidence—even when these faults may have been reactivated in subsequent tectonic movements (e.g., [54, 79]). Likewise, volcanic deposits, and especially those derived from explosive eruptions, constitute a valuable tool for establishing stratigraphic correlations within and outside the limits of the basin, as well as a precise geochronology of the host sedimentary successions (e.g., [80]). On the other hand, the interaction between volcanic processes (which are generally catastrophic) and sedimentary processes sometimes leads to the appearance of "anomalous" deposits within the sedimentary successions, which can be predisposed to erroneous interpretations if the nature of volcanic processes is not well known [81, 82]. Thanks to the current approach of volcanology that pursues the study and understanding of volcanic processes, bringing together many other aspects besides the pure identification and classification of volcanic rocks, it is possible to obtain a much broader vision of these phenomena, which helps in the interpretation of other geological problems, such as basin analysis.

The formation of a sedimentary basin is a geodynamic process that frequently implies the existence of a fracture network that allows the progressive subsidence of the blocks it delimits, thus accommodating sedimentation [83]. Similarly, volcanic episodes respond to geodynamic processes that lead to the formation of magmas at depth and hence facilitate their rise to the surface. However, the formation and ascent of magmas do not always imply the existence of eruptive processes. Only when tectonic conditions are adequate (especially in the upper crust) can magma reach the surface. These conditions imply a locally distended stress field that favors the opening of fractures and consequently the rise of magma through them (e.g., [84]). In many cases, these fractures are the ones that delimit the basin and control its subsidence, so the location of the volcanic centers is directly related to the structure of the basin. Therefore, in paleovolcanic terrains, the reconstruction of volcanic stratigraphy that indicates the position of vents may help to infer the structure of the basin where volcanic deposits have been emplaced.

Due to the fact that the physical conditions that control the release of magma to the surface do not vary with time, the study of volcanic processes is useful, above all, in the reconstruction of those basins that have undergone subsequent tectonic transformations. In current basins, the application of geophysical methods allows obtaining an adequate understanding of their structure and dynamics—although these methods may be of little value in the interpretation of ancient basins. However, the reconstruction of the volcanic episodes helps to know the initial structural conditions that controlled them and, therefore, allows one to deduce which were the tectonic features that directed the dynamics of the basin. Moreover, in deeply eroded paleovolcanic terrains, it is sometimes possible to observe the roots of large volcanic complexes (stratovolcanoes, collapse calderas, etc.) represented by different sets of subvolcanic intrusions and faults [85–87], whose orientation may depart from the regional ones; hence, the structural reconstruction of such paleovolcanic settings needs to be conducted and understood at different spatial and temporal scales when these complexities appear.

The influence of volcanic activity on sedimentation can be significant in various aspects. The sedimentation rate in a basin with volcanism can be much higher than in a non-volcanic basin with similar characteristics. This may represent a significant increase in the rate of subsidence of the basin, while it can significantly reduce the time required to become clogged. This fact can be accentuated in the case of volcano-tectonic basins or especially in the case of large collapse calderas, where the deposition of successions of volcano-sedimentary materials, several hundreds of meters thick, is carried out over very short periods of time (e.g., [43]). This can be misleading if the observer does not properly separate both processes on the timeline.

In a sedimentary basin where there is a direct influence of volcanic activity, sedimentation will be significantly affected by the simultaneous presence of eruptions that generate large volumes of pyroclastic materials and by the growth and subsequent dismantling of volcanic edifices. When studying the response of the sedimentary system to the presence of volcanism, we must make a distinction between syn-eruptive periods and inter-eruptive periods [82]. The syn-eruptive periods are characterized by the instantaneous production, geologically speaking, of large volumes of volcaniclastic sediments and other volcanic products that may be remobilized and deposited through different sedimentation processes (e.g., [88]). These periods are short and are separated by relatively longer inter-eruptive periods during which volcanism has little or no influence on the sedimentary system and which will consequently be characterized by a significant decrease in sediment production. In the stratigraphic record, the existence of these syn- and inter-eruptive periods can be identified based on the lithological and sedimentological characteristics of the deposits. In this sense, we must take into account that the resulting deposits will depend on the relative importance of these two types of periods.

The presence of volcaniclastic sedimentation implies some notable differences with respect to typical siliciclastic sedimentation [9, 82, 89, 90]. First, the resulting deposits will mostly be made up of fragments derived directly from eruptive activity rather than by weathering of preexisting rocks (**Figure 14**). In contrast, pyroclastic deposits are sediments generated over very short intervals of time and can be emplaced in the form of thick layers that may cover the topography more or less homogeneously or fill valleys and topographically depressed areas, resulting in efficient erosion. In a volcanic terrain with a predominance of explosive activity, erosion rates are high not only due to the existence of a high volume of unconsolidated material, but also to the destruction of the vegetation, which acts as a regulating agent for sedimentation from volcanic processes [82, 88, 91]. The loss of vegetation and the relative impermeability of the pyroclastic material, due to its fine grain size or poor sorting compared with soils, causes an increase in the amount of material that can be remobilized, which significantly increases the volume and periodicity of the total discharge into the basin [82].

The style of volcanism is of great importance to the development of the basin infilling successions. The volume of volcaniclastic material determines the extent of the influence of eruptions on sedimentation. In paleovolcanic terrains where a large part of the vent areas may have been eroded, it is necessary to identify the primary or secondary character of all the deposits that form the stratigraphic record if we

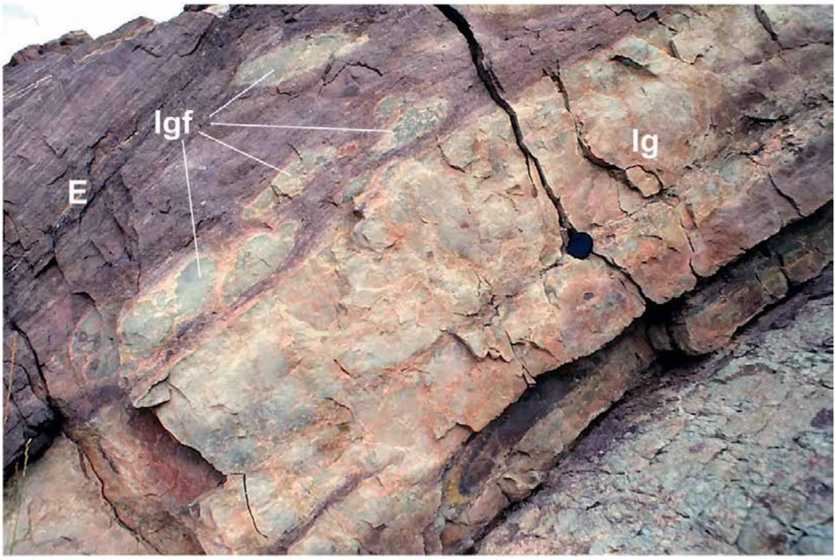

Figure 14.
Field example of an ignimbrite deposit (Ig) eroded by an epiclastic crystal-rich sandstone (E) which incorporates fragments of the ignimbrite (Igf). The lack of a paleosoil separating both deposits is indicative of a short time lapse between the two (credit: Joan Martí).

want to know the evolution of the non-volcanic sedimentation in the basin and the influence of eruptive activity on it. The identification of the syn- and inter-eruptive periods serves to interpret the stratigraphic record in terms of cycles of eruptive activity, which, when combined with the identification of compositional criteria, allows establishing the relationship between sedimentation and magma compositions. In this way, we can observe how variations in the volume and extension of volcanic material supplied by the eruptions to the basin may depend on variations in the degree of explosiveness of magmas, this in turn being related to variations in their chemical composition (and volatile content).

Finally, we should note that the epiclastic processes that act in volcanic terrains do not differ from those that can be found in non-volcanic terrains. However, differences may exist in the resulting deposits due variations in the density of fragments, as a consequence of their variable degrees of vesiculation; this may affect their hydraulic classification and, consequently, the texture and sedimentary structures of the resulting deposits [1, 92]. A common feature of most paleovolcanic sequences is the presence of crystal-rich deposits of a different nature (e.g., [1, 58, 66, 93–95]). The main features that these rocks present can be relatively similar despite their potential diversity of origins (**Figure 9c, d, f**), making it possible that they could be materials of pyroclastic or epiclastic origin or a combination of both. The correct characterization of these crystal-rich deposits, particularly those of epiclastic origins, will permit us to know the influence of volcanism on sedimentation in the basin, its nature, and quite possibly the location of the source areas of the volcaniclastic materials. For example, in the description of many ancient terrains we can find rocks of an ambiguous nature, rich in crystals and with a clay matrix, which are generically called graywackes (e.g., [96, 97]), and which in many cases, among other origins, correspond to volcaniclastic (pyroclastic or epiclastic) deposits. The presence of these deposits in the stratigraphic record remark the importance of volcanism as a source of sediments and offer good samples for radiometric dating because of the minerals (e.g., zircon) they usually contain.

7. Final remarks and future perspectives

In the previous sections, we have briefly outlined some of the main aspects that need to be considered when working in paleovolcanic terrains. Probably, the most important is the fact that volcanic activity has not fundamentally changed over time (uniformitarianism), so that we can confidently assume that the volcanic processes and products that we observe at present are the same as those represented in the geological past. Therefore, their characterization and interpretation may be carried out in the same way. This observation, however, also allows us to consider another important aspect of volcanic activity, which is that, despite the existence of certain broad similarities, each volcanic area may have particular characteristics, which suggest that it should be studied independently. The criteria that must be taken into account when studying an ancient volcanic terrain should be as similar as possible to the ones used in recent volcanic areas. At present, it is not enough to give a good description of the different volcanic or volcano-sedimentary deposits, an essential step in any volcanological study, but they must be interpreted in terms of their volcanological significance and their influence on associated depositional environments. Therefore, the same should be applied to the study of paleovolcanic terrains.

Many paleovolcanic terrains are associated with important mineral deposits (e.g., Kurokos, in Japan [98, 99]; the Pyrite Belt of the Iberian Peninsula [40, 100]). Volcanic areas represent regions with a high thermal flux and the existence of hydrothermal fluids, many of them directly associated with the magmatic source, which means a high possibility for the accumulation of mineralizing elements. Likewise, volcaniclastic materials can constitute important hydrocarbon reservoirs (e.g., [42, 101]). Diagenetic changes of fresh volcanic deposits can reduce their permeability; however, the dissolution of volcaniclastic materials can contrastingly increase permeability and increase reservoir quality. The study of paleovolcanic terrains in terms of modern volcanology may also provide results that are quite helpful in the study of recent terrains with similar characteristics, where such processes may be inferred, yet not observed directly due to the lack of deep erosion and tectonics. Similarly, the exploration of high-enthalpy geothermal reservoirs in active volcanic areas can greatly benefit from the study of ancient analogs coming from deeply eroded volcanic terrains where the roots of the volcanic edifices are well exposed and the geometry and distribution of fossil geothermal reservoirs can be observed (e.g., [102–104]).

Another aspect to highlight in the study of ancient volcanic terrains is that they offer a good source of information to analyze plate tectonic evolution and the formation of sedimentary basins (e.g., [105]). In this sense, we can deduce the geodynamic framework in which the basins develop by studying the nature of the associated volcanism. The reconstruction of the position of eruptive vents will give information on the tectonic structure of the basin, since it will allow us to infer the distribution of the fractures through which the magma ascended to the surface; this will thereby provide clues for the reconstruction of the corresponding stress field. Therefore, the presence of volcanic products in the sedimentary record of a basin should not be necessarily considered as an isolated event. Volcanic activity must be interpreted as an effect with the same causes that condition the existence of some sedimentary basins, although on some occasions it can even become the direct cause that conditions their formation, as is the case of some collapse calderas and volcano-tectonic depressions (e.g., [106, 107]).

Based on what has been exposed in this contribution, I hope that a clear idea can be drawn for the importance of a correct interpretation of the volcanic episodes that we find in the geological record. A good description of the products generated by these volcanic processes is the first step to be able to understand their true meaning. However, the reconstruction of the volcanic episodes, in terms of their geodynamic framework, volcano-tectonic environment, basin dynamics, and eruptive mechanisms, based on a correct identification and interpretation of deposits, should be the main objective that we must consider when beginning a study of paleovolcanic terrains.

Acknowledgements

This research has been partially funded by the Spanish grants MINECO CGL2017-84901-C2 and MICINN PID 2020-114273GB-C21. I warmly thank the scientific editor Karoly Nemeth and the IntexOpen reviewers for their comments, which have contributed to improve the manuscript. English text has been reviewed and revised by Grant George Buffett (www.terranova.barcelona).

Author details

Joan Martí
Geosciences Barcelona, CSIC, Barcelona, Spain

*Address all correspondence to: joanmartimolist@gmail.com

References

[1] Cas RAF, Wright JV. Volcanic Successions. London: Allen & Unwin; 1987. p. 528

[2] Martí J, Groppelli G, Brum da Silveira A. Volcanic stratigraphy: A review. Journal of Volcanology and Geothermal Research. 2018;**357**:68-91. DOI: 10.1016/j.jvolgeores.2018.04.006

[3] Druitt TH. Pyroclastic density currents. Geological Society, London, Special Publication. 2007;**145**(1):145. DOI: 10.1144/GSL.SP.1996.145.01.08

[4] Sulpizio R, Dellino P, Doronzo DM, Sarocchi D. Pyroclastic density currents: State of the art and perspectives. Journal of Volcanology and Geothermal Research. 2014;**283**:36-65. DOI: 10.1016/j.jvolgeores.2014.06.014

[5] Nagasawa K. Chapter 2 weathering of volcanic ash and other pyroclastic materials. Developments in Sedimentology. 1978;**26**:105-125. DOI: 10.1016/S0070-4571(08)70683-6

[6] Fisher RV. Proposed classification of volcaniclastic sediments and rocks. Geological Society of America Bulletin. 1961;**72**:1409-1414

[7] Fisher RV. Rocks composed of volcanic fragments and their classification. Earth-Science Reviews. 1966;**1**:287-298

[8] Fisher RV, Schmincke HU. Pyroclastic Rocks. Berlin: Springer-Verlag; 1984. p. 472

[9] Fisher RV, Smith GA. Volcanism, tectonics and sedimentation, In: Fisher RV, Smith GA, editors. Sedimentation in Volcanic Settings. Broken Arrow, OK, USA: SEPM Special Publication n° 45; 1991. pp. 1-5

[10] Walker RG. editor. Facies Models, 2nd ed. Geological Association of Canada. Geoscience Canada. Repr. Ser. 1. 1984

[11] Walker RG. Facies modelling and sequence stratigraphy. Journal of Sediment Petroleum. 1990;**60**:777-786

[12] Suthren RJ. Facies analysis of volcaniclastic sediments: A review. Geological Society, London, Special Publications. 2007;**18**(1):123. DOI: 10.1144/GSL.SP.1985.018.01.07

[13] Pettijohn FJ. Sedimentary Rocks. 3ª ed. New York: Harper and Row, Publishers; 1975. p. 628

[14] Cas RAF, Busby-Spera C, editors. Volcaniclastic sedimentation, Sediment. Geological, Special Issue. 1991;**74**:362

[15] Cowlyn J, Kennedy BM, Gravley DM, Cronin SJ. A confidence-based assessment method for distinguishing pyroclastic density current deposits from other volcaniclastic units. Frontiers in Earth Science, 30 November 2020, Sec. Volcanology. 2020;**8**. Available from: https://www.frontiersin.org/articles/10.3389/feart.2020.581195. DOI: 10.3389/feart.2020.581195. ISSN: 2296-6463

[16] Sarocchi D, Borselli L, Macías JL. New tools to investigate textures of pyroclastic deposits. Collapse Calderas Workshop IOP Publishing IOP Conf. Series: Earth and Environmental Science. 2008;**3**:012009. DOI: 10.1088/1755-1307/3/1/012009

[17] Branney MJ, Sparks RSJ. Fiamme formed by diagenesis and burial-compaction in soils and subaqueous sediments. Journal of the Geological Society of London. 1990;**147**:919-922

[18] Martí J. Caldera-like structures related to Permo-carboniferous volcanism of the Catalan Pyrenees (NE Spain). Journal of Volcanology and Geothermal Research. 1991;**45**:173-186

[19] Jiang B, Harlow G, Wohletz K, et al. New evidence suggests pyroclastic flows are responsible for the remarkable preservation of the Jehol biota. Nature Communications. 2014;**5**:3151. DOI: 10.1038/ncomms4151

[20] Bell B, Williamson IT. Fossil trees, tree moulds and tree casts in the Palaeocene Mull lava field, NW Scotland: Context, formation and implications for lava emplacement. Earth and Environmental Science Transactions of the Royal Society of Edinburgh. 2017;**107**(1):1-19. DOI: 10.1017/S175569101700007X

[21] Luthardt L, Rößler R, Schneider JW. Palaeoclimatic and site-specific conditions in the early Permian fossil forest of Chemnitz—Sedimentological, geochemical and palaeobotanical evidence. Palaeogeography, Palaeoclimatology, Palaeoecology. 2016;**441**:627-652. DOI: 10.1016/j.palaeo.2015.10.015

[22] Tosal A, Pàmies J, Martín-Closas C. Plant taphonomy and palaeoecology of Pennsylvanian wetlands from the Erill Castell Basin of the eastern Pyrenees, Catalonia, Spain. Palaeogeography, Palaeoclimatology, Palaeoecology. 2022;**605**:111234. DOI: 10.1016/j.palaeo.2022.111234

[23] Fritz WJ, Harrison S. Transported trees from the 1982 Mount St. Helens sediment flows: Their use as paleocurrent indicators. Sedimentary Geology. 1985;**42**:49-64

[24] Wilson CNJ. The Taupo eruption. In: New Zealand II. The Taupo Ignimbrite. Vol. A.314. London: Phil. Trans. R. Soc; 1985. pp. 229-310

[25] Kovács J, Nemeth K, Szabó P, Kocsis L, Kereszturic K, Újvárie G, et al. Volcanism and paleoenvironment of the Pula maar complex: A pliocene terrestrial fossil site in Central Europe (Hungary). Palaeogeography, Palaeoclimatology, Palaeoecology. 2020;**537**:109398. DOI: 10.1016/j.palaeo.2019.109398

[26] Bordy EM, Rampersadh A, Abrahams M, Lockley MG, Head HW. Tracking the Pliensbachian–Toarcian Karoo firewalkers: Trackways of quadruped and biped dinosaurs and mammaliaforms. PLoS One. 2020;**15**(1):e0226847. DOI: 10.1371/journal.pone.0226847

[27] Hall K, Thorn C, Sumner P. On the persistence of 'weathering'. Geomorphology. 2012;**149-150**:1-10. DOI: 10.1016/j.geomorph.2011.12.024

[28] Price DG. Weathering and weathering processes. Quarterly Journal of Engineering Geology and Hydrogeology. 1995;**28**:243-252. DOI: 10.1144/GSL.QJEGH.1995.028.P3.03

[29] Di Figlia MG, Bellanca A, Neri R, Stefansson A. Chemical weathering of volcanic rocks at the island of Pantelleria, Italy: Information from soil profile and soil solution investigations. Chemical Geology. 2007;**246**(1-2):1-18. DOI: 10.1016/j.chemgeo.2007.07.025

[30] Wedekind W, López-Doncel R, Dohrmann R, Kocher M, Siegesmund S. Weathering of volcanic tuff rocks caused by moisture expansion. Environment and Earth Science. 2013;**69**:1203-1224. DOI: 10.1007/s12665-012-2158-1

[31] Pirajno F, Cawood PA. Hydrothermal Processes and Mineral System. Berlin: Springer; 2009. p. 1250

[32] Schwartz GM. Hydrothermal alteration. Economic Geology. 1959;**54**(2):161-183. DOI: 10.2113/gsecongeo.54.2.161

[33] Friedman I, Long W. Volcanic glasses, their origins and alteration processes. Journal of Non-Crystalline Solids. 1984;**67**:127-133

[34] Marshall RR. Devitrification of natural glass. Geological Society of America Bulletin. 1962;**72**(1961):1493-1520. DOI: 10.1130/0016-7606(1961)72[1493:DONG]2.0.CO;2

[35] Perez-Torrado FJ, Martí J, Queralt I, Mangas J. Alteration processes of the Roque Nublo ignimbrites (gran Canaria, Canary Islands). Journal of Volcanology and Geothermal Research. 1995;**65**:191-204

[36] Smith RL. Zones and zonal variations in ash-flows. U.S. Geological Survey Professional Paper. 1960;**354-F**:149-159

[37] Sparks RSJ, Tait SR, Yanev Y. Dense welding caused by volatile resorption. Journal of the Geological Society. 1999;**156**:217-225

[38] McPhie J, Cas RAF. Chapter 49 - volcanic successions associated with ore deposits: Facies characteristics and ore–host relationships. In: The Encyclopedia of Volcanoes (Second Edition). Amsterdam, The Netherlands: Elsevier, Academic Press; 2015. pp. 865-879. DOI: 10.1016/B978-0-12-385938-9.00049-3

[39] Allen R l. False pyroclastic textures in altered silicic lavas, with implications for volcanic associated mineralizations. Economic Geology. 1988;**83**:1424-1446

[40] Soriano C, Martí J. Facies analysis of volcano-sedimentary successions hosting massive sulfide deposits in the Iberian pyrite belt, Spain. Economic Geology. 1999;**94**(6):867-882. DOI: 10.2113/gsecongeo.94.6.867

[41] Richardson SM, McSween HY. Geochemistry: Pathways and Processes. Englewood Cliffs, New Jersey: Prentice-Hall, Inc; 1989. p. 488

[42] Mathisen ME, McPherson JG. Volcaniclastic deposits: Implications for hydrocarbon exploration. In: Fisher RVY, Smith GA, editors. Sedimentation in Volcanic Settings. Broken Arrow, OK, USA: SEPM Special Publication n° 45; 1991. pp. 27-36

[43] Lipman PW. Caldera-collapse breccias in the western San Juan Mountains, Colorado. Geological Society of America Bulletin. 1976;**87**:1397-1410

[44] Smith RL, Bailey RA. Resurgent cauldrons. Geological Society of American Memoris. 1968;**116**:613-662

[45] Hay RL, Ijima A. Nature and origin of palagonite tuffs of the Honolulu group on Oahu, Hawaii. Geological Society of America Memoirs. 1968;**116**:331-376

[46] Jakobsson SP. Envoronmental factors controlling the palgonitization of the Surtsey tephra, Iceland. Bulletin Geology Society Denmark. 1978;**27**:91-105

[47] Jakobsson SP, Moore JG. Hydrothermal minerals and alteration rates at Surtsey volcano, Iceland. Geological Society of America Bulletin. 1986;**97**:648-659

[48] Walton AW. Zeolitic diagenesis in Oligocene volcanic sediments, trans-Pecos, Texas. Geological Society of America Bulletin. 1975;**86**:615-624

[49] Stroncik NA, Schmincke HU. Palagonite – A review. International Journal of Earth Science (Geol Rundsch).

2002;**91**:680-697. DOI: 10.1007/s00531-001-0238-7

[50] Walker GPL. Palagonite Petrology. Encyclopedia of Earth Science. Boston, MA: Springer; 1989. DOI: 10.1007/0-387-30845-8_172

[51] Höskuldsson A, Sparks RSJ. Thermodynamics and fluid dynamics of effusive subglacial eruptions. Bulletin of Volcanology. 1997;**59**:219-230

[52] Spears DA. The origin of tonsteins, an overview, and links with seatearths, fireclays and fragmental clay rocks. International Journal of Coal Geology. 2012;**94**(1):22-31. DOI: 10.1016/j.coal.2011.09.008

[53] Huff W. K-bentonites: A review. American Mineralogist. 2016;**101**(1): 43-70. DOI: 10.2138/am-2016-5339

[54] Soriano C, Martí J, Casas JM. Palinspastic reconstruction of Permo-carboniferous basins involved in alpine deformation: The Erill castell-Estac basin, southern Pyrenees, Spain. Geologie en Mijnbouw. 1996;**75**:33-55

[55] Catuneanu O, Galloway WE, Kendall CGSC, Miall AD, Posamentier HW, Pratt BR, et al. Sequence stratigraphy: Methodology and nomenclature. Newsletters on Stratigraphy. 2011;**44**(3):173-245. DOI: 10.1127/0078-0421/2011/0011

[56] Salvador A, editor. International stratigraphic guide. In: A Guide to Stratigraphic Classification, Terminology, and Procedure. Boulder, CO, USA: The International Union of Geological Sciences and the Geological Society of America; 1994. p. 214

[57] Roche O. Nature and velocity of pyroclastic density currents inferred from models of entrainment of substrate lithic clasts. Earth and Planetary Science Letters. 2015;**418**:115-125

[58] Martí J. Genesis of crystal-rich volcaniclastic facies in the Permian red beds of the Central Pyrenees (NE of Spain). Sedimentary Geology. 1996;**106**:1-19

[59] Hailwood EA. Magnetostratigraphy Geological Society of Special Report. 1989;(19):84. ISSN: 0309-670X

[60] Perroud H, Calza F, Khattach D. Paleomagnetism of the Silurian volcanism at Almaden, southern Spain. Journal of Geophysical Research. 1991;**96**:1949-1962

[61] Nemeth K, Palmer J. Geological mapping of volcanic terrains: Discussion on concepts, facies models, scales, and resolutions from New Zealand perspective. Journal of Volcanology and Geothermal Research. 2019;**385**:27-45. DOI: 10.1016/j.jvolgeores.2018.11.028

[62] Hackett WR, Houghton BF. A facies model for a quaternary andesitic composite volcano: Ruapehu, New Zealand. Bulletin of Volcanology. 1989;**51**:51-68

[63] Smith GG. Sedimentology of proximal to distal volcaniclastics dispersed across an active foldbelt: Ellensburg formation (late Miocene), Central Washington. Sedimentology. 1988;**35**:953-977

[64] Allen SR, Hayward BW, Mathews E. A facies model for a submarine volcaniclastic apron: The Miocene Manukau subgroup, New Zealand. Bulletin of the Geological Society of America. 2007;**119**:725-742

[65] Busby CJ. Large-volume rhyolite ash flow eruptions and submarine caldera collapse in the lower

Mesozoic Sierra Nevada, California. Journal of Geophysical Research. 1984;**89**:8417-8427

[66] Cas RAF. Submarine “crystal-tuffs”: Their origin using a lower Devonian example from southeastern Australia. Geological Magazine. 1983;**120**:471-486

[67] Cas RAF, Wright JV. Subaqueous pyroclastic flows and ignimbrites: An assessment. Bulletin of Volcanology. 1991;**53**:357-380

[68] Schneider JL, Fourquin C. y Picheler, JC. Two examples of subaqueously welded ash-flow tuffs: The Visean of southern Vosges (France) and the upper cretaceous of northern Anatolia (Turkey). Journal of Volcanology and Geothermal Research. 1992;**49**:365-383

[69] Soriano C, Giordano G, Cas RAF, Riggs N, Porreca M. Facies architecture, emplacement mechanisms and eruption style of the submarine andesite El Barronal complex, Cabo de Gata, SE Spain. Journal of Volcanology and Geothermal Research. 2013;**264**:210-222. DOI: 10.1016/j.jvolgeores.2013.07.001

[70] Stix J. Subaqueous, intermediate to silicic-composition explosive volcanism: A review. Earth-Science Reviews. 1991;**31**:21-53

[71] Carey SN, Sigurdsson H. Deep-sea evidence for distribution of tephra from the mixed magma eruption of the Soufrière on St. Vincent 1902: Ash turbidites and air fall. Geology. 1978;**6**:271-274

[72] Carey SN, Sigurdsson H. The Roseau ash: Deep-sea tephra deposits from a major eruption on Dominica, Lesser Antilles arc. Journal of Volcanology and Geothermal Research. 1980;**7**:67-86

[73] Cole RB, Decelles PG. Subaerial to submarine transitions in early Miocene pyroclastic flow deposits, southern San Joaquin basin, California. Geological Society of America Bulletin. 1991;**103**(2):221-235. DOI: 10.1130/0016-7606(1991)103<0221:STSTIE>2.3.CO;2

[74] Sigurdsson H, Sparks RSJ, Carey SN, Huang TC. Volcanogeneic sedimentation in the Lesser Antilles arc. Journal of Geology. 1980;**88**:523-540

[75] Sparks RSJ, Sigurdsson H. y Carey SN. The entrance of pyroclastic flows into the sea, I. oceanographic and geologic evidence from Dominica Lesser Antilles. Journal of Volcanology and Geothermal Research. 1980;**7**:87-96

[76] Busby C. Possible distinguishing characteristics of very Deepwater explosive and effusive silicic volcanism. Geology. 2005;**33**:845-848

[77] White JDL, Smellie JL, Clague DA. Introduction: A deductive outline and topical overview of subaqueous. In: Explosive Volcanism Explosive Subaqueous Volcanism. Washington, DC, USA: AGU, Geophysical Monograph 140; 2003. DOI: 10.1029/140GM01

[78] Willians H, McBirney AR. Volcanology. San Fracisco: Freeman, Cooper & Co.; 1979. p. 397

[79] Saura E, Martí J, Cirés J. Structural reconstruction of volcano-tectonic Permian-carboniferous basins of the Catalan Pyrenees (NE Iberia). Geological Society of America Bulletin. 2022 (under revision)

[80] Alloway BV, Larsen G, Lowe DJ, Shane PAR, Westgate JA. In: Elias SA, editor. Tephrochronology, Encyclopedia of Quaternary Science. Amsterdam, The Netherlands: Elsevier; 2007.

pp. 2869-2869. Available from: https://www.elsevier.com/books/encyclopedia-of-quaternary-science/elias/978-0-444-51919-1

[81] Smith GA. The influence of explosive volcanism on fluvial sedimentation: The Deschutes formation (Neogene) in Central Oregon. Journal of Sedimentary Research. 1987;**57**:614-629

[82] Smith GA. Facies sequences and geometries in continental volcaniclastic sediments. In: Fisher RVY, Smith GA, editors. Sedimentation in Volcanic Settings. Broken Arrow, OK, USA: SEPM Special Publication n° 45; 1991. pp. 109-121

[83] Cloetingh S, Burov E. Lithospheric folding and sedimentary basin evolution: A review and analysis of formation mechanisms. Basin Research. 2011;**23**(3):257-290. DOI: 10.1111/j.1365-2117.2010.00490.x

[84] Gudmundsson A. Rock Fractures in Geological Processes. Cambridge, UK: Cambridge University Press; 2011. DOI: 10.1017/CBO9780511975684

[85] Gautneb H, Gudmundsson A. Effect of local and regional stress fields on sheet emplacement in West Iceland. Journal of Volcanology and Geothermal Research. 1992;**51**:339-356

[86] Gudmundsson A. Infrastructure and mechanics of volcanic systems in Iceland. Journal of Volcanology and Geothermal Research. 1995;**64**:l-22

[87] Holohan EP, Troll VR, Errington M, Donaldson CH, Nicoll GR, Emeleus CH. The Southern Mountains zone, isle of rum, Scotland: Volcanic and sedimentary processes upon an uplifted and subsided magma chamber roof. Geological Magazine. 2009;**146**(3):400-418. DOI: 10.1017/S0016756808005876 Printed in the United Kingdom

[88] Cuitino JI, Scasso RA. Reworked pyroclastic beds in the early Miocene of Patagonia: Reaction in response to high sediment supply during explosive volcanic events. Sedimentary Geology. 2013;**289**:194-209

[89] Kataoka KS, Manville V, Nakajo T, Urabe A. Impacts of explosive volcanism on distal alluvial sedimentation: Examples from the Pliocene–Holocene volcaniclastic successions of Japan. Sedimentary Geology. 2009;**220**:306-331

[90] Rossignol C, Hallot E, Bourquin S, Poujol M, Jolivet M, Pellenard P, et al. Using volcaniclastic rocks to constrain sedimentation ages: To what extent are volcanism and sedimentation synchronous? Sedimentary Geology. 2019;**381**:46-64. DOI: 10.1016/j.sedgeo.2018.12.010

[91] Wilson CJN. Ignimbrite morphology and the effects of erosion: A New Zealand case study. Bulletin of Volcanology. 1991;**53**:635-644

[92] Sohn C, Sohn YK. Distinguishing between primary and secondary volcaniclastic deposits. Scientific Reports. 2019;**9**:12425. DOI: 10.1038/s41598-019-48933-4

[93] Breitkreuz C, Cortesogno L, Gaggero L. Crystal-rich mass flow deposits related to the eruption of a sublacustrine silicic cryptodome (early Permian Collio Basin, Italian Alps). Journal of Volcanology and Geothermal Research. 2002;**114**(3-4):373-390. DOI: 10.1016/S0377-0273(01)00297-9

[94] Repstock A, Breitkreuz C, Lapp M, Schulz B. Voluminous and crystal-rich

igneous rocks of the Permian Wurzen volcanic system, northern Saxony, Germany: Physical volcanology and geochemical characterization. International Journal of Earth Sciences (Geol Rundsch). 2017;**107**:1485-1513. DOI: 10.1007/s00531-017-1554-x

[95] Sohn YK, Son M, Jeong JO, Jeon YM. Eruption and emplacement of a laterally extensive, crystal-rich, and pumice-free ignimbrite (the cretaceous Kusandong tuff, Korea). Sedimentary Geology. 2009;**220**(3-4):190-203. DOI: 10.1016/j.sedgeo.2009.04.020

[96] Kemnitz H. The Lausitz graywackes, Saxo-Thuringia, Germany—Witness to the Cadomian orogeny. Special Paper of the Geological Society of America. 2007;**423**:97-141. DOI: 10.1130/2007.2423(04)

[97] Schärer U, Allègre CJ. Investigation of the Archaean crust by single-grain dating of detrital zircon: A greywacke of the Slave Province, Canada. Canadian Journal of Earth Sciences. 1982;**19**(10):1910-1918. DOI: 10.1139/e82-169

[98] Skinner BJ, editor. The Kuroko and related volcanogenic massive sulfide deposits. Economic Geology Monograph. 1983;**5**:604

[99] Yamada R, Yoshida T. Relationships between Kuroko volcanogenic massive sulfide (VMS) deposits, felsic volcanism, and island arc development in the Northeast Honshu arc, Japan. Mineralium Deposita. 2011;**46**:431-448. DOI: 10.1007/s00126-011-0362-7

[100] Rosa CJP, McPhie J, Relvas JMRS. Type of volcanoes hosting the massive sulfide deposits of the Iberian Pyrite Belt. Journal of Volcanology and Geothermal Research. 2010;**194**:107-126

[101] Klarner S, Klarner O. Identification of paleo-volcanic rocks on seismic. In Updates in Volcanology - A Comprehensive Approach to Volcanological Problems. Intechopen; 2012. DOI: 10.5772/24943

[102] Liotta D, Brogi A, Ruggieri G, Zucchi M. Fossil vs, Active geothermal systems: A field and laboratory method to disclose the relationships between geothermal fluid flow and geological structures at depth. Energies. 2021;**2021**(14):933. DOI: 10.3390/en14040933

[103] Mahwa J, Li D, Ping J, et al. Mapping the spatial distribution of fossil geothermal manifestations and assessment of geothermal potential of the Tangyin rift, southeast of Taihang Mountain in China. Journal of Mountain Science. 2022;**19**:2241-2259. DOI: 10.1007/s11629-022-7329-2

[104] Person M, Banerjee A, Hofstra A, Sweetkind D, Gao Y. Hydrologic models of modern and fossil geothermal systems in the Great Basin: Genetic implications for epithermal Au-Ag and Carlin-type gold deposits. Geosphere. 2008;**4**(5):888-917. DOI: 10.1130/GES00150.1

[105] Stern RJ. The evolution of plate tectonics. Philosophical Transactions of the Royal Society A. 2018;**376**:20170406. DOI: 10.1098/rsta.2017.0406

[106] Aguirre-Díaz GJ, Labarthe-Hernández G, Tristán-González M, Nieto-Obregón J, Gutiérrez-Palomares I. Chapter 4, ignimbrite flare-up and graben calderas of the Sierra Madre occidental, Mexico. In: Gottsmann J, Martí J, editors. Caldera Volcanism: Analysis, Modelling and Response. Developments in Volcanology. Vol. 6. Amsterdam: Elsevier; 2008. pp. 143-180

[107] Branney MJ. Eruption and depositional facies of the Whorneyside tuff formation, English Lake District: An exceptionally large-magnitude phreatoplinian eruption. Geological Society of America Bulletin. 1991;**103**:886-897

Chapter 3

The Ampferer-Type Subduction: A Case of Missing Arc Magmatism

Mohamed A. Abu El-Rus, Ali A. Khudier, Sadeq Hamid and Hassan Abbas

Abstract

Ampferer-type subduction is a term that refers to the foundering of hyper-extended continental or embryonic oceanic basins (i.e., ocean-continent transitions) at passive continental margins. The lithospheric mantle underlying these rift basins is mechanically weaker, less dense, and more fertile than the lithospheric mantle underlying bounded continents. Therefore, orogens resulting from the closure of a narrow, immature extensional system are essentially controlled by mechanical processes without significant thermal and lithologic changes. Self-consistent, spontaneous subduction initiation (SI) due to the density contrast between the lithosphere and the crust of ocean-continent transitions is unlikely to occur. Additional far-field external horizontal forces are generally required for the SI. When the lithosphere subducts, the upper crust or serpentinized mantle and sediments separate from the lower crust, which becomes accreted to the orogen, while the lower crust subducts into the asthenosphere. Subduction of the lower crust, which typically consists of dry lithologies, does not allow significant flux-melting within the mantle wedge, so arc magmatism does not occur. As a result of melting inhibition within the mantle wedge during Ampferer-type subduction zones, the mantle beneath the resulting orogenic belts is fertile and thus has a high potential for magma generation during a subsequent breakup (i.e., magma-rich collapse).

Keywords: A-type subduction, B-type subduction, orogeny, missing arc magmatism, subduction, subduction initiation (SI), ocean-continent transitions (OCT)

1. Introduction

The term "subduction" was first used by Amstutz [1] to describe the original concept of the downward thrusting of oceanic lithosphere beneath a continental or oceanic upper plate bounded by a Wadati-Benioff zone of earthquake foci [2, 3]. This process is essential for maintaining Earth's surface constant as new oceanic lithosphere (crust and upper mantle) is formed at mid-ocean ridges, and older lithosphere is destroyed at convergent plate boundaries. With application to the various mechanisms of lithospheric convergence, foundering, and recycling, the term subduction has become broader over time and has lost some of its original meaning. It now refers to a series of processes in which material from the Earth's uppermost layer is submerged into the asthenospheric mantle, and its chemical constituents are recycled back into the Earth's interior. Regardless of submerging Earth's lithosphere process into the convective asthenosphere, two categories of subduction zones on the modern Earth (ca, 1 Ga, [4]) can be distinguished based on the association of magmatism: (a) The subduction zones associated with volcanism and (b) subduction zones missing arc-volcanicity.

The subduction zones associated with giant volcanism are referred to as Benioff-type (or B-type or Pacific-type) subduction, which is characterized by the spontaneous initiation of giant oceanic lithosphere foundering, previously formed at a mid-ocean ridge into the convective upper mantle beneath oceanic or continental upper plates [5–8]. While at the ocean-ocean convergence boundary, the older and colder plate (i.e., the denser plate) often subducts the younger and warmer oceanic plate, at the ocean-continental convergence boundary, the oceanic plate subducts beneath the less dense continental plate. Although the density contrast between the oceanic lithosphere and the asthenosphere may be a possible driving force for the initiation of subduction, it is considered a second order of importance compared to convective currents in the asthenosphere that exert drag forces on the base of the lithosphere [9, 10]. However, the negative buoyancy of the sinking lithosphere (which is denser than the underlying asthenosphere) results in slab pulls, which are thought to be the dominant driving forces of plate motions [6, 11–13]. One or two planar zone(s) of seismicity in the down-going slab (the Wadati-Benioff plane) [3, 14] can reach the mantle transition depth of ~660 km [15]. In addition, heating of the subducting crust releases a significant volume of water from the hydrated lithologies of the subducting material, leading to the fluid-flux melting within the overlying mantle wedge and the generation of hydrous, near-continuous arc magmatism [4, 8, 15–19]. The generated magma is lighter than the surrounding mantle material and rises through the mantle and overlying crust [20]. It creates a chain of volcanic islands on the ocean floor known as an island arc at ocean-ocean convergence margins, or it forms a mountain chain with many volcanoes known as a volcanic arc at ocean-continental convergence margins. The hydrous, calcareous magmatism with low FeO content "calc-alkaline" is predominant in the magmatic arcs [21–24]. A deep trench usually forms parallel to the convergence boundary as the crust sinks downward. More volcanic material and sedimentary rocks accumulate around the island arcs, eventually thrust into an accretionary wedge and onto the continental plate [15]. As a result, high-pressure, low-temperature metamorphic facies series are common at these convergent boundaries [25–27].

The term Ampferer-type subduction was first used to describe the "missing" continental crust in the Alpine orogen (European Alps) [28]. The term was recently revived considering a new understanding of hyper-extended basins and passive margins by [7, 8, 29], who interpreted the mechanism of lithospheric recycling in the Pyrenees and Western and Central Alps. The Ampferer-type (or A-type) subduction occurs when a continent or large island collides with another continent by subducting hyperextended continental basins that contain minor oceanic crust formed at rift margins [7, 8, 20]. These hyper-thinned basins and their mechanically weak serpentinized mantle beneath serve as focal points for initiating convergence and down-thrusting of these basins beneath passive margins [7, 20, 30–32]. Only the dry root lithosphere is subducting, while hydrated lithologies from the descending plate (hydrated mantle rocks and sedimentary deposits) are sequentially accreted into a nascent orogenic wedge, resulting in amagmatic closure associated with tremendous deformation of preexisting continental rocks, forcing the material upward, creating high mountains [7, 32–34].

Since the advent of plate tectonic theory in the 1960s, which assumes that subduction of the oceanic lithosphere primarily controls rigid plate motions [35, 36], alternative concepts for the lithosphere's foundering process have been neglected [7, 8, 20, 37]. Many convergent boundaries that exhibit Ampferer-type subduction features could have been considered Benioff-type subduction in the strict sense. Therefore, this chapter presents the well-known cases of Ampferer-type subduction zones and addresses the challenging questions of when, where, and how subduction initiation (SI) occurs at/around passive margins and the reasons for missing arc magmatism along these margins.

2. The Ampferer-type subduction: convergence and assembly of the previously rifted lithosphere

Ampferer-type subduction occurs only at passive continental margins that hyper-extend into rift basins, often accompanied by exhumation of the (subcontinental) mantle and may reach the stage of (magma-poor) embryonic oceans [7]. Such an embryonic basin-margin system is likely to be more laterally homogeneous than ocean basins, which contain significant spreading ridges. Under these conditions, the mechanical weakness of the serpentinized mantle and the hyper-thinned continental lithosphere serve as focal points for the initiation of convergence and downward thrusting of these basins beneath passive continental boundaries [7, 30–32]. The main features for recognizing Ampferer-type subductions are (i) coherent structural units or nappes (flake tectonics) transported over long distances modified by moderate deformation and comprising the (ultra-) high-pressure continental and oceanic fragments and (ii) the lack of Penrose-type oceanic crustal fragments [7, 38]. The Ampferer-type subductions instead comprise fragments of basins flooded by exhumed subcontinental mantle, like the magma-poor Iberia-Newfoundland ocean-continent transition zones (OCTs) [39–41].

3. Architecture and embryonic oceans and hyperextend rift basins

Although the Wilson cycle is often used to describe the continental collision zones as formed by the closure of broad oceans floored with Penrose-type crust [42], there are numerous orogenic belts (e.g., Pyrenees, Alps, and European Variscides) having conjugate precollisional margins separated by immature extensional zones (i.e., narrow oceans or hyperextended continental rift basins) [7, 29, 34, 43, 44]. Immature extension systems are rift systems that begin when the continental crust has been stretched to complete embrittlement, typically at a crustal stretching factor of about 3–4 [45], and whose development stopped before or with the initiation of seafloor spreading [43, 44, 46, 47] (**Figure 1**). These rift systems involve thinning continental crust to the exhumation of the subcontinental lithospheric mantle at the floor of rift basins [43, 44, 46, 47]. In these basins, the entire remaining crust and the uppermost part of the subcontinental mantle are subject to intense hydrothermal circulation that forms sericite and illite in the crustal rocks [48–50] and serpentine, chlorite, and talc up to 4–6 km deep in the lithospheric mantle [51–54]. The hyperextension of the continents can also lead to decompression melting of the underlying asthenospheric mantle [55], commonly without the formation of mid-ocean ridge basalt (MORB)-type melts, or they are only partially extracted and tend to stagnate in and

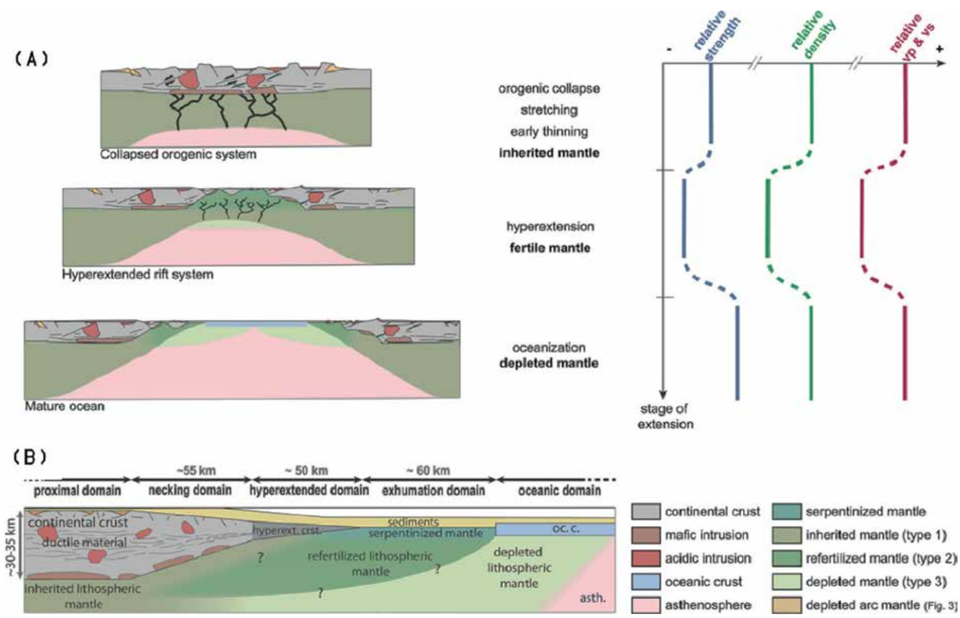

Figure 1.
(a) Various stages of extension and corresponding physical properties of the lithospheric mantle at the center of the rift. (b) Architecture and lithology of a typical magma-poor rifted margin [44].

fertilize the overlying lithospheric mantle [56]. This process tends to homogenize (on a large scale) the uppermost lithospheric mantle (~30 km) beneath the rift basins into plagioclase-bearing lherzolite [41, 56]. However, growing evidence suggests that fertilization of the lithospheric mantle beneath the rift basins is uneven and gradually increases from the proximal to the unstretched continental part to an ideal homogeneous plagioclase-bearing peridotite beneath the distal part of the rift basin [41].

The fertilized mantle under immature oceanic basins, such as beneath the southern part of the Porcupine Basin [57] or at hyperextended rifted margins such as the Iberian margin [58], the Newfoundland margin [59], and the Flemish Cap [60], is also characterized by a reduction in seismic velocities of about 1% at pressures up to 1 GPa and by >2% at higher pressures [44]. Although serpentinization is likely the main cause of the velocity decreases up to 6 km below the seafloor, it may not be responsible for reducing the seismic velocity at greater depths as the serpentine becomes unstable [44]. However, the presence of plagioclase in the fertilized mantle strongly affects the rheology of the lithospheric mantle because plagioclase is weaker than pyroxene and olivine [44]. As a result, the fertilized mantle behaves semi-brittle (i.e., the plagioclase stability field) between 18 and 40 km below the embryonic oceans and hyperextended rift basin. This mantle domain, where deformation can be accommodated along localized anastomosing shear zones, is broader than in the lithospheric mantle beneath the bounded continental margins and could have significance as a stress guide for subduction initiation of rift basins beneath passive continental margins at greater depths up to 30 km [44].

The absence of significant subduction-related magmatism in orogens formed from Ampferer-type subduction zones is interpreted because of the narrow width of the closing ocean, which did not allow significant decompression and/or flux melting [61, 62]. Therefore, the mantle beneath orogens resulting from the closure

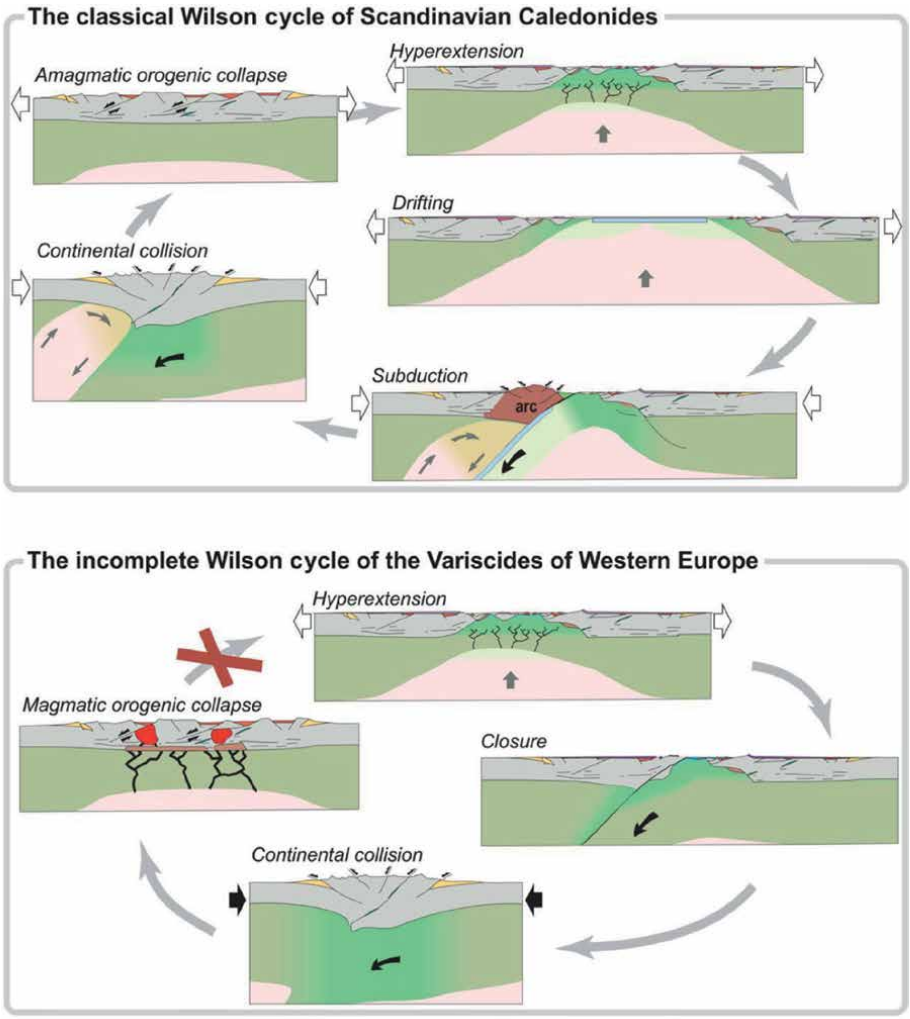

Figure 2.
Two end-members proposed for the Wilson cycle in the North Atlantic as it is resulting from the closure of both broad, mature oceans (the Scandinavian Caledonites), and narrow oceans (<500 km) or immature, hyperextended rift systems (the Variscides of Western Europe) [44].

of a hyperextended rift basin or narrow embryonic ocean is likely fertile because it is hydrated and enriched in mobile constituents derived from subducting sediments, oceanic crust, and dehydrating serpentinite but lacks significant flux melting [63]. This fertile mantle could provide fusible components for intense magmatism during subsequent collapse (magma-rich orogenic collapse [43, 44]. This is shown in the widespread mafic to acidic intrusions, for instance in the crust in the Variscan region, Basin and Range province, and Canadian Cordillera [64–67]. Conversely, orogenic belts formed by the closure of a large ocean are associated with intense flux melting within the mantle wedge due to the release of substantial fluids from dehydration of the large, subducted slab and decompression melting of the hot asthenosphere that rises to compensate for the down dragged mantle wedge material by the slab [68–70]. These melting processes form island arcs at the sea-flower or volcanic arcs at the continental margin [71] and deplete the source mantle wedge

[72]. Orogens formed by the closure of a large ocean may therefore be underlain by a relatively depleted mantle [43]. Therefore, the subsequent collapse of these orogenic belts is devoid of magma (magma-poor collapse). The Western Europe-North Atlantic region is an ideal example to examine how shortening or incomplete Wilson cycles may differ from classic Wilson cycles, as it consists of orogens resulting from the closure of both narrow oceans (< 500 km) or immature, hyperextended rift systems (the Variscides of Western Europe) and broad, mature oceans (the Scandinavian Caledonides) (**Figure 2**) [44, 73].

4. Subduction zone initiation (SZI)

Two concepts are commonly proposed for subduction zone initiation (SZI): (i) spontaneous or vertically forced and (ii) induced or horizontally forced SZI [74–76]. Vertically forced SZI is caused by the contrast between the underlying convicting mantle and the cooling lithosphere above. The viability of this scenario is controversial [77], especially for SZI at passive margins [78]. The body force resulting from density differences is most likely insufficient to break up and initiate a subduction zone if the rift basin lithosphere is older than 20 My after the continental breakup [79]. This assumption is not consistent with the ages of descending, hyperextended continental basins, which are generally older than 20 My (e.g., ~34 My for Oligocene subduction of the New Caledonia Basin beneath the northern Norfolk Ridge, SE Pacific; [20] and ~ 60–65 My for initiation of subduction of Piemonte-Liguria Ocean beneath the Adriatic continental margin, [78]. Moreover, data from recent and ancient subduction zones [76, 80] suggest that vertically forced SZI was probably not the dominant scenario during the last 100 million years. Therefore, the horizontally forced SZI model is preferred to overcome the increasing strength of the cooling lithosphere [76, 78, 81]. The far-field external horizontal forces can be caused by the mid-ocean ridge, mantle plume, neighboring sinking slab, and large-scale mantle convection [82]. However, [83] argues that vertical forces can accelerate, propagate, and facilitate the development of self-sustaining subduction zones that are initially dominated by horizontal forces.

It is most likely that the initiation of subduction zones by horizontal compressive forces requires a process that mechanically weakens or softens the lithosphere to aid in the localization stresses that eventually lead to the breakup [20]. Several mechanisms have been proposed for softening the lithosphere during SZI including mineral reaction and transformation [84], fluid-induced [20, 85, 86], microstructural evolution and anisotropy [87], mineral grain damage and plunging [88, 89], and thermal softening [78, 90, 91]. Petrological thermomechanical models show that a temperature increase of only ca. 50°C is sufficient for successful SZI [78, 92]. Therefore, thermal softening is considered a potential mechanism to form a shear zone transecting the lithosphere [90, 93–97] and initiate subduction at a hyperextended continental [78]. Serpentinization within the lithosphere may also serve as a stress conductor during subduction initiation because it is weaker than peridotite, continental crust, and oceanic crust [98–100]. In addition, greater serpentinization would reduce the coherence of the rift basin lithosphere [7], which generally exhibits shallow slab detachment (SD) early after the SZI [78]. In contrast, the low-serpentinized lithosphere is coherent and requires more compressional forces for SZI [79, 101]. The strong lithosphere may be able to maintain a continuous subducting slab down to 660 km depth for more than 20 Myr after basin closure [78].

5. Missing arc magmatism

Well-documented examples of subduction initiation involving mature oceanic lithosphere (Benioff-type subduction zones, e.g., the Neotethys supra subduction zone and the Izu-Bonin-Mariana arc) are characterized by an initial phase of upper plate extension and tholeiitic to boninitic magmatism [102, 103]. Once initiated, partial eclogitization and densification of the subducting oceanic lithosphere results in a slab-pull mechanism that is a driving force for self-sustaining subduction and ocean closure [6]. Dehydration of oceanic crust drives flux melting of the overlying mantle wedge and lower crust of the overriding plate, resulting in predominantly "calc-alkaline" magmatism [104–108]. Therefore, the presence of ophiolites associated with calc-alkaline magmatism and low-temperature, high-pressure metamorphic rocks are interpreted as unequivocal evidence for paleosubduction zones [109]. In contrast, subduction zones with the immature oceanic lithosphere (Ampferer-type subduction zones, e.g., the European Variscides, Pyrenean Belt, and Alpine Mountains) are characterized by ophiolites, subduction-related metamorphism, accretionary prisms, and syn-orogenic clastic sediments but and lacking calc-alkaline magmatism [7, 8, 20, 29]. Although the absence of calc-alkaline magmatism within the Ampferer-type subduction zone is commonly attributed to the narrow width of the closing ocean (<500 km), which did not allow for significant decompression and/or flux melting and thus habitable arc magmatism [61, 62], a recent study of a case of Ampferer-type subduction zones beneath New Caledonia in the Oligocene revealed that other causes of missing arc magmatism are also relevant [20]. The Oligocene subduction zone beneath New Caledonia is an ideal Ampferian-type paradigm for investigating the reason for missing the arc magmatism associated with Ampferian-type subduction zones because its paleogeographic elements have not been jumbled together by collisional deformation or dismembered by strike-slip faulting. In addition, the well-documented evolutionary history of New Caledonia and its relative tectonic simplicity is appropriate for specifying the operational processes within the Oligocene Ampferer-type subduction zone [20].

The New Caledonia Island is a remnant of Gondwana continental crust that is part of the Norfolk Ridge (**Figure 3**), which began to drift away from the eastern Australian margin during the opening of the Tasman Sea in the Late Cretaceous [110–112]. Norfolk Ridge is a suitable location for commencing Ampferer-type subduction due to the hyperextension of the east border of the Australian continent, which curtailment in tiny slivers in this region [20, 112]. The magmatism associated with the Oligocene subduction zone is rare and represented by in situ minor eruptive basalt-andesite lava flows of La Conception (c. 29.12 My Ar/Ar age, [20]) and two small isolated Oligocene granodiorite massifs (c. 24 My [113]) that are not far from the La Conception lavas: the Saint Louis Massif, located about 2 km to the east, and the Koum/Borindi Massif, located ~55 km to the northeast (**Figure 3**). Thus, the correlation of La Conception lava with Saint Louis and Koum/Borindi Massifs is of great importance for studying the cross-geochemical trend associated with the Ampferer subduction zone, which is critical for understanding the dynamics of the mantle wedge, including how it convects, where and how much melting occurs, how much melt extraction affects source heterogeneity, and how non-subduction heterogeneity affects arc lavas. However, a recent study of the Oligocene subduction zones beneath New Caledonia [20] revealed the following reasons that may result in missing the arc magmatism in association with Ampferer-type subduction zones:

5.1 Cold subduction zone

The opening of the New Caledonian Basin occurred during the rifting of the eastern margin of the Australian-Gondwanan continent in the Late Cretaceous time [114, 115]. This implies that the crust of the New Caledonian Basin was about 34 Ma old (i.e., cold crust) [79–108] at the time of its subduction beneath the northern Norfolk Ridge in the early Oligocene (ca. 32 Ma) [116]. The mantle wedge overlying the descending plate was also cold. Its potential temperature (Tp °C), estimated from the composition of the La Conception lava, ranges from 1268 to 1316°C [20]. This estimate is below the potential temperatures of the ambient mantle (i.e., ~1400°C) [117] and below the 1350°C required for arc basalt magma formation within the mantle wedge [118]. In addition, trace element modeling of the La Conception lavas suggests that the melting source was 119–129 km within the mantle wedge [20]. These constraints are consistent with cold subduction zones, where large amounts of water can be transported in the gabbro and peridotite layers of the subducted slabs to depths greater than 200 km, where it hydrates and partially melting the mantle wedge, in contrast to warm subduction zones, where the entire subducted slab becomes anhydrous at shallow to intermediate depths and the mantle wedge only at shallow depths [119, 120].

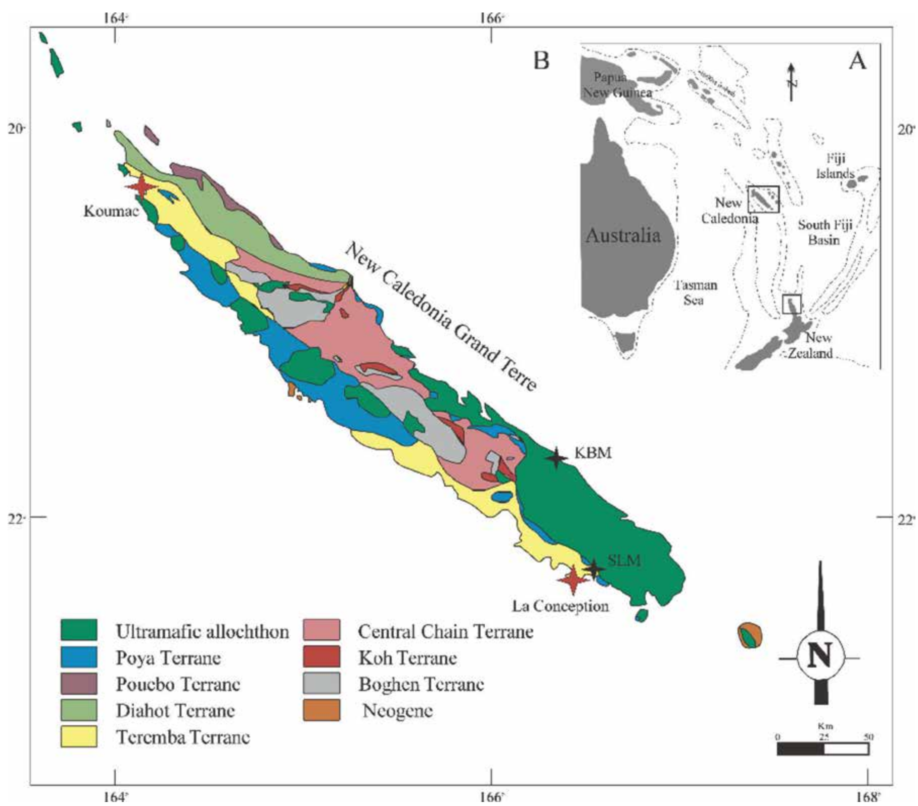

Figure 3.
The generalized geology map of New Caledonia shows the locations of all eight terranes. Red stars show locations of Oligocene magmatism (La conception lava quarry, the Saint Louis Massif [SLM], and the Koum/Borindi Massif [KBM]) [20].

5.2 The high sinking velocity of the subducted slab

Given that the emplacement of the La Conception lavas occurred around 29.12 Ma and that the Oligocene subduction zone began at approximately 33.7–35 Ma at a location about 50 km west of New Caledonia (as indicated by a + 100 mGal gravity anomaly, [121, 122], the sinking velocity of the subducted slab to depth ~119–129 km within the mantle wedge where the La Conception lavas generated [20] ranges from 4.0 to 5.1 cm/year. Such a rapid sinking velocity, combined with the cold nature of the subducting slab, may not allow enough interaction between the sinking slab and the mantle wedge to produce significant volumes of arc magmas [123, 124].

5.3 The depletion inheritance of the mantle beneath the continental border

The depletion heritage of the mantle beneath the continental border considering that Nb and Ta are least effectively transferred from the subducted oceanic slab to the overlying mantle melting column, the ratio of elements to Nb (or Ta) would measure the non-conservative character of the elements (% sz), which expresses the extent of their displacement from the average MORB at a given Nb [125]. Calculations of % sz for the elements in La Conception show that Rb, Pb, Th, Ba, U, K, and Pb are strongly non-conservative with % sz > 80%; LREE, Sr., and P_2O_5 are moderately non-conservative with a % sz range of 80–40%; Sm and Nd are non-conservative to slightly non-conservative with % sz from 40% to the detection limit, whereas other elements exhibited negative % sz values (**Figure 4**) [20]. The negative % sz values suggest that the mantle beneath the Norfolk Ridge was relatively depleted before the onset of the Oligocene subduction zone, which may partially inhibit the arc magmatism.

5.4 The continental nature of the subducting slab

The nature of the New Caledonian Basin itself may also play a significant role in reducing arc volcanism because the New Caledonian Basin is a continental crust that is commonly dominated by dry granitic material [126, 127]. Furthermore, unlike the oceanic lithosphere, the lithospheric mantle underlying continental crust does not contain voluminous hydrous mineral phases [7, 29]. Therefore, the sinking slab of the New Caledonian Basin beneath the Norfolk Ridge did not provide the hydrous fluids necessary to lower the solidus of the mantle wedge and produce the arc volcanism associated with the Oligocene subduction zone [20].

5.5 Formation of a magmatic barrier at the base of the overriding plate

Seismic tomography shows evidence of a deep reflector at a depth of 60 km (~18 kbar) beneath the west coast of New Caledonia, and this structure was found to dip northward by at least 30° [115]. This deep seismic discontinuity was attributed to a remnant of a sinking slab of a subduction zone that formed in response to the blocking of an older subduction east of the Norfolk Ridge in the early Oligocene (ca. 32 My) [116]. However, this depth estimate for the subducted slab is not consistent with the fractionated REE and high Sr/Y content of the La Conception lava [20], suggesting the presence of residual garnet in the melting source (i.e., melting within the garnet stability field >25 kbar) [128]. Therefore, we believe that the seismic mirror beneath New Caledonia is the solidification front of accumulated mantle-derived melts at the base of the overriding plate. The incipient melt slowly

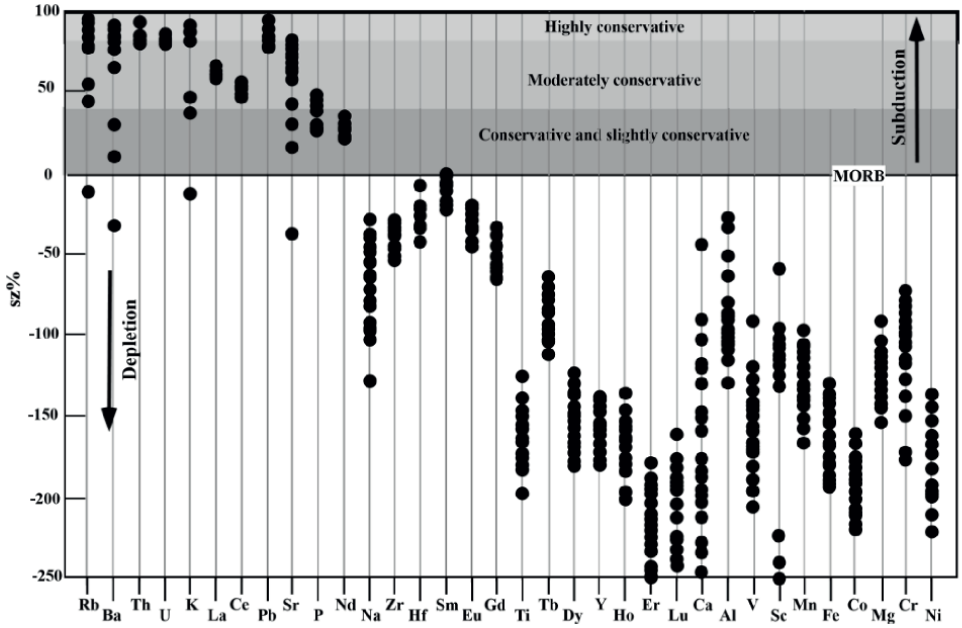

Figure 4.
The percentage of the subduction component (%sz) of the La Conception lavas is estimated from the displacement of the average mid-oceanic-ridge basalt (MORB) at a given Nb [20].

percolates upward (i.e., porous flow), mainly in a vertical direction due to the buoyancy of magma and the high permeability of partially molten systems [129, 130], and eventually, it enters the cooler lithosphere where it begins to solidify [131]. This would cause of the development of a low-permeability zone or permeability barrier [131, 132], under which the subsequent pluses of magma accumulate, forming a melt-rich zone [133–135].

6. Examples of Orogenic belts resulting from Ampherer-subduction zones

Ideal examples of orogens resulting from the closure of a hyperextended rift system or an immature ocean include the Alps [34], Pyrenees [136, 137], and European Variscides [138, 139]. These orogens often occurred without significant subduction-related magmatic activity, so the original rock units before the collision were relatively well preserved [34, 43, 44, 137, 140].

6.1 Closure of the Piemonte-Liguria Ocean and Alpine orogeny

The Alpine orogen, upon subduction initiation at ~85–100 Ma [30, 141, 142], shows no evidence of magmatic activity during subduction initiation combined with a ~ 50 Ma hiatus in magmatism, or "arc gap" [29]. The orogen contains fragments of the Piemont-Liguria Ocean, which was not a Penrose-type oceanic crust. The Piemont-Liguria Ocean was formed in the Jurassic period when the paleocontinents Laurasia (to the north, with Europe) and Gondwana (to the south, with Africa) started to move away from each other [143]. The Piemont-Liguria Ocean contained several continental blocks such as the Adriatic plate (also known as the Apulian Plate) and Sesia-Dent Blanche unit separated from Gondwana and Briançonnais block separated from Laurasia (**Figure 5**). The Gondwanan continental block Adriatic plate was moving northward into Laurasia. In the Cretaceous period, the Piemont-Liguria Ocean lay between Europe (and a smaller plate called the Iberian plate) in the northwest and the Adriatic plate in the southeast. The European and Adriatic passive margins were likely hyperextended, while the Piemonte-Liguria ocean basin was mainly floored by an exhumed mantle and hyperextended continental crust rather than mature oceanic crust (e.g., [7, 34, 78, 144]. At ca. 85–80 Ma, subduction at the Adriatic margin led to subduction of the Sesia-Dent Blanche unit [145], and progressed from southeast to northwest across the PL Ocean (ca. 50–45 My), the Briançonnais (ca. 45–42 My), and the Valais Basin (ca. 42–35 My) as indicated by the tectono-metamorphic evolution of those units (**Figure 5** [142, 145–148]. However, the onset of subduction initiation at the passive margins of Laurasia allowed the accretion of the hydrated portion of the subducting of the remaining Piemont-Liguria Ocean plate within an orogenic Alpine wedge (**Figure 5**) [29]. It is unclear whether the subducted slab is currently separated or remains attached to the European plate (**Figure 5**) [149].

6.2 Iberian plate kinematics and Pyrenees orogeny

The Pyrenean orogeny in southwestern Europe is an ~E-W trending mountain belt, about 450 km long and 125 km wide (**Figure 6**) that formed in the Late Cretaceous to Paleogene in response to convergence between the hyperextension NE continental margins of the Iberian Microplate and the Southwest Eurasian Plate [150]. The Iberia microplate was part of Pangea in the Paleozoic [151] but separated in the Late Jurassic [152–154]. Based on magnetic lineation in the Atlantic Ocean and Bay of Biscay to the west, the separation of the Iberian Microplate was N-S directional rifting before it rotated counterclockwise early Aptian (e.g., Scissor-type opening) (**Figure 7**) [155–158]. Analysis of the paleomagnetic record suggests a ~ 35° counterclockwise rotation of the Iberia microplate completed in the early Aptian (126 ~ 118 My) [150]. Such a high amount of rotation should be associated with subduction beneath the Eurasian margin [150, 157, 158] and the North Pyrenean fault zone represents the suture between Iberia and southwest Eurasia (**Figure 6**) [150]. Structural and deep seismic studies have shown that the orogen is asymmetric, with the Iberian continental lithosphere underthrust at least ~80 km beneath Europe [159, 160]. However, several tomographic studies show no evidence of a subducted slab anywhere beneath the Pyrenees [161–163], ruling out the opening of a broad oceanic basin prior to Late Cretaceous convergence [161]. Vissers et al. [150] explained the absence of a remnant subducted slab by the motion of Iberia/Eurasia relative to the mantle, where the Pyrenean region may have laterally displaced from a subducting slab remnant after slab break-off. Mantle tomography indicates that such a slab remnant may exist today between 1900 and 1500 km depth beneath southern Algeria [150].

6.3 Closure of the Paleozoic Rheic ocean and Variscan orogeny

The Variscan Belt is a segment of a mountain system that has existed all around the world because of a sequence of Paleozoic collisional orogenic events (e.g., the Appalachians in America, Mauritanides in Africa, the Caledonides in Scandinavia

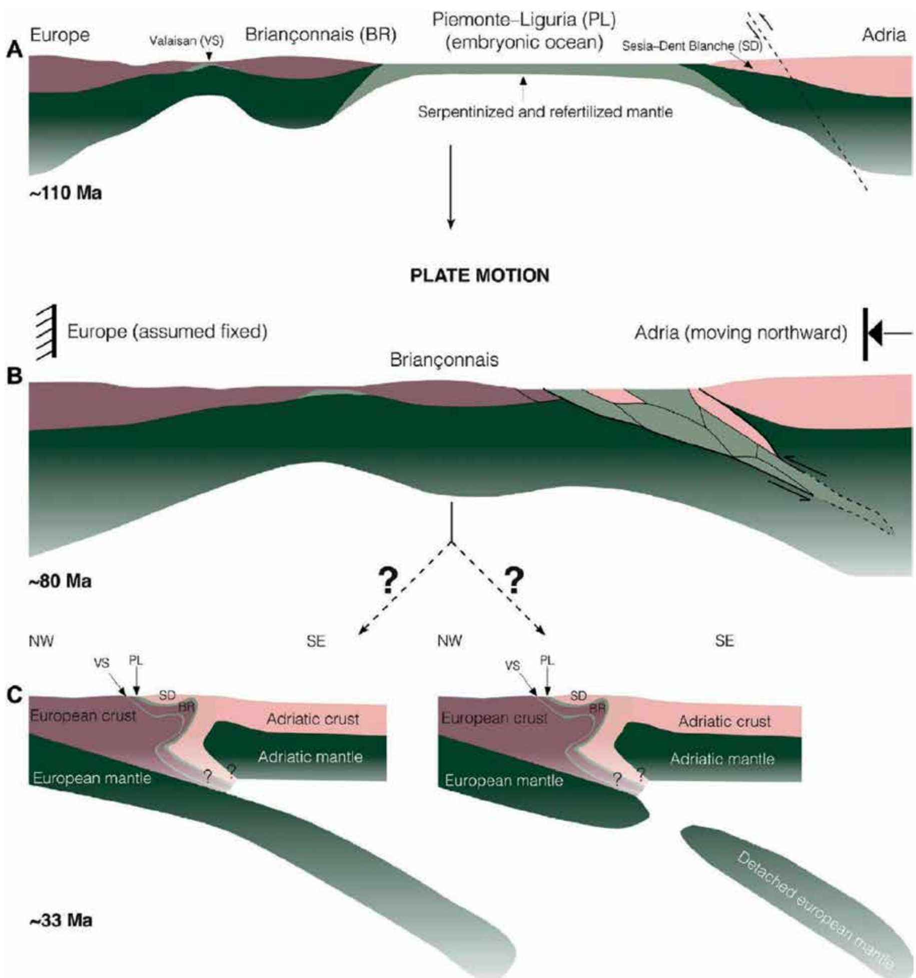

Figure 5.
Simplified conceptual geodynamic sketch of the Alpine orogeny after Candioti et al. [78]. (a) Passive margin geometry and embryonic oceans after the rifting phase. (b) Horizontally forced SZI on the Adriatic passive margin and subduction of the Sesia-Dent Blanche unit. (c) Possible scenarios for the collisional phase of Alpine orogeny with a slab that is continually subducting (left) or a slab that is separated (right).

and Scotland, the Urals in Russia, the Tien Shan in Asia, and the Lachlan Fold Belt in Australia) that marked the amalgamation of the supercontinent Pangea [138, 139] (**Figure 8**). The Variscan belt extends across Europe, with the best exposure in central and western Europe and parts of Morocco and Algeria to the north of the West African Craton [138, 165]. It formed between 480 and 250 My after the collision of Gondwana to the south and Baltica-Laurentia to the north [164, 166–167]. The Variscan belt is a much more complex paleogeographic orogenic belt whose elements were not only shuffled together by collisional deformation but were also dismembered by strike-slip faults and the formation of oroclines [167]. Reviewing the evolution of the main tectonic units and their paleogeography position within the Variscan is beyond the scope of our work, and the reader may refer to [138, 167–169] for further details. However, the presence of suture zones characterized by ophiolites, subduction-related metamorphism and magmatism, accretionary prisms, and foreland basins with syn-orogenic clastic sediments within the

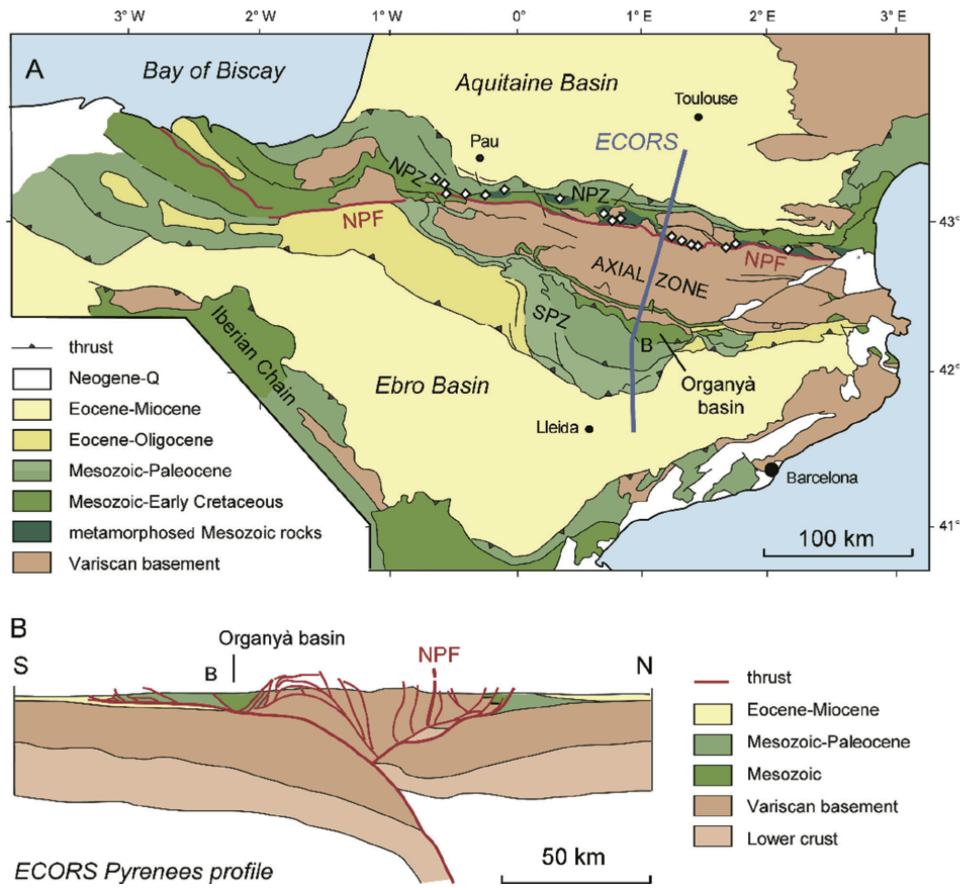

Figure 6.
(a) Geological sketch map of the Pyrenees [150]. Blue line indicates ECORS seismic section shown in (b). White diamonds denote mantle peridotite bodies. NPZ, North Pyrenean Zone; NPF, North Pyrenean Fault; SPZ, Southern Pyrenean Zone; B, Boixols thrust. (b) ECORS crustal-scale cross-section Pyrenees [150].

European Variscides confirms the existence of several microcontinents between Laurussia and Gondwana. These microcontinents include the blocks of Avalonia, North Armorica (Franconia + Thuringia, separated by the failed Vesser Rift), and South Armorica (southwestern central Iberia, north-central Armorican Massif, Bohemia, all probably united, and Paleo-Adria) (**Figure 9**) [138, 139, 166, 167, 170, 171]. Several authors [138, 170, 171] have proposed that the Variscan microcontinents separated from the north-Gondwana margin by back-arc spreading and southward subduction. Although this model may apply to the Avalonia microcontinent and the opening of the Rheic Ocean, it cannot explain the existence of other microcontinents and intervening rift/drift zones during the Cambrian and Ordovician [167]. Alternatively, a system of mantle plume activity beneath the North Gondwanan margin has been hypothesized to result in the opening of the Rheic and other peri-Gondwanan oceans [172–174]. Only the Rheic (between Avalonia and the Armorican microcontinents) evolved into a sizeable ocean documented by biogeography and paleomagnetism [167]. The other basins (i.e., the Saxo-Thuringian Ocean between north and South Armorica and the Galicia-Moldanubian Ocean between South Armorica and Palaeo-Adria) did not grow beyond the narrow ocean stage and did not pass through the complete Wilson Cycles [167]. Closure of the narrow oceans and their subduction

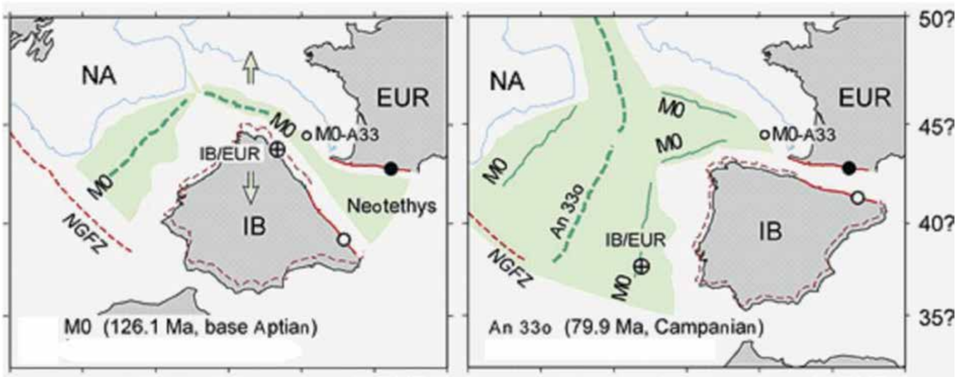

Figure 7.
Scissor-type scenario [159], for the plate kinematic of the Late Mesozoic motion of the Iberian Peninsula to Europe, with the inferred position of the Iberian Peninsula at M0 times (left panel) and the onset of the Alpine collision (right panel). NA, North America; IB, Iberia; EUR, Europe; NGFZ, Newfoundland-Gibraltar Fracture Zone. Circles with crosses denote the poles of the overall reconstruction. Circles labeled M0-A33 denote the poles of the phase describing the opening of the Bay of Biscay.

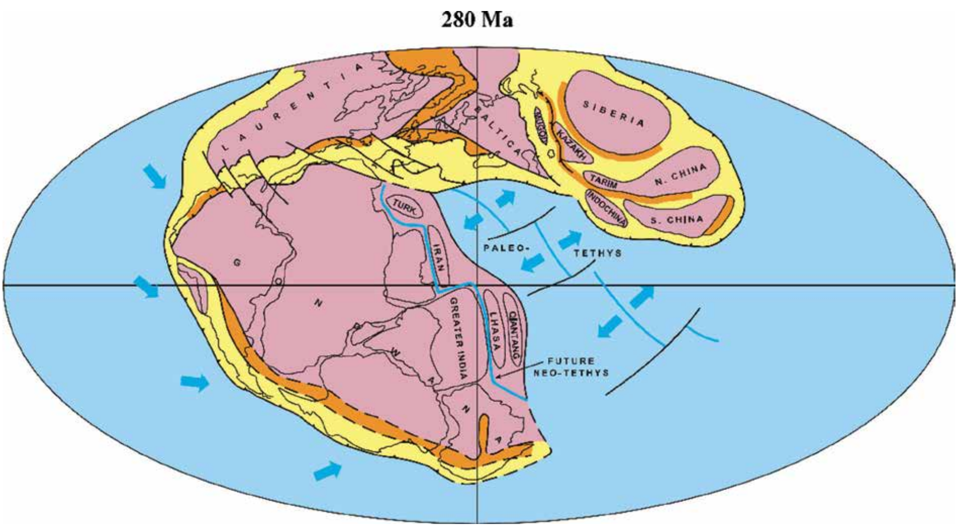

Figure 8.
Permian (at 280 Ma) assembly of the continents showing the Paleozoic belts. Yellow, 400 ± 250 Ma; orange, 450 ± 400 Ma [164].

beneath microcontinents in order from south to north, between the middle Devonian and the Tournaisian gave birth to orogenic belts with HP-UHP metamorphism with missing arc magmatism (i.e., Ampferer-type subduction).

7. Conclusions

Orogenic and post-orogenic magmatism is primarily controlled by the size and maturity of the basin/oceanic crust involved in the subduction zones. Orogenic belts formed from the closure of narrow oceans or hyperextended rift basins (Ampferer-type subduction) are characterized by the absence of arc magmatism

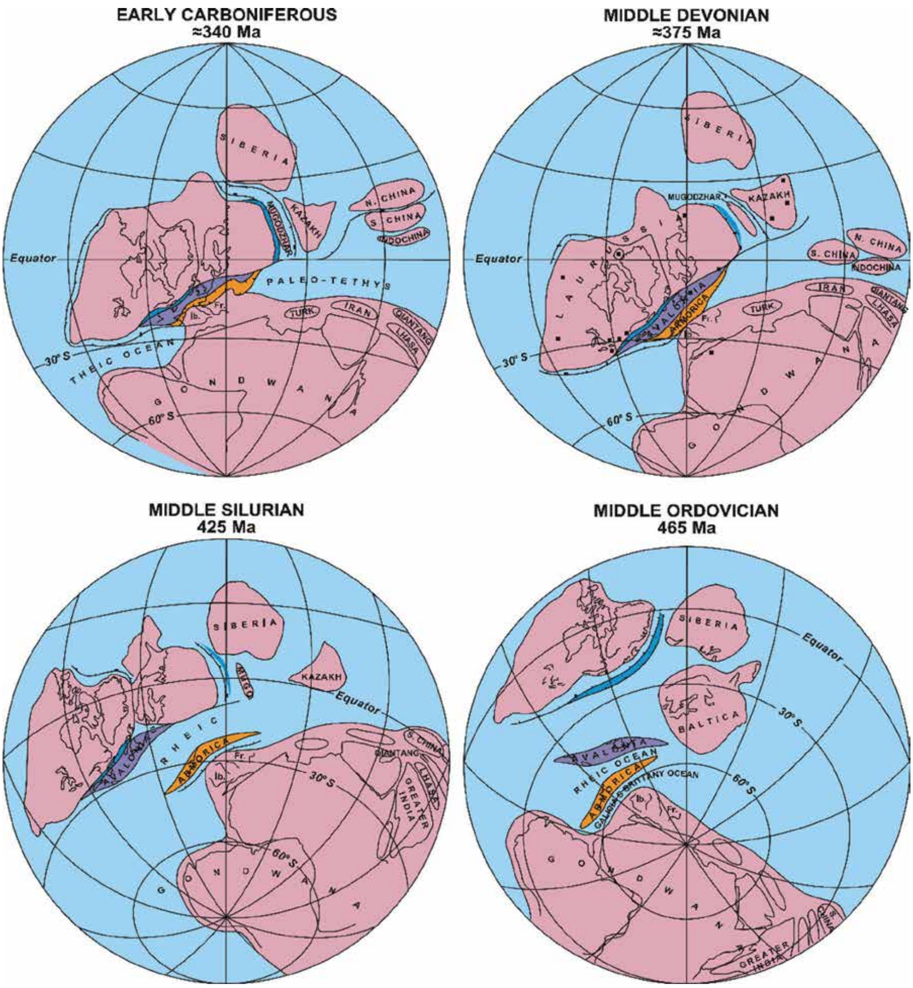

Figure 9.
Tentative reconstruction of the Variscan and surrounding areas at successive intervals from middle Ordovician (465 Ma) to Lower Carboniferous (340 Ma) [166] continental microplates. Blue, island arcs; black squares, distribution of Callixylon (petrified trees) in the Late Devonian (375 Ma).

but post-orogenic magma-rich collapse. In contrast, orogenic belts formed from the closure of broad oceans floored with Penrose-type crust (Benioff-type subduction) are characterized by arc magmatism but post-orogenic magma-poor collapse.

Acknowledgements

The present work was carried out with logistical and financial support from the Geology Department of Assiut University.

Conflict of interest

All figures are used with permission.

Author details

Mohamed A. Abu El-Rus*, Ali A. Khudier, Sadeq Hamid and Hassan Abbas
Faculty of Science, Geology Department, Assiut University, Assiut, Egypt

*Address all correspondence to: mmahmad@aun.edu.eg

References

[1] Amstutz A. Structures Alpines: Subductions Successives Dans l'Ossola. Vol. 241. Paris: Comptes rendus de l'Acad'emie des sciences; 1955. pp. 967-969

[2] Wadati K. On the activity of deep-focus earthquakes in the Japan islands and neighbourhoods. The Geophysical Magazine. 1935;**8**:305-325

[3] Benioff H. Seismic evidence for the fault origin of oceanic deeps. Geological Society of America Bulletin. 1949;**60**:1837-1856. DOI: 10.1130/00167606(1949)60[1837:SEFTFO]2.0.CO;2

[4] Stern RJ. The evolution of plate tectonics. Philosophical Transactions. Series A, Mathematical, Physical, and Engineering Sciences. 2018;**376**:20170406. DOI: 10.1098/rsta.2017.0406

[5] Carlson RL, Hilde TWC, Uyeda S. The driving mechanism of plate tectonics: Relation to age of the lithosphere at trenches. Geophysical Research Letters. 1983;**10**:297-300. DOI: 10.1029/GL010i004p00297

[6] Cloos M. Lithospheric buoyancy and collisional orogenesis: Subduction of oceanic plateaus, continental margins, island arcs, spreading ridges, and seamounts. Geological Society of America Bulletin. 1993;**105**:715-737. DOI: 10.1130/0016-7606(1993)105<0715:LBACOS>2.3.CO;2

[7] McCarthy A, Tugend J, Mohn G, Candioti L, Chelle-Michou C, Arculus R, et al. A case of Ampferer-type subduction and consequences for the Alps and the Pyrenees. American Journal of Science. 2020;**320**:313-372. DOI: 10.2475/04.2020.01

[8] Chelle-Michou C, McCarthy A, Moyen JF, Cawood PA, Capitanio FA. Make subductions diverse again. Earth Science Reviews. 2020;**226**:103966. DOI: 10.1016/j.earscirev.2022.103966

[9] Doglioni C. A proposal for the kinematic modelling of W-dipping subductions-possible applications to the Tyrrhenian-Apennines system. Terra Nova. 1991;**3**:423-434. DOI: 10.1111/j.1365-3121.1991.tb00172.x

[10] Ziegler PA. Plate tectonics, plate moving mechanisms and rifting. Tectonophysics. 1992;**215**:9-34. DOI: 10.1016/0040-1951(92)90072-E

[11] Ueda K, Gerya T, Sobolev SV. Subduction initiation by thermal–chemical plumes: Numerical studies. Physics of the Earth and Planetary Interiors. 2008;**171**:296-312. DOI: 10.1016/j.pepi.2008.06.032

[12] Ganguly J, Freed AM, Saxena SK. Density profiles of oceanic slabs and surrounding mantle: Integrated thermodynamic and thermal modeling, and implications for the fate of slabs at the 660 km discontinuity. Physics of the Earth and Planetary Interiors. 2009;**172**:257-267. DOI: 10.1016/j.pepi.2008.10.005

[13] Boonma K, Kumar A, Garcia-Castellanos D, Jimenez-Munt I, Fernandez M. Lithospheric mantle buoyancy: The role of tectonic convergence and mantle composition. Scientific Reports. 2019;**9**:17953. DOI: 10.1038/s41598-019-54374-w

[14] Hasegawa A, Umino N, Takagi A. Double-planed structure of the deep seismic zone in the northeastern Japan arc. Tectonophysics. 1978;**47**:43-58. DOI: 10.1016/0040-1951(78)90150-6

[15] Webb P. Introduction to Oceanography. Mountain View, CA: Roger Williams University; 2021. p. 383 Available from: http://rwu.pressbooks.pub/webboceanography

[16] Gill JB. Orogenic Andesites and Plate Tectonics. Berlin Heidelberg: Springer; 1981. p. 392. DOI: 10.1007/978-3-642-68012-0

[17] Tatsumi Y, Sakuyama M, Fukuyama H, Kushiro I. Generation of arc basalt magmas and thermal structure of the mantle wedge in subduction zones. Journal of Geophysical Research - Solid Earth. 1983;**88**:5815-5235. DOI: 10.1029/JB088iB07p05815

[18] Abu El-Rus M A: Geological studies on Abu Ghalaga area, Eastern Desert, Egypt [M.Sc. thesis]. Assiut: Assiut University; 1991: p. 255

[19] Arculus RJ. Evolution of arc magmas and their volatiles: The state of the planet. Frontiers and Challenges in Geophysics, Geophysical Monograph Series. 2004;**150**:95-108. DOI: 10.1016/0024-4937(94)90060-4

[20] Nicholson KN, Abu El-Rus MA. A case of Ampferer-type subduction beneath the New Caledonia arc: Evidence for inefficient subduction of hydrated lithologies into the upper mantle. Geological Society of America Bulletin. DOI: 10.1130/B36166.1

[21] Ahmed AA, Abu El-Ru MA. Pre-orogenic magmatic phases of Baranis Area, southeastern Desert, Egypt. Bulletin of Faculty of Sciences, Assiut University. 2002;**32**:73-97

[22] Arculus RJ. Use and abuse of the terms calcalkaline and calcalkalic. Journal of Petrology. 2003;**44**:929-935. DOI: 10.1093/petrology/44.5.929

[23] Khudier AA, Abu El-Rus MA, El-Gaby S, El-Nady O. Geochemical and geochronological studies on the infrastructural rocks of Meatiq and Hafafit swells, Eastern Desert, Egypt. Egyptian Journal of Geology. 2006;**50**:190-214

[24] Khudier AA, Abu El-Rus MA, El-Gaby S, El-Nady O, Bishara WW. Sr-Nd isotopes and geochemistry of the infrastructural rocks in the Meatiq and Hafafit core complexes, Eastern Desert, Egypt: Evidence for involvement of pre-Neoproterozoic crust in the growth of Arabian-Nubian Shield. Island Arc. 2008;**17**:90-108. DOI: 10.1111/j.1440-1738.2007.00599.x

[25] Maekawa H, Shozui M, Ishii T, Fryer P, Pearce JA. Blueschist metamorphism in an active subduction zone. Nature. 1993;**364**:520-523. DOI: 10.1038/364520a0

[26] El-Fadly MA, Hamid SA, El-Rus MA, Khudeir AA. An inquiry into the structural evolution of the Neoproterozoic Shait Granite Complex, south Eastern Desert, Egypt. Assiut University Journal of Geology. 2018;**47**:41-56

[27] Hamid S, Abu El-Rus MA, El Kazzaz YA, Khudeir AA. Neoproterozoic tectono-metamorphic evolution of Hafafit Dome "A" and the abutting Shait ophiolitic mélange domain at Gabel Mudargag area, central Eastern Desert, Egypt. Assiut University Journal of Geology. 2020;**49**:1-25

[28] Ampferer O, Hammer H. Geologischer Querschnitt durch die Ostalpen vom Allgäu zum Gardasee. Jahrbuch der Kaiserlich Königlichen Geologischen Reichsanstalt. 1911;**61**:631-710

[29] McCarthy A, Chelle-Michou C, Müntener O, Arculus R,

Blundy J. Subduction initiation without magmatism: The case of the missing Alpine magmatic arc. Geology. 2018;**46**:1059-1062. DOI: 10.1130/g45366.1

[30] Zanchetta S, Garzanti E, Doglioni C, Zanchi A. The Alps in the cretaceous: A doubly vergent pre-collisional orogen. Terra Nova. 2012;**24**:351-356. DOI: 10.1111/j.1365-3121.2012.01071.x

[31] Tugend J, Manatschal G, Kusznir NJ, Masini E, Mohn G, Thinon I. Formation and deformation of hyperextended rift systems: Insights from rift domain mapping in the Bay of Biscay-Pyrenees. Tectonics. 2014;**33**:1239-1276. DOI: 10.1002/2014tc003529

[32] Auzemery A, Yamato P, Duretz T, Willingshofer E, Matenco L, Porkol'ab K. Influence of magma-poor versus magma-rich passive margins on subduction initiation. Gondwana Research. 2022;**103**:172-186. DOI: 10.1016/j.gr.2021.11.012

[33] Ernst WG. Alpine and Pacific styles of Phanerozoic mountain building: Subduction-zone petrogenesis of continental crust. Terra Nova. 2005;**17**:165-188. DOI: 10.1111/j.1365-3121.2005.00604.x

[34] Mohn G, Manatschal G, Beltrando M, Haupert I. The role of rift-inherited hyper-extension in Alpine-type orogens. Terra Nova. 2014;**26**:347-353. DOI: 10.1111/ter.12104

[35] Wilson JT. Did the Atlantic close and then re-open? Nature. 1966;**211**:676-681. DOI: 10.1038/211676a0

[36] Wilson JT. Static or mobile earth: The current scientific revolution. Proceedings of the American Philosophical Society. 1968;**112**:309-320

[37] Trümpy R: Why plate tectonics was not invented in the Alps. International Journal of Earth Sciences 2001; 90:477-483. https://doi.org/ 10.1007/s005310000175

[38] François C, Pubellier M, Robert C, Bulois C, Jamaludin SNF, Oberhänsli R, et al. Temporal and spatial evolution of orogens: A guide for geological mapping. Episodes. 2022;**45**:265-283. DOI: 10.18814/epiiugs/2021/021025

[39] Manatschal G, Müntener O. A type sequence across an ancient magmapoor ocean–continent transition: The example of the western Alpine Tethys ophiolites. Tectonophysics. 2009;**473**:4-19. DOI: 10.1016/j.tecto.2008.07.021

[40] Mohn G, Manatschal G, Masini E, Müntener O. Rift-related inheritance in orogens: A case study from the Austroalpine nappes in Central Alps (SE-Switzerland and N-Italy). International Journal of Earth Sciences. 2011;**100**:937-961. DOI: 10.1007/s00531-010-0630-2

[41] Picazo S, Müntener O, Manatschal G, Bauville A, Karner G, Johnson C. Mapping the nature of mantle domains in Western and Central Europe based on clinopyroxene and spinel chemistry: Evidence for mantle modification during an extensional cycle. Lithos. 2016;**266-267**:233-263. DOI: 10.1016/j.lithos.2016.08.029

[42] Dewey JF, Burke K. Hot spots and collisional break-up: Implications for collisional orogeny. Geology. 1974;**2**:57-60. DOI: 10.1130/00917613(1974)2<57:HSACBI>2.0.CO;2

[43] Chenin P, Manatschal G, Picazo S, Müntener O, Karner GD, Johnson C, et al. Influence of the architecture of magma-poor hyperextended rifted margins on orogens produced by the closure of narrow versus wide oceans. Geosphere. 2017;**13**:559-576. DOI: 10.1130/GES01363.1

[44] Chenin P, Picazo S, Jammes S, Manatschal G, Müntener O, Karner GD. Potential role of lithospheric mantle composition in the Wilson cycle: A North Atlantic perspective. In: Wilson R W, Wilson RW, editors. Fifty Years of the Wilson Cycle Concept in Plate Tectonics. London: Geological Society; 2018. p. 470. DOI: 10.1144/SP470.10

[45] Perez-Gussinyé M, Reston TJ. Rheological evolution during extension at non-volcanic rifted margins: Onset of serpentinization and development of detachments leading to continental breakup. Journal of Geophysical Research. 2001;**106**:3961-3975. DOI: 10.1029/2000JB900325

[46] Sutra E, Manatschal G, Mohn G, Unternehr P. Quantification and restoration of extensional deformation along the Western Iberia and Newfoundland rifted margins. Geochemistry, Geophysics, Geosystems. 2013;**14**:2575-2597. DOI: 10.1002/ggge.20135

[47] Doré T, Lundin E. Hyperextended continental margins – knowns and unknowns. Geology. 2015;**43**:95-96. DOI: 10.1130/focus012015.1

[48] Manatschal G. Fluid-and reaction-assisted low angle normal faulting: Evidence from rift-related brittle fault rocks in the Alps (Err Nappe, eastern Switzerland). Journal of Structural Geology. 1999;**21**:777-793. DOI: 10.1016/S0191-8141(99)00069-3

[49] Manatschal G. New models for evolution of magma-poor rifted margins based on a review of data and concepts from West Iberia and the Alps. International Journal of Earth Sciences. 2004;**93**:432-466. DOI: 10.1007/S00531-004-0394-7

[50] Pinto VHG, Manatschal G, Karpoff AM, Viana A. Tracing mantle-reacted fluids in magma-poor rifted margins: The example of Alpine Tethyan rifted margins. Geochemistry, Geophysics, Geosystems. 2015;**16**:3271-3308. DOI: 10.1002/2015GC005830

[51] Hess H. Serpentines, orogeny, and epeirogeny. In: Poldervaart A, editor. Crust of the Earth: A Symposium, Geological Society of America Special Papers. Vol. 62. Boulder, USA: The Geological Society of America; 1955. pp. 391-408. DOI: 10.1130/SPE62-P391

[52] Christensen NI. Composition and evolution of the oceanic crust. Marine Geology. 1970;**8**:139-154. DOI: 10.1016/0025-3227(70)90002-2

[53] Früh-Green GL, Connolly JA, Plas A, Kelley DS, Grobéty B. Serpentinization of oceanic peridotites: Implications for geochemical cycles and biological activity. In: Wilcock WS, Delong EF, Kelley DS, Baross JA, Craig Cary S, editors. The Subseafloor Biosphere at Mid-Ocean Ridges. Vol. 144. Washington, DC: American Geophysical Union, Geophysical Monographs; 2004. pp. 119-136. DOI: 10.1029/144GM08

[54] Picazo S, Cannat M, Delacour A, Escartín J, Roumé-Jon S, Silantyev S. Deformation associated with the denudation of mantle-derived rocks at the Mid-Atlantic Ridge 13-15°N: The role of magmatic injections and hydrothermal alteration. Geochemistry, Geophysics, Geosystems. 2012;**13**:Q04G09. DOI: 10.1029/2012GC004121

[55] Latin D, White N. Generating melt during lithospheric extension: Pure shear vs. simple shear. Geology. 1990;**18**:327-331. DOI: 10.1130/0091-7613(1990)018<0327:GMDLEP>2.3.CO;2

[56] Müntener O, Manatschal G, Desmurs L, Pettke T. Plagioclase

peridotites in ocean–continent transitions: Refertilized mantle domains generated by melt stagnation in the shallow mantle lithosphere. Journal of Petrology. 2010;**51**:255-294. DOI: 10.1093/petrology/egp087

[57] O'reilly B, Hauser F, Ravaut C, Shannon P, Readman P. Crustal thinning, mantle exhumation and serpentinization in the Porcupine Basin, offshore Ireland: Evidence from wide-angle seismic data. Journal of the Geological Society. 2006;**163**:775-787. DOI: 10.1144/0016-76492005-07

[58] Afilhado A, Matias L, Shiobara H, Hirn A, Mendesvictor L, Shimamura H: From unthinned continent to ocean: The deep structure of the West Iberia passive continental margin at 38°N. Tectonophysics 2008; 458: 9-50. https://doi.org/10.1016/j.tecto.2008.03.002

[59] Lau KWH, Louden KE, Funck T, Tucholke BE, Holbrook WS, Hopper JR, et al. Crustal structure across the Grand Banks–Newfoundland Basin continental margin – I. Results from a seismic refraction profile. Geophysical Journal International. 2006;**167**:127-156. DOI: 10.1111/j.1365-246X.2006.02988.x

[60] Funck T, Hopper JR, Larsen HC, Louden KE, Tucholke BE, Holbrook WS. Crustal structure of the ocean-continent transition at Flemish Cap: Seismic refraction results. Journal of Geophysical Research. 2003;**108**:2531. DOI: 10.1029/2003JB002434

[61] Boillot G, Capdevila R. The Pyrenees: Subduction and collision? Earth and Planetary Science Letters. 1977;**35**:151-160. DOI: 10.1016/0012-821X(77)90038-3

[62] Sengör AMC. Orogenic architecture as a guide to size of ocean lost in collisional mountain belts. Bulletin of the Technical University of Istanbul. 1991;**44**:43-74

[63] Anderson DL. Speculations on the nature and cause of mantle heterogeneity. Tectonophysics. 2006;**416**:7-22. DOI: 10.1016/j.tecto.2005.07.011

[64] Costa S, Rey P. Lower crustal rejuvenation and growth during post-thickening collapse: Insights from a crustal cross section through a Variscan metamorphic core complex. Geology. 1995;**23**:905-908. DOI: 10.1130/0091-7613(1995)023<0905:LCRAGD>2.3.CO;2

[65] Vanderhaeghe O, Burg J-P, Teyssier C. Exhumation of migmatites in two collapsed orogens: Canadian Cordillera and French Variscides. In: Ring U, Brandon MT, Lister GS, Willett SD, editors. Exhumation Processes: Normal Faulting, Ductile Flow and Erosion. Vol. 154. London: Geological Society; 1999. pp. 181-204. DOI: 10.1144/GSL.SP.1999.154.01.08

[66] Rey P, Vanderhaeghe O, Teyssier C. Gravitational collapse of the continental crust: Definition, regimes and modes. Tectonophysics. 2001;**342**:435-449. DOI: 10.1016/S0040-1951(01)00174-3

[67] Petri B, Mohn G, Štípská P, Schulmann K, Manatschal G. The Sondalo gabbro contact aureole (Campo unit, Eastern Alps): Implications for midcrustal mafic magma emplacement. Contributions to Mineralogy and Petrology. 2016;**171**:1-21. DOI: 10.1007/s00410-016-1263-7

[68] Iwamori H. Transportation of H_2O and melting in subduction zones. Earth and Planetary Science Letters. 1998;**160**:65-80. DOI: 10.1016/S0012-821X(98)00080-6

[69] Sisson TW, Bronto S. Evidence for pressure release melting beneath magmatic arcs from basalt at Galunggung, Indonesia. Nature. 1998;**391**:883-886. DOI: 10.1038/36087

[70] Jagoutz O, Müntener O, Schmidt MW, Burg J-P. The roles of flux- and decompression melting and their respective fractionation lines for continental crust formation: Evidence from the Kohistan arc. Earth and Planetary Science Letters. 2011;**303**:25-36. DOI: 10.1016/j.epsl.2010.12.017

[71] Uyeda S. Subduction zones and back arc basins – a review. Geologische Rundschau. 1981;**70**:552-569. DOI: 10.1007/BF01822135

[72] Martinez F, Taylor B. Mantle wedge control on back-arc crustal accretion. Nature. 2002;**416**:417-420. DOI: 10.1038/416417a

[73] Chenin P, Manatschal G, Lavier LL, Erratt D. Assessing the impact of orogenic inheritance on the architecture, timing, and magmatic budget of the North Atlantic rift system: A mapping approach. Journal of the Geological Society. 2015;**172**:711-720. DOI: 10.1144/jgs2014-139

[74] Stern R. Subduction initiation: Spontaneous and induced. Earth and Planetary Science Letters. 2004;**226**:275-292. DOI: 10.1016/j.epsl.2004.08.007

[75] Stern RJ, Gerya T. Subduction initiation in nature and models: A review. Tectonophysics. 2018;**746**:173-198. DOI: 10.1016/j.tecto.2017.10.014

[76] Crameri F, Magni V, Domeier M, Shephard GE, Chotalia K, Cooper G, et al. A transdisciplinary and community-driven database to unravel subduction zone initiation. Nature Communications. 2020;**11**:3750. DOI: 10.1038/s41467-020-17522-9

[77] Mueller S, Phillips RJ. On the initiation of subduction. Journal of Geophysical Research. 1991;**96**:651-665. DOI: 10.1029/90JB02237

[78] Candioti L, Duretz T, Schmalholz SM. Horizontal force required for subduction initiation at passive margins with constraints from slab detachment. Frontiers in Earth Science. 2022;**10**:785418. DOI: 10.3389/feart.2022.785418

[79] Cloetingh S, Wortel R, Vlaar NJ. On the initiation of subduction zones. Pure and Applied Geophysics. 1989;**129**:7-25. DOI: 10.1007/BF00874622

[80] Lallemand S, Arcay D. Subduction initiation from the earliest stages to self-sustained subduction: Insights from the analysis of 70 Cenozoic sites. Earth Science Reviews. 2021;**221**:103779. DOI: 10.1016/j.earscirev.2021.103779

[81] McKenzie DP. The initiation of trenches: A finite amplitude instability. In: Talwani M, Pitman WC III, editors. Island Arcs, Deep Sea Trenches and Back-Arc Basins, Volume 1. Washington, DC: American Geophysical Union; 1977. pp. 57-61. DOI: 10.1029/me001p0057

[82] Zhong X, Li Z-H. Subduction initiation at passive continental margins: A review based on numerical studies. Solid Earth Sciences. 2021;**6**:249-267. DOI: 10.1016/j.sesci.2021.06.001

[83] Shuck B, Gulick SPS, Van Avendonk HJA, Gurnis M, Sutherland R, Stock J, et al. Stress transition from horizontal to vertical forces during subduction initiation. Nature Geoscience. 2022;**15**:149-155. DOI: 10.1038/s41561-021-00880-4

[84] White SH, Knipe RJ. Transformation- and reaction-enhanced ductility in rocks. Journal of the Geological Society. 1978;**135**:513-516. DOI: 10.1144/gsjgs.135.5.0513

[85] Regenauer-Lieb K, Yuen DA, Branlund J. The initiation of subduction: Criticality by addition of water? Science. 2001;**294**:578-580. DOI: 10.1126/science.1063891

[86] Dymkova D, Gerya T. Porous fluid flow enables oceanic subduction initiation on Earth. Geophysical Research Letters. 2013;**40**:5671-5676. DOI: 10.1002/2013GL057798

[87] Montési LG. Fabric development as the key for forming ductile shear zones and enabling plate tectonics. Journal of Structural Geology. 2013;**50**:254-266. DOI: 10.1016/j.jsg.2012.12.011

[88] Bercovici D, Ricard Y. Mechanisms for the generation of plate tectonics by two-phase grain-damage and pinning. Physics of the Earth and Planetary Interiors. 2012;**202-203**:27-55. DOI: 10.1016/j.pepi.2012.05.003

[89] Mulyukova E, Bercovici D. Collapse of passive margins by lithospheric damage and plunging grain size. Earth and Planetary Science Letters. 2018;**484**:341-352. DOI: 10.1016/j.epsl.2017.12.022

[90] Yuen DA, Fleitout L, Schubert G, Froidevaux C. Shear deformation zones along major transform faults and subducting slabs. Geophysical Journal International. 1978;**54**:93-119. DOI: 10.1111/j.1365-246X.1978.tb06758.x

[91] Regenauer-Lieb K, Yuen DA. Rapid conversion of elastic energy into plastic shear heating during incipient necking of the lithosphere. Geophysical Research Letters. 1998;**25**:2737-2740. DOI: 10.1029/98GL02056

[92] Kiss D, Podladchikov Y, Duretz T, Schmalholz SM. Spontaneous generation of ductile shear zones by thermal softening: Localization criterion, 1D to 3D modelling and application to the lithosphere. Earth and Planetary Science Letters. 2019;**519**:284-296. DOI: 10.1016/j.epsl.2019.05.026ff

[93] Thielmann M, Kaus BJP. Shear heating induced lithospheric-scale localization: Does it result in subduction? Earth and Planetary Science Letters. 2012;**359-360**:1-13. DOI: 10.1016/j.epsl.2012.10.002

[94] Jaquet Y, Schmalholz SM. Spontaneous ductile crustal shear zone formation by thermal softening and related stress, temperature and strain rate evolution. Tectonophysics. 2018;**746**:384-397. DOI: 10.1016/j.tecto.2017.01.012

[95] Kiss D, Candioti LG, Duretz T, Schmalholz SM. Thermal softening induced subduction initiation at a passive margin. Geophysical Journal International. 2020;**220**:2068-2073. DOI: 10.1093/gji/ggz572

[96] Auzemery A, Willingshofer E, Yamato P, Duretz T, Beekman F. Kinematic boundary conditions favouring subduction initiation at passive margins over subduction at mid-oceanic ridges. Frontiers in Earth Science. 2021;**9**:765893. DOI: 10.3389/feart.2021.765893

[97] Auzemery A, Willingshofer E, Yamato P, Duretz T, Sokoutis D. Strain localization mechanisms for subduction initiation at passive margins. Global and Planetary Change. 2020;**195**:103323. DOI: 10.1016/j.gloplacha.2020.103323

[98] Ulmer P, Trommsdorff V. Serpentine stability to mantle depths and subduction-related magmatism. Science. 1995;**268**:858-861. DOI: 10.1126/science.268.5212.858

[99] Escartm J, Hirth G, Evans B. Strength of slightly serpentinized peridotites: Implications for the tectonics of oceanic lithosphere. Geology. 2001;**29**:1023-1026. DOI: 10.1130/0091-7613(2001)029<1023:SOSSPI>2.0.CO;2

[100] Hilairet N, Reynard B, Wang Y, Daniel I, Merkel S, Nishiyama N, et al. High pressure creep of serpentine, interseismic deformation, and initiation of subduction. Science. 2007;**318**:1910-1913. DOI: 10.1126/science.1148494

[101] Zhong X, Li Z-H. Forced subduction initiation at passive continental margins: Velocity-driven versus stress-driven. Geophysical Research Letters. 2019;**46**:11054-11064. DOI: 10.1029/2019GL084022

[102] Shervais JW. Birth, death, and resurrection: The life cycle of suprasubduction zone ophiolites. Geochemistry, Geophysics, Geosystems. 2001;**2**:1010. DOI: 10.1029/2000GC000080

[103] Maffione M, van Hinsbergen DJJ, de Gelder GINO, van der Goes FC, Morris A. Kinematics of late cretaceous subduction initiation in the neo-Tethys ocean reconstructed from ophiolites of Turkey, Cyprus, and Syria. Journal of Geophysical Research. 2017;**122**:3953-3976. DOI: 10.1002/2016JB013821

[104] Plank T, Langmuir CH. An evaluation of the global variations in the major element chemistry of arc basalts. Earth and Planetary Science Letters. 1988;**90**:349-370. DOI: 10.1016/0012-821X(88)90135-5

[105] Lee C-TA, Luffi P, Plank T, Dalton H, Leeman WP. Constraints on the depths and temperatures of basaltic magma generation on earth and other terrestrial planets using new thermobarometers for mafic magmas. Earth and Planetary Science Letters. 2009;**279**:20-33. DOI: 10.1016/j.epsl.2008.12.020

[106] Grove TL, Till CB, Krawczynski MJ. The role of H_2O in subduction zone magmatism. Annual Review of Earth and Planetary Sciences. 2012;**40**:413-439. DOI: 10.1146/annurev-earth-042711-105310

[107] Perrin A, Goes S, Prytulak J, Davies DR, Wilson C, Kramer S. Reconciling mantle wedge thermal structure with arc lava thermobarometric determinations in oceanic subduction zones. Geochemistry, Geophysics, Geosystems. 2016;**17**:4105-4127. DOI: 10.1002/2016GC006527

[108] Khudeir AA, Paquette JL, Nicholson K, Johansson Å, Rooney TO, El-Fadly MA, et al. On the cratonization of the Arabian-Nubian Shield: Constraints from granite gneisses in south eastern desert, Egypt. Geoscience Frontiers. 2021;**12**:101148. DOI: 10.1016/j.gsf.2021.101148

[109] Stern RJ. Evidence from ophiolites, blueschists, and ultrahigh-pressure metamorphic terranes that the modern episode of subduction tectonics began in Neoproterozoic time. Geology. 2005;**33**:557-560. DOI: 10.1130/G21365.1

[110] Crawford AJ, Meffre S, Symonds PA. 120 to 0 Ma tectonic evolution of the Southwest Pacific and analogous geological evolution of the 600 to 220 Ma Tasman fold belt. In: Hills RR, Muller RD, editors. Evolution and Dynamics of the Australian Plate. Geological Society of America Special Paper; Vol. 372. Boulder, USA: The Geological Society of America; 2003; Paper 372. pp. 383-404. DOI: 10.1130/0-8137-2372-8.383

[111] Schellart WP, Lister GS, Toy VG. A late Cretaceous and Cenozoic

reconstruction of the Southwest Pacific region: Tectonics controlled by subduction and slab rollback processes. Earth Science Reviews. 2006;**76**:191-233. DOI: 10.1016/j.earscirev.2006.01.002

[112] Nicholson KN, Maurizot PP, Black PM, Picard C, Simonetti AA, Stewart A, et al. Geochemistry and age of the Nouméa Basin lavas, New Caledonia; Evidence for Cretaceous subduction beneath the eastern Gondwana margin. Lithos. 2011;**125**:659-674. DOI: 10.1016/j.lithos.2011.03.018

[113] Sevin B, Maurizot P, Cluzel D, Tournadour E, Etienne S, Folcher N, et al. Post-obduction evolution of New Caledonia. In: Maurizot P, Mortimer N, editors. New Caledonia: Geology, Geodynamic Evolution and Mineral Resources. Vol. 51. London: Geological Society; 2020. pp. 147-188. DOI: 10.1144/M51-2018-74

[114] Falvey DA, Mutter JC. Regional plate tectonics and the evolution of Australia's passive continental margin. BMR Journal of Australian Geology and Geophysics. 1981;**6**:1-29

[115] Régnier M. Lateral variation of upper mantle structure beneath New Caledonia determined from P-wave receiver function: Evidence for a fossil subduction zone. Geophysical Journal. 1988;**95**:561-577. DOI: 10.1111/j.1365-246X.1988.tb06704.x

[116] Cluzel D, Bosch D, Paquette J, Lemennicier Y, Montjoi P, Menot R. Late Oligocene post-obduction granitoids of New Caledonia: A case for reactivated subduction and slab break-off. The Island Arc. 2005;**14**:254-271. DOI: 10.1111/j.1440-1738.2005.00470.x

[117] Putirka K. Excess temperatures at ocean islands: Implications for mantle layering and convection. Geology. 2008;**36**:283-286. DOI: 10.1130/G24615A.1

[118] Tatsumi Y. Some Constraints on Arc Magma Genesis in Inside the Subduction Factory. Vol. 138. Washington, D.C.: American Geophysical Union, Geophysical Monograph; 2003. pp. 277-292. DOI: 10.1029/138GM12

[119] Stern RJ. Subduction zones. Reviews of Geophysics. 2002;**40**:3.1-3.38. DOI: 10.1029/2001RG000108

[120] van Keken PE, Hacker BR, Syracuse EM, Abers GA. Subduction factory: 4. Depth-dependent flux of H_2O from subducting slabs worldwide. Journal of Geophysical Research. 2011;**116**:B01401 DOI: 10.1029/2010JB007922

[121] Cluzel D, Chiron D, Courme MD. Discordance de l'Eoce'ne supérieur et e've'nements pré-obduction en Nouvelle-Cale'donie (Pacifique sud-ouest): Compte Rendus de l'Académie des Sciences, Série II. Sciences de la Terre et des Planètes. 1998;**327**:485-449

[122] Paquette J-L, Cluzel D. U–Pb zircon dating of post-obduction volcanic-arc granitoids and a granulite-facies xenolith from New Caledonia, Inference on Southwest Pacific geodynamic models. International Journal of Earth Sciences. 2007;**96**:613-622. DOI: 10.1007/s00531-006-0127-1

[123] Yumul, Jr GP, Dimalanta CB, Marquez EJ, Queaño KL. Onland signatures of the Palawan microcontinental block and the Philippine mobile belt collision and crustal growth process: A review. Journal of Asia Earth Sciences. 2009;**34**:610-623. DOI: 10.1016/j.jseaes.2008.10.002

[124] Yumul, Jr GP, Armada LT, Gabo-Ratiob JAS, Dimalanta CB,

Austria RSP. Subduction with arrested volcanism: Compressional regime in volcanic arc gap formation along east Mindanao, Philippines. Journal of Asia Earth Sciences. 2020;**4**:100030. DOI: 10.1016/j.jaesx.2020.100030

[125] Pearce JA, Peate DW. Tectonic implications of the composition of volcanic arc magmas. Annual Review of Earth and Planetary Sciences. 1995;**23**:251-285. DOI: 10.1146/annurev.ea.23.050195.001343

[126] Shor GG, Kirk HK, Maynard GL. Crustal structure of the Melanesian area. Journal of Geophysical Research. 1971;**76**:2562-2586. DOI: 10.1029/JB076i011p02562

[127] Dubois J, Aubertin RA, Louis J, Guillaume R, Launay J, Montadert L. Continental margins near New Caledonia. In: Burk CA, Drake CL, editors. The Geology of Continental Margins. New York: Springer Science and Business Media; 1974. pp. 521-1029

[128] Kinzler RJ. Melting of mantle peridotite at pressures approaching the spinel to garnet transition: Application to mid-ocean ridge basalt petrogenesis. Journal of Geophysical Research. 1997;**102**:853-874. DOI: 10.1029/96JB00988

[129] Faul UH. Melt retention and segregation beneath mid-ocean ridges. Nature. 2001;**410**:920-923. DOI: 10.1038/35073556

[130] Zhu W, Hirth G. A network model for permeability in partially molten rocks. Earth and Planetary Science Letters. 2003;**212**:407-416. DOI: 10.1016/S0012-821X(03)00264-4

[131] Rondenay S, Montési LGJ, Abers GA. New geophysical insight into the origin of the Denali volcanic gap. Geophysical Journal International. 2010;**182**:613-630. DOI: 10.1111/j.1365-246X.2010.04659.x

[132] Korenaga J, Kelemen PB. Origin of gabbro sills in the Moho transition zone of the Oman ophiolite: Implications for magma transport in the oceanic lower crust. Journal of Geophysical Research. 1997;**102**:27729-27749. DOI: 10.1029/97JB02604

[133] Sparks DW, Parmentier EM. Melt extraction from the mantle beneath spreading centers. Earth and Planetary Science Letters. 1991;**105**:368-377. DOI: 10.1016/0012-821X(91)90178-K

[134] Spiegelman M. Physics of melt extraction: Theory, implications and applications. Philosophical Transactions of the Royal Society of London: Physical Sciences and Engineering. 1993;**342**:23-41. DOI: 10.1098/rsta.1993.0002

[135] Katz RF, Spiegelman M, Langmuir CH. A new parameterization of hydrous mantle melting. Geochemistry, Geophysics, Geosystems. 2003;**4**:1073. DOI: 10.1029/2002GC000433

[136] Lagabrielle Y, Labaume P, de Saint BM. Mantle exhumation, crustal denudation, and gravity tectonics during Cretaceous rifting in the Pyrenean realm (SW Europe): Insights from the geological setting of the lherzolite bodies. Tectonics. 2010;**29**:TC4012. DOI: 10.1029/2009TC002588

[137] Tugend J, Manatschal G, Kusznir N. Spatial and temporal evolution of hyperextended rift systems: Implication for the nature, kinematics and timing of the Iberian–European plate boundary. Geology. 2015;**43**:15-18. DOI: 10.1130/G36072

[138] Kröner A, Romer RL. Two plates-many subduction zones: The Variscan orogeny reconsidered. Gondwana Research. 2013;**24**:298-329. DOI: 10.1016/j.gr.2013.03.001

[139] Regorda A, Lardeaux J-M, Roda M, Marotta AM, Spalla MI. How many subductions in the Variscan orogeny? Insights from numerical models. Geoscience Frontiers. 2020;**11**:1025-1052. DOI: 10.1016/j.gsf.2019.10.005

[140] Beltrando M, Manatschal G, Mohn G, Dal Piaz GV, Vitale Brovarone A, Masini E. Recognizing remnants of magma-poor rifted margins in high-pressure orogenic belts: The Alpine case study. Earth Science Reviews. 2014;**131**:88-115. DOI: 10.1016/j.earscirev.2014.01.001

[141] Rosenbaum G, Lister G S: The Western Alps from the Jurassic to Oligocene: Spatio-temporal constraints and evolutionary reconstructions: Earth Science Reviews 2005;**69**:281-306. DOI: 10.1016/j.earscirev.2004.10.001

[142] Handy KR, Schmid SM, Bousquet R, Kissling E, Bernoulli D. Reconciling plate-tectonic reconstructions of Alpine Tethys with the geological–geophysical record of spreading and subduction in the Alps. Earth Science Reviews. 2010;**102**:121-158. DOI: 10.1016/j.earscirev.2010.06.002

[143] Le Breton E, Brune S, Ustaszewski K, Zahirovic S, Seton M, Müller RD. Kinematics and extent of the Piemont-Liguria basin: Implications for subduction processes in the Alps. Solid Earth. 2021;**12**:885-913. DOI: 10.5194/se-12-885-2021

[144] Schenker FL, Schmalholz SM, Moulas E, Pleuger J, Baumgartner LP, Podladchikov Y, et al. Current challenges for explaining (ultra)high-pressure tectonism in the Pennine domain of the Central and Western Alps. Journal of Metamorphic Geology. 2015;**33**:869-886. DOI: 10.1111/jmg.12143

[145] Manzotti P, Bosse V, Pitra P, Robyr M, Schiavi F, Ballèvre M. Exhumation rates in the Gran Paradiso Massif (Western Alps) constrained by in situ U–Th–Pb dating of accessory phases (monazite, allanite and xenotime). Contributions to Mineralogy and Petrology. 2014;**173**:1-28. DOI: 10.1007/s00015-014-0172-x

[146] Rubatto D, Gebauer D, Fanning M. Jurassic formation and Eocene subduction of the Zermatt-Saas-Fee ophiolites: Implications for the geodynamic evolution of the Central and Western Alps. Contributions to Mineralogy and Petrology. 1998;**132**:269-287. DOI: 10.1007/s004100050421

[147] Manzotti P, Ballèvre M, Zucali M, Robyr M, Engi M. The tectonometamorphic evolution of the Sesia-Dent Blanche Nappes (Internal Western Alps): Review and synthesis. Swiss Journal of Geosciences. 2014;**107**:309-336. DOI: 10.1007/s00015-014-0172

[148] Schmid SM, Kissling E, Diehl T, van Hinsbergen DJJ, Molli G. Ivrea Mantle Wedge, Arc of the Western Alps, and Kinematic Evolution of the Alps-Apennines Orogenic System. Swiss Journal of Geosciences. 2017;**110**:581-612. DOI: 10.1007/s00015-016-0237-0

[149] Kästle ED, Rosenberg C, Boschi L, Bellahsen N, Meier T, El-Sharkawy A. Slab break-offs in the alpine subduction zone. International Journal of Earth Sciences. 2020;**109**:587-603. DOI: 10.1007/s00531-020-01821-z

[150] Vissers RL, van Hinsbergen DJ, van der Meer DG, Spakman W. Cretaceous slab break-off in the Pyrenees: Iberian plate kinematics in paleomagnetic and mantle reference frames. Gondwana Research. 2016;**34**:49-59. DOI: 10.1016/j.gr.2016.03.006

[151] Ziegler PA. Geological Atlas of Western and Central Europe. Vol. 121. The Hague, Shell Internationale Petroleum Maatschappij; 1982. pp. 371-372. DOI: 10.1017/S0016756800 029344

[152] Carey WS. The orocline concept in Geotectonics. Papers and Proceedings of the Royal Society of Tasmania. 1958;**89**:255-288

[153] Van der Voo R, Spakman W, Bijwaard H. Tethyan subducted slabs under India. Earth and Planetary Science Letters. 1999;**171**:7-20

[154] Le Pichon X, Sibuet JC. Western extension of boundary between European and Iberian plates during the Pyrenean orogeny. Earth and Planetary Science Letters. 1971;**12**:83-88. DOI: 10.1016/0012-821X(71)90058-6

[155] Srivastava SP, Roest WR, Kovacs LC, Oakey G, Lévesque S, Verhoef J, et al. Motion of Iberia since the late Jurassic: Results from detailed aeromagnetic measurements in the Newfoundland basin. Tectonophysics. 1990;**184**:229-260

[156] Srivastava SP, Sibuet JC, Cande S, Roest WR, Reid ID. Magnetic evidence for slow seafloor spreading during the formation of the Newfoundland and Iberian margins. Earth and Planetary Science Letters. 2000;**182**:61-76. DOI: 10.1016/S0012-821X(00)00231-4

[157] Sibuet J-C, Srivastava SP, Spakman W. Pyrenean orogeny and plate kinematics. Geophysical Research. 2004;**109**:B08104. DOI: 10.1029/ 2003JB002514

[158] Vissers RLM, Th MP. Mesozoic rotation of Iberia: Subduction in the Pyrenees? Earth Science Reviews. 2012;**110**:93-110. DOI: 10.1016/j.earscirev. 2011.11.001

[159] Beaumont C, Muñoz JA, Hamilton J, Fullsack P. Factors controlling the alpine evolution of the central Pyrenees inferred from a comparison of observations and geodynamical models. Journal of Geophysical Research. 2000;**105**:8121-8145. DOI: 10.1029/1999JB900390

[160] Roure F, Choukroune P, Berástegui X, Muñoz JA, Villien A, Matheron P, et al. ECORS deep seismic data and balanced cross sections: Geometric constraints on the evolution of the Pyrenees. Tectonics. 1989;**8**:41-50. DOI: 10.1029/TC008i001p00041

[161] Souriau A, Chevrot S, Olivera C. A new tomographic image of the Pyrenean lithosphere from teleseismic data. Tectonophysics. 2008;**460**:206-214. DOI: 10.1016/j.tecto.2008.08.014

[162] Bronner A, Sauter D, Manatschal G, Péron-Pinvidic G, Munschy M. Reply to problematic plate reconstruction by Tucholke B E, Sibuet J-C. Nature Geoscience. 2012;**5**:677

[163] Clerc C, Lahfid A, Monié P, Lagabrielle Y, Chopin C, Poujol M, et al. High-temperature metamorphism during extreme thinning of the continental crust: A reappraisal of the North Pyrenean passive paleomargin. Solid Earth. 2015;**6**:643-668. DOI: 10.5194/ se-6-643-2015

[164] Mc Carthy A, Tugend J, Mohn G. Formation of th e Alpine orogen by amagmatic convergence and assembly of previously rifted lithosphere. Elements. 2021;**17**:29-34. DOI: 10.2138/ gselements.17.1.29

[165] Michard A, Ouanaimi H, Chr H, Soulaimani A, Baidder L. Reply to the comment by Michard et al. on "Tectonic relationships of Southwest Iberia with the allochthons of Northwest Iberia and the Moroccan Variscides" by J F Simancas

et al. (Comptes Rendus Geoscience 2009;**341**:103-113). Comptes Rendus Geoscience. 2010;**342**:170-174. DOI: 10.1016/j.crte.2010.01.008

[166] Matte P. The Variscan collage and orogeny (480-290 Ma) and the tectonic definition of the Armorica microplate: A review. Terra Nova. 2001;**13**:122-128. DOI: 10.1046/j.1365-3121.2001.00327.x

[167] Franke W, Cocks LRM, Torsvik TH. The Palaeozoic Variscan oceans revisited. Gondwana Research. 2017;**48**:257-284. DOI: 10.1016/j.gr.2017.03.005

[168] Franke W. The mid-European segment of the Variscides: Tectonostratigraphic units, terrane boundaries and plate tectonic evolution. In: Franke W, Haak V, Oncken O, Tanner D, editors. Orogenic Processes: Quantification and Modelling in the Variscan belt. Vol. 179. London: Geological Society; 2000. pp. 35-61. DOI: 10.1144/GSL.SP.2000.179.01.05

[169] Winchester JA, Pharaoh TC, Verniers J. Palaeozoic amalgamation of Central Europe. Vol. 201: 343. London: Geological Society; 2002. DOI: 10.1144/gsl.sp.2002.201

[170] Kröner U, Hahn T, Romer RL, Linnemann U. The Variscan orogeny in the Saxo-Thuringian Zone – heterogeneous overprint of Cadomian/Paleozoic Peri-Gondwana crust. In: Linnemann UR, Nance D, Kraft P, editors. The Evolution of the Rheic Ocean: From Avalonian-Cadomian Active Margin to Alleghenian-Variscan Collision. Geological Society of America Special Paper; Vol. 423. Boulder, USA: The Geological Society of America; 2007. pp. 153-172. DOI: 10.1130/SPE423

[171] Cogné J. The Cadomian Orogeny and its influence on the Variscan evolution of western Europe. In: D'Lemos RS, Strachan RA, Topley CG, editors. The Cadomian Orogeny. Vol. 51. London: Geological Society; 1990. pp. 305-311. DOI: 10.1144/GSL.SP.1990.051.01.19

[172] Crowley QG, Floyd PA, Winchester GA, Franke W, Holland G. Early Palaeozoic rift-related magmatism in Variscan Europe: Fragmentation of the Armorican Terrane Assemblage. Terra Nova. 2000;**12**:171-180. DOI: 10.1046/j.1365-3121.2000.00290.x

[173] Floyd PA, Winchester J, Seston R, Kryza R, Crowley QG. Review of geochemical variation in Lower Palaeozoic metabasites from the NE Bohemian Massif: Intracratonic rifting and plume-ridge interaction. In: Franke W, Haak V, Oncken O, Tanner D, editors. Orogenic Processes: Quantification and Modelling in the Variscan Belt. Vol. 179. London: Geological Society; 2000. pp. 155-174. DOI: 10.1144/GSL.SP.2000.179.01.1

[174] Nowak I, Żelaźniewicz A, Dörr W, Franke W, Larionov AN. The Izera metabasites, West Sudetes, Poland: Geologic and isotopic U–Pb evidence of Devonian extension in the Saxothuringian Terrane. Lithos. 2011;**126**:435-454. DOI: 10.1016/j.lithos.2011.07.006

Chapter 4

Eruption Scenario Builder Based on the most Recent Fissure-Feed Lava-Producing Eruptions of the Arxan-Chaihe Volcanic Field (ACVF), NE China

Bo'xin Li, Károly Németh, Julie Palmer, Alan Palmer, Vladyslav Zakharovskyi and Ilmars Gravis

Abstract

Fissure eruption is the most prominent type of Pleistocene to Holocene volcanism in Arxan-Chaihe Volcanic Field recording vent migration along fissures. This research is examined Sentinel Satellite Images to outline the youngest lava flows in the region in conjunction with field observations. Also, GIS-based analyses were performed with the aim to calculate the volumes of lava flows to determine the length of the lava flow emissions. Topographic cross sections and various geomorphological parameters (e.g., geomorphon and topographic position index) were used to reconstruct the pre-eruptive geomorphology of the region to simulate lava flow inundation using Q-LAVHA plug in the QGIS package. Pre-eruptive topography was created, and various simulations were used to obtain the best-fit lava inundation. This process yielded to estimate an average of 5 m lava flow thickness. The same parameters of the lava flow simulations were used to run on the post-eruptive topography to simulate future lava flow inundation. Results showed that the lava flows best simulate if they emitted along a NE–SE trending fissure between two young vent zones or in an extensive elongated area following the NW–SE trending valley axis initiated from the Yanshan vents.

Keywords: scoria cones, pyroclastic, lava flow, fissure eruption, lava fountaining, strombolian eruption, satellite imagery, GIS

1. Introduction

Lava flows in every volcanic field represent the major volcanic events and significant phases of volcanism [1]. The most distinctive characteristics of lava flows are their surface morphology. Such surface "shapes and patterns" not only represent the interests of tourism and scientific exhibitions but also reveal great value for

IntechOpen

interpretations of how volcanism occurred, potential indicators of petrogenesis, shifting of eruption phases, eruptive magnitudes (volumes and ejection pressures), and geochronology of how long an eruption last. In general, two types of the morphology of lava flows have been described in the literature: ʻaʻā type and pāhoehoe [1]. pāhoehoe lava flows commonly emerge during events of Strombolian style eruptions with low viscosity and high-temperature basaltic eruptions [2, 3]. This type of lava flow is usually known for its smooth surfaces and gentle undulations, with occasional hummocky surfaces and tumuli. In general, pāhoehoe lava flows can extend tens of kilometers in distance from their sources [3]. Small outflows alternatively emerge from the chilled crust of the surface and can feed small "toes", which are approximately no more than few dm thick, several m long, and dm-to-m wide. Pāhoehoe lava flows are associated with low outflux velocity; this means the volumetric flow rates are about 2–5 m^3/s and slow flow front velocities are approximately 1–10 m/hr. [3]. These behaviors of the emplacement are shown by the low flux velocity profile allowing the flows to develop a chilled crust keeping the melt able to move. Thus, the forehead of flows commonly proceeds moving slower than the lateral partitions of the flow body; this indicates not only the flow can maintain undisrupted with smooth and intact surfaces but also preserve "toe" structures while the flows keep moving. Like its counterpart, aa-type lava flows commonly present as extremely rough surfaces with spikes and swarmed gullies [1]. ʻaʻā lava type generally has denser inner parts. The emplacement behavior shows that the flows commonly have a thick (1–2 m) chilled shield surrounding the main lava body. The forehead of rough surfaces with clinkers can be broken while the flow moves [4–6]. The fallen part will eventually be buried by the bottom of the flows. Topography can affect significantly how the flow moves, and facilitate ponding or cascading effects in steep steps or behind obstacles or valleys. Pāhoehoe lava can also become rubble where chilled crusts can be broken apart and carried rapidly further. In this case, morphotypes could work better to describe the flows (e.g., [7]).

Following the regional tectonic trends, fissure eruptions always generate large volumes of lava, which form the continental flood basaltic lava provinces [8, 9]. Commonly, the lava provinces can stretch into hundreds to thousands of km^2 areas. Due to the volumes of the lava that ejected, a basaltic flood lava province usually was formed over long time, extreme in a period of 1 to 2 million years [10, 11]. The fissure eruptions generally are related to the continental rift zones, such as East African Great Rift [12]. The stretching or rifting property usually produces large lava volumes These geological settings are usually defined by monogenetic volcanic fields. They are defined by tens to hundreds of small vents formed due to mainly two eruptive styles, such as Strombolian, Hawaiian, and phreatomagmatic types [13]. Those small vents usually swarm and confine in a large region (e.g., thousands of km^2). The occurrences of monogenetic volcanic fields are commonly shown by the linear trend of vents, clustering, or randomly distributed all strongly influenced by the crustal structure of the region where they erupted [14, 15]. In old continental crusts inherited structural elements commonly influence the vent distribution of monogenetic volcanic fields and can be controlled by the regional fracture zones, which could subsequently form fissure-aligned volcanic systems [14].

The products of monogenetic volcanism are commonly revealed as scoria cones, cinder cones, tuff cones, tuff rings, lava flows, and pyroclastic materials (formations of ashes and density currents). Those straight-generated and primitive volcanic products can be easily affected by the local environments and climates; in other words, the surface processes (Kereszturi et al. 2011). When the surface processes influenced the young volcanism, it could vastly change the outlines of the topography and landforms [16]. Also, the pre-existed landforms play an important role in forming subsequent volcanic landforms, such as hydrogeology-controlled lowlands and complexities of country rocks.

Modeling for lava flow emplacement is one of the interests of interpretations of lava eruptions in some ways that are beyond human records. Long lava flow commonly indicates flows extending approximately more than 100 km from their sources [17] (Stephenson et al. 1998). In general, long flows can generate rapid and insulated emplacements. The rapid model can expect lava flows exceeding 100 km from sources [17], with less than 0.5°C/km of chilling stages under the transporting velocity of approximately 2–15 m/s. The insulated models prefer flows outfluxing under low velocities [3, 12, 17], for example, 0.1–1.4 m/s. Also, insulated emplacements can be expected the thickness of flows to be no more than 23 m at the maximum, with effusive rates at about 8–7100 m^3/s [3]. Slope datasets are the essence of all the above-mentioned assessments. The flows that were emplaced by rapid aspect should be distinguished by the channel-fed structures, for example, lava channels on the surfaces of ʻaʻā type, and expected as generated from short-lived lava fountaining. On the other hand, the insulated aspect can be expected to produce a range of inflated tube-feeding, and sheet pāhoehoe flows within a long distance from their sources/vents. Such flows are also marked as an indicator of a long-lived ponding system [3].

Volcanic eruptions commonly reveal themselves as multi-phases and prolonged event during the syn-eruptive stages. Also, building a range of eruption scenarios can allow researchers to have a better view of the complexities of volcanic eruptions and volcanic uncertainties [18]. In general, the eruption scenarios contain four major aspects: eruption locations, types of eruptive phases, duration of a single phase, and occurrence and frequency of hazards. Eruption locations indicate short-lived and small vents with their distributions and a single large composite volcano, which produces long-lived and complex volcanic events. The transitions between different eruptive types show that the diversities of volcanism are the current and future preceding states of volcanoes. Durations of eruptive phases analyze the potential magnitudes of local volcanism and are considered either discrete or prolonged eruptions. Hazards' frequencies and occurrence are considered as the influences of erupted gas, blast styles, pyroclastic density current-triggered syn-eruptive disasters, and post-eruptive lahar events.

In NE China, numerous mafic monogenetic volcanic fields formed through the Cenozoic. Among these fields, there are volcanic fields that had historic volcanic eruptions including lava effusions such as those known from Wudalianchi [19, 20] and the Arxan-Chaihe Volcanic Fields [21]. Two young volcanoes located in the southeast part of the Arxan-Chaihe Volcanic Field (ACVF), that is, Yanshan-the "triple vent" and Gaoshan (eastern side of YS), have been dated under the C^{14} method, which revealed the ages of those two vents about 1900–1990 cal a BP [21, 22].

The major aim of this research is to focus on providing the best possible eruption model to understand the potential impact of a similar eruption in the future based on the youngest eruptive event in the region that occurred approximately 2000 years ago in ACVF. To constrain this, we employed satellite images that show the surface successions of lava flows as a range of typical indicators of how to build the possible chronicle of the vent onset events and the subsequent ponding processes in the volcanic histories of ACVF. Thus we propose that the youngest eruption in the region took place along fissure-dominated vents. As the ACVF is part of the UNESCO Global Geopark network [23], volcanic hazard needs to be treated seriously and this work provides valuable geology-based information and lava flow simulation to envision the likely eruption scenario the region may face in a future volcanic eruption.

2. Geological settings

ACVF is located on the eastern side of Inner Mongolia, northeast of China (**Figure 1a**). The Great Xing'an Mountain is the basement holding ACVF's volcanism as a distinctive geomorphological outline, which vastly distracts and draws the interests of both tourism and commercial behaviors.

The volcanism of ACVF is the most targeted element of local interest, not only its rareness but also the value of research. ACVF is a distinctive volcanic field due to its distance away from Japan Subduction Zone, about 200 km. Such a long spatial span indicates that the general background of ACVF is mostly controlled by the intra-continental settings, which are influenced by a distant convergent plate margin [24]. ACVF is located on the western side of Song'liao Graben, which is an enormous geological and structural subsidence in the center of NE China in consideration of a rifting-zone environment. One of the conventional concepts is that the delamination of supra-crustal layers takes place on the weak points so that the rifting processes can generate large subsidence areas, that is, grabens, on the local territories [25]. The subduction zone fueled the delamination processes, which manifested the increasing activities of rifting. The basement of ACVF is approximately formed in the middle to late Mesozoic eras. Previous pieces of research show that the major components of the basement of the Great Xing'an Range are composed of Mesozoic volcanic and granitoid materials. The dwelling elements such as zircon, whole-rock elements, and Hf isotopic composition indicate the properties of the Great Xing'an Range. Geochronology (mostly K-Ar and Ar-Ar techniques) shows that there are at least three stages of the evolutionary histories of the ranges. The felsic volcanic rocks were formed in the Middle-Late Jurassic periods about 174–148 Ma; intermediate and intermediate-felsic volcanic

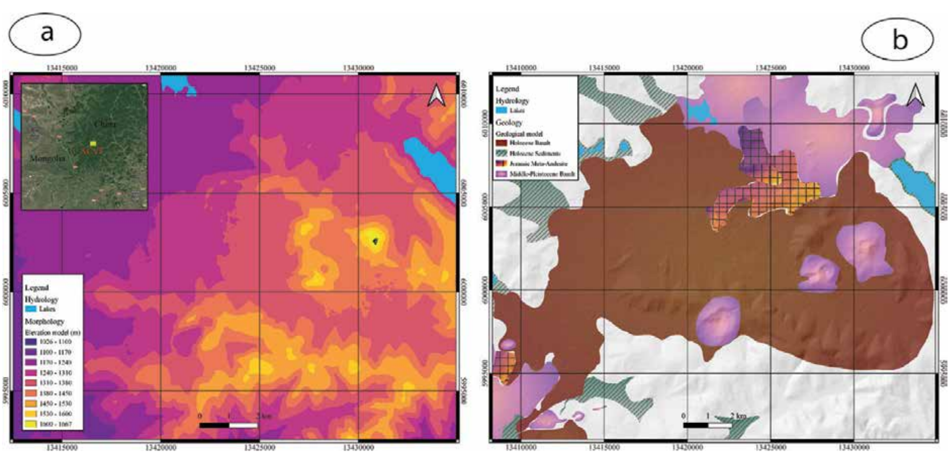

Figure 1.
The general morphological aspect of the Arxan-Chaihe volcanic field (a) and its simplified geological architecture (b). Topography is based on SRTM 30 m resolution digital elevation model. Geology information is derived from (Wang et al. 2014). Please note that the young lava flow extent is greatly overestimated. Reconnaissance mapping indicated that many regions shown on this map covered by the youngest lava flows are not accurate and they are rather part of old lava flow fields. Maps are on WGS84 projection using NE China local coordinate system.

rocks were created in the Early Cretaceous intervals about 142–138 Ma, with no later than 125 Ma; normal felsic volcanic rocks were generated in the Early Cretaceous about 140–120 Ma, with the major volcanic events at 125 Ma. Upwelling mantle movements are the general factor of the compositions of Mesozoic volcanic rocks; this very well corresponds to the methods rifting system of Song'liao Graben [25].

The youngest activities of volcanism at ACVF occurred approximately 2000 years ago. Previous research shows that the lava flows cover the major areas of the Arxan UNESCO Global Geopark with several intervals of the ages. K-Ar method (whole rock) reveals the ages of the bulk lava flows in multiple vent locations of AVCF. Lava flows on both riverbanks of Halaha River erupted at about 0.587 ± 0.18 Ma [21, 26]. Among them, the youngest lava flows were generated from Yanshan's "triple vent" about 1990 to 2000 years ago. All these flow or bulk volcanic rocks are basalt or trachybasalt. The mafic property makes those flows follow the specific rheology and emplacement mechanisms of forming a range of young landforms of volcanism [21, 26, 27].

Up to now, 47 vents have been recognized by various field trips or through satellite images (Li et al. 2021). The ACVF occupies an area of about 2000 km^2 in hill country (**Figure 1a**). Those vents are aligned from southwest to northeast, especially along the study area (**Figure 1b**). For instance, on the eastern side of Tianchi Lake, two paralleled fissures indicate the propagation processes during the syn-erupted stages (**Figure 2a**-**d**). This feature is also found on the eastern side of Dichi Lake (**Figure 2a**-**d**). From the satellite images, the two ends of ACVF are marked by Wusulangzi Lake in the southwest corner (**Figure 2a**-**d**) and Tongxin Lake in the northeast corner. Between those two lakes, at least 15 vents are aligned through a distinctive orientation, which is SW-NE. Thus, vent distributions of ACVF show that the local tectonic trends, such as fissure orientations, follow a general direction, which is SW-NE directed trend [23, 24].

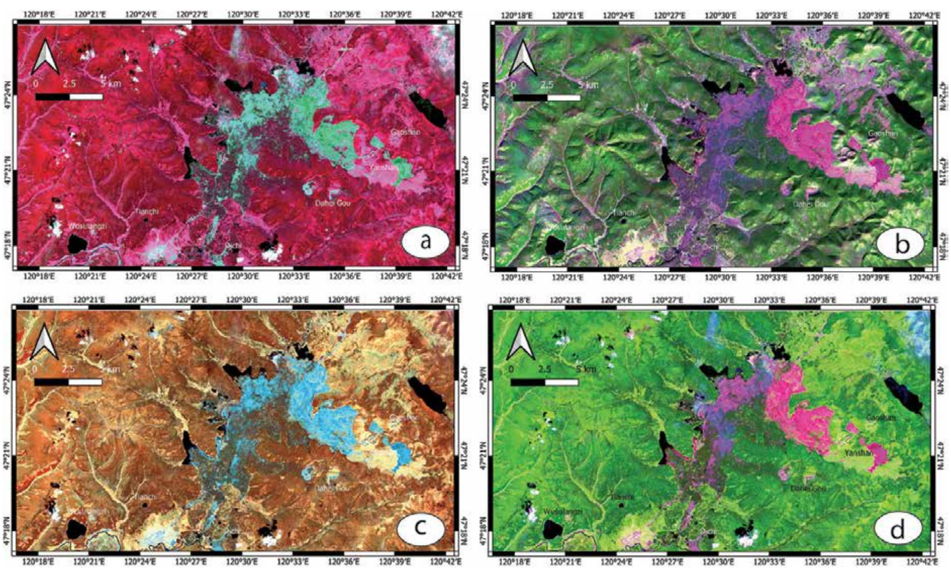

Figure 2.
Sentinel satellite images of the Arxan – Chaihe volcanic field showing the distinct texture of the young lava flows. a) False color image; b) SWIR image; c) geology – Band 8, 11, 12; d) geology – Band 12, 8, 2. Maps are in WGS84 projection using geographical coordinate systems.

Present-day geomorphology of the region of ACVF is revealed by a range of post-eruptive landscapes with volcanic products. The currently available geological map (**Figure 1b**) shows an extensive lava-covered region marked as Holocene basalt. Interestingly, in this maps the three volcanic cone complexes, Gaoshan, Yanshan, and Dahei Gou marked as Middle Pleistocene basalts distinctly separated from the young lava flows (**Figure 1b**). The targeted two vent complexes (Yanshan and Dahei Gou) are scoria cones with welded cores and various clastogenic lava units indicating eruptions where Hawaiian and Strombolian style eruptions alternated over the activity. On the present-day Halaha riverbanks, the youngest lava flows extend over 10 km on average and are suspected to reach about 16 km SW from their source following the paleo-Halaha River valley (**Figure 2a**-**d**). The surface structures of the flows represent the two distinctive pāhoehoe and ʻaʻā types. Also, pāhoehoe flows preserve a range of ponded fabrics such as ponded lakes, lave tubes, whalebacks, and tumuli. Lava channels can be observed in a partially collapsed SW side of the Yanshan scoria cones.

3. Methods

Sentinel imagery is a ground-breaking aerospace technology, which was carried out by European Space Agency in 2014 (https://apps. sentinel-hub.com). The missions aim at the goals of agricultural monitoring, emergency management, land cover classification, and water quality. This research applies the satellite images depicted from the Sentinal-2 orbital system. The main reason for this research by utilizing the Sentinel images is that lava flows or products of volcanism can vastly reveal a range of different textures or visual effects of imagery on the satellite photography system compared to the textures of surrounding areas. Yanshan (YS) and Dahei Gou (DHG) are the two vents that generated the youngest morphologies of lava flows covering an area of at least about 70 km^2. Please note that on the geological map, the young lava flows are marked in an area significantly larger than the real extent of the lava flows suggested by our reconnaissance mapping. The images from the Sentinal-2 system reveal a series of flow textures under different observation methods (**Figure 2a**-**d**). Thus, the targeted two vents, that is, YS and DHG, and their eruptive products (mostly lava flows) might be outlined by systematical analyses of remote sensing and GIS methods in relation to the observed lava successions. DEM images downloaded from the ALOS-PALSAR dataset (https://asf.alaska.edu/data-sets/sar-data-sets/alos-palsar/) that offers digital elevation data with a resolution of 12.5 m. The accessed DEMs were reprojected to the WGS 84/UTM zone 51 N map datum and coordinate system. Using QGIS (version 3.26 – Tisler) and its SAGA and GrassGIS we created slope maps, hill shades, and topography position index maps to check the general geomorphological details of the region. Cross-sections were utilized to understand the general trends of the morphology of the study area (**Figure 3**).

The Q-LAVHA plugin of QGIS software can provide a general model or a simulation with analyses of pre-eruptive and post-eruptive topography to interpret lava flow evolution histories and future hazard assessments [28, 29] (Mossoux et al. 2016). In general, the Q-lavHA program is a QGIS plugin that simulates probabilities of ʻaʻā lavas distributions from one or multiple distributed eruptive vents on a DEM satellite image [29]. The inserted models, such as probabilistic and deterministic models, can

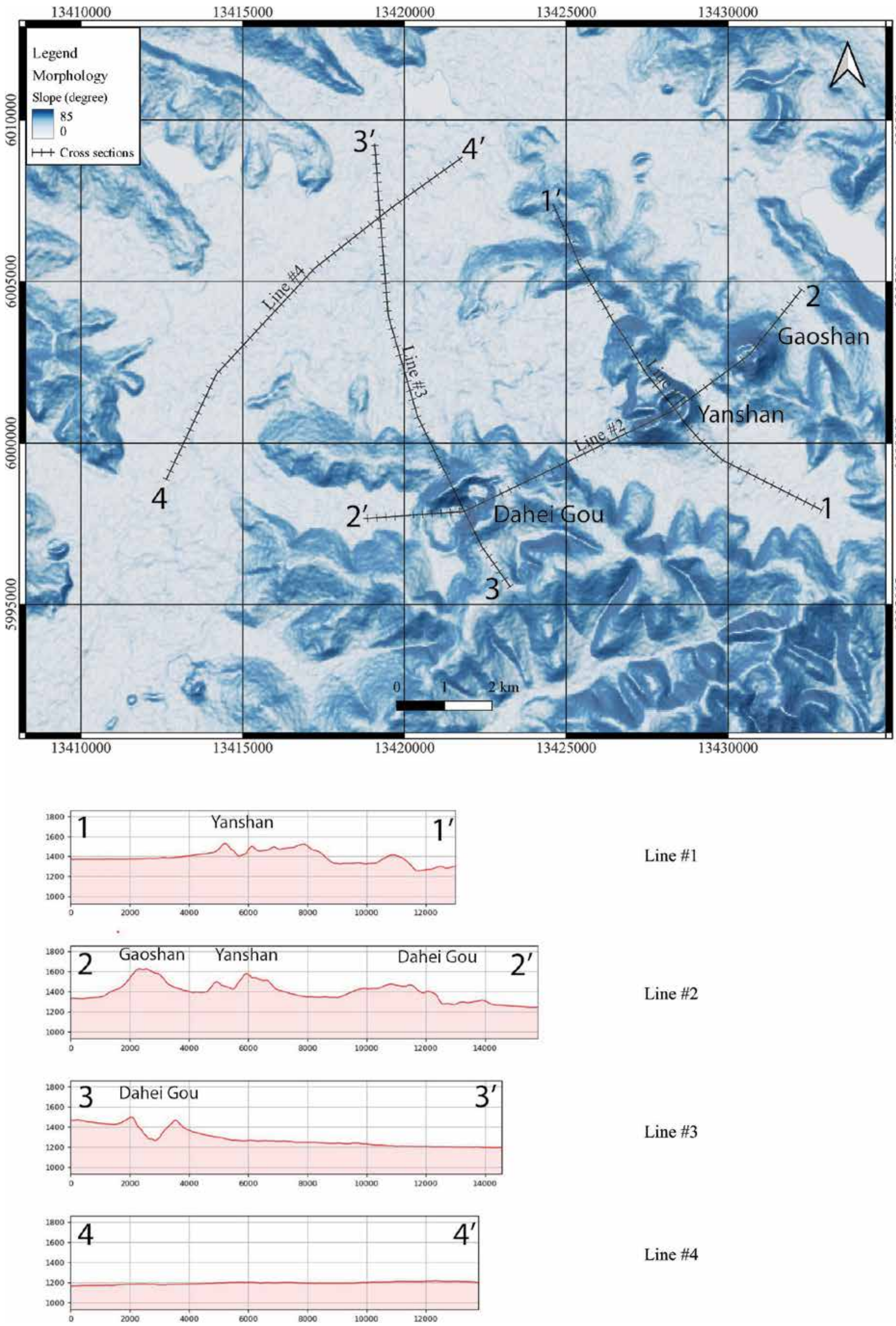

Figure 3.
Slope map of the ACVF showing the characteristic texture of the region with scoria cones and extensive lava flows. Cross sections (lines with numbers on the map) revealed a very gentle sloping landscape upon the lava emplaced. Map is on WGS84 projection using NE China local coordinate system.

provide a range of calculations in relation to probabilities for lava flow propagation and terminal length under spatial aspects [28–32]. The confine of this program is the probabilistic steepest slope on parameters of spatial spreads. The corrective factors are the major algorithm to even the "pits," which may jeopardize the lava modeling processes by obstacles from DEM images. To overcome this issue, the DEM upon the simulation runs need to go through a prescribed preparation outlined in the plug-in manual. We have completed these steps. Moreover, we created a pre-eruptive topography by removing the lava flows on the current DEM. To do this, we created a contour map based on the ALOS-PALSAR 12.5 m resolution DEM and then we manually modified – in a supervised fashion – the contour lines fitting them to the general morphology unaffected by the youngest lavas (**Figure 4a** and **b**).

Based on the new contour lines, we recreated a new pre-eruptive DEM (**Figure 4c**) and visually compared it to the current DEM (**Figure 4d**). To see the validity of the pre-eruptive topography we created slope maps for the pre- and post-eruptive-scenario (**Figure 5a** and **b**) as well as aspect maps (**Figure 5c** and **d**) to have visual control over the process. We decided to follow this manual process, in spite of it being more time-consuming as during the supervised process we had continuous connection to the landscape and we were able to self-evaluate the scenes based on our own field experiences. In the end, we also created pre- and post-eruptive topographic position index maps just to see how the lava flow removal affects this parameter (**Figure 6a** and **b**). Finally, we created a geomorphon map for the present-day situation (**Figure 6c**).

For the Q-LAVHA simulation, we tested all the in-built methods and we found the Euclidian simulation performed the best due to the general low slope angle at our

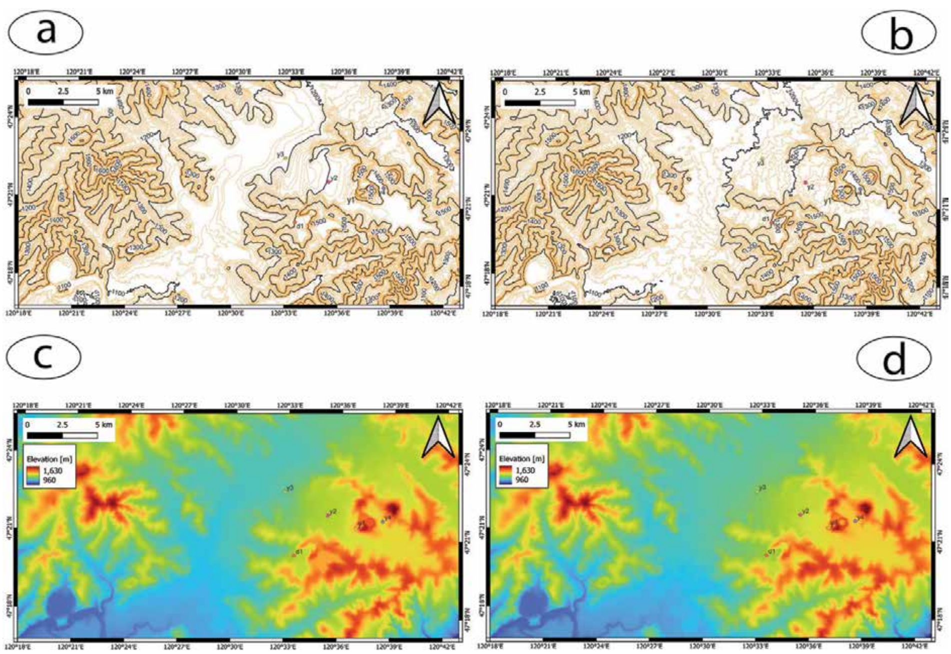

Figure 4.
Contour map of the pre-eruptive (a) and post-eruptive (b) surface. Regenerated DEM of the pre-eruptive surface (c) was used to simulate lava flow emplacement. Post-eruptive DEM (d) was used to simulate future lava flow inundation. Maps are on WGS84 projection using geographical coordinate system.

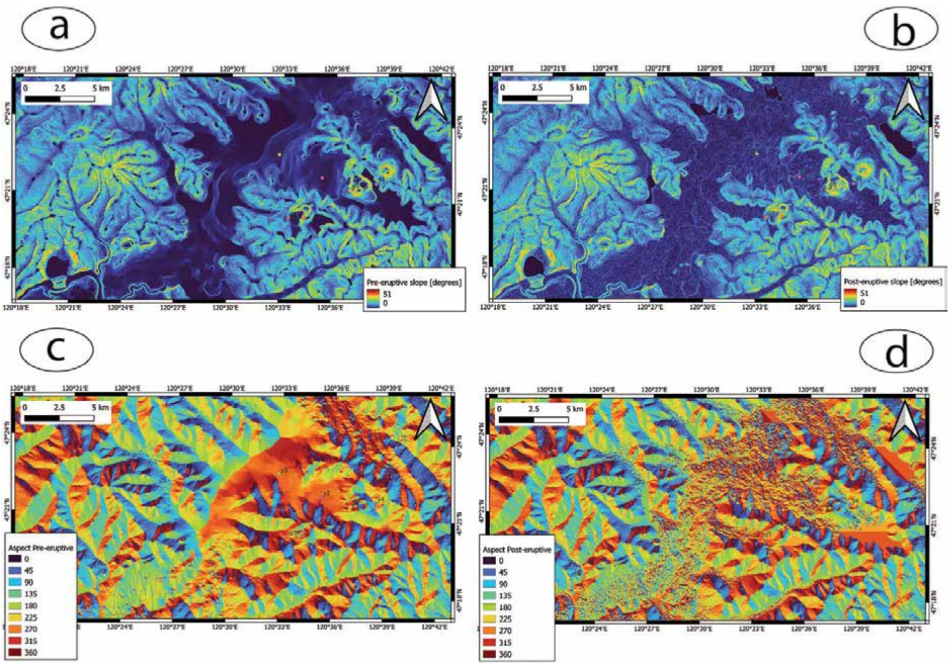

Figure 5.
Pre-eruptive slope map (a) shows the general trend of the landscape, while post-eruptive slope map demonstrates the rugged flow fields (b). Aspect maps of the pre-eruptive morphology (c) indicate a good trend to the general landscape characteristics. Aspect map of the post-eruptive surface (d) shows the rugged nature of the lava flow field. Maps are on WGS84 projection using geographical coordinate system.

lava flows emplaced (an average of less than 1 degree). Within the simulations, we increased the simulation distances from the measured maximum lava flow runout distances. As other researchers used Q-LAVHA on regions of low slope angles (e.g., flat surface) such as Paricutin in Mexico [33], we followed their recommendations to increase the simulation length well over 10 times of the measured lava flow length. In Paricutin, even 50 times longer simulation length has been applied. In our work, we find the simulation distance about 25 times longer than the average lava flow runout distances provided good results, hence in our work we followed this simulation distance (e.g., 250 km for a 10 km long, or 100 km for a 4 km long lava flow).

The terminal length is considered as FLOWGO Model [31] through the definitions of fixed length values, a function of statistical length probabilities, and thermal-rheological properties of open-channel lava flow [7]. While Q-LAVHA offers the FLOWGO simulation, it requires numerous physico-chemical parameters [19]. As we do not have most of those data, we have not explored the FLOWGO to the full extent, instead run some tests with likely parameters drafted from variable literature [34–36]. As field evidence indicates that the eruption, at least in the Yanshan vent complex reached high intensity in times as evidenced by the presence of abundant clastogenic lava flows, we applied high magma mass flux rates, mafic composition, high-temperature conditions, and wide flow channel parameters.

The lava flow simulation method was performed by Q-LAVHA within QGIS. Three different modeling concepts have been carried out: points, a line, and a polygon [29]. A single point or multiple points are the envisions of vents that probably erupted flows around Yanshan areas. Lines are the simulations of fissure vents. Polygons

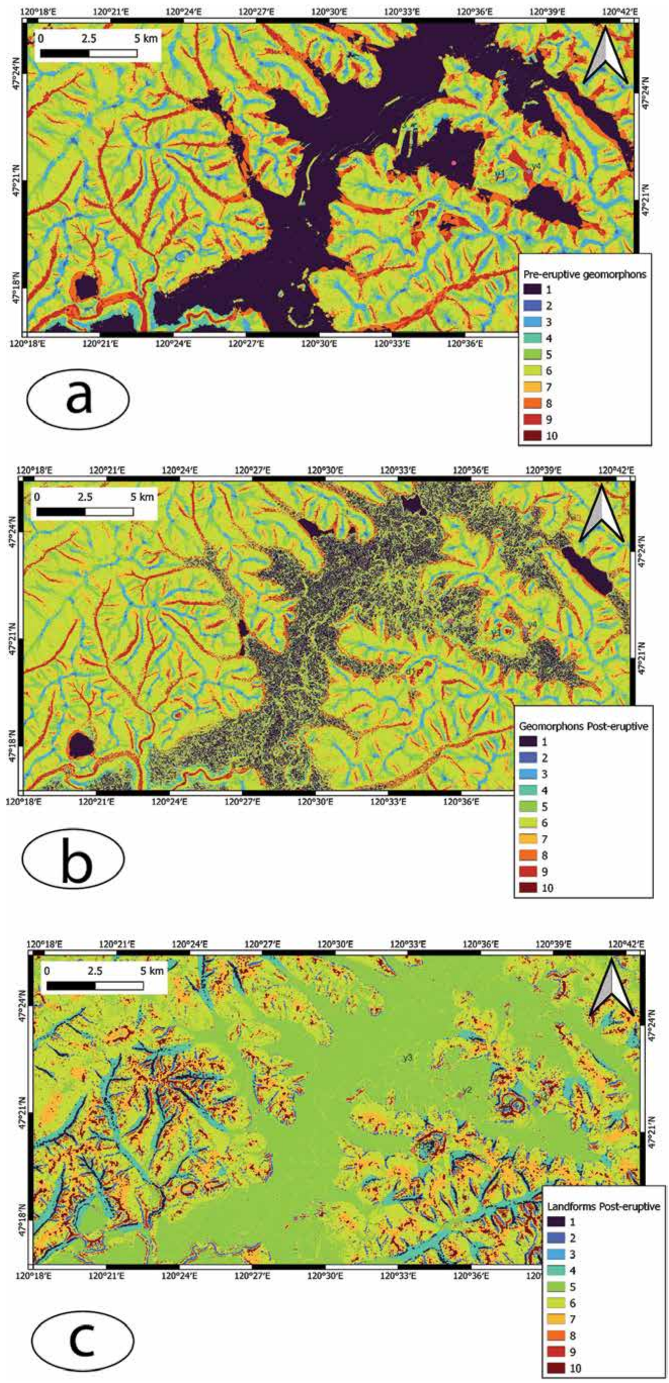

Figure 6.
Pre-eruptive (a) and post-eruptive geomorphon maps show clearly the topographical differences the landscape received through the lava inundation. Codes refer to the following parameters: 1) flat; 2) summit; 3) ridge; 4) shoulder; 5) spur; 6) slope; 7) hollow; 8) footslope; 9) valley; 10) depression. Topographic position index map (c) of the post-eruptive (present-day) landforms show the variety of landforms the region has. Codes are: 1) canyons, deeply incised streams; 2) midslope drainages, shallow valleys; 3) upland drainages, headwaters; 4) U-shaped valleys; 5) plains; 6) open slopes; 7) upper slopes, mesas; 8) local ridges, hills in valleys; 9) midslope ridges, small hills in plains; 10) mountain tops, high ridges. Maps are on WGS84 projection using geographical coordinate system.

imply vent swarms. For the simulation processes, the preparation of DEM images is necessary. The resolution of a DEM image used is approximately 12.5 m in pixel sizes. Then, the contour map was treated in a supervised fashion, essentially adjusting the contours where the lava flow clearly acts as an addition to the morphology. Utilizing the GrassGIS plugin of QGIS is the next step to rebuilding a DEM image with a new corrected pre-eruptive contour line. It is also important that all the maps must be projected properly to UTM coordinate with the NE China sections.

In the end, we applied 5 m average lava flow thickness and run the flow simulation on the current topography to see potential lava inundation in case a similar eruption take place in the same vent locations as those created in the 2000 AD lava flow fields. As mentioned above, several methods of Sentinel Imagery have been applied to the areas of YS and DHG.

False-color imagery (**Figure 2a**) aims at observations of at least one non-visible wavelength to image Earth, which is generally composed of red and green bands in a very popular recognition of images. False-color imagery is most used to assess plant density and healthy conditions since plants reflect near-infrared and green light while they absorb red. Cities and exposed grounds are gray or brown, and water appears blue or black. In this image, the youngest lava flows appear as green color regions with specific flow-banded patterns. Ash is shown up in pink smooth pattern that fills topography lows. From ash, loose alluvial deposits can be difficult to distinguish but their surface pattern is slightly different.

Short wave infrared composite (SWIR) measurements (**Figure 2b**) can estimate how much water is present in plants and soil as water absorbs SWIR wavelengths in the optical spectrum. Shortwave-infrared bands are also helpful in distinguishing between cloud types (e.g., water clouds vs. ice clouds), snow and ice, all of which appear to be white in visible light. In this classification, vegetation appears in green gradients, soils and infrastructures are in brown gradients, and water appears to be black. Newly burned lands are strongly reflected in SWIR bands, making them visible for mapping fire events. Each rock type differently reveals shortwave infrared light, making it possible to map geology by comparing different colors of reflected SWIR light. Barren lava flow surfaces appear in pink tones reflecting the quick depletion of moisture from porous, dark lava surfaces.

Geology 8, 11, and 12 composite uses both shortwave infrared (SWIR) bands 11 and 12 to differentiate among different rock types (**Figure 2c**). Each rock and mineral type reflects shortwave infrared light differently, making it possible to map out geology by comparing reflected SWIR light. Near-infrared (NIR) band 8 highlights vegetation, contributing to the differentiation of ground materials. Vegetation in the composite appears red. The composite is useful for differentiating vegetation and land, especially geologic features that can be useful for mining and mineral exploration. In the Arxan region, young lava flows appear bright blue and differ significantly from the background brownish-reddish (mostly dry vegetated) regions (**Figure 2c**).

Geology 12, 8, and 2 composite use shortwave infrared (SWIR) band 12 to differentiate among different rock types. Each rock and mineral type reflects shortwave infrared light differently, making it possible to map out geology by comparing reflected SWIR light. Near-infrared (NIR) band 8 highlights vegetation, and band 2 detects moisture, both contributing to the differentiation of ground materials. The composite is utilized for finding geological formations and features (e.g., faults and fractures), lithology (e.g., granite and basalt), and mining applications. At Arxan, the image shows clearly the young lava surfaces against the vegetated background (**Figure 2d**).

4. Results

4.1 Lava flow morphology and the sources of the youngest AD2000 eruption

Field observations have already determined that YS (**Figure 7a**) and DHG are the two large scoria cone complexes that generated significant morphologies of lava flows.

YS, The Triple Vent, preserves three distinctive scoria cones with visual successions from the observations of satellite images (**Figure 2a-d**). As **Figure 2a-d** depict, YS composes of three distinct volcanic edifices overlapping each other with a total area of 2.2 km^2. Fieldworks indicate that the highest elevation (approximately 1597 m above sea level) is observed on the top of the jointing point between the southeast one and the southwest one (**Figure 7b**). Scoria caps cover the top of the triple vent. The steepest slope is located on the southern flank of the edifice, which is nearly 47 degrees due to the welded nature of the proximal scoria and spatter beds. A breakage merges on the southwestern cone with outpouring lava flows that form a range of influxes at least 3.77 km long into the broad fluvial valley of the Halaha River. Scoria ash and lapilli formed deposits that blanketed at least 1 m thick units in an area mostly to the east of the Yanshan vents (**Figure 7c**). The Sentinel images reveal that ash plain extends about 4 km from the Yanshan volcanic complex and traces of valley accumulated ash up to 10 km from the source are likely based on the satellite image pattern. The eastern side of the Yanshan edifice is truncated and a hummocky surface can be traced about a km from the cone flank indicating an early collapse of the vent toward the east. The rafted cone fragments were subsequently covered by the ash plain (**Figure 2a, b** and **d**). Lava flows preserve a range of distinctive features of morphologies, such as

Figure 7.
a) Yanshan complex scoria cone from the south. Note the steep slope and the wide-open crater toward the SW. b) Extensive ash plain over lava flows indicate that explosive eruption took place after the first effusive stage. C) the broad and deep crater of Yanshan is surrounded by steep crater rim formed by clastogenic lavas.

rubbly pāhoehoe (**Figure 8a**), rugged surface textures (**Figure 8b**), lava channels, and tumuli. Similar to YS, DHG is located in the southwest direction of YS, about 5 km.

The total area of the vent is approximately 2 km^2. In the areas of lava flows influenced by DHG, raft-shaped spatter sections and large slabs of lava that randomly pack in chaotic nature are shreds of evidence of the outpouring of lava from the vent. Inside the crater areas, individual tumuli, ramped-up lava rubble/talus, and large piles of ʻaʻā lava blocks form a range of rough surface topography. Lava flows along the crater margin preserve several meter-long cracks parallel to the crater margin. These zones, as mentioned above, are represented as fractures along the inflated and ponded intra-crater, where ponded lava collapsed upon the partial evacuation of the large crater. DHG is composed of at least three major nested crater systems (**Figure 2b** and **d**), which indicate vent migration, crater infill, and sudden releases of lava forming a pit-like crater system. Those extended lava fields and morphologies of the vents have drawn interest in eruption histories and geoconservation purposes [23, 24].

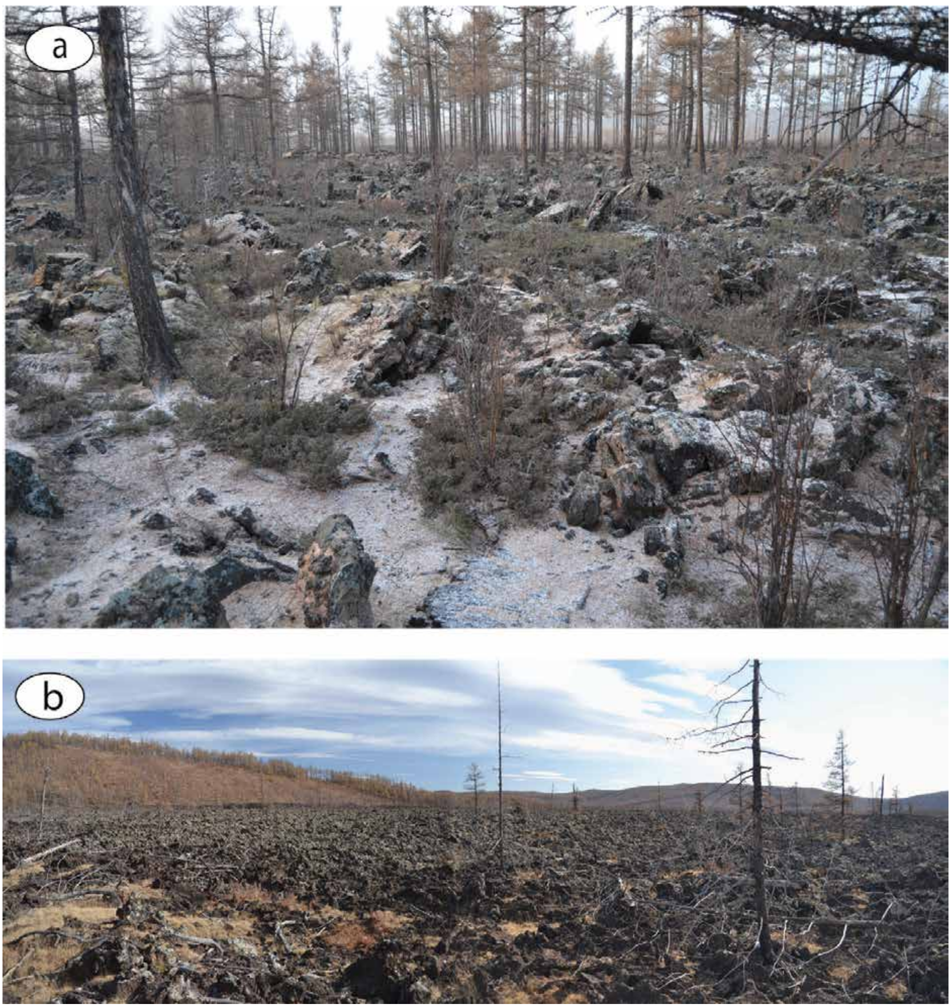

Figure 8.
a) Typical distal lava flow field along the Halaha River valley, about 8 km from the source. b) Typical proximal lava flow field in the upper basin just east of the Yanshan volcano group.

General observations on satellite images such as the Sentinel image sets reveal a complex lava flow emplacement history. Three vents of the YS are clearly overlapping each other. On the basis of the overlap, a relative chronology can be established. The northern edifice formed first followed by a new edifice grown in its southeastern flank. Later on, a third edifice was built on the western margin of the second cone. It is evident that the northern, first cone likely suffered a collapse event and a large part of the edifice was rafted away, forming a hummocky landscape in the eastern regions. It is also evident that the majority of the youngest lava flow is not covered by ash, hence the main ash-producing eruption, inferred to be sub-Plinian (based on the estimated extent of its deposits), was followed by the main lava effusion toward the west and from a small fissure just NE from the first Yanshan cone.

The main lava flow can be distinguished into at least five satellite image patterns not including the valley filling flow segment inferred to be derived from Dahei Gou (**Figure 9a**). The patterns are very similar in each sentinel image; hence they are likely to be reasoned from some geological feature. The main lava flow has a whirlpool-like pattern (**Figure 9b** and **c**), indicating flow movement and interaction with obstacles like tumuli; pressure ridges formed slightly earlier in the same flow field. All the sentinel images show that the main lava flow from YS made into the paleo-valley of the Halaha River. They are not covered by ash; hence they clearly represent the youngest eruptive event in the region. The whirlpool-like pattern on the main flow indicates a higher portion of the lava margin on its N-NE side of the confining valley than on the S-SW side, suggesting that the flow likely made a curved move anticlockwise (**Figure 9a**). The elevation difference between the two edges of the flow (on profile 2) is about 40 m indicating a slightly westward inclined surface on what the lava emplaced (over 3660 m, about 40 m elevation difference yield to a slope of no more than 1 degrees, a very flat landscape). A low slope angle means that the lava emplaced in a very gentle sloping landscape, so no wonder it generated some ponding once entered the main flow channels of the paleo-Halaha River. On the NE-SW sections of the main YS lava flow, the flow thickness is estimated to be less than 10 m in proximal areas but in the flow edges the flow became thin, often only around 1–2 m thick. On the basis of the geological observation, a 5 m average flow thickness is a realistic estimate. In the thickest part of the lava flow fields and some ponded sections, the lava thickness may reach 20 m in localized sections. Topography profile from YS and to the far end of the lava field in the SE, over 16,000 m distances, 225 m drop has been recorded, yielding a less than 1° slope again. A low slope angle also indicates relatively thin lava coverage, especially in distal regions which the direct observations confirmed. DHG longitudinal topography profile across the lava flow emitted from DHG also shows a clear drop of 94 m over 6638 m distance, yielding less than a 1° slope. This section forms the main DHG flow part. The satellite image pattern shows the textures of flows from DHG smoother than the ones of Yanshan flows, indicating that the main DHG flow might predate YS. About 1186 m above sea level, a clear 2–4 m drop, and a topography gap was recognized that separated a younger satellite image pattern suggesting that a young flow probably YS origin formed the axis of the river valley fill flows.

Flow thickness is estimated to be similar to YS and fixed to an average of 5 m. DHG topography profile perpendicular to the main flow axis indicates about 7 m higher lava surfaces on the N-NE side of the flow channel, suggesting that the flow slightly climbed in the southern valley margin, just as expected by the movement of the flow from DHG. YS lava flow initiated about 125 m higher than DHG (1381 m versus 1256 m). Judging that both flows emplaced on flat areas with less than 1° slopes, it is

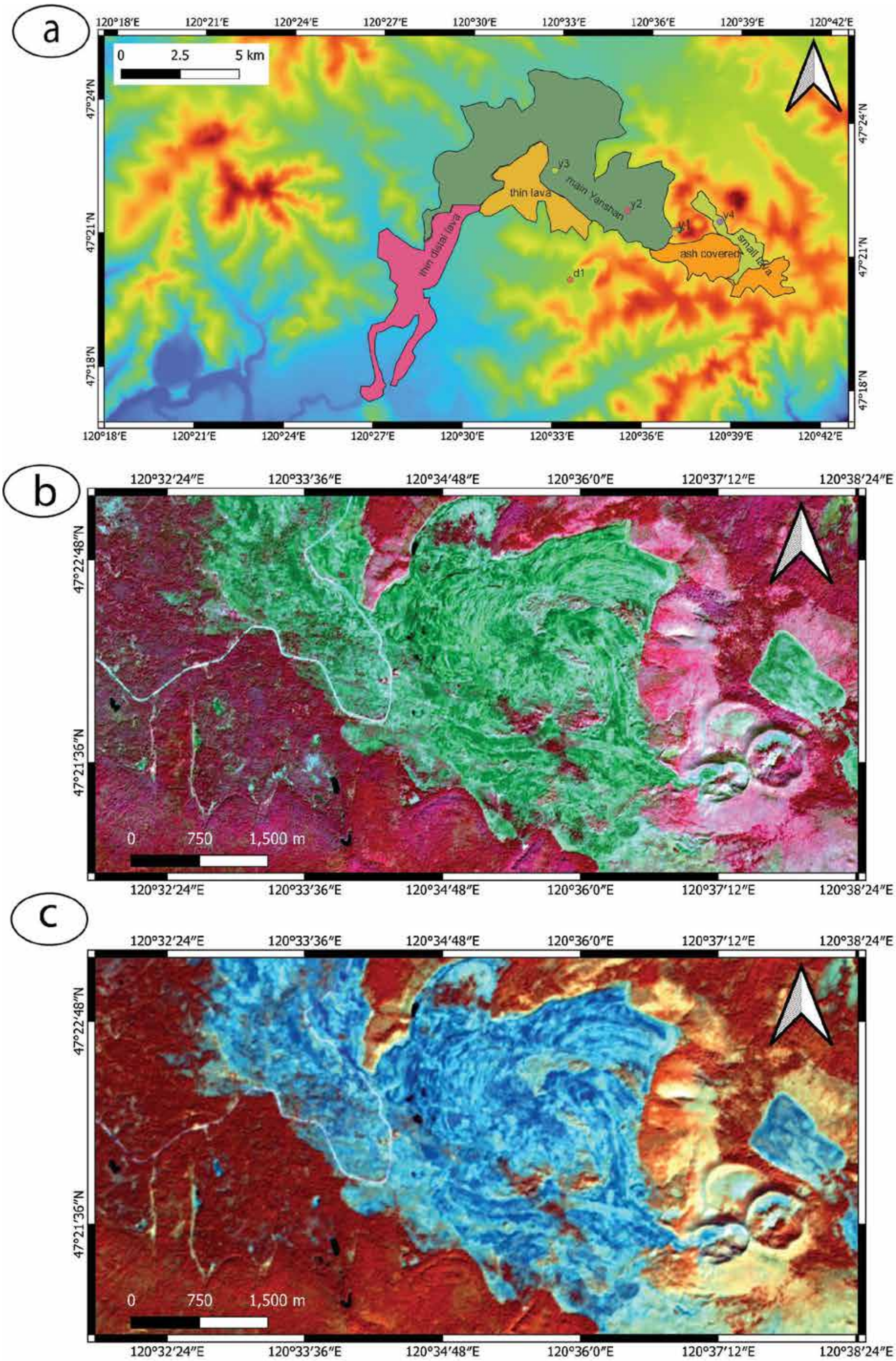

Figure 9.
a) Distinct lava flow regions of the youngest lava flow of Arxan. b) Whirlpool-like lava flow pattern on false color (c) and geology band 8, 11, 12 sentinel satellite images. Maps are on WGS84 projection using geographical coordinate system.

expected that flows, if similar effusion rates are expected, will go further distances rather than go higher elevations (16,000 m vs. 6638 m, YS vs. DHG, respectively). Following the above-mentioned logical steps, it can be assumed that at low lands, some mixing and interflow of lava flows take place, what we recognized as different satellite image textures. From field investigations, we can see that young lava flows are covered by an ash plain of about 2–4 m thick scoriaceous ash in the SE of YS. Light color patterns on satellite images indicate that the ash covers are extensive in the SE of YS and likely reach over 10 km from their source. Field mapping confirms that beneath the ash cover, young lava flows to fill the valley in the SE of YS with a new channel of lava flow probably not thicker than 5 m. These lava flows formed before the ashfall. Satellite image textures indicate that lavas likely erupted and formed after the main ash fall events toward the NW, feeding main YS flows to the Halaha River valley. Thin ash coverages were recorded in NW of YS, in elevated regions and beneath some proximal flows. Satellite image textures indicate that young lava flow erupted from a fissure and filled the valley between YS and Gaoshan and some local lows SE from YS. As Gaoshan is fully covered by ash, following the points mentioned above, it can be stated that the fissure formed after the main ash fall event. In summary, Sentinel images reveal different textures from various methods of waveband observations. Those textures might be the indicators of lava successions and possible eruption histories of major territories of ACVF.

5. Discussion

5.1 Eruption scenarios and possible magnitudes of the events

From the previous research, YS and DHG are two volcanoes formed by effusive or even violent Strombolian eruptions. Successions of lava flow distributed in surrounding areas of these two vents indicate a range of typical histories of syn-eruptive stages and volcanic edifice constructions.

DHG vent opened first in the youngest eruptive events and formed a scoria cone in the NE, gradually shifting fissures toward the SW. Lava outpour from the SW vent of DHG. At least three closely spaced vent/volcano formed, most of them still preserving young volcano morphology. Satellite image textures indicate that some lava flows spill over the SW vent of DHG and feed the main DHG flow. It cannot be ruled out that the flow was not fed from some western flank fissure in the SW vent of DHG, but the satellite image pattern is more indicative of spillover. The dense vegetation cover over the main DHG flow indicates some soil formation over the lava flow surface. Some ash recorded on top of DHG flow indicates that subsequent, probably early Yanshan-sourced ash covered the main flow and the mixed flows in the far valley. The main SW crater is a 1 km wide and about 50 m steep pit crater filled with fresh lava that shows similar satellite image textures to the youngest lava flows and no sign of ash cover. This indicates that this fresh lava must have been emplaced after the main ash falls from YS.

Shortly after the emplacement of the DHG main flow, the complex YS vent system formed. While earlier Gaoshan was assigned to be part of the Yanshan vent system, based on the satellite image pattern and the general morphological architecture of the edifice, Gaoshan is clearly the oldest landform of the YS region as it has erosional gullies typical for older landforms in the region. It is also completely covered by ash inferred to come from YS.

The YS first vent y1 (**Figure 2**) is the northern edifice, a scoria cone with relatively fine-grained deposits. It is not easy to establish if this vent sourced any lava or not. It seems that its SE side might have suffered some collapse as some hummocky surface was observed in the SE of this edifice about a km from its rim, which is in the right position to have some rafted cone there. In addition, in the same scar region, the second set of vents formed y2. This volcanic edifice reached about 100 m elevation and formed a steep scoria cone. The deepest point of the funnel-shaped crater is only about 25 m above the lava fields in the east. This cone must have been active for a long time to build such a substantial size of cone. The cone also evolved in at least two phases as magma withdrawal must have created a crater. After rejuvenation, it formed an intra-crater cone that nearly filled the original crater zone but never grew out of it. This eruption phase was also purely explosive, but its deposits were likely to form localized deposit piles within the major crater and probably the outer flank. This complex explosive activity produced ash plumes that deposited ash that covered earlier lava flows. Such flows are probably emitted due to magma withdrawal during the main cone growth phase. The eruption subsequently built the third volcano just SW from the y2, defined as y3. The y3 built a scoria cone as well, forming an attached cone nearly as high as y2. Gradual SW-ward shift of the activity gradually built another edifice that subsequently changed its activity dominated by Hawaiian-style lava fountaining and building a complex spatter system. This side of the volcanic complex probably suffered some collapse and rafting, letting the magma find its way out toward the west feeding the main lava flow of YS, reaching the Halaha River valley about 16 km away from the emission point.

At the time of the main lava emission, explosive activity was ceased or limited only to small lava fountains and/or localized ash emission toward the east, as the young lava flow surface has no ash cover. Probably at the same time (not really possible to establish relative chronology), a small fissure opened between YS and Gaoshan and emitted a flow that filled the depression just east of the YS system and between Gaoshan and YS. This event also postdates the ash fall event and is likely the youngest phase of the eruption. Interestingly, the Sentinel image textures in the DHG crater also exhibit very young lava morphology, raising the question that DHG probably had experienced an intermittent lava effusion phase that partially refilled the crater. Thus, a complex fissure is an aligned eruption sequence that puts DHG and YS on the same time horizon. Gaoshan is likely part of an older phase of eruptions. Thus, it can be assumed that this eruption was really an extensive event that occurred in a structural alignment (fissure or fault?) about 15 km in length.

The calculations of the estimated volumes of lava pouring can reveal how long the eruption events last. The lava flows are unlikely to form more than 20 m in thickness in ponded regions on valley floors. The estimated volumes of lava emplacements are calculated by a range of standards, such as the eruption types of other volcanic fields (e.g., Mt. Etna in 2001 and Hawaii in 1985). So far, the field identifications and observations, or even classifications, have already yielded an outcome that YS and DHG were formed by a series of violent lava fountaining or effusive eruption events. Also, the steps on the field are indicated that the slope of lava fields is relatively flattened. Thus, the simulations carried out on YS and DHG from the volcanoes with this similar eruptive style can be considered to be valid assumptions of eruption scenarios. In **Table 1**, the rates of lava emplacements are based on different scenarios from varieties of volcanic fields in the world.

From **Table 1**, it can be assumed probably about 14–30 m^3/s interval of the realistic one (green color). These two values mean that the eruption periods lasted about half a

Lava flow	Surface area [m2]	Average estimated thickness (m)	Volume (km^3)	Estimated emplacement time – Negros de Aras (Chile) (m^3/s): 14	Estimated emplacement time Negros de Aras (Chile) (m^3/s): 113	Estimated emplacement time Nyíamuragira 2006 (m^3/s): 145	Estimated emplacement time Mt. Etna 2001 (m^3/s): 30	Estimated emplacement time Lentiscal (m^3/s): 100	Estimated emplacement time Hawaii 1985 (m^3/s): 2
Small YS (y2)	2,845,217	3	0.00853565	7.056589782	0.874267761	0.68132591	3.293075231	0.987922569	49.39612847
Thin mixed lava (yd mix)	12,014,075	4	0.0480563	78.82095929	4.922187398	3.835911558	18.5402392	5.562071759	278.103588
Thin YS (y-d)	7,363,514	4	0.02945406	4.325035232	3.016844477	2.35105811	11.36344753	3.409034259	170.451713
Ash covered YS (y1)	8,537,547	3	0.02561264	68.54108424	2.623385878	2.044431753	9.881420139	2.964426042	148.2213021
Major DHG (d)	10,923,970	8	0.08739176	14.7572615	8.951138971	6.975715198	33.71595679	10.11478704	505.7393519
Mayor YS (y)	37,086,705	8	0.29669364	232.6958946	30.38897493	23.68244253	114.4651389	34.33954167	1716.977083
Total	78,771,028		0.49574405	406.1968246	50.77679941	39.57088506	191.2592778	57.37778333	2868.889167
				In realistic		In min	In realistic		In max

Table 1.
Estimated eruption scenarios of YS and DHG that were calculated by different standards from similar volcanic fields. Color codes are referred to the information outlined in the main text.

year to one and a half years with the continuous development of the entire flow field. However, considering the distinctive flow fields, it can be inferred that major effusive phases, either explosive phases or quiet time, have taken place. Overall, the possible assumption can be estimated that a similar eruption probably took a few years with distinctive explosive phases and separate lava effusion stages from vents along the main structural zones.

The 1983 eruption on Hawai'i was fed by effusion rates of up to 22–44 m^3/s, and flows extended 7 km^2 to form a 6 km^2, 100 × 10^6 m^3 flow field (Trusdell 1995). In contrast, the 1985 eruption (also in Hawai'i) was fed by effusion rates of 0.5–4.5 m^3/s, which resulted in flows extending 1.8 km to form a 2.2 km^2, 19 × 10^6 m^3 flow field (Harris et al. 1997). Effusion rate also appears to control the basic flow dynamics. In Hawaii, effusion rates determine the manner in which flows are emplaced. Effusion rates at 120 m^3/s produce rapidly advancing channelized ʻaʻā lava flows, and effusion rates of approximately 20 m^3/s (but typically more than 5 m^3/s) produce slowly advancing tube-fed pāhoehoe flows (Rowland and Walker 1990). The lava flows at ACVF are somewhere between. In the upper flow regime, they are more like aa-type of lava flows with lots of slabs and rubbly pahoehoe; once they reach the valley floor, they slow down, inflate, and make whaleback features. Considering that the region is very flat, it can be imagined that the flow had to go at a reasonable speed (higher effusion rate) to retain heat to make the lava able to advance. In the end, the flow advanced over 16 km from its source, and even in DHG, the flow reached nearly 7 km. This is a large number and requires a relatively fast-moving flow.

5.2 Lava flow simulation

Sentinel images in different observation methods show the different textures of lava flows around YS and DHG. Those textures indicate the different lava batches, which were systematically emplacing and overlapping each other. As mentioned above, the flow thickness is estimated to be about 5 m on average. While flows accumulated on a very flat surface (less than 1 degree), the program needs a substantial L value of simulation distance to put in as the measured lava runout distance [33]. If given a specific runout distance of the flows, for example, 10 km, the L value would be 10 km. Thus, if given 25 times of runout distance, the L value is actually 250 km. Eventually, the best simulation outcome is 250 km for the lava flow runout distance as the modeling pattern successfully covers the estimated flow areas (i.e., from YS). Field works have already proven that the slope of the flow areas is low, which might be no more than 1°. Such large volumes of flow can only be pushed on the flattened surface by a high effusion rate. Also, the low value of flow thickness with such an effusion rate that leads to large coverage areas of lava flows is approximately 5 m. Eventually, 5 m thickness of the flow pluses and 10 m of the given buffer thickness can help the modeling process switch on the quadrant, and the "16-point" aid makes sure that the simulation does not stop on flat surfaces [29]. The best modeling pattern was created by Euclidean Length, which is that each iteration stops when the flowline reaches the specified Euclidean Length (m). The Euclidean represents the crow-fly distance between the point where the simulation starts and the front of the flow line. This calculation way can let flow patterns freely distribute in confined areas. From the above-mentioned modeling processes, geological implications can be:

1. The flow thickness is probably the best to fix at 5 m, knowing that this might be higher up to 10 in proximal areas or far less in the far end of the flow lobes. This

envision is very well corresponded with geological observations in two seasonal field works.

2. The lava flows probably cannot be in the 3 m range as they are too thin, and the model stops too early, whatever parameters that are fitted in the program.

3. The flows also cannot be more than 10 m range as that creates edifice-like flow patterns with far less lava flow runoff.

Especially applying another single point marking as the vent location shows the model can reach the far north and northeast boundaries of the flow. This newly assumed emission point was put on the territory of a whirlpool-like feature that was apparent in satellite images (**Figure 9b** and **c**), which is suspected to be a buried vent beneath the lava flows.

In addition, this location also falls in the zone where another SW-NE fissure may exist lying on the old Tianchi Lake fissures. The points simulations likely provide the flow from YS in the flow inundation areas (**Figure 10a**-**d**).

However, the problem is that this simulation cannot simulate the flow flowing through the Halaha River channel, which has a lower elevation than YS's. In order to solve this issue, one possibility is that those fields had been inundated by flows from DHG earlier.

The line simulation yields a distinctive outcome that may indicate YS and DHG were lying on the same fissure (**Figure 11a** and **b**). If the program is carried out YS and DHG within a 1 km wide, 7 km long fissure line, also let the program select random vents along this assumed line with an average distance of about 500 m spacing. In this way, almost the entire lava flow area is covered by the simulated pattern. Thus,

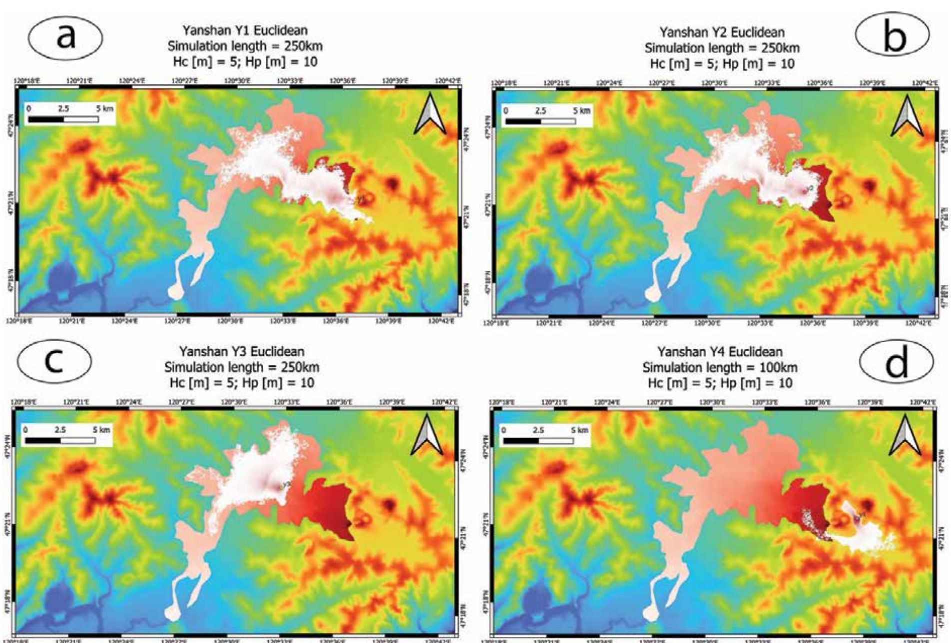

Figure 10.
Lava flow simulations from four different point sources; a) from y1; b) from y2; c) from y3; d) from y4. Maps are on WGS84 projection using geographical coordinate system.

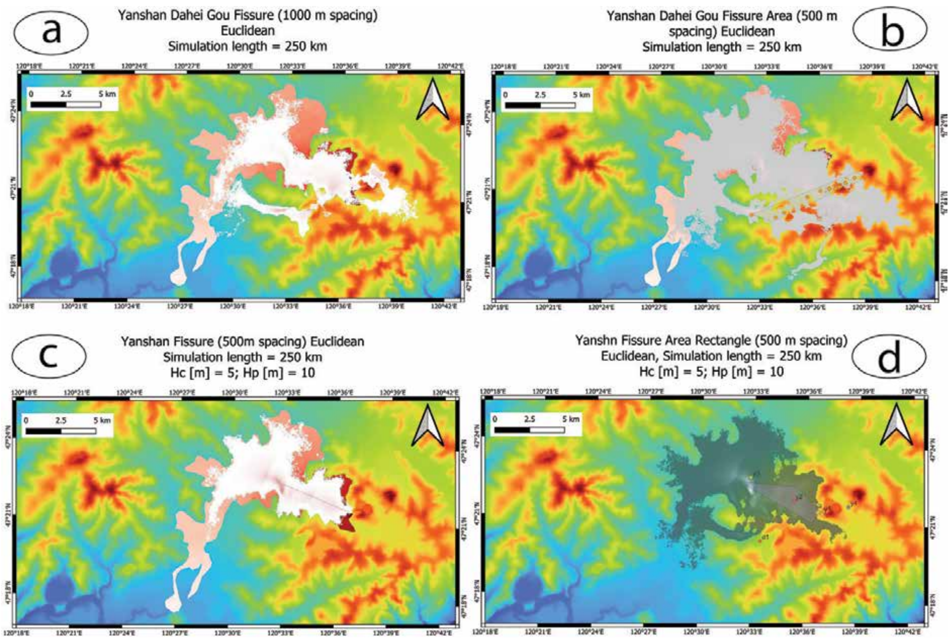

Figure 11.
Lava flow simulation through a fissure between Dahei Gou and Yanshan (a) or a rectangle shape area of vents between Dahei Gou and Yanshan (b). Fissure eruption along an NW-SE axis valley centerline (c) and along a rectangle shape area (d) near Yanshan. Maps are on WGS84 projection using geographical coordinate system.

the line simulation may imply that the Triple Vent and DHG probably erupted at the same time along a fissure about 1 km wide and 7 km long. Furthermore, flow thickness is no more than 5 m on average.

In addition, we explored the simulation if we envision a fissure from Yanshan toward the Halaha River valley and simulating a fissure eruption event (**Figure 11c**) and treating the region as a potential vent zone within a rectangular region (**Figure 11d**). Both modeling was able to reproduce the upper flow fields of Yanshan. The vent area model however generated a potential scenario that lava may have overspilled from the Yanshan valley to Dahei Gou which is a unique but apparently not impossible scenario (**Figure 11d**).

On the basis of the simulations, we fixed the lava flow thickness at 5 m and applied the same parameters we used on the current DEM to test how a lava flow would behave if future eruptions would take place from the same vent. This is an unlikely situation within monogenetic volcanic fields but not unknown. In addition, the two main vent complexes clearly show geological evidence that they are amalgamated complex edifices where subsequent eruptions took place at least in the vicinity of the previous vents.

The four-vent simulation on the current topography created a lava flow field nearly completely covered the lava fields in the Yanshan and upper Halaha River Valley (**Figure 12**). It is clear that such eruptions would produce enough lava flow to disrupt the two main roads crossing the region.

5.3 Implications for the geopark

Applying the simulation to a theoretical fissure opening between Dahei Gou and Yanshan produced very extensive lava flow fields that clearly would be a devastating event for the operation of the geopark (**Figure 13**).

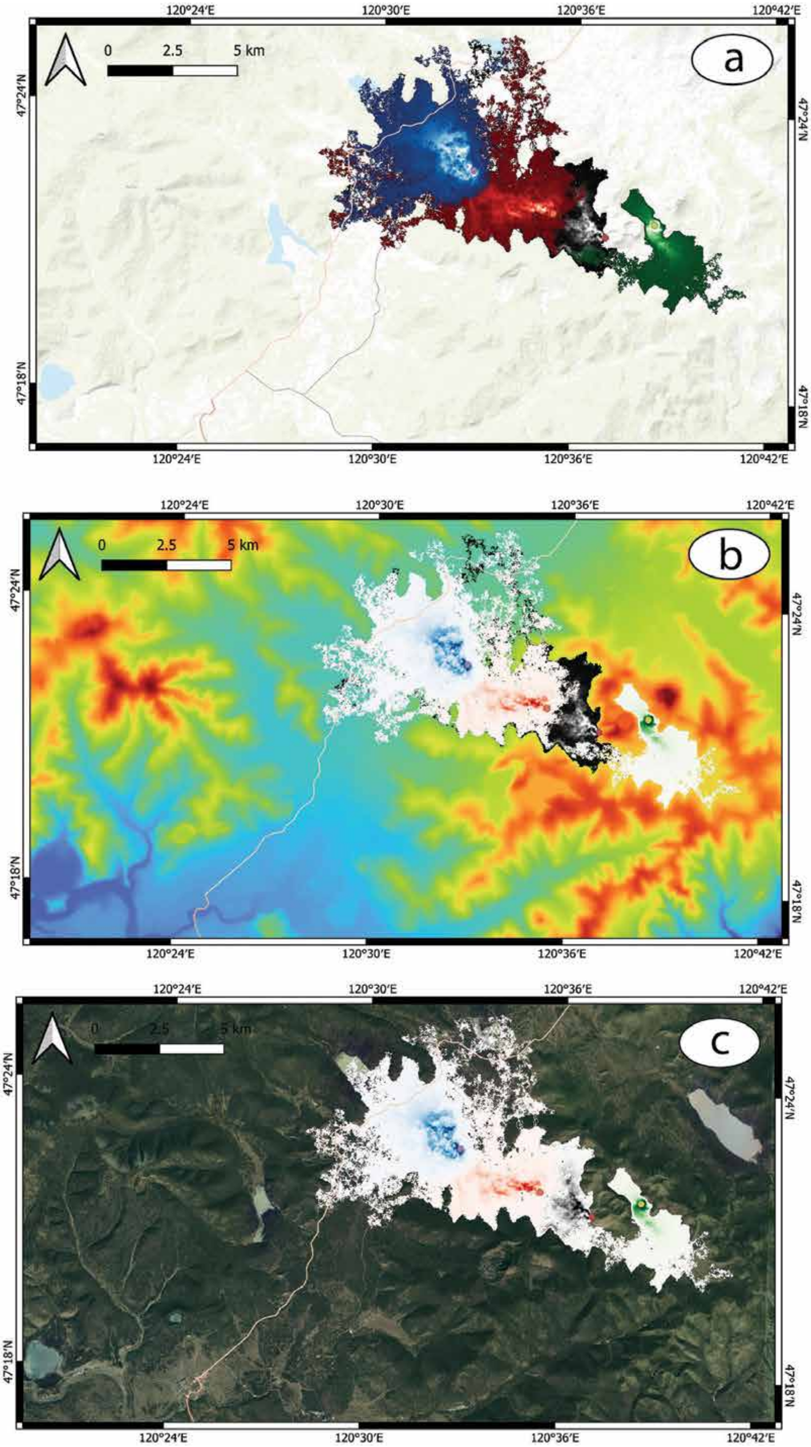

Figure 12.
Set of lava flow simulations run over the current topography (post-eruptive) simulating lava effusion from the four vents along the NW-SE trending valley near Yanshan. Shaded relief map (a) with roading, post-eruptive DEM with roading (b), and GoogleEarth satellite imagery with roading showing the potential inundation if effusive eruptions would take place from y1, y2, y3, and y4 vents in this time sequence.

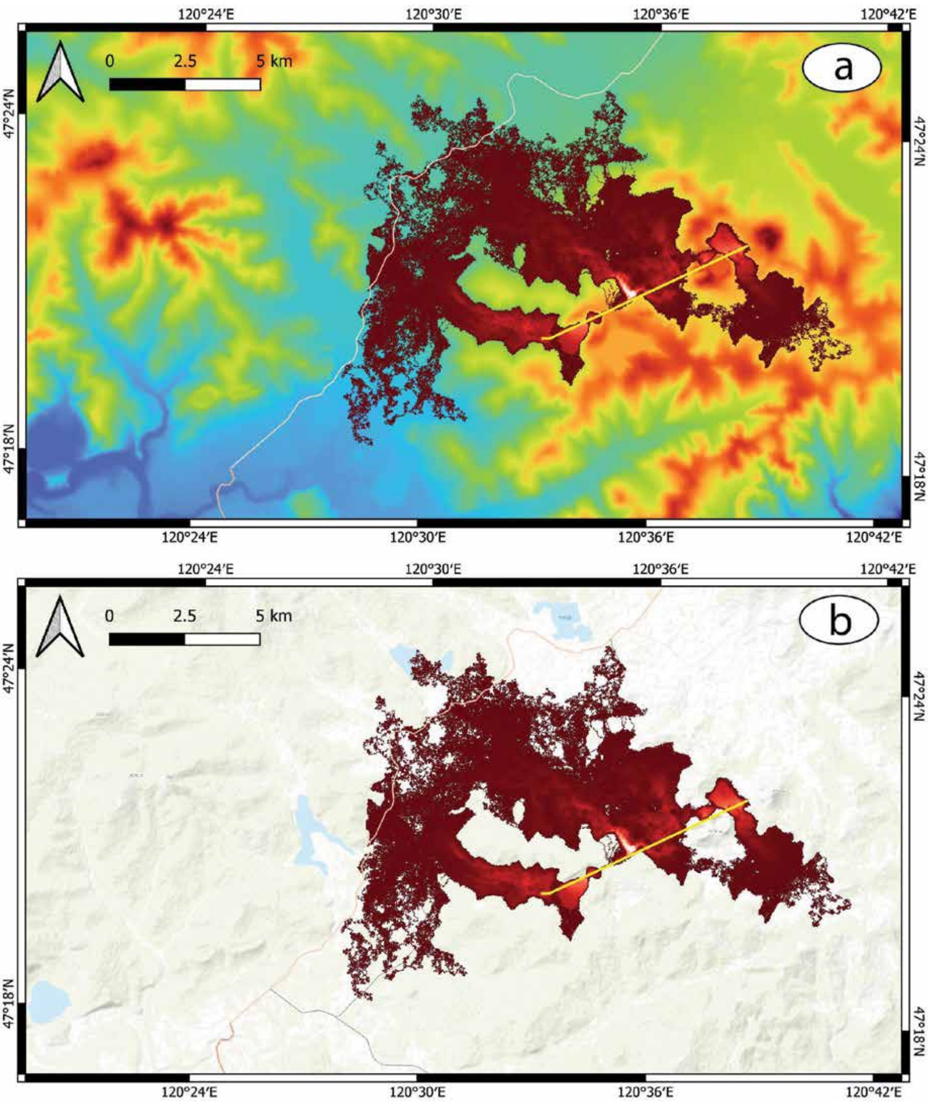

Figure 13.
Simulating lava effusion along a fissure running between Dahei Gou and Yanshan on a post-eruptive DEM (a) and shaded relief (b) maps showing an extensive lava inundation that would fill the two parallel NE-SW valley within Dahei Gou and the Yanshan group situated. Maps are on WGS84 projection using geographical coordinate system.

Surprisingly, if we envision a vent swarm within a rectangle area in the Yanshan valley, it is likely that lava will enter the Dahei Gou valley and be able to produce extensive flow inundation, posing a substantial volcanic hazard for the geopark (**Figure 14**).

ACVF is located in a territory of a UNESCO Global Geopark, which was established in 2016 [23]. The annual tourism visitation rate is high, especially in high season and Chinese holidays, hence the volcanic risk is evident. The infrastructures of this geopark are mostly well constructed but lava flow inundation simulations showed they are beyond the potential destruction zones. The current lack of volcanic hazard management in consideration can be a critical issue not only for wealth engagements but also for the safety of local people.

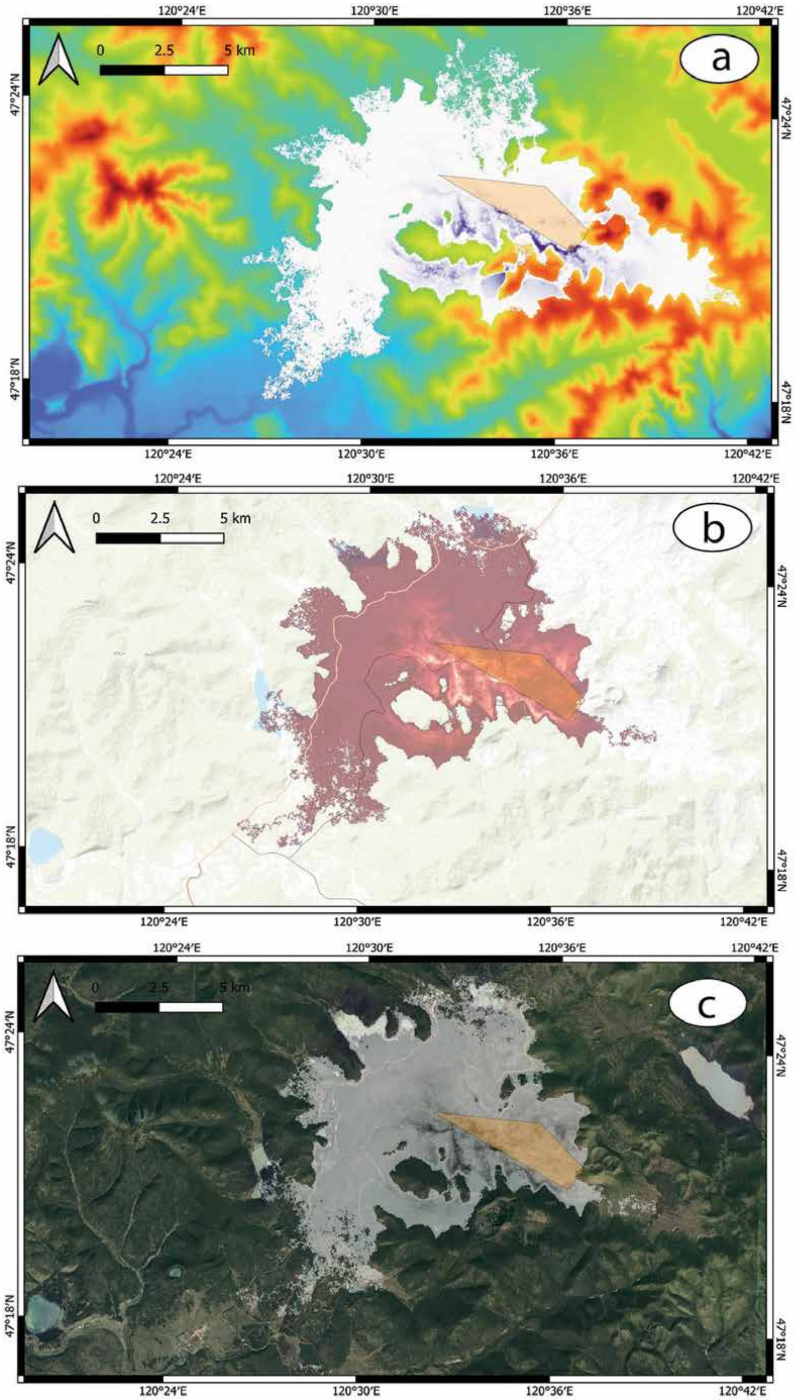

Figure 14.
Lava flow inundation simulation applying rectangle shape vent zones along the NE-SW axis valley within the Yanshan group sits. On the digital elevation model (a) it is clearly visible that lava flows can reach the Dahei Gou valley and the maximum run-out distance of the flow can reach the broad alluvial valley near to the local tourism center of Tianchi township. On the shaded relief, (b) and Google earth satellite image (c) illustrate well the potential extent of the lava flows and its impact on the infrastructure. Maps are on WGS84 projection using geographical coordinate system.

As mentioned above, ACVF is still an active volcanic field; YS and DHG are the two major vents in magnificent scales (e.g., volumes and areas). DHG and YS are observed from the Google satellite images and located from the main Tianchi Town, about 12.6 km and 17.3 km, respectively. From the observations of slope maps, the town is on the west side of these two vents, and elevations on the western side of ACVF are generally lower than the elevations on its east. Satellite images show that lava flows are the basement of constructions in relation to the town. The Halaha River cuts through from the western end of ACVF and then flows to the south, which is also the southern side of the town. Assessments and evaluations from **Table 1** are sufficient indicators that a possible effusion rate of lava flows might be a significant parameter of local risk management. Under the relatively high effusion rates and considered flattened surfaces of local territories, basaltic flows always influenced tremendous areas surrounding the vents. The total area of flows in targeted destinations of ACVF is approximately 90 km^2. In comparison to the Hawaii eruptions in 2018, the flow areas generated from YS and DHG are less than the mentioned one, which was about 144 km^2. Another thing is that a 90 km^2 area of lava flows has already succeeded the total area of Wudalianchi flows, which is approximately 65 km^2 [37, 38]; this could mean that the potential hazards from ACVF are needed to pay attention to most aspects of safety prospects. Local geomorphology shows that YS and DHG were formed in intra-mountainous settings. Valleys are the confines for the lava flowing. The low viscosity properties of basaltic lavas make the hazard areas even more dangerous than other areas with open topography; specifically, the town was built in the central part of the valley bottoms. ACVF is a national geopark in an active volcanic zone; this is very different from other volcanic geoparks that are commonly far away from the major vents. The low population in the region prevents generating primary interest in volcanic hazards within the community. In addition, people have low information and understanding of volcanic hazards hence the Arxan UNESCO Global Geopark could be an excellent avenue to pass knowledge on the volcanic hazard to the local communities and visitors.

6. Conclusion

This preliminary research about lava flows erupted from YS and DHG tries to bring a new insightful result of lava evolutionary histories and subsequent hazard evaluations. Sentinel imagery plays an essential role in this research. Calculations for the lava volumes and effusion rates are the major outcomes of this research for the first time providing geologically validated and modeled lava flow eruptive volumes for ACVF. GIS-based techniques provided new information on the nature and extent of lava flow inundation. Applying STRM, ALOS-PALSAR Digital Elevation Models and applying GIS techniques to analyze the morphological assets of the ACVF provided a complex framework to simulate lava flow inundation. Lava flow simulations in concert with direct field observations revealed that future lava flow effusion would generate significant lava flow infill along the NE-SW trending valley within Dahei Gou and Yanshan volcanoes sit. As these lava flow likely would reach the main transport routes of the region, complex volcanic hazard studies and probabilistic estimates are needed to mitigate future volcanic hazards. Future research is needed to concentrate on the chronologies of lava successions, and predictions of future eruptions along with the local fissures which formed the lava flows in ACVF.

Author details

Bo'xin Li[1], Károly Németh[1,2]*, Julie Palmer[1], Alan Palmer[1], Vladyslav Zakharovskyi[1] and Ilmars Gravis[3]

1 School of Agriculture and Environment, Massey University, New Zealand

2 Institute of Earth Physics and Space Science, Sopron, Hungary

3 Geoconservation Trust Aotearoa, Ōpōtiki, New Zealand

*Address all correspondence to: knemeth69@gmail.com

References

[1] Kilburn CRJ. Lava flows and flow fields. In: Sigurdsson H et al., editors. Encyclopedia of Volcanoes. San Diego: Academic Press; 2000. pp. 291-306

[2] Macdonald GA. Pahoehoe, aa and block lava. American Journal of Science. 1953;**251**(3):169

[3] Self S, Keszthelyi L, Thordarson T. The importance of pahoehoe. Annual Review of Earth and Planetary Sciences. 1998;**26**:81-110

[4] Kilburn CRJ, Lopes RMC. The growth of AA lava flow fields on Mount Etna, Sicily. Journal of Geophysical Research: Solid Earth. 1988;**93**(B12):14759-14772

[5] Sato H. Textural difference between Pahoehoe and aa lavas of Izu-Oshima volcano, Japan - an experimental-study on population-density of plagioclase. Journal of Volcanology and Geothermal Research. 1995;**66**(1-4):101-113

[6] Rossi MJ. Morphology of the 1984 open-channel lava flow at Krafla volcano, northern Iceland. Geomorphology. 1997;**20**(1-2):95-112

[7] Murcia H et al. Late Holocene lava flow morphotypes of northern Harrat Rahat, Kingdom of Saudi Arabia: Implications for the description of continental lava fields. Journal of Asian Earth Sciences. 2014;**84**:131-145

[8] Thordarson T, Self S. The Laki (Skaftar fires) and Grimsvotn eruptions in 1783-1785. Bulletin of Volcanology. 1993;**55**(4):233-263

[9] Wylie JJ et al. Flow localization in fissure eruptions. Bulletin of Volcanology. 1999;**60**:432-440

[10] de Silva S, Lindsay JM. Chapter 15 - primary volcanic landforms. In: Sigurdsson H, editor. The Encyclopedia of Volcanoes (Second Edition). Amsterdam: Academic Press; 2015. pp. 273-297

[11] Sheth H. Morphology and architecture of flood basalt lava flows and sequences. In: A Photographic Atlas of Flood Basalt Volcanism. Cham, Germany: Springer; 2018. pp. 33-79

[12] Hutchison W et al. The eruptive history and magmatic evolution of Aluto volcano: New insights into silicic peralkaline volcanism in the Ethiopian rift. Journal of Volcanology and Geothermal Research. 2016;**328**:9-33

[13] Smith IEM, Németh K. Source to surface model of monogenetic volcanism; a critical review. Special Publication - Geological Society of London. 2017;**446**(1):1-28

[14] Le Corvec N et al. Spatial distribution and alignments of volcanic centers: Clues to the formation of monogenetic volcanic fields. Earth-Science Reviews. 2013;**124**:96-114

[15] Mazzarini F et al. Volcanic field elongation, vent distribution, and tectonic evolution of a continental rift: The Main Ethiopian rift example. Geosphere. 2016;**12**(3):706-720

[16] Murcia H, Németh K. Effusive Monogenetic Volcanism. In: Németh K, editor. Updates in Volcanology - Transdisciplinary Nature of Volcano Science. London, UK, London, UK: inTech Open: Rijeka, Croatio; 2021. pp. 133-147

[17] Stephenson PJ et al. Three long lava flows in North Queensland. Journal of Geophysical Research-Solid Earth. 1998;**103**(B11):27359-27370

[18] Kereszturi G et al. Numerical simulation of basaltic lava flows in the Auckland volcanic field, New Zealand-implication for volcanic hazard assessment. Bulletin of Volcanology. 2014;**76**(11):1-17

[19] Sun CQ et al. Tephra evidence for the most recent eruption of Laoheishan volcano, Wudalianchi volcanic field, Northeast China. Journal of Volcanology and Geothermal Research. 2019;**383**:103-111

[20] Wei H et al. Three active volcanoes in China and their hazards. Journal of Asian Earth Sciences. 2003;**21**(5):515-526

[21] Bai ZD et al. Yanshan, Gaoshan - two active volcanoes of the volcanic cluster in Arshan, Inner Mongolia (in Chinese with English abstract). Earthqua Research Chi-Chi. 2005;**19**:402-408

[22] Cui XG et al. Understanding the Yanshan volcano eruption in the Chaihe-Arxan volcanic field, northeastern China. Arabian Journal of Geosciences. 2021;**14**(21):2174

[23] Németh K et al. Update on the volcanic geoheritage values of the Pliocene to quaternary Arxan-Chaihe volcanic field, Inner Mongolia, China. Geoheritage. 2017;**9**(3):279-297

[24] Li B et al. Basic volcanic elements of the Arxan-Chaihe volcanic field, Inner Mongolia, NE China. In: Németh K, editor. Updates in Volcanology - Transdisciplinary Nature of Volcano Science. London, UK, London, UK: IntechOpen: Rijeka, Croatia; 2021

[25] Zhang ZC et al. Geochemistry and geochronology of the volcanic rocks associated with the Dong'an adularia-sericite epithermal gold deposit, lesser Hinggan range, Heilongjiang province, NE China: Constraints on the metallogenesis. Ore Geology Reviews. 2010;**37**(3-4):158-174

[26] Liu JQ et al. The role of melt-rock interaction in the formation of quaternary high-MgO potassic basalt from the greater Khingan range, Northeast China. Journal of Geophysical Research - Solid Earth. 2017;**122**:1-19

[27] Fan QC et al. Studies on quaternary volcanism stages of Halaha river and Chaoer river area in the great Xing'an range: Evidence from K-Ar dating and volcanic geology features. (in Chinese with English abstract). Acta Petrologica Sinica. 2011;**27**:2827-2832

[28] Rodriguez-Gonzalez A et al. Comparison of real and simulated lava flows in the Holocene volcanism of gran Canaria (Canary Islands, Spain) with Q-LavHA: Contribution to volcanic hazard management. Natural Hazards. 2021;**107**(2):1785-1819

[29] Mossoux S et al. Q-LAVHA: A flexible GIS plugin to simulate lava flows. Computers & Geosciences. 2016;**97**:98-109

[30] Harris AJL et al. Calculation of lava effusion rates from Landsat TM data. Bulletin of Volcanology. 1998;**60**(1):52-71

[31] Harris AJL, Rowland SK. FLOWGO: A kinematic thermo-rheological model for lava flowing in a channel. Bulletin of Volcanology. 2001;**63**(1):20-44

[32] Vilches M et al. Effusion rate estimation based on solidified lava flows: Implications for volcanic hazard assessment in the Negros de Aras monogenetic volcanic field, northern Chile. Journal of Volcanology and Geothermal Research. 2022;**422**:107454

[33] Becerril L et al. The historical case of Paricutin volcano (Michoacan,

Mexico): Challenges of simulating lava flows on a gentle slope during a long-lasting eruption. Natural Hazards. 2021;**107**(1):809-829

[34] Rowland SK, Garbeil H, Harris AJL. Lengths and hazards from channel-fed lava flows on Mauna Loa, Hawai'i, determined from thermal and downslope modeling with FLOWGO. Bulletin of Volcanology. 2005;**67**(7):634-647

[35] Wantim MN et al. Numerical experiments on the dynamics of channelised lava flows at Mount Cameroon volcano with the FLOWGO thermo-rheological model. Journal of Volcanology and Geothermal Research. 2013;**253**:35-53

[36] Harris AJL, Rowland SK. FLOWGO 2012: An Updated Framework for Thermorheological Simulations of Channel-Contained Lava. In: Carey R, Cayol V, Poland M, Weis D, editors. Hawaiian Volcanoes: From Source to Surface. 2015;**208**:457-481

[37] Xiao L, Wang CZ. Geologic features of Wudalianchi volcanic field, northeastern China: Implications for Martian volcanology. Planetary and Space Science. 2009;**57**(5-6):685-698

[38] Gao W et al. Geological and geomorphological value of the monogenetic volcanoes in Wudalianchi National Park, NE China. Geoheritage. 2013;**5**(2):73-85

Chapter 5

Physical Volcanology and Facies Analysis of Silicic Lavas: Monte Amiata Volcano (Italy)

Luigina Vezzoli, Claudia Principe, Daniele Giordano, Sonia La Felice and Patrizia Landi

Abstract

Monte Amiata (Italy) is a middle Pleistocene silicic volcano characterized by the extrusion of extensive (5–8 km long and 60 m thick on average) sheet-like lava flows (SLLFs). It is one of the prime volcanoes that have been involved in the volcanological debate on the genetic interpretation of large silicic flows. We performed integrated stratigraphic, volcanological, and structural field survey and petrochemical study of Monte Amiata SLLFs to describe their volcanic facies characteristics and to elucidate their eruptive and emplacement processes. Individual flow units exhibit basal autoclastic breccia beds or shear zones, frontal ramp structures, massive cores with subvertical cooling columnar jointing, coherent non-vesicular upper parts, and plain surfaces with pressure ridges. Internal shear-bedding and crystals and vesicles lineations define planar to twisted and straightened outflow layering. The absence of fragmental textures, both at micro- and macro-scale, supports the effusive nature for the SLLFs. The most common lithology is a vitrophyric trachydacite of whitish to light-gray color, showing a homogeneous porphyritic texture of K-feldspar, plagioclase, pyroxene, and biotite, in a glassy perlitic or microcrystalline poorly vesicular groundmass. Morphological features, facies characteristics, internal structure, and petrographic textures of these silicic sheet-like and long-lasting flows suggest that their effusive emplacement was governed by peculiar physicochemical and structural conditions.

Keywords: sheet-like silicic lava flow, volcanic facies, emplacement dynamics, volcano-tectonics, perlite, Monte Amiata

1. Introduction

Due to their relatively high viscosity and volatile content, silicic (SiO_2 > 63 wt%) magmas are mainly erupted explosively producing voluminous fallout and ignimbrite deposits, which can reach areal extension of thousands of square kilometers and thickness of hundreds of meters (e.g., [1]). In contrast, silicic effusive eruptions are correlated with domes and short and thick flows. The emplacement of silicic lavas is commonly governed by physical variables such as the high viscosity, low temperature and volatile content, and low eruption rates. Moreover, silicic lava effusions are poorly constrained because of a paucity of direct observations on historical eruptions (i.e., Colima, Mexico, 1998–1999, [2]; Santiaguito, Guatemala, 1922 to present, [3]; Chaitén, Chile, 2008–2009, [4]; Cordón Caulle, Chile, 2011–2012, [5–7]). Overall, the best known and described silicic effusive products are rhyolite lava domes [8] and stubby obsidian flows restricted to the near-vent areas [9, 10]. Since the 1960s, more extensive silicic volcanic units have been the object of controversy over their origin because of volcanological characteristics typical of either lava flows and welded or rheomorphic pyroclastic rocks (ignimbrite). In more recent times, several of these extensive sheet-like silicic volcanic units were interpreted as lava flows and distinguished from rheomorphic ignimbrites in well-documented geological records worldwide [11–21]. However, some key questions regarding the eruption and emplacement mechanisms of large volume silicic lavas remain still open [22–25].

Monte Amiata is a silicic (mainly trachydacite) middle Pleistocene volcano (**Figure 1**) of the Tuscan Magmatic Province (Italy; [26]) that focused on the interest of volcanologists and petrologists for about 300 years since the eighteenth century [27] and was one of the prime volcanoes that have been involved in the volcanological debate on the genetic interpretation of the enigmatic sheet-like silicic volcanic rocks [28–33].

Monte Amiata is that volcano for which the word “rheoignimbrite” was first coined by Alfred Rittmann [30] to indicate a volcanological process explaining the concomitant lava- and pyroclastic-like textural and geological characteristics found in some silicic volcanic rocks [33]. The pristine interpretation of Monte Amiata ignimbrites and rheoignimbrites by Rittmann was not universally accepted (e.g., [34]; G.P. L. Walker in [32]). However, the concept of rheomorphism, considered such as a post-depositional gravitational flow and deformation process, has been subsequently recognized and applied in volcanology to ignimbrites (e.g., rheomorphic ignimbrites; [35, 36]), pyroclastic fall deposits [32], and lavas. After the Rittmann assumption, the various studies present in the literature [37–44] have in fact suggested not conclusive data and interpretations about the eruption processes of Monte Amiata silicic rocks, mainly because of the lack of exhaustive physical volcanological observations and their interpretations in a modern volcanological framework.

Nowadays, we accept that Monte Amiata is a completely effusive silicic volcano whose activity was dominated by the emplacement of silicic lava flows, exogenous lava domes, and coulées [45]. To support our interpretation, we have performed

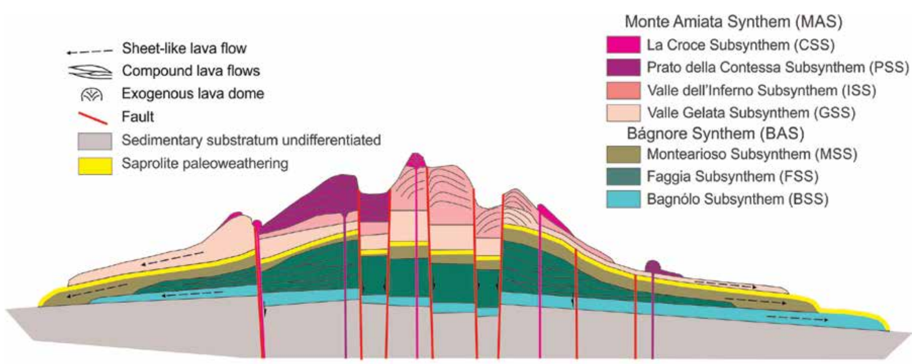

Figure 1.
Idealized cross section showing the stratigraphic relationships and the internal architecture of the completely effusive silicic Monte Amiata composite volcano. Not in scale.

detailed and systematic field-based investigations on the stratigraphy, structure, physical features, volcanic facies, and macroscopic and microscopic structures and textures of Monte Amiata deposits.

Specifically, this chapter focuses on several sheet-like lava flows (SLLFs) that constitute the main part of the Monte Amiata volcanic edifice and offer an excellent opportunity to learn more about extensive and voluminous silicic lavas. The goals of our study are (1) to discuss some criteria to distinguish silicic lava flows from welded tuffs and rheoignimbrites, (2) to interpret ascent, eruption, and emplacement mechanisms for Monte Amiata trachydacite through physical and observational data, (3) to produce a model of emplacement for the SLLFs, and (4) to suggest reading keys for the interpretation of the eruptive activity, which originates for such kind of magmatic, structural, and volcano-tectonic environments. We are convinced that the conclusions obtained for Monte Amiata can be applied to improve the general understanding of the volcanic processes at the origin of the emplacement of large silicic effusive bodies and to enhance the assessment of their associated volcanic hazard.

2. Geological setting

2.1 Overview of Monte Amiata volcano

Monte Amiata (42°53′15″N, 11°37′24″E) is a middle Pleistocene polygenetic volcano culminating at 1738 m above sea level (a.s.l.) and located in southern Tuscany (Italy) within the Tuscan Magmatic Province [26]. The province formed in the inner sector of the Late Cretaceous–Early Miocene Northern Apennine thrust-and-fold belt [46, 47] and appears related to crustal thinning and asthenosphere upwelling [48, 49] associated with a Miocene-Pleistocene extensional tectonic regime [50, 51] that favored the partial melting in lower crust and mantle [26]. Magmatism in the province extended from 8 Ma to 0.2 Ma and includes plutonic and volcanic rocks. Monte Amiata is the youngest volcanic activity of the province. Its volcanic products overlay a sedimentary substratum represented by marly limestones and calcareous sandstones of Mesozoic-Cenozoic age [52].

Monte Amiata was active in a short interval of time (305–231 ka, [53, 54]). The source vents are eruptive fissures forming a 7 km-long, NE-SW-trending volcanic rift zone (**Figures 1** and **2**; [45]) related to a regional transtensional fault system (Bágnore—Bagni S. Filippo Shear Zone; [55]). Times and modes of the volcanic activity and evolution, such as the volcano-tectonic deformations of the edifice and the periodic refilling of the shallow silicic reservoir with new basaltic magmas ([56], and references therein), were probably controlled by the tectonic deformations along this shear zone [45].

The main composition of Monte Amiata lavas is trachydacite, with subordinate latite [40, 42, 44, 57]. Mafic magmatic enclaves (ME) are present within the silicic lava flows [58] and reflect the indirect mantle input to the volcanic activity and geological evolution [44, 45].

Based on a new accurate stratigraphic and structural geological survey [45, 59–62], we have innovatively proposed that the Monte Amiata geological evolution consists of two main periods of activity corresponding to two Unconformity Bounded Stratigraphic Units (UBSUs; [63]): the older Bágnore Synthem (BAS) and the younger Monte Amiata Synthem (MAS) (**Figure 1**). They are separated by a period of volcanic quiescence represented by a major geological unconformity during which a surface of intravolcanic saprolite paleo-weathering and associated tectonic deformations

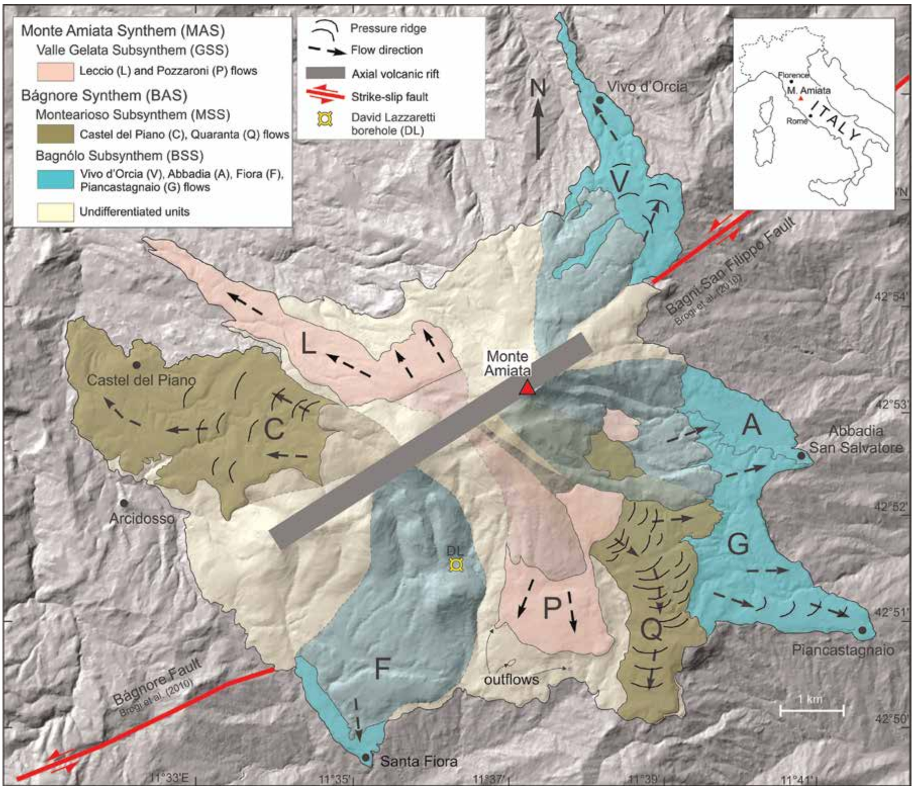

Figure 2.

*Geologic sketch map of Monte Amiata showing the sheet-like lava flows (SLLFs) object of the study. The last phases of activity (Valle dell'Inferno, Piano della Contessa, and La Croce Subsynthems; see **Figure 1**), which not include SLLFs, are omitted. Colors of stratigraphic units are as in **Figure 1**. The more intense color tone indicates exposed SLLFs, and the lighter one indicates the inferred portions covered by younger units. Letters for name of SLLFs: A—Abbadia San Salvatore, C—Castel del Piano, F—Sorgente del Fiora, G—Piancastagnaio, P—Pozzaroni, Q—Quaranta, V—Vivo d'Orcia. The presence of ogive structure on some flow surface is depicted. Front and margins of the Pozzaroni lava flow show outflow lobes. Geologic mapping from your original field survey. Digital terrain model (DEM) basis from the technical map of the Tuscany Region at the 1: 10,000 scale.*

developed at expense of the BAS rocks [62]. Then, the recognition of other surfaces of discontinuity of lower rank has made it possible to divide these two synthems into seven subsynthems (**Figure 1**). Monte Amiata succession does not record pyroclastic deposits, on the contrary to common composite silicic volcanoes that show packages of intercalated tuffs and lava flows.

From its earliest stages, BAS volcanic activity is characterized by the emplacement of several extensive, individual SLLFs (Bagnólo Subsynthem-BSS; **Figure 1**) that flowed N, SE, and S for very long distances (up to 8 km) and crop out in the distal portion of the volcanic edifice (**Figure 2**; [45]). After the construction of an effusive cone formed by the successive emplacement and overlap of channelized compound lava flows (Faggia Subsynthem-FSS; **Figure 1**), more localized individual SLLFs are once again extruded (Montearioso Subsynthem-MSS; **Figures 1** and **2**; [45]). Younger units, composing MAS, comprise long individual SLLFs that reach 5–6 km in length (**Figure 2**) associated with extrusive lava domes and coulées (Valle Gelata Subsynthem-GSS; **Figure 1**), followed by numerous exogenous lava domes with associated coulées (Valle dell'-Inferno-ISS and Prato della Contessa-PSS Subsynthems) and, finally, by some smaller channelized lava flows (La Croce Subsynthem-CSS; **Figure 1**; [45]).

2.2 Previous studies and open questions

Two fundamental geological problems on Monte Amiata volcano emerged from previous studies carried out during the last 60 years including the issues associated with the correct definition of the stratigraphic units and, consequently, of the interpretation of the geological evolution in light of the revised volcanological interpretation of the eruption dynamics and the emplacement processes.

In all previous studies, the reconstruction of the stratigraphic framework was founded mainly on lithological and petrographic characteristics rather than on objective geological criteria applying the principal approach of volcano geology. Consequently, based on supposedly homogeneous and indistinguishable textures, geochemical composition, and mineral paragenesis of rocks, the resulting volcanic history was represented by only three units [39, 40, 43]. This tri-fold division of the volcanic activity of Monte Amiata includes (1) an initial and single extended sheet of vitrophyric flows (Basal Complex Auctorum), (2) a cluster of lava domes and coulées extruded from the axial summit crest of the volcano, and (3) two final trachyandesite (olivine-phyric latite) small lava flows.

In fact, in all previous studies on Monte Amiata, the SLLFs of the lower portion of the stratigraphic succession (Basal Complex Auctorum) were all assigned to a single eruptive event (in turn explosive, effusive, or mixed), which would have marked the beginning of the activity of the volcano. Differently, the stratigraphic reconstruction presented in our works ([45, 59–62], this paper) demonstrates that the SLLFs are not a large indistinct unit produced by a single eruptive event, but that they consist of numerous eruptive units that are distinct in the source area, areal distribution, and volcanological and petrographic features. Moreover, these single eruptive units until now included in the former Basal Complex Auctorum are actually individual lithostratigraphic units found at different levels of the stratigraphic succession (**Figures 1** and **2**).

After the initial definition as ignimbrites and rheoignimbrites [30, 37–39], the genetic interpretation of the extensive sheet-like trachydacite flows of Monte Amiata has been the subject of various conjectures, which, however, was not supported by stratigraphic and structural field data and by an accurate volcanological definition of the depositional facies. Ref. [40] proposed a mixed complex eruption, with an initial explosive phase followed by an effusive phase. The effusive nature of these flows has been generically supposed by various authors [41, 42], albeit in contexts focused on other topics and without any objective observation. Refs. [43, 44] proposed a highly speculative mechanism of the collapse of an endogenous summit mega-dome generating a single predominantly gravitational flow of fragmented and still hot material that was distributed all around the volcano and evolved in a rheomorphic sheet, which flowed like lava after emplacement.

On the basis of the various physical and compositional indicators, stratigraphic relations, and our geologic mapping, we do not agree with these previous interpretations for any of the Monte Amiata sheet-like trachydacite flows.

3. Materials and methods

This chapter focuses on the volcanological and stratigraphic characterization and interpretation of the SLLFs of Monte Amiata volcano. The stratigraphic identification and cartography of the geological units studied are based on the stratigraphic criteria of the Unconformity Bounded Stratigraphic Units (UBSUs; [63]), following the suggestions of the International Stratigraphic Guide (that can be accessed online http://www.stratigraphy.org). This type of stratigraphic unit is defined as a rocky body bounded to the top and bottom by specific, significant, and demonstrable surfaces of geologic discontinuity. The basic synthem unit can be divided into two or more subsynthems. Names of units adopted in this work have been introduced and described in previously published papers [45, 62].

The description of lava flows studied is based on the analysis of volcanic facies [64, 65]. For depositional facies, we mean the set of lithological characters of a rock, which allows its distinction according to some combination of physical features and composition, without nor genetic neither stratigraphic significance. Different facies record variations in conditions and processes of formation and deposition; consequently, they can lead to the interpretation of volcanological genetic processes and emplacement mechanisms. For each of the identified volcanic facies, we describe physical and morpho-structural features, internal and surface structures, and macroscopic and microscopic textures, and we propose their genetic interpretation. The internal arrangement of facies in terms of vertical and horizontal sequence and association contributes to recognize the architecture of the effusive volcano. We refer to a flow unit as the deposit of a discrete flow within an eruption event, whereas to an eruptive unit as all the products effused during a time- and space-distinct eruption event which can also be composed of several successive flow units. Individual eruptive unit outlines have been delineated and mapped from field evidence, and patterns and textural differences.

The petrographic observation of the Monte Amiata rock samples allowed to recognize several different exposed lithotypes [57] on the basis of different paragenesis, groundmass textures, and content in mafic magmatic enclaves and meta-sedimentary xenoliths. About 30 rock samples belonging to the SLLFs discussed in this work were analyzed under a polarizing microscope at Institute of Geosciences and Earth Resources (National Research Council of Italy), Pisa (Italy), in order to carry out a textural, petrographic, and mineralogical characterization. In addition, further textural investigations were performed at the National Institute of Geophysics and Volcanology (INGV), Pisa (Italy), using a Zeiss EVO MA 10 Scanning Electron Microscope (SEM), capturing selected back-scattered electron (BSE) images.

The morphometric parameters of Monte Amiata lava flows were determined in the field and with reference to the geologic map (**Figure 2**; see also [45]). The area, minimum length, and slope of each flow were calculated by means of the ruler tool of Google Earth on the basis of the performed geological mapping. The average thickness of each eruptive unit was estimated from outcrop relief scaled from the topographic base maps. Most calculated volumes are less than real volumes because a great part of the SLLFs are covered by the overlying volcanic units, and their extent to the source zone is actually unknown. Anyway, the calculated volume is essentially a dense-rock equivalent, since porosity in these lavas is generally very low to absent.

4. Results on Monte Amiata trachydacite SLLFs

4.1 Stratigraphic relationships and physical features

The long, trachydacite SLLFs span over the stratigraphic succession of the volcano and are not restricted to a particular stratigraphic level (**Figure 1**). They are more abundant but not exclusive in Bágnore Synthem (BAS), as they are found also in Monte Amiata Synthem (MAS).

Among the BAS trachydacite, we have identified two stratigraphically distinct groups of SLLFs. The oldest SLLFs group crops out at the base of the volcanic stratigraphic sequence (BSS; **Figure 1**) and comprises the Sorgente del Fiora, Piancastagnaio, Abbadia San Salvatore, and Vivo d'Orcia lithostratigraphic and eruptive units (**Figure 2**). They spread NW and SE over a wide area unconformably overlying the pre-volcanic sedimentary substratum and are extensively exposed along the external perimeter of the volcano. They reach distances up to 5–8 km from the probable vent area, with widths up to 1.5–2 km and thickness of 30–90 m (**Table 1**). A second BAS series of SLLFs (MSS; **Figure 1**) is in the NW and S sides of the edifice and comprises the Castel del Piano and Quaranta lithostratigraphic and eruptive units (**Figure 2**). They reached a distance of about 7 km from the probable emission centers, with thicknesses of 50–80 m (**Table 1**). After an interval of weathering (saprolite) and faulting, the resumed MAS volcanic activity (GSS; **Figure 1**) produced extensive SLLFs along the N and S slopes forming Leccio and Pozzaroni lithostratigraphic and eruptive units (**Figure 2**) with length of 5–6 km and thickness ranging 50–70 m (**Table 1**).

The two younger SLLFs (GSS; Leccio and Pozzaroni) show about the same area (5–6 km^2) that is the smallest of the Monte Amiata SLLFs. The greatest extent (10–11 km^2) is reached by the SLLFs of MSS (Quaranta and Castel del Piano). Intermediate areas (7–9 km^2) are typical of SLLFs effused during BSS, considering in this case the incertitude in vent positioning and the related error in the area calculations (**Table 1**).

The calculated average volume of the SLLFs spans between 0.30 and 0.72 km^3. To be considered that the error associated with these volumes is quite high, with the exception of Pozzaroni and Leccio SLLFs (**Figure 3a**), due to the incertitude on the thickness distribution along the lava flow's path. There is a faint linear correlation between the calculated volumes and the flows lengths (R: 0.423) (**Table 1** and **Figure 3a**). Moreover, two different alignments are recognizable in both area/length and volume/length graphs (**Figure 3a** and **b**). In particular, (i) there is a very good linear correlation (R: 0.994) between both volume and area and the length of the three

SLLF	Label	S/SS	Area (km^2)	Length (km)	Slope (%)	Thickness range (m)	Average thickness (m)	Volume (km^3)	Average volume (km^3)
Pozzaroni	P	MAS/GSS	5.83	4.75	9.7	70–50	60	0.41–0.29	0.35
Leccio	L	MAS/GSS	5.00	6.33	18.6	70–50	60	0.35–0.25	0.30
Quaranta	Q	BAS/MSS	9.98	6.94	13.0	80–50	65	0.80–0.50	0.65
Castel del Piano	C	BAS/MSS	11.23	7.00	5.3	80–50	65	0.90–0.56	0.73
Piancastagnaio	G	BAS/BSS	8.66	7.72	13.2	90–30	60	0.78–0.26	0.52
Fiora	F	BAS/BSS	9.76	5.57	11.2	90–30	60	0.88–0.29	0.59
Abbadia	A	BAS/BSS	7.36	5.07	8.0	90–30	60	0.66–0.22	0.44
Vivo d'Orcia	V	BAS/BSS	6.50	6.76	9.2	90–30	60	0.59–0.20	0.39

*Slope is average from the inferred vent to the terminus of the flow. S: synthem, SS: subsynthem, and labels of eruptive units as in **Figure 2**.*

Table 1.
Morphometric parameters for the sheet-like lava flow (SLLF) of Monte Amiata.

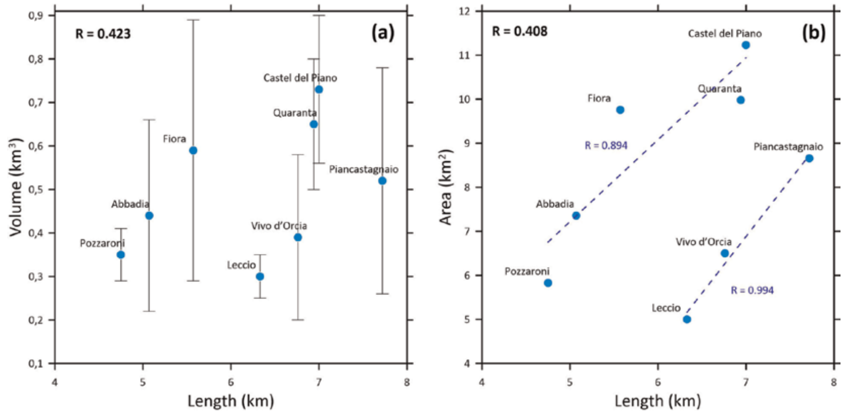

Figure 3.
Plots (a) length vs. volume and (b) length vs. area for the Monte Amiata SLLFs. R is the linear correlation coefficient. See text for explanation.

valley-controlled lava flows of Leccio, Vivo d'Orcia, and Piancastagnaio (in its terminal portion), and (ii) a quite good linear correlation (R: 0.894) for the other five lava flows that distributed in larger lava bodies. In this last case, the poor correlation can be attributed to the exposure condition of the lava flows that influence the accuracy of the area calculation. No correlation is observed between area and slope values, suggesting that the different areal distribution of SLLFs can be independent of the underlying morphology [66], but depending probably on the physicochemical properties of the erupted magma (see discussion in Section 5.2).

The present topographic surface of Monte Amiata volcano represents the primary volcanic surface of the subsequent constructional bodies that concurred to build the volcanic edifice, with the little effects of exogenous erosion and tectonic deformation. All SLLFs are characterized by low- or moderate-relief surfaces forming large tabular areas on the slopes of Monte Amiata. Different lava plateaus developed at different altitudes and formed a stepped relief consisting of overlapping plains separated by breaks of slope [45, 62]. This morphology suggests that flows were not confined by channels and spread along the low-relief sides of the volcano. In the case of Vivo d'Orcia (BAS) and Leccio (MAS) eruptive units (**Figure 2**), lavas moved down the outer flank of the volcano following tectonically controlled preexisting drainage, entering and filling river furrows where they stopped.

The source areas of SLLFs are mainly buried by younger volcanic units and probably correspond to the present elongated summit crest of the volcano (**Figure 2**). Exposures of the flows are largely their surficial part; abrupt but irregular scarps identify the flow fronts and margins. Due to the relatively old age of the volcano, the outcrops are subject to possible surface erosion and front collapses (for this reason, the measured lava length and area have to be considered as minimum values) and the exposed logs are often discontinuous.

The opportunity to access to the complete succession of a SLLF was a continuously cored deep borehole (David Lazzaretti borehole; [67–69]) that intersected top-to-bottom the Sorgente del Fiora eruptive unit. This drilling is located on the southern slope of the volcano about 2 km NNE of the lava flow front (DL in **Figure 2**) and displays well-preserved lithofacies and internal textures. The Sorgente del Fiora lava was recovered between 147 m and 265 m of depth from the ground level (i.e., between 939 and 821 m a.s.l.) and shows a thickness of 118 m (**Figure 4a**). It overlies a lower volcanic sequence of trachydacite predating the exposed units and is overlain by trachydacite belonging to FSS.

4.2 Lithofacies, structures, and textures

4.2.1 Macroscopic lithofacies and facies association

Based on observations of outcrops, hand specimens, and drill cores in the Monte Amiata SLLFs trachydacite (**Figure 4**), we have identified four main coherent lithofacies based on variations in groundmass texture, color, and vesicularity. In addition, three fragmental lithofacies have also been recognized based on differences in texture and composition of clasts and matrix. In all these lithofacies, trachydacite is characterized by nearly identical mineral paragenesis (K-feldspar, plagioclase, biotite, and subordinate pyroxene) and phenocrysts size. The characteristics of these lithofacies and their facies association are well exemplified by the lithostratigraphic log of the Sorgente del Fiora eruptive unit in the David Lazzaretti borehole compared with the correlate outcropping sequence (**Figure 4**).

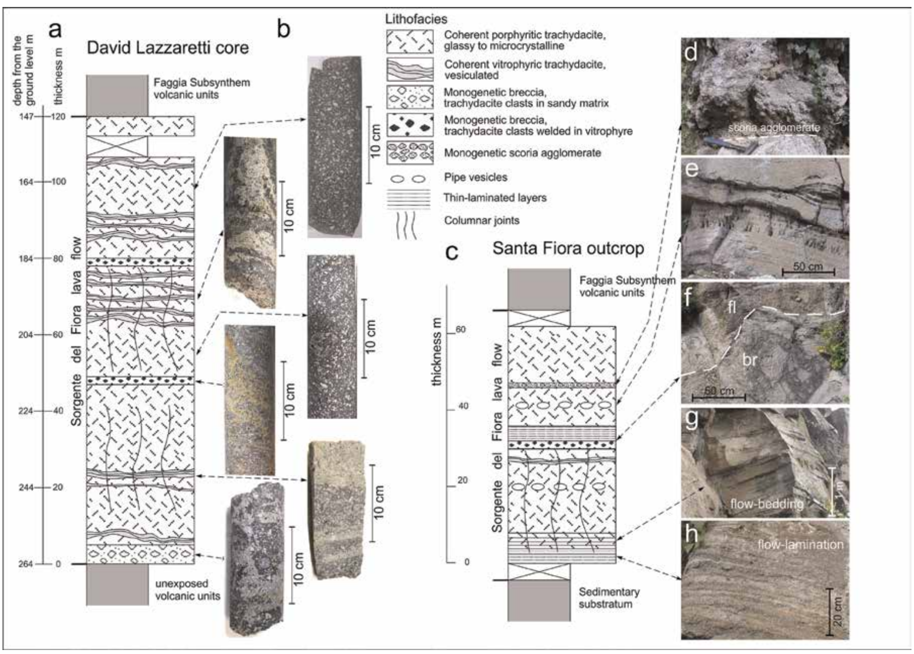

Figure 4.
The Sorgente del Fiora eruptive unit is representative of the trachydacite SLLFs of Monte Amiata, showing the vertical distribution and association of the coherent and fragmental lithofacies identified. (a) Lithostratigraphy of the drill core David Lazzaretti (DL in ***Figure 2****) that intersected top-to-bottom the Sorgente del Fiora unit. (b) Examples of the main lithofacies identified and described in the DL core. (c) Generalized lithostratigraphic log through the Sorgente del Fiora unit from outcrops along flow margins and front. (d) Interflow scoria agglomerate (lithofacies g). Hammer for scale. (e) Vesicle layering. Some beds show tubular vesicles a few cm high. In the upper right part of the image, flow bands have been deflected around a lens of coarse vesiculation, implying that the vesicles formed while the lava was still ductile, probably during flowage. (f) Interflow monogenetic breccia with welded vitrophyric matrix (br; lithofacies f) overlain by thin-laminated lava beds (fl). (g) Flow bedding composed of massive porphyritic lava beds separated by sheet joints. (h) Thin flow lamination alternating massive porphyritic, vesicular, and glassy lava layers at mm to cm scale.*

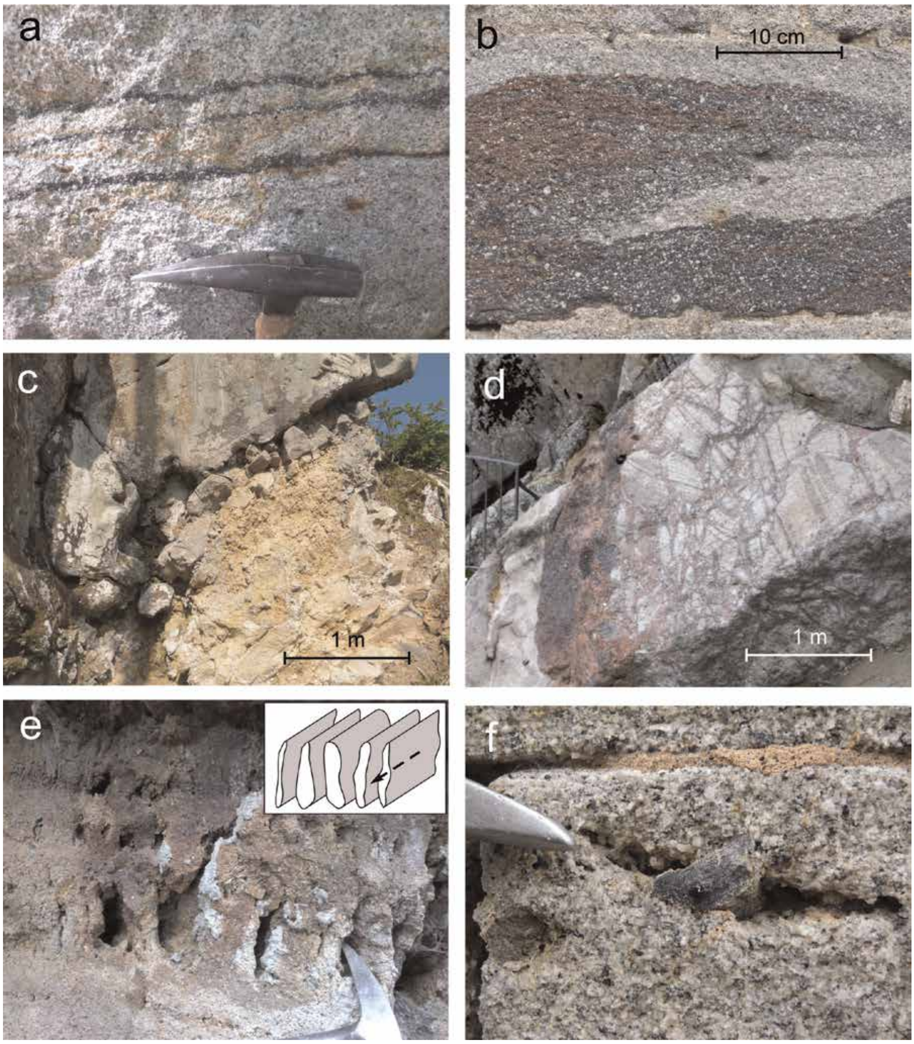

Figure 5.
Outcrop photo of lithofacies and physical volcanological features of the trachydacite SLLFs of Monte Amiata. (a) Bands of black obsidianaceous vitrophyric trachydacite (lithofacies c) in white perlitic vitrophyric trachydacite (lithofacies a; Quaranta unit). (b) Deformed mingling texture between black-to-red obsidianaceous vitrophyric trachydacite (lithofacies c) and white perlitic vitrophyric trachydacite (lithofacies a; Abbadia unit). (c) Basal monogenetic breccia with clastic matrix (lithofacies e) separating two flow units (Piancastagnaio unit). Note the inverse gradation with the larger angular clasts at the top. (d) Interflow monogenetic breccia with laminated trachydacite clasts welded in vitrophyric matrix (lithofacies f; Piancastagnaio unit). (e) Coarse vesicularity with tubular-shaped gas cavities confined in layers (Sorgente del Fiora unit). Inset shows the tridimensional geometry of these cavities that are elongated parallel to the flow direction (arrow). (f) An irregular elongate cavity developed around a meta-sedimentary xenolith (Sorgente del Fiora unit). Hammer for scale where not indicated.

The four coherent lithofacies identified (**Figures 4** and **5**; **Table 2**) are as follows: (a) whitish coherent vitrophyric perlitic trachydacite; (b) gray coherent porphyritic microcrystalline trachydacite; (c) black-to-red coherent vitrophyric obsidianaceous trachydacite; and (d) cream-colored coherent vitrophyric microvesiculated trachydacite. Each of these coherent lithofacies shows internal subtle textural variations that include dimensions and abundance in phenocrysts (from fine-grained to coarse-grained porphyricity), vesicles and crystal concentration zones, vesicles layers, and crystals preferential alignment in fluidal texture. Moreover, lithofacies are arranged in variable vertical and horizontal facies association. At the outcrop scale, the contact between texturally distinct lithofacies is usually sharp.

The three fragmental lithofacies (**Figures 4** and **5**; **Table 2**) are as follows: (e) monogenetic, clast-supported to matrix-supported breccia with fine-grained clastic matrix; (f) monogenetic matrix-supported breccia with clasts welded in a vitrophyric matrix; and (g) monogenetic clast-supported scoria agglomerate. All these fragmental lithofacies have to be considered primary volcanic and autoclastic deposits. In particular:

i. Texture and composition of breccia of lithofacies (e) suggest a formation involving brittle fragmentation at temperatures below the glass transition field [70] of already solidified and flow-laminated lava (**Figures 4** and **5c**).

ii. In lithofacies (f), clast shape and texture suggest that trachydacite was yet rigid at the time of brecciation and that fragmentation occurred *in situ* with scarce disaggregation and transport. Texture and composition of this breccia suggest an initial fracturing and fragmentation at the base of a cooling lava flow unit, followed by its successive welding, as a consequence of the reheating due to the heat advection from the flow to the basal breccia [70, 71]. The overlying coherent trachydacite shows a planar, undeformed flow lamination that parallels the irregular breccia top (**Figure 4f** and **5d**).

4.2.2 Internal structures and textures

Internal structures and textures, such as vesiculation and gas cavities, flow banding, cooling joints, and deformations, have been observed in Monte Amiata SLLFs.

Vesicles and gas cavities are segregation structures of fluids and show different shape, orientation, and dimension in function of their temporal and genetic relationships with the flowing molten lava [72]. In Monte Amiata SLLFs, the dominant coherent lithofacies are poorly or evenly microvesiculated. Vesicles, ranging from less than a millimeter across to cavities more than 10 cm large, are concentrated in trains that form discrete interlayers defining flow layering (**Figure 4e**) and the local flow directions. In coarsely vesicular beds, tubular gas cavities occur together in zones that form planar lenses and layers (**Figure 4e**). The tridimensional geometry of these cavities is complex and unusual (**Figure 5e**). They are apparently continuous for several tens of centimeters in length, horizontally elongated with the main axis parallel to the flow foliation and flow direction. They show an irregular ellipsoidal section, up to 1 cm across and 10 cm along the vertical axis, with scalloped bubble walls (**Figure 5e**). These peculiar gas cavities show some differences as compared with the pipe vesicle typically occurring in basaltic lava [73] that is characterized by individual, subvertical cylindrical tubes with a subcircular section whose formation is attributed to the upward migration of a single bubble of magmatic gas. In the case of Monte Amiata SLLFs, tubular vesicles are formed probably by both the upward coalescence of smaller bubble and lateral migration along the flow direction under the influence of a strong volatile segregation in not-quenched lava. The bubbles confinement in discrete levels may suggest gas entrapment in discrete superimposed domains impermeable among them to the further upward volatile migration. This molten lava partitioning resulted from laminar flow processes, possibly enhanced by the mingling

	Lithofacies	Compositional characteristics	Architecture and occurrence
Coherent lithofacies			
a	Coherent vitrophyric perlitic whitish trachydacite	Massive, evenly porphyritic, equigranular, medium-fine grain (2–5 mm). Groundmass limpid and unaltered glassy, poorly vesiculated, and perlite fractures (2–3 mm). Glomerophyres px + bt + plg; sieved and zoned plg (max 5 cm) and rare K-fs (max 1–2 cm) megacrysts. Poor ME; frequent Msx	Nonuniformly distributed strips and lenses of lithofacies (c). Dominant lithofacies, mainly in Q, C and V units. (**Figure 5a**)
b	Coherent porphyritic microcrystalline gray-to-pink trachydacite	Massive and flow banded, porphyritic, equigranular or seriated, coarse-medium grain. Groundmass microcrystalline—aphyric, locally spherulitic, poorly vesiculated, patches of vesicular pink glass. Glomerophyres plg + bt + px (5–20 mm); sieved and zoned plg (max 5 cm) and rare K-fs (max 1 cm) megacrysts. Abundant ME and Msx.	Interlayer with beds of lithofacies (c) and (d). Well-represented lithofacies, in both flow-banded marginal and frontal parts and massive cores of lava bodies. (**Figure 4g**)
c	Coherent vitrophyric obsidianaceous black-to-red trachydacite	In beds 0.1–10 cm thick, porphyritic, equigranular, medium-fine grain. Groundmass glassy, dense obsidianaceous, not vesiculated, partly perlitic. Glomerophyres plg + bt + px; sieved and zoned plg; rare K-fs (max 1 cm) megacrysts.	Layers and small lenticular patches in lithofacies (a) and (b), planar to very irregular mingling textures [69]. Never outcropping in large individual bodies. (**Figure 5b**)
d	Coherent vitrophyric vesiculated cream-colored trachydacite	In beds 0.1–10 cm thick, poorly porphyritic, medium-fine grain. Groundmass glassy vesiculated, patches of highly vesicular fibrous glass (**Figure 4e**).	Interlayers in the other coherent lithofacies defining a compositional flow lamination. Never outcropping in large individual bodies. (**Figure 4h**)
Fragmental lithofacies			
e	Monogenetic clast- to matrix-supported breccia, fine-grained clastic matrix	Poorly sorted, sometimes inverse-graded. Clasts (cm to dm scale) of blocky, roughly equant, angular to sub-rounded fragments of lithofacies (a) and (b) with flow laminations. Matrix loose to poorly indurated, composed of finer fragments of the same composition.	Thickness 0.5–2 m, lateral extension 1–20 m; after lateral extinction, encasing flow units become para-concordant. Basal breccia in Q and P units, interflow breccia in F and G units, surface breccia in L unit. (**Figures 4** and **5c**)
f	Monogenetic matrix- to clast-supported breccia, clasts welded in a vitrophyric matrix	Poorly sorted. Clasts (cm to dm scale), angular to sub-rounded fragments of lithofacies (a) and (b) with flow laminations, lacking deformation structures. Red and gray coherent vitrophyric matrix welding the clasts, with sharp boundaries; sometimes, matrix is injected in fractures within clasts.	Thickness 0.5–5 m, lateral extension 2–5 m. Clasts' flow lamination evidences little rotation and jigsaw-fit texture. Interflow breccia in F and G units. (**Figure 4f** and **5d**)

	Lithofacies	Compositional characteristics	Architecture and occurrence
g	Monogenetic clast-supported scoria agglomerate	Sub-rounded clasts (dm scale) of coarsely vesiculated, dense fragments (scoriae) of lithofacies (a) and (b). Open framework with scarce and irregularly distributed fine-grained clastic matrix with the same composition of clasts.	Thickness 0.3–1 m, lateral extension limited to few meters. Interflow layer in F and G units.

bt: biotite, K-fs: K-feldspar, plg: plagioclase, px: pyroxene. ME: magmatic enclave, Msx: meta-sedimentary xenolith.

Table 2.
Summary of the macroscopic lithofacies of SLLFs of Monte Amiata trachydacite.

of different lithofacies. Another characteristic of the Monte Amiata SLLFs is the presence of cavities with irregular shape formed around meta-sedimentary xenoliths and megacrysts of plagioclase and sanidine (**Figure 5f**). In this case, gas segregation may result directly from the inclusions.

A layered banded aspect, often flat-lying, is well developed in the Monte Amiata SLLSs, defined both by the interlayering of different lithofacies and by variation in vesicularity, crystallinity, grain size, color, and groundmass texture. Flow bands are laterally continuous, parallel, and dominantly quite planar.

Two types of flow banding must be distinguished in the Monte Amiata SLLFs. A pervasive fine-scale flow banding structure (flow lamination) is produced by interlayering of mm- to cm-sized dark and light laminae of different coherent lithofacies (**Figure 4h**). In addition, sheeting joints, generally attributed to shear partings developed during laminar flow, form well-developed bedding (**Figure 4g**). The stratified structure (flow bedding) comprises massive beds (cm- to m-thick) of porphyritic and vitrophyric coherent lithofacies enclosed at top and bottom by inter-layers (mm- to cm-thick) of microvesicular or obsidian lithofacies (**Figure 4a** and **b**). Several processes have been taken into account for the formation of bedding in silicic lavas [74]: (i) mingling of different parts of the magma [75–77]; (ii) welding and rheomorphism [78]; (iii) repeated brecciation followed by reannealing into the conduit [79, 80]; and (iv) laminar flowage inherited during flow in the conduit in response to shear stresses along the conduit walls that continue and propagate upward during the lava advance for the shear stresses at the lava flow base [9].

The flow bands define local sinuosity, steep dips, folding, and convolution in frontal and margin zones of SLLFs (see Section 4.2.3).

Some of the Monte Amiata SLLF trachydacite (Sorgente del Fiora and Piancastagnaio) shows parallel columnar cooling joints that post-date the flow bedding and flow lineation. They are roughly defined, with spacing of 1.5–2.5 m, vary from subvertical to dipping at moderate angles toward the flow front.

4.2.3 Surface and margin structures

At Monte Amiata, *in situ* paleo-weathering, overlaying by younger volcanic units, and current poorly exposure preclude the detection of SLLF original surface structures, such as creases [81] and fractures [82], typical of large silicic lava flows. At the meso-scale, the only surface structures that were preserved in SLLFs include surface ridges or ogives.

Surface ridges or ogives are arcuate reliefs, transversely oriented to the downslope flow. Their convexity indicates the direction of flow. The arcuate shape is caused by the increase in frictional resistance toward the margins of the flow [38, 83]. At Monte Amiata, the presence of surface ridges or ogives is mainly evident on the Quaranta and Castel del Piano units (**Figure 2**). Both these trachydacite SLLFs are stratigraphically below the surface of saprolite paleo-weathering that marks the boundary between BAS and MAS. The Monte Amiata ogives look as linear accumulations of lava boulders. Boulders are rounded-shaped, stacked in an open framework, and arranged in transversal arcuate ridges that are spacing 50–100 m apart from each other with apparent amplitudes averaging 5–15 m upon the topographic surface. These structures have already been distinguished by [30], which, however, considered ogives as the discriminating structure supporting his interpretation of Monte Amiata rheoignimbrites.

Several interpretations have been proposed to explain the formation of ogives on silicic lava flows. Taking Monte Amiata as a model, Rittmann [30] first explained the formation of ogives as pressure ridges due to the differential viscosity between the hot and fluid core and the rigid surface of flows that is compressed and corrugated in folds. The boulders forming the ridges are considered by [30] of primary volcanic origin, resulting as the remnant of rootless dikes of molten material intruded from below in the fractured core of the anticlinal-like ridges subjected to extensive stresses. These seminal ideas of Alfred Rittmann are the premise for various subsequent interpretations. However, most of the observations and models on surface ridges have been addressed to rhyolite obsidian domes and coulées rather than to the structures present on the surface of long silicic lava flows. Macdonald [84] proposed that the ridges on rhyolitic block lava flows are the surface expression of the upward bending—named ramp structure—of the shear planes of the internal flowing lava. The conception that ogives are folds of the lava crust produced by ductile deformation in compression (pressure ridges) as due to differential movements between two layers (center and outside crust of the flow) having temperature and viscosity contrasts was applied by previous scientists [9, 83, 85] among others. Another interpretation proposes that surface ridges are evidence of an extensional regime due to the inflation and deformation of a rigid crust. The moving fluid-rich melt beneath the insulation crust extrudes through regularly spaced cracks forming diapir-like structures [9, 86, 87]. In a more extreme way, Andrews and colleagues [88] challenged the "fold theory" of Fink and proposed that ogives are tensile fracture-bound structures that record brittle failure and stretching of the crust as the lava advances and spreads.

Based on our field observations (**Figure 6**), we interpret the ogives developed on the surface of Monte Amiata SLLFs as compressional structures [89] produced during downslope flowage of viscous silicic lava. The core of these small antiform folds is fractured, enhancing a stronger spheroidal *in situ* weathering of lava in rounded boulders (corestones) during the paleo-weathering processes (**Figure 6**; [62]). Being prominent on the topographic surface, ogives are also the site of more intense surface erosion that removed the sandy saprolite matrix. Consequently, the residual blocks have collapsed in place on themselves forming the boulder accumulations exposed on flow surface [62].

Previous authors [39, 40, 43] have interpreted the surface ridges and boulder accumulations on Monte Amiata SLLFs surface as the evidence of the emplacement of block lava flows. Block lava flows are defined [84, 90, 91] as lava flows in which a highly irregular surface is completely covered by continuous, open clast-supported debris of dense and solidified lava blocks, up to several meters in size, with a

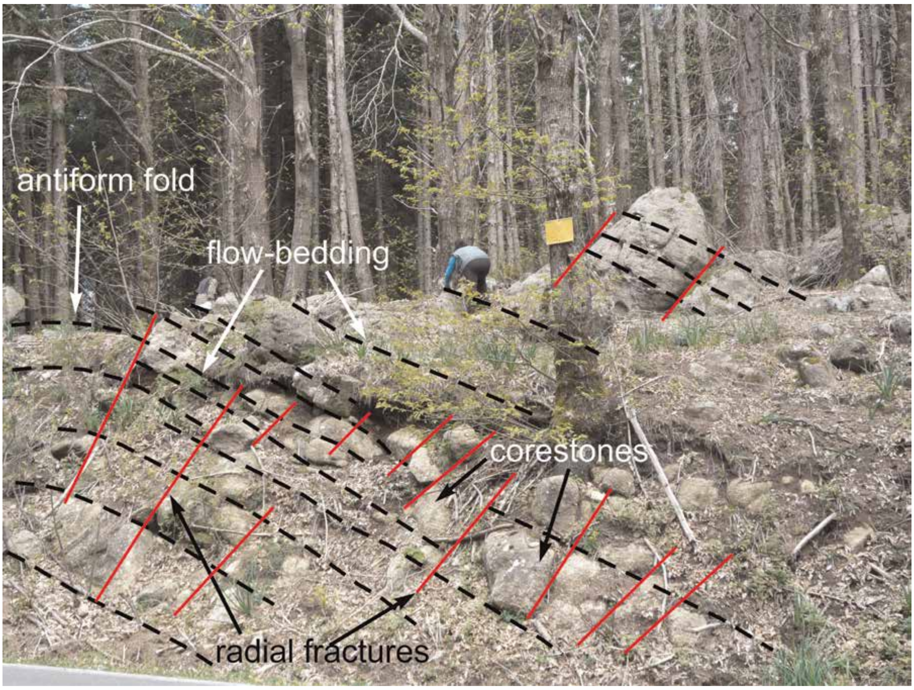

Figure 6.
Natural section showing the internal structure of a ridge (ogive) on the surface of the Quaranta SLLF. The flow banding (dashed black lines) defines an antiform fold. Radially distributed fractures (red solid lines) are related to the extension in the anticline hinge. At the intersection between joints defined by the flow banding and extensional fractures, in situ *saprolite paleo-weathering isolated subrounded corestones of trachydacite. As an extreme effect of this alteration, the ridge resulted as an accumulation of residual lava blocks. Geologist for scale.*

polyhedral shape delimited by smooth, slightly curved faces and angular edges. Normally in the block lava body, a central mass of massive lava is preserved, but the fragmented material remains predominant [84]. Block lavas formed from magmas with silicic to intermediate composition and high viscosity. The mechanism of formation of a blocky breakage of lava is interpreted as dependent on the rapid growth on the flow surface of a thick, more or less glassy crust, which shatters due to the movement of the warmer underlying flow [90]. The extensive deposits of large subrounded lava boulders arranged in arcuate ridges on the surface of the SLLFs of Monte Amiata are not identifiable with the block lava flow as defined above.

The typical structural model of silicic lava flows comprises an internal coherent core enveloped with flow-generated breccia that forms loose deposits on the surface, along the flow margins (levées; [3]) and at the flow front [12]. In Monte Amiata SLLFs, evidence of the presence of lateral levées and accumulation of auto-brecciated debris at the flow front were not observed.

Surface breccia is also absent, but of a localized exception in the Leccio eruptive unit. In the outcrop of Pian di Ballo quarry, located in the medial part of the Leccio lava flow, coherent trachydacite is enveloped with flow-generated breccia (**Figure 7**). Based on texture of the deposit, we distinguished five lithofacies: (1) coherent massive trachydacite with concentric flow foliation forming a monolithic core; (2) coherent stratified trachydacite protruding laterally from the massive core; (3) fractured trachydacite (both massive and stratified) with close fractures and jigsaw cracks; (4)

fragmented and poorly disaggregate trachydacite; and (5) monogenetic, structure-less matrix-supported lithic breccia. These lithofacies undergo lateral transitions with grading boundaries and complex sedimentary architecture (**Figure 7**). Fragmented and poorly disaggregated lava (lithofacies 4) is characterized by polyhedral blocks, up to 1 m large (**Figure 7**) with low intra-clast matrix. Even though most of the blocks are

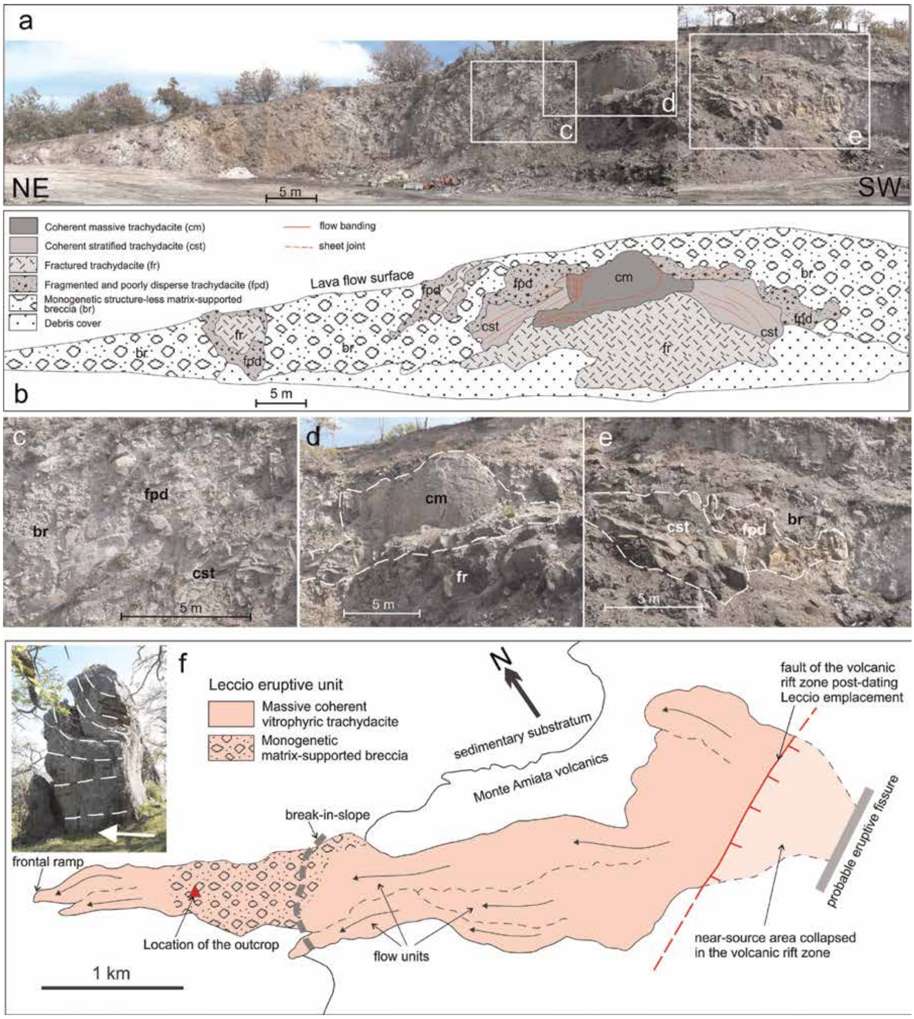

Figure 7.
Quarry escarpment in the locality Pian di Ballo (red triangle in f) showing a complete section transversal to the flow direction of the Leccio SLLF. The structure of the lava flow shows the development of a surface autobreccia. (a) Photo and (b) sketch of the outcrop. A central core of massive trachydacite (cm) with concentric flow foliation is embedded in a monogenetic breccia (br) through progressive fragmentation and dispersion of lava blocks. Although the different lithofacies on the sketch are separated by solid lines, the contacts are gradational. Flow direction is toward the observer. (c) Particular of the gradational transition from coherent trachydacite (cst), to fragmented and poorly dispersed trachydacite (fdp), and to chaotic breccia (br). (d) Close-up of the massive lava core (cm). While the outermost part of the flow was breaking, the center was still molten and moving lava. (e) The flow banded lava (cst) is progressively pervasively fractured by a network of jigsaw cracks but remaining coherent, then is fragmented in a jigsaw-fit breccia that retains the original stratification (fpd), and, finally, is dispersed in the breccia (br). Location of boxes c, d, and e is depicted in a. (f) Map of the Leccio eruptive unit showing the areal distribution of lithofacies and structures. In the inset is the frontal ramp at the edge of the SLLF.

shattered, they retain a recognizable geometry of original bedding and jointing of the primary depositional and cooling structures of lava flows. Bigger blocks are either fractured or shattered, and many of the block interiors exhibit pervasive jigsaw cracks and jigsaw-fit fractures. This lithofacies represents portions of the coherent pre-fragmentation lavas, slightly disaggregated and displaced. The monolithologic massive and poorly sorted breccia (lithofacies 5) is a chaotic assemblage of matrix-supported clasts from medium to well consolidated. Angular to sub-rounded fragments of trachydacite, ranging from a few centimeters to more than a few decimeters in size, are completely disaggregated and dispersed in the prevailing sandy matrix with the composition of the adjacent clasts. This matrix was likely produced by the disaggregation of the same clasts during transport.

Geologic relationships indicate that fragmentation of a rhyolite lava flow occurred mainly when the flow was spreading [92]. The spatial distribution of the breccia deposit present at the surface of the Leccio eruptive unit (**Figure 7f**) indicates that this unusual (for Monte Amiata SLLFs) volcanic facies probably formed as a function of the change in topography that the lava has encountered during emplacement. From the source area, represented by an eruptive fissure of the summit volcanic rift zone (**Figures 2** and **7f**), the Leccio trachydacite flowed for up to 3 km along a slope of about 15° and then reached a low gradient area (2–3° in slope) without confining walls at the edge of the volcanic edifice. When the flow arrived at the abrupt break-in-slope, it decelerated, and a dynamic block fragmentation occurred at the margins and surface of the flow, forming the monogenetic matrix-supported breccia observed in this part of the Leccio eruptive unit (**Figure 7**). The increase in the degree of fragmentation suggested by the textural characteristics of the breccia (grain size reduction, jigsaw cracks, and jigsaw-fit fragmentation), proceeding from the internal coherent core to external surfaces of flow, is probably the consequence of progressive fracturation, disaggregation, and dilation processes that have occurred during this deceleration phase [93, 94]. Then, the massive coherent trachydacite core (**Figure 7d**) resulted in a thermally insulated internal part of the lava that continued to flow downstream confined through a paleo-valley, attaining a total length of more than 6 km (**Table 1**), and terminated with a frontal ramp structure (**Figure 7f**).

Monte Amiata SLLFs have steep flow front, tens of meters thick, exhibiting ramp structures and monoclinal folds outlined by the orientation of the flow bedding (**Figure 8**). In ramp structures, the flow bedding varies from a flat foliation parallel to the base of the flow to an upward curved, steeply dipping to vertical shape. The stack of layers involved in the upward spoon-shaped deformation overrides along a plane of shearing and discontinuity the underlying gently dipping layers (**Figure 8a**). Contact occurs without the interposition of breccia. Moving upstream away from the ramp, the attitude of the flow bedding becomes para-concordant. These ramp structures have been observed near the frontal portion of several flow units and are probably to be attributed to an increased stress regime owing to an increasing frictional resistance toward the base of the flow ramp. Indeed, they are well developed at the front of flow that was channelized and ponded in paleo-valleys (Leccio and Vivo d'Orcia; **Figure 7f**, **8a** and **b**). The ramp structures observed in Monte Amiata SLLFs are different from both the sheet-like flow ramps described in obsidian block lava flows and attribute to individual flow units having upper and lower surfaces that are composed of *in situ* brecciated, brittle glassy carapaces (i.e., the Rocche Rosse flow at Lipari; [95]) and ramps triggered by shear planes inside the lava interior and related to the formation of surficial ogive structures [96].

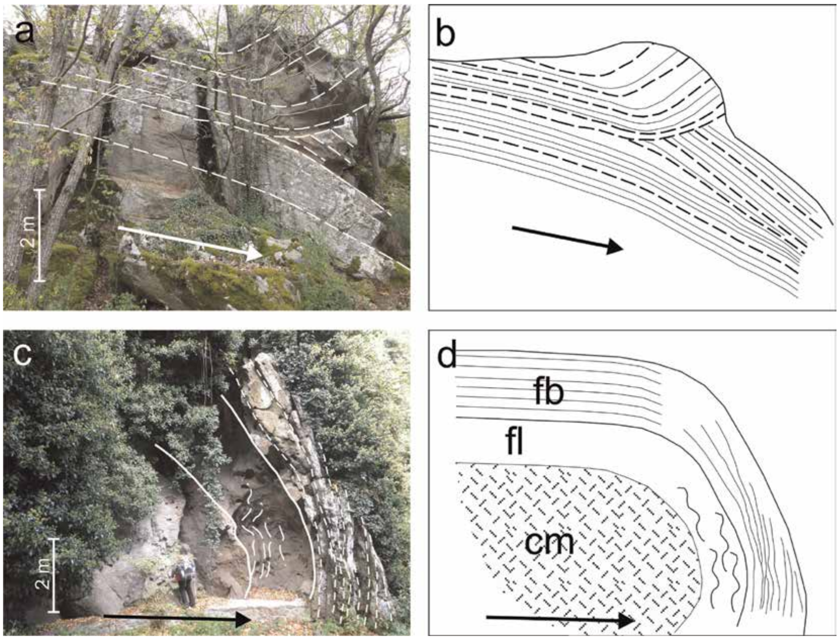

Figure 8.
Flow front structures in SLLFs of Monte Amiata. (a) Outcrop exposure and (b) interpretative sketch of flow ramp structure at the flow front of Vivo d'Orcia eruptive unit composed of fine laminated vitrophyric trachydacite with perlitic glassy groundmass. Arrow is the flow direction. Note the transition from para-concordant to discordant bedding and the absence of breccia deposits. (c) Outcrop exposure and (d) interpretative sketch of monoclinal fold structure of the flow front of Piancastagnaio eruptive unit. The core of the fold is composed of coherent massive trachydacite (cm), enveloped in flow-laminated (fl) and flow-banded (fb) trachydacite. Along the subvertical limb of the fold, the flow-laminated lava is deformed in small asymmetric parasitic folds and the flow-banded lava is stretched.

Another type of flow front observed at Monte Amiata consists of layers which, instead of being bent upward, as in the ramps, are bent downward to form a monoclinal fold (**Figure 8c** and **d**). In this case, flow bedding is planar and sub-horizontal in the upper part of the flow body, whereas near the front, it curves sharply downward until it becomes subvertical. Flow bedding experienced a stratal stretching and thinning caused by the extension in the fold limb (**Figure 8c** and **d**). The core of the fold is composed of coherent massive trachydacite, enveloped by faintly tiny laminated trachydacite with layers deformed in crumpled minor folds. Locally, a detachment surface has been observed at the base of the frontal fold. Also in this case, the deformation occurs without the presence of breccia. This type of flow front has been observed in the Piancastagnaio and Sorgente del Fiora eruptive units.

Flow front of lavas usually is obscured by a talus apron. At Monte Amiata, the presence of frontal breccia has never been observed. It cannot be excluded *a priori* that breccia has been completely removed by erosion, but the lack of both any deposit remains and its continuation in a basal breccia lead to the interpretation of an emplacement mechanism different from that of rhyolite lava flows.

4.3 Facies architecture

Within a single flow unit, the vertical and lateral lithofacies distribution and association allows to recognize a characteristic structural partitioning of lava flow interior [11, 97]: (i) basal zone; (ii) core or central zone; and (iii) upper zone.

i. The basal zone [12, 98] of BAS SLLFs typically rests directly on the surface of the underlying unit (sedimentary substratum or older volcanic units in core drill DL) without intervening pyroclastic, volcaniclastic, sedimentary, or pedogenetic layers. MAS SLLFs overlay the paleo-weathering saprolite deposit developed at the expense of BAS units. The SLLF basal zone is generally 2–5 m thick and comprises a breccia bed (lithofacies e; **Table 2**) or a shear zone (**Figure 9**). The occurrences of basal breccia are localized; the contact between the basal breccia and the overlying lava is typically sharp. In the classic models [12, 99], basal breccia is interpreted as originated as crumble breccia at the surface of slowly moving masses of lava, which concurs to form the steep flow front talus and then was overridden as the lava advanced. In Monte Amiata SLLFs, both the absence of surface and frontal breccia deposits and the texture of the basal breccia observed suggest that the basal breccia is produced *in situ* by shear fragmentation. In most cases, the basal breccia is lacking, and the bottom of SLLF is composed of bedded facies with flow layering of glassy and microcrystalline trachydacite (lithofacies a, b, and d; **Table 2**), planar or tightly folded, and sparse—greatly stretched—shrinkage gas cavities.

ii. The central (lava core) zone [12] in SLLFs of Monte Amiata is typically 20–40 m thick and comprises massive and bedded facies, with joints and flow

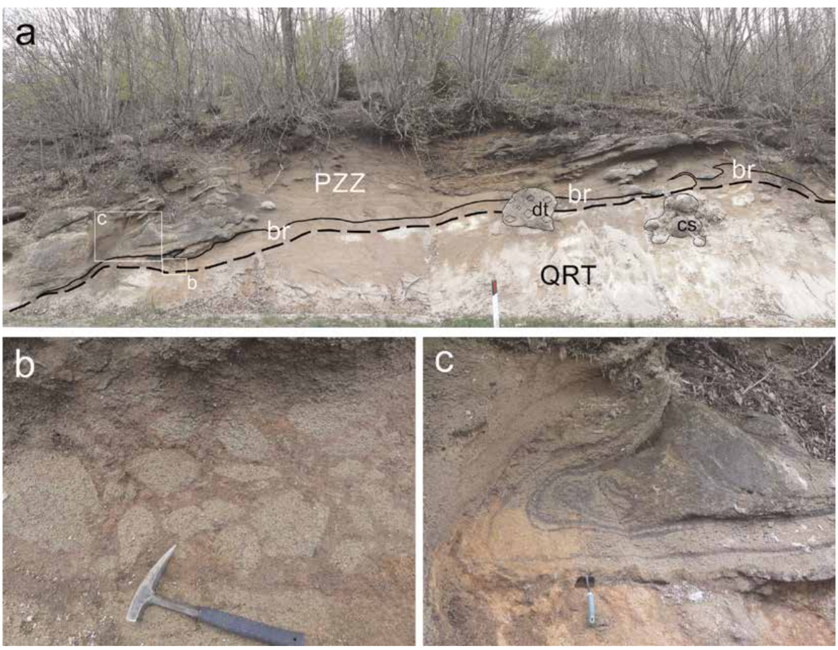

Figure 9.
(a) Overview of the outcrop showing the contact between the Quaranta (QRT) and Pozzaroni (PZZ) SLLFs. The upper portion of the Quaranta lava flow (BAS-MSS) has been in situ *paleo-weathered into a whitish sandy saprolite with groups of corestones (CS). The basal zone of the Pozzaroni lava flow is composed of a discontinuous bed of monogenetic matrix-supported breccia (br) overlaid by flow-bedded trachydacite. Both breccia and stratified basal trachydacite are deformed in convoluted folds. dt =debris. Boxes refer to b and c details. (b) Close-up of the breccia at the base of PZZ eruptive unit. The flow lamination in the clasts is randomly oriented. (c) Detail of the recumbent fold and convoluted structures at the base of PZZ formed during the flow for the high viscosity of the lava.*

layering. Massive lava is generally uniform and dense. Lava shows poorly developed, vertical, or locally inclined columnar joints a few to several meters across (i.e., Sorgente del Fiora and Piancastagnaio eruptive units). Subhorizontal sheeting joints are also present and are more conspicuous near the top and base of the central zone. Flow layering is parallel to aligned crystals and vesicle-rich layers and is interpreted as planes of weakness imparted by the flowage. In some units (i.e., Sorgente del Fiora and Vivo d'Orcia eruptive units), lenses and irregular zones of welded breccia (lithofacies f; **Table 2**) and scoriaceous agglomerate (lithofacies g; **Table 2**), with an individual thickness of 0.5–1.5 m, form interlayers between otherwise massive lava banks. We interpret that these interlayers resulted from intra-flow fragmentation processes within a single eruptive unit, probably related to stresses caused by movement in the overlying flow.

iii. The upper zone of Monte Amiata SLLFs trachydacite is characterized by a moderately more vesicular groundmass and a planar morphology forming subhorizontal plateaus and poorly inclined sides. It does not show the typical structure of lithophysae, strong vesiculation, and scoriaceous or blocky autobreccia classically described for the top of large silicic lava flows [12, 92]. The absence of these surface structures is confirmed by the stratigraphic log of the Sorgente del Fiora unit in the DL core (**Figure 4**), even if it cannot be excluded that in other units, they were present but currently poorly exposed or subsequently eroded.

4.4 Geochemical and petrographic characteristics

The whole chemical composition of the lava flows (LF) and domes (LD) at Monte Amiata ranges from latite to trachydacite (SiO_2 = 57–68 wt%; $Na_2O + K_2O$ = 7–9 wt%; **Figure 10**) [40, 42, 44, 57, 58, 100]. In variable proportion through the entire sequence, millimetric to pluri-decimetric in size, meta-sedimentary xenoliths and microgranular magmatic enclaves (ME) are present. The ME compositions range from trachybasalt to latite (SiO_2 = 47–59 wt%; $Na_2O + K_2O$ = 5–8 wt%; **Figure 10**; [58]). A careful selection (**Table 3**) of data from literature shows that all the SLLF samples are among the most evolved rocks of the suite and classify them as trachydacite (SiO_2 = 64–68 wt%; $Na_2O + K_2O$ = 8–9 wt%; **Figure 10**) having a normative q > 20% (q = Q/(Q + or + ab + an)*100) [101].

The SLLFs are highly porphyritic (about 40% according to [41]), medium- to coarse-grained, with maximum dimensions of the phenocrysts rarely exceeding 1 cm (**Table 4**). The most abundant phenocrysts are plagioclase, K-feldspar, orthopyroxene, and biotite, and less abundant are apatite, ilmenite, and quartz, rarely present clinopyroxene (**Table 4**). The presence of fragmented crystals is peculiar, especially of K-feldspar (**Figure 11a** and **b**). Content in mafic magmatic enclaves is scarce, while tabular meta-sedimentary xenoliths are more frequent.

Instead, the lava domes, coulées, and short lava flows are medium to high porphyritic ranging from 26 to 34% [41, 56], with similar mineral paragenesis, but are characterized by the distinctive presence of K-feldspar megacrysts (from 1 to 5–6 cm long) coupled with abundant microgranular magmatic enclaves [40, 42, 44, 57].

The SLLFs are generally porphyritic to glomeroporphyritic with a glassy groundmass commonly showing perlitic fractures. Different groundmass microtextures are observed, also in the same unit: (i) glassy groundmass microlite-free (**Figure 11c**) or

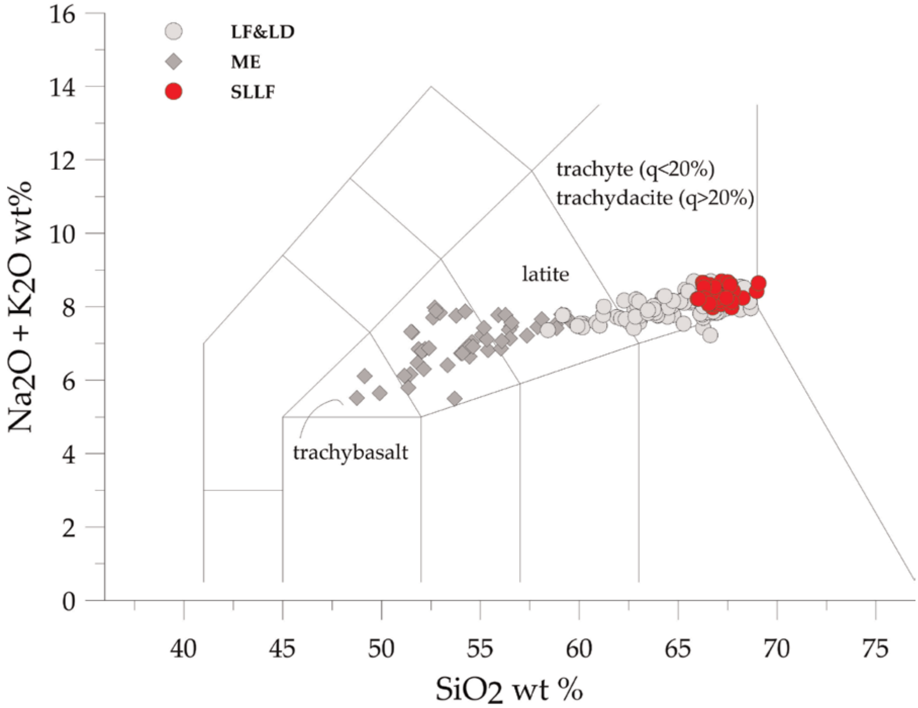

Figure 10.
T.A.S. (Total Alkali-Silica) diagram for products of Monte Amiata volcano: Silicic lava flows and lava domes (LF + LD; light gray dots), magmatic enclaves (ME; dark gray diamonds), and SLLF units studied in this work (red dots; ***Table 2****). Data from [39–42, 44, 57].*

(ii) with ultra-microlites aligned to the flow direction (**Figure 11d**); (iii) glassy groundmass locally devitrified with scattered spherulites (**Figure 11e**); and (iv) heterogeneous groundmass with flow banding in elongated bands or lenses generally of a darker color (**Figure 11f**). Flow bands are normally enriched in crystal fragments (**Figure 11g**); (v) highly vesicular with fibrous glass and large flattened vesicles (**Figure 11h**).

4.5 Temperature, pressure, and dissolved volatile content in Monte Amiata magmas

In order to retrieve the conditions (i.e., pressure, P; temperature, T; and volatile content) of magma in the storage system and during the dynamics of ascent toward the surface, and to understand eruption dynamics of Monte Amiata SLLF generating magmas, we have applied the numerous geothermobarometers and geohygrometers so far available in the literature, accounting for both "crystal," "crystal-crystal," and "crystal-residual liquid" equilibria. The compositions of the lavas for which calculations were performed are reported in **Table 3**. More details about the contour conditions (e.g., mineral-liquid duplets; preliminary estimations by independent variables; necessary equilibrium tests) necessary to apply each specific model are reported in [102].

The list of geothermobarometers and hygrometers adopted is reported in **Table 5** [103–107], together with the temperature interval of application of magma ascent and

Label	SLLF[1]	Ref[2]	SiO_2 wt%	TiO_2	Al_2O_3	$Fe_2O_3^*$	FeO	MnO	MgO	CaO	Na_2O	K_2O	P_2O_5	LOI	Sum
84 BB	A	3	64.67	0.52	16.30	3.19		0.04	1.53	2.75	2.03	5.70	0.18	2.97	99.88
AMT 47	A	2, 4	66.28	0.52	16.33	1.11	2.00	0.05	1.23	2.75	2.14	6.16	0.18	1.26	100.00
AMT 48	A	2, 4	65.69	0.52	16.67	0.38	2.72	0.05	1.27	2.71	2.12	5.99	0.17	1.72	100.00
AMT 94	A	4	67.43	0.49	16.27	0.59	2.26	0.04	1.31	2.13	2.17	5.97	0.13	1.22	100.00
AMT 17–145	A	5	64.30	0.51	15.70	3.46		0.05	1.36	2.72	2.26	6.04	0.16	1.85	98.52
84 AV	C	3	65.89	0.49	16.08	3.67		0.05	1.28	3.02	2.21	5.74	0.16	1.28	99.87
AM 11	C	1	66.57	0.52	15.90	2.06	1.38	0.05	1.43	3.01	2.26	5.73	0.20	0.87	99.98
AM 13	C	1	66.11	0.50	15.70	2.07	0.91	2.41	0.05	2.53	2.13	5.90	0.19	1.51	100.01
AM 19	C	1	66.98	0.54	16.05	2.56	0.59	0.05	1.33	2.76	1.96	5.93	0.18	1.06	99.99
AMT 06	C	2, 4	65.82	0.59	16.36	0.61	2.72	0.06	1.19	2.96	2.20	6.06	0.18	1.26	100.00
AMT 08	C	4	66.25	0.56	15.52	0.83	2.48	0.06	1.21	2.97	2.22	6.35	0.15	1.40	100.00
AMT 09	C	4	66.81	0.51	15.63	0.85	2.20	0.05	1.13	2.95	2.28	6.23	0.15	1.22	100.00
Amt 10	C	2, 4	66.40	0.53	15.70	0.72	2.52	0.06	1.32	2.99	2.37	5.91	0.16	1.25	99.93
AMT 10	C	2, 4	66.73	0.56	15.54	0.60	2.52	0.05	1.19	2.96	2.28	6.29	0.17	1.12	100.00
AM 37	F	1	68.27	0.48	15.26	2.14	0.64	0.05	1.11	2.56	2.20	6.14	0.15	1.01	100.01
AMT 50	F	4	65.74	0.58	15.80	0.48	2.76	0.05	1.36	3.16	2.14	6.04	0.16	1.74	100.00
AMT 51	F	2, 4	65.70	0.54	16.06	0.43	2.76	0.05	1.33	2.98	2.13	5.95	0.16	1.91	100.00
84 BD	G	3	65.42	0.47	16.22	3.69		0.05	1.28	3.11	2.19	5.74	0.15	1.56	99.88
AMT 56	G	2, 4	66.90	0.50	15.64	0.16	2.80	0.05	1.27	2.93	2.18	6.14	0.15	1.28	100.00
AM 16	L	3	68.34	0.48	15.19	2.41	0.36	0.05	1.13	2.30	2.30	6.25	0.15	1.20	100.16
AMT 01	L	2, 4	66.91	0.58	15.51	0.50	2.56	0.05	1.19	3.00	2.25	6.24	0.16	1.05	100.00
AMT 03	L	2, 4	66.14	0.62	15.83	0.49	2.76	0.06	1.27	3.20	2.23	6.09	0.18	1.14	100.00
AMT 04	L	2, 4	66.01	0.56	15.87	0.77	2.68	0.06	1.28	3.08	2.18	6.11	0.16	1.25	100.00

Label	SLLF[1]	Ref [2]	SiO_2 wt%	TiO_2	Al_2O_3	$Fe_2O_3^*$	FeO	MnO	MgO	CaO	Na_2O	K_2O	P_2O_5	LOI	Sum
AMT 13–10	L	5	65.70	0.51	16.10	3.66		0.06	1.41	3.00	2.40	6.19	0.17	1.41	100.73
AMT 13–21	P	5	66.00	0.55	16.00	3.74		0.06	1.40	2.39	2.17	6.26	0.17	1.58	100.42
AM 71	Q	3	66.87	0.51	15.95	2.18	0.97	0.05	1.29	2.72	2.40	5.63	0.18	1.25	100.00
AMT 60	Q	2, 4	65.36	0.63	16.36	0.53	2.76	0.06	1.34	2.87	2.29	6.22	0.17	1.41	100.00
AMT 14–57	Q	5	66.00	0.54	15.90	3.74		0.06	1.45	3.20	2.39	6.10	0.18	1.51	101.17
84 AZ	V	3	65.01	0.50	16.62	3.85		0.06	1.43	2.80	2.16	5.93	0.17	1.72	100.25
84 BA	V	3	65.60	0.50	16.03	3.75		0.05	1.45	3.21	2.21	5.93	0.16	0.98	99.87
AMT 96	V	4	65.22	0.51	17.55	1.23	1.72	0.04	1.30	2.31	2.17	5.75	0.17	2.04	100.00
AMT 97	V	2, 4	66.60	0.50	16.12	1.75	1.64	0.04	1.21	2.61	2.18	5.95	0.15	1.25	100.00
AMT 95	V	2, 4	64.81	0.55	17.47	0.19	2.84	0.05	1.44	2.54	2.16	5.90	0.19	1.86	100.00

[1]*Label of SLLF units as in **Figure 2**: A. Abbadia, C. Castel del Piano, F. Fiora, G. Piancastagnaio, L. Leccio, P. Pozzaroni, Q. Quaranta, V. Vivo D'Orcia).*[2]*References: 1: [58], 2: [40], 3: [42], 4: [44], 5: [57].* **Total iron as* Fe_2O_3.

Table 3.
Representative chemical whole rock compositions of selected samples of SLLF from Monte Amiata.

Groundmass texture	Glassy with perlitic fractures, subordinate aphanitic, and devitrified in spherulites (unit P); variable amount and distribution of vesiculation, stretched and folded vesicles aligned according to flow foliation (units F, P, Q, and V), sometimes filled by secondary precipitation minerals (e.g. cristobalite) (unit P); variable amount (few to abundant) of microlites and spider- and needle-shaped ultra-microlites (mainly K-fs and px) aligned according to flow foliation
Phenocrysts assemblage[1]	K-fs (medium 5 mm, rare up to 1.5 cm); plg (3–5 mm); opx (2–3 mm); bt (medium 1–3 mm, abundant, euhedral and up to 4 mm in units A, P, Q, and V); rare cpx (unit F); glomeroporphyres of plg + opx + bt units F, G, Q, and V)
Mineral phases and microstructures[1]	K-fs: mainly fragments of larger crystals, Carlsbad twinning (unit F), rounded and lobate rims; some poikilitic texture including melts and crystals (plg, bt and crystal aggregate of plg + opx) (units A, L, Q, and V) Plg: complex zoned crystals with sieve-textured and patchy-zoned resorbed nucleii (highly altered into alluminosilicate minerals e.g., allophane) and oscillatory-zoned rims., often host fluid, glass and mineral inclusions(e.g., bt, opx, Fe-Ti oxides), commonly as crystal cluster (C, F, G, P, and V) Bt: abundant, sometimes opacized; folded, broken in thin lamellae, and containing sub-spherical holes (sieve texture) and mineral inclusions Opx: deep embayments and rounded opacized rims include small euhedral apatite and Fe-Ti oxides. Cpx: rare, in microphenocrysts and microlites Fe-Ti oxides: microphenocrysts: commonly included in other minerals Quartz: abundant highly resorbed crystals (unit L)
ME/xenoliths	Holocrystalline aggregates (plg + opx + bt), abundant in units P and Q Meta-sedimentary xenoliths, dark gray, platy, fine-grained, composed of: (i) green spinel+bt + feldspar, unit A, (ii) green spinel + graphite, with a feldspar corona, and "baked clay"-like fragments, unit L, (iii) green spinel + quartz + cordierite with plg + bt corona, unit Q, and iv) aggregates of acicular crystals bt/phlogopite + plg + K-fs + cpx + glass, unit V

[1]*Mineral phases: K-fs = K-feldspar; plg = plagioclase; cpx = clinopyroxene; opx = orthopyroxene; bt = biotite. ME: mafic magmatic enclave. Labels of SLLF units as in* ***Figure 2.***

Table 4.
Microscopic petrographic characteristics of Monte Amiata SLLFs.

lava flow dynamics. Our results all show that the lavas emitted at Monte Amiata represent, in terms of temperature, an extreme end member for each of the compositions and mineral assemblages investigated here.

On the basis of the results provided in **Table 5**, we can distinguish two sample subsets: (1) a first group (PES, preeruptive stage) characterized by crystalline liquid balances associated with a phase of initial crystallization, where the liquid is the total rock, representative of a preeruptive or initial phase of ascent; (2) a second group (ES, eruptive stage) where the liquid phase in equilibrium with a specific crystalline phase is the interstitial fluid. This group has been related to a late phase of the crystallization occurred during the ascent of the magma and/or during the mass emplacement of lavas. The PES group shows temperature estimates between 900°C and 1070°C, whereas ES group has temperature range between 800°C and 900°C. These temperature ranges constitute the entire temperature interval provided by the employment of all the geothermometers analyzed and constitute therefore an enlarged estimate of the real intervals of expected temperature.

The estimation of dissolved water content (hereafter reported as H_2O and expressed in wt%) is of fundamental importance to comprehend the storage and

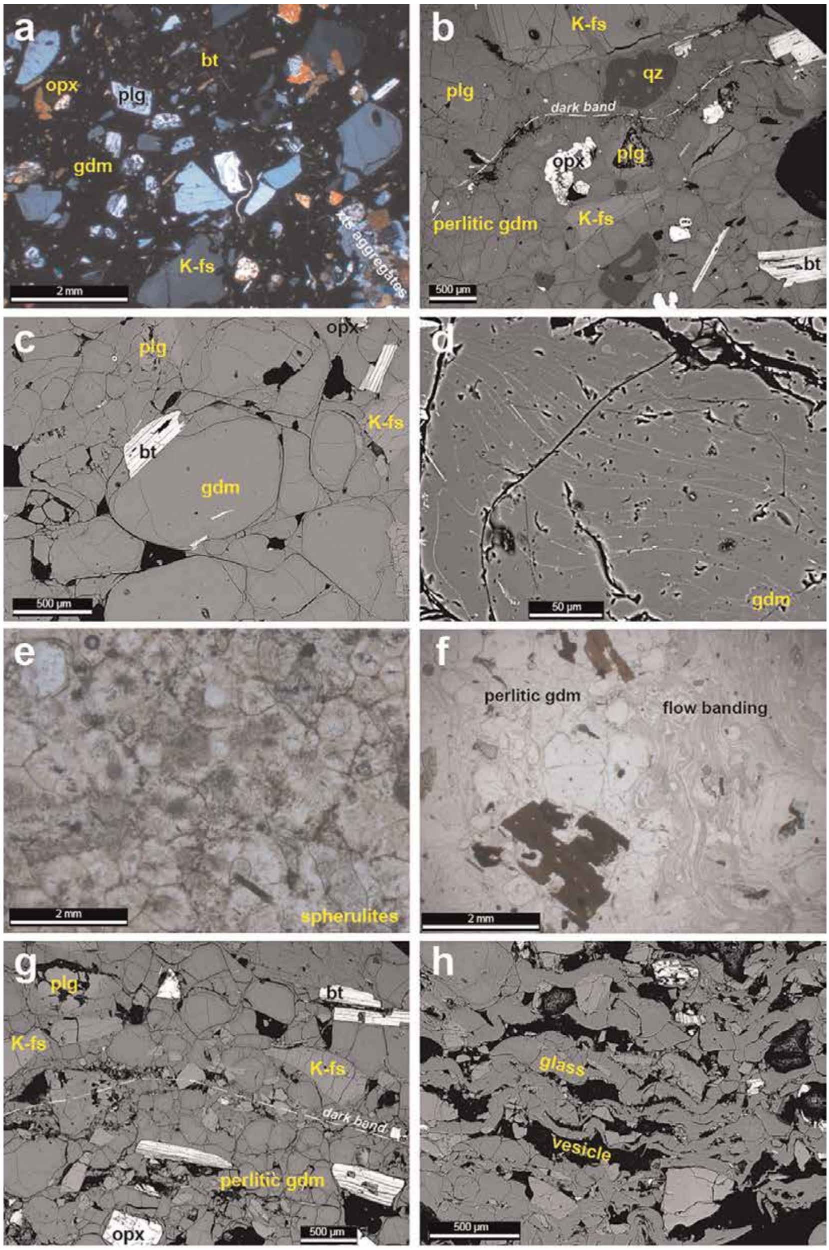

Figure 11.
(a) Highly porphyritic texture: The phenocrysts are fragmented crystals of K-feldspar, plagioclase, orthopyroxene, biotite set in a glassy groundmass (optical microscopic image crossed polarized, unit Q, sample AMT 14–51); (b) broken crystals of K-feldspar, zoned plagioclase, orthopyroxene, biotite, and resorbed quartz set in a perlitic glassy groundmass (BSE-SEM image, unit L, sample AMT 14–71b); (c) glassy groundmass, microlite-free, with perlitic texture (BSE-SEM image, unit L, sample AMT 13–10b); (d) glassy groundmass with ultra-microlites (probably Fe-Ti oxides) aligned to the flow direction (BSE-SEM image, unit L, sample AMT 13–10b); (e) devitrified groundmass with spherulites (optical microscopic image plane polarized, unit P, sample AMT 14–54); (f) heterogeneous glassy groundmass with perlitic texture and darker flow bands (optical microscopic image plane polarized, unit L, sample AMT 14-71b); (g) glassy groundmass with perlitic texture and flow band enriched in crystal fragments (BSE-SEM image, unit L, sample AMT 13–10); (h) highly vesicular glassy groundmass with large flattened vesicles (BSE-SEM image, unit L, sample AMT 13–10). Labels of SLLFs as in ***Figure 2****. bt: biotite; gdm: groundmass; K-fs: K-feldspar; opx: orthopyroxene; plg: plagioclase; qz: quartz, xts: crystals.*

	Plg-liquid			Cpx-liquid				Apatite
*	Eq. 23	Eq. 24a	Eq. 26	Talk1	Talk2	Talk3	Talk4	
Unit								
Total rock (TR)								
SLLF	(1030–1050)	(993–1015)	(965–993)	980	(955–998)	965	(914–1014)	(905–940)
Glass matrix (GM)								
SLLF	(877–888)	(824–838)	(832–845)	—	—	—	—	(879–883)

Temperature calculated by using ([103, 104]; Eqs. 23, 24a, 26) plagioclase model for only the Plg-liquid couples which passed equilibrium test (2.2.1.). GM and TR are the groundmass liquids and the total rock liquids, respectively. Talk1, Talk2, Talk3, and Talk4 are the temperature intervals calculated for each Cpx-liquid equilibrium combination which passed the equilibrium tests. Temperature values referred to as Talk1, Talk2, Talk3, and Talk4 correspond to the re-calibration of [105] models of [106]. The apatite geothermometer, reported as apatite, is the value calculated for the [104] geothermometer. More details can be found in [102]. A temperature interval between 900°C and 1070°C is assumed to be ideal for the initial crystallization at depth, whereas a lower temperature interval (800°C and 900°C) is likely characteristic of the late crystallization condition at the shallow levels, emplacement, or post-emplacement.
**Reported equations are as from [103, 104].*

Table 5.
Summary of the minimum and maximum temperature values estimated by using the geothermometers proposed by [102] for the SLLF of the BAS and MAS.

ascent conditions of magma, as well as the eruption style and emplacement of the volcanic products. H_2O, in fact, more than any other component, affects the physical properties of the magmatic and volcanic materials as well as the associated processes (diffusivity, crystallization, and degassing). One weight percent of H_2O dissolved in a SiO_2-rich magma may change its viscosity of ca. 6 orders of magnitude and its glass transition temperature (i.e., the temperature at which, upon certain stress conditions, there a transition between a viscous to a brittle mechanical behavior occurs) of 200°C.

Since there are no data on the CO_2 concentration of melt inclusions, the H_2O-CO_2 saturation model of [108] (https://melts.ofm-research.org/CORBA_CTserver/GG-H2O-CO2.html) was used to estimate the fluid content of the magma stored in the Monte Amiata magma chamber positioned at 6 km depth [49, 109, 110], where the expected external pressure is 106 MPa and temperature is 900–1070°C (see before). The average oxide percentage was considered (**Table 3**) in calculations. The H_2O and CO_2 mole fractions in the fluid phase were varied to compute the H_2O and CO_2 in the coexisting melt at 900–950°C, whereas no results were obtained at higher temperatures. Outcomes are reported in **Figure 12**, showing that maximum H_2O concentration is 3.96–3.98 wt% for zero CO_2 and maximum CO_2 concentration is ca. 500 ppm for zero H_2O.

Of course, the H_2O and CO_2 concentrations in the deep magma might be everywhere along these lines. Nevertheless, it must be recalled that in the Monte Amiata edifice and surrounding area, a strong degassing of magmatic/mantellic CO_2 occurs as indicated by high CO_2 fluxes from soil [111, 112], the presence of CO_2 in the fluid inclusions [113], and the composition of geothermal fluids ([114]; and references therein).

Therefore, owing to this occurrence of magmatic/mantellic CO_2, the magma in the Monte Amiata chamber might be saturated with CO_2 and consequently water concentration would be low or even very low, although this possibility is a hypothesis to be proven or rejected by means of melt inclusions data. If this hypothesis is true, CO_2 would be readily lost upon degassing and H_2O concentration would weakly decrease, thus explaining the lack of explosive activity at Monte Amiata.

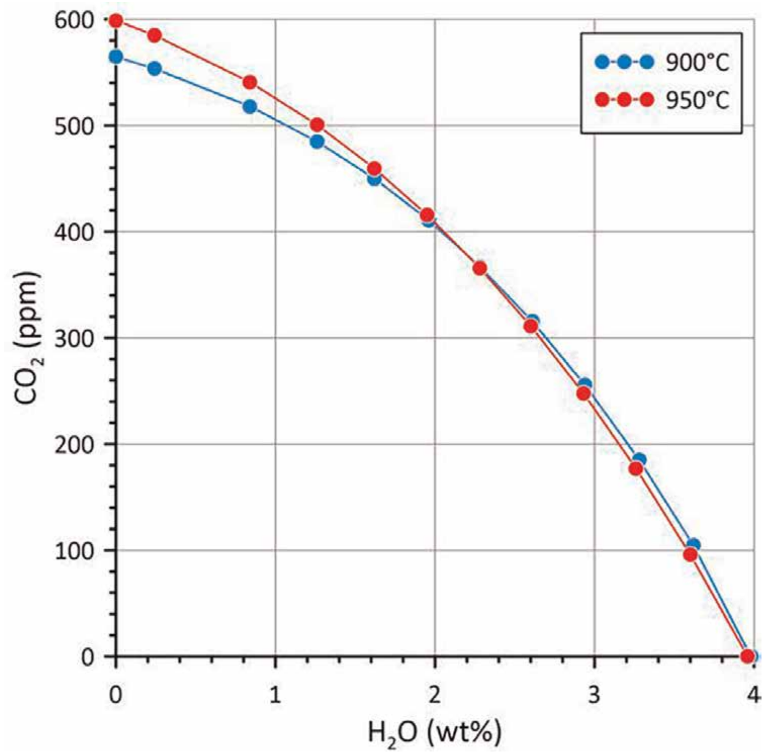

Figure 12.
CO_2 vs. H_2O coexistence in melt calculated by means of the saturation model of [108] for temperature of 900°C (blue line and dots) and 950°C (red line and dots).

4.6 Rheological properties

In order to quantify the effect of rheology on Monte Amiata eruptive style, in this study we combine two empirical models. The first model (GRD) [115] allows to calculate the residual liquid viscosity as a function of the temperature (T) and the composition (X). The second model (CM) [116] allows to estimate the rheological effects due to the presence of crystals in strained magmas, through the calculation of the relative viscosity (i.e., the ratio between the viscosity of the mixture and the viscosity of the pure liquid). The input data are constituted by the textural data providing the crystal fraction (Section 4.4), the temperature estimation, and dissolved fluid content (Section 4.5).

Figure 13 reports the pure liquid viscosity vs. the inverse of the temperature. The calculations are performed on the entire temperature range, but we put in evidence the interval 900–1070°C, representative of an early-stage-crystallization (PES) magma and the interval 800–900°C, representative of the late-stage-crystallization magma and erupted products (ES). Considering the total content of fluids present inside this magma, which is strongly influenced by the presence of CO2—see Section 4.5—and considering that the latter is completely separated from the magma during the ascent and the emplacement process, a quantitative of 0.3 wt% of residual water appears acceptable as an input parameter into the proposed models. The crystal fraction of the suspended crystals presents in each SLLF is based on the average values proposed by [41]. These values are reported in

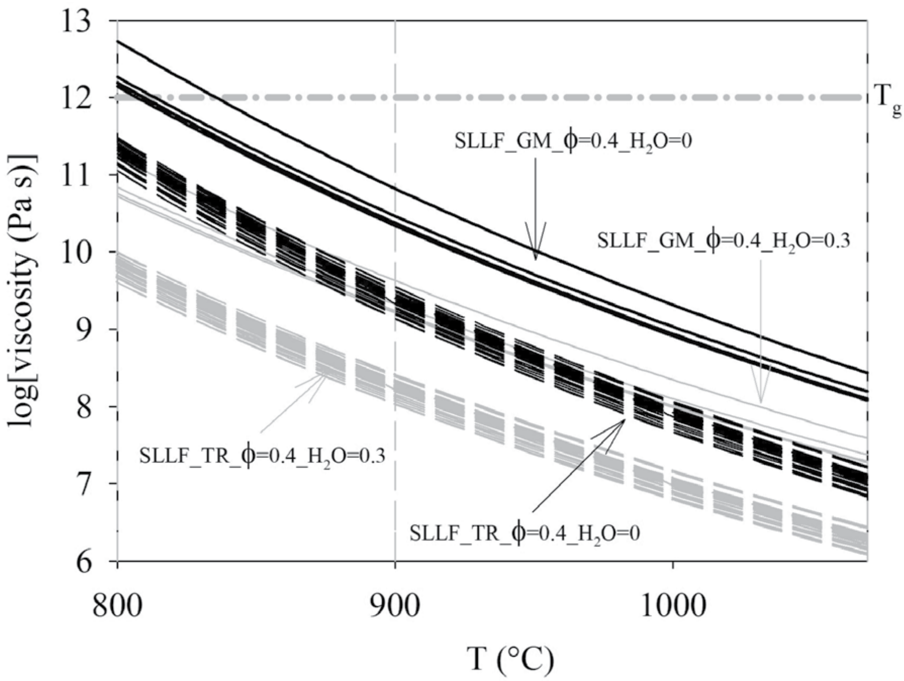

Figure 13.
Diagram of the calculated liquid + crystal suspension viscosity values for the investigated Monte Amiata SLLFs. Here, the suspending liquid is taken as the residual glass matrix (GM) or as the total rock (TR), whereas the crystal content (ϕ) is taken as the value proposed by [45] of 40 volume % (ϕ=0.4). Water content (H_2O) is considered to be 0 or 0.3 wt% as potentially presence as dissolved at the basis of the most tick lava flows. The calculations provided here do not account for the effect of suspended vesicles in the multiphase magmatic and volcanic mixture. For that reason, we could assume that the calculated values are an upper limit of the real volcanic mixture viscosity (vesicles in fact have an important effect in reducing magmatic and volcanic mixture viscosity), which may be representative of the most glassy crystal rich (vesicle free) lavas as those found at Monte Amiata. The figure also reports (at 10^{12}Pa s, in dash and dot thick gray) the line which marks the glass transition, that is, at first approximation, representative of the limit of viscous flow of lava flows [70]. In all cases, the calculated volcanic mixture viscosities estimated in the temperature interval (900–1070°C) are well below the flow limit as above defined. Both GM and TR, at any crystal and water content conditions in the (800–900°C) temperature interval, mostly fall below Tg and, only at the very lowest T, they overpass it.

volume percent (the number in the parenthesis followed by the symbol %). All the calculations are carried out by assuming the lowest strain rate value (10^{-5} s^{-1}), which provides the highest viscosity value.

In **Figure 13,** we also report the value of the glass transition temperature (Tg) as taken at a viscosity of 10^{12} Pa s [70]. Tg constitutes that barrier below which most of processes (e.g., diffusion, crystallization, vesiculation, flow, and welding) are significantly inhibited, if not halted. On the other hand, above the glass transition, the above-mentioned processes are still active and potentially rapid enough to still influence somehow the magmatic and volcanic processes. Ref. [117] published a comprehensive review of the ways how the various magmas and volcanic bodies may cross the glass transition temperature (e.g., conventional thermal cooling; cooling along a retrograde solubility curve; effective raising of Tg as due to degassing) and enhance the welding of pyroclastic materials or the flow of silicic lavas, other than affecting the depth of the fragmentation depth.

5. Discussion

5.1 Distinguishing silicic lavas from welded tuffs and rheomorphic ignimbrites

Several scholars have attempted to compare and define diagnostic textures and structures to explain how silicic lava flows differ from high-temperature pyroclastic density currents (welded and/or rheomorphic ignimbrites) (e.g., [11, 15, 71, 99]). In this section, we discuss the geological and volcanological features (field physical features and rock's textures and structures) that support the interpretation of trachydacite sheet-like silicic flows of Monte Amiata as lavas and reject the attribution as welded ignimbrites and rheoignimbrites deriving from the emplacement of pyroclastic density currents emitted during a single large explosive eruption.

In **Table 6**, we summarize (i) the diagnostic depositional characteristics of ignimbrite [1, 118–120] that have not found in Monte Amiata trachydacite SLLFs despite careful search, and (ii) the discriminating internal textures and structures of the Monte Amiata trachydacite SLLFs that help to identify them as silicic lava flows [12, 121–123].

In conclusion, the volcanological observations, the field geological evidence, and the petrographic analyses performed on the trachydacite SLLFs of Monte Amiata are consistent with a genetic interpretation by effusive eruptions, which gave rise to long and extensive silicic lava flows.

5.2 Defining a model of silicic lava flows (SLLFs) for Monte Amiata trachydacite

Observations and models on silicic lava flows have been mainly carried out on small rhyolite obsidian domes and coulées [9, 87, 89] that have some characteristics that were extended to other silicic lavas. The idealized structural model of rhyolite lava flow [92] consists of three principal zone: (1) a basal pyroclastic deposit emplaced during the initial phase of the eruption, (2) a lava dome or short flow formed by the relatively quiet effusion of magma, and (3) an envelope of carapace breccia that grows around the molten core of the lava body as the chilled and brittle outer crust breaks in response to internal expansion and growth. The lava body is further subdivided in a vertical sequence of: basal part composed of breccia of pumice and obsidian blocks, interior part composed of either coarsely vesicular pumice, coherent even flow-foliated glassy obsidian, and finely vesicular pumice, and surface breccia [89].

More recently, a certain number of studies have been carried out so far it concerns the emplacement mechanisms of very large lava flow sequences in the Brazilian sector of the early Cretaceous Paranà Etendeka Magmatic Province (PEMP) [19–21]. Apparently, these huge effusive silicic sequences (> thousands of km^3) were not accompanied by explosive activity. The same authors have invoked mechanisms, which explain the emplacement of the investigated lava flows as mainly due to the emission of degassed dacitic and rhyolitic low-viscosity lavas.

The peculiarity of Monte Amiata sheet-like trachydacite lava flows appear to have some point in common with those found in the products reported in the PEMP and, with respect to other described silicic flows, their main features, without considering the greater length of the SLLF, are as follows:

a. Absence of tephra or air-fall pumice deposits testifying explosive activity associated with the lava emplacement. Commonly, sequence of explosive

Textural discriminating characteristics	Diagnostic value
Features distinguishing SLLFs from ignimbrite	
Fragmentary vitroclastic textures (bubble-wall shards, small pumice fragments, fiamme) none observed.	Even in the very densely welded ignimbrites occurrences of shards and pumice are generally anyway recorded.
Evidence of welding not observed.	Also in strongly welded tuffs, some remains of welding textures are preserved due to vertical and lateral gradation from completely non-welded to fully welded facies.
Lithofacies do not record gradational changes in texture and structure from near source to distal areas of flow.	Adjacent to vent, ignimbrites show only particulate flow facies varying from vitrophyric welded tuffs and polygenetic lithic-rich breccia, and grade to massive pumice-and-ash flows, and finally to mass flows completely managed by gravity (lahars, debris flow) [118–120].
Vertical and lateral association of facies, derived from different eruptive and emplacement mechanisms, but still generated by the same explosive eruptive event, not observed.	Basal Plinian fallout, co-ignimbrite ash fallout, and low-density pyroclastic flows can be present in the basal, intermediate, and top parts of the ignimbrite deposit.
Features indicative of effusive style of emplacement	
Coherent texture with high content in phenocrysts (40 vol%, [41]) in a homogenous transparent vitrophyric or microcrystalline groundmass.	Texture indicating crystallization from a non-particulate melt.
Very little vertical and lateral variation in mineral paragenesis and chemical composition, within individual trachydacite flows.	Textures indicating crystallization from a non-particulate melt.
Fluidal texture due to well-developed crystals lineation and elongated vesicles, preservation of delicate-textured glomerocrysts.	Textures indicating effusion and spreading of lava; in ignimbrites, the prominent development of foliation is by flattening of pumice fragments during welding.
Flow-layered structures due to banding (color, lithofacies, and vesicularity), and parting along flow planes.	Structures suggesting laminar flow of coherent lava; layering is favored by shear near the base of the flow.
Folding of flow bands, mainly at the flow front and margins.	Suggests high viscosity of a non-particulate melt.
Small to large-scale mingling domains of obsidian glassy, microcrystalline, and vesicular glassy coherent lithofacies, in bands and lenses [75].	Textures indicating emplacement from a non-particulate melt. In an explosive event, magma mingling textures are destroyed by disruption of the magma and exhibited only in discrete pyroclasts.
Small content (<10%) in broken crystals.	The presence of low percentages of broken crystals is therefore characteristic of silicic viscous lavas and is interpreted as the response to shear stress during laminar flow [121].
Lithic inclusions of mafic magmatic enclaves and meta-sedimentary xenoliths of basement units that were at a deep of about 6 km in the upper crust, where the magmatic chamber formed [109, 122].	In ignimbrites, lithic fragments derived from the disaggregation of the wall rocks by shallow explosion [123] (near vent) or incorporation from the ground during flowage (near base).
Basal and internal monolithologic autoclastic breccia, composed of coarse scoria clasts or blocky co-genetic lithic clasts in a sandy matrix with the same composition as clasts.	Indicative of lava-like viscous flow rather than particulate flow.

Textural discriminating characteristics	Diagnostic value
Step flow front a few tens of meters thick with ramp structures; and marginal flow lobes [12].	Indicative of lava-like viscous flow that suddenly stopped; ignimbrite shows gradual thinning at edges of unit.
Arcuate ogives on flow surface.	Formed as folds while the lava was in motion; viscosity decreases downward from the surface to the interior of the flow.
Well-defined areal distribution of individual flows, also in a relatively flat topography; several flows ponded in paleo-valleys.	An ignimbrite would have inundated the flanks of the volcano and climbed over many barriers.

Table 6.
Characteristics of Monte Amiata SLLFs supporting the interpretation as lava flows.

eruptions of tephra preceding (and/or following) the extrusion of silicic lava flows and domes is observed [89, 124]. In similar cases, the early-stage explosive activity was considered functional to gas escape from magma and to the subsequent effusive activity.

b. Absence of talus debris commonly mantling the steep front, margins (levées), and surface (upper breccia) of silicic lava flows and domes and originating by syn-eruptive rockfall of highly disrupted surficial portions of lava. This implies that we cannot apply to Monte Amiata SLLFs the interpretation that the basal breccia derived by the fracturing of the cooler, finely vesicular, pumiceous crust during lava movement that fall off at the front and are overridden by the advancing lava, forming a nearly continuous envelope around the more viscous flow interior [89].

c. Some SLLFs show several lobe outflows (i.e., Pozzaroni; **Figure 2**) deriving from the breakout of the lava front and margins, similar to basaltic lavas. This process extended the lava field and suggests that the thick lavas are maintained, even for a long time, substantially above the glass transition temperature, representative of the temperature of flow halting [70], favoring their mobility and the run-out of long distances [5, 6, 102].

d. A high porphyricity in a glassy fresh groundmass that is commonly not devitrified and lacking of spherulitic texture, whereas most described silicic lavas show aphyric or non-porphyritic glassy (obsidian or pumiceous) texture.

e. Absence of a quenched or highly vesicular crust.

f. No correlation is observed between area and slope values, suggesting that the different areal distribution of SLLFs can be substantially independent from the underlying morphology.

The recognition of large-volume, extensive silicic lava flow units at Monte Amiata introduces questions regarding the mechanisms of emplacement. Into the literature, the uncommon sheet-like silicic lava flows are related to the effect of large erupted volume and the effectively lava heat retained due to a thick solidified crust, whereas the dome-forming eruptions of silicic lavas are related to low-magma production rates [125].

Thanks to the direct observation of the events of silicic lava flow emplacement occurred in historical time [2–7], we have understood that the emplacement of large volume and great thickness silicic lava flows with high proportions of suspended crystals should not surprise us.

In fact, it has demonstrated by [5, 6, 126] and, more recently, [19, 20], that the large thickness of a lava flow constitutes the most efficient thermal barrier, which reduces heat loss and allows to maintain the lavas at high temperature well above their glass transition temperatures. This will favor, for years, or even for decades, in the cases of the largest fluxes, the flow. To favor flow will favor other important processes, such as the crystallization of the spherulitae and the contribution of the volatile resorption [117, 127].

In conclusion, the unusual length and the main characteristics described above (absence of related tephra deposits, absence of talus debris, presence of outflow lobes, high porphyricity, glassy fresh groundmass, and absence of quenched or highly vesicular crust) of the SLLFs of Monte Amiata may be referred to the high temperature, high thicknesses, and relatively large volume of each one of these lava flows. In this picture, morphological factors and volatile content seem to have played a minor role.

5.3 Volcano-tectonic and structural implication into the silicic volcanism of Monte Amiata

At Monte Amiata, the association of silicic volcanism with transtensive shear zones [45, 55] was significant in determining the volcanological character of the silicic volcanism. In this work, we were able to define the near-vent features, buried under younger units, and to infer the source area on the basis of thickness, physical features, and distribution of Monte Amiata SLLF eruptive units. The vent area of SLLFs was possibly identified with an eruptive fissure system located near the crest of the summit ridge and fed by linear dike swarms (**Figure 2**). A multi-vent source is recorded by changes in location of eruption source (**Figure 2**).

Monte Amiata magmas were vented by faults related to regional transtension along the Bagnore-Bagni San Filippo shear zone that has been active during the volcano activity [45, 55], leading to dominantly effusive eruptions.

Referring to this structural framework, the SLLFs of Monte Amiata are put in place following the ascent along a system of faults which in their upper portion define a summit axial rift zone, rather than real volcanic conduits. The geometry of these upwellings and the reduced quantity of gas present in the magma are probably the main factors that inhibit the formation of a fragmentation surface [45]. While the ability of this lava flows to maintain their viscosity, their anomalously high temperature for a long time determines the style of emplacement in long and thick lava flows.

6. Conclusions and future researches

The outstanding questions on Monte Amiata sheet-like trachydacite that we discuss in this work are mainly related to the interpretation of its eruption mechanisms (effusive vs. explosive volcanism) that we have faced with an unprecedented physical and volcanological characterization of the products and by comparing our results with the updated models of ignimbrite and rheoignimbrite. The identification of several lava flow eruptive units (referring to different eruptive events and vents location) having different stratigraphic position and composed of several flow units separated by scoria or breccia beds is the first argument for this discussion. The second main discussion point is the manner of flowing of single lava flows and the reasons for producing the different volcanic facies and structures we observed and described. Our results point out to a model for the formation of the Monte Amiata SLLFs which could possibly be extended to other silicic composite volcanoes.

In major detail, our field-based study of the trachydacite SLLFs of Monte Amiata supports these conclusions:

1. The volcanic deposits of Monte Amiata, both outcropping and present in the subsoil of the volcano, recently crossed by deep drilling, are exclusively made up of a set of silicic lava flows, lava domes, and associated coulées.

2. The SLLFs include different individual effusive eruptive units that are well recognizable from each other and well traceable on the field. They have different stratigraphic position in the volcanic succession that prevents to consider all these lavas as coeval and/or emitted in a single episode of magmatic feeding and eruption.

3. The arcuate ridges of trachydacite boulders present on the surface of SLLFs are to be referred to pervasive phenomena of *in situ* paleo-weathering of lavas at the expense of surficial fold structures (ogives).

4. The repeated presence of SLLFs at different levels of the stratigraphic volcanic sequence implies that, during the geological history of the volcano, there have been conditions for a recurrence of an eruptive mechanism emplacing long and extensive silicic lava flows. This peculiar behavior of a silicic magma can possibly be attributed to the ascent along eruptive fractures of batches of magma with low gas content and anomalously high temperatures. These physicochemical conditions enabled lavas to flow slowly but inexorably up to the distances granted to them by the internal thermal balance. For this reason, the lavas morphologically forced by valley incisions flow at major distances in proportion to the others that flow unconfined (**Table 1**), because the greater thickness and the smaller exchange surface with the soil and the atmosphere allow a greater conservation of the temperature inside them. This temperature surplus could be originally due to a higher value of the ratio between the temperature times the volume of the melt still residing in the magma chamber and the temperature times the volume of the more basic magma coming from the deep.

5. The tectonic control on the feeding system has meant that the magma supply was managed by the activity of the various deep and superficial fracturing trends. This type of control is able to create the conditions to inhibit the formation of a fragmentation surface and generate an entire volcano through a succession of exquisitely fissural eruptions in a regime of volcano-tectonic rift.

Looking to the future, the data still missing on Monte Amiata products are represented by the quantification of the volatile content in magmas, and by the definition of the silicic-magma/mafic-magma ratio characterizing the feeding of the single events. Obtaining these further pieces of information will allow us to further refine the model presented here for the formation of SLLFs and, in a broader perspective, the model of the other lithofacies (lava domes and coulées) that have been emplaced during the various phases of the life of the completely silicic Monte Amiata volcano.

Acknowledgements

This work has been initially funded by the Regione Toscana (Italy) by means of the LAMMA Consortium in the framework of the project of a volcanological monograph of Monte Amiata edited at the end of 2017, and then by JRC-EPOS project. Prof. Luigi Marini is acknowledged for the fruitful discussion on fluid fraction inside Monte Amiata magmas. SLF is grateful to T. Abebe Adhana for priceless help in optical microscope observations.

Author details

Luigina Vezzoli[1,2*], Claudia Principe[2], Daniele Giordano[2,3,4], Sonia La Felice[2] and Patrizia Landi[2,5]

1 Science and High Technology Department, Insubria University, Como, Italy

2 Institute of Geosciences and Earth Resources, National Research Council, Pisa, Italy

3 Earth Sciences Department, Torino University, Torino, Italy

4 Institute of Sciences and Technologies for Ceramic Materials, National Research Council, Faenza, RA, Italy

5 National Institute of Geophysics and Volcanology, Pisa Section, Pisa, Italy

*Address all correspondence to: luigina.vezzoli@gmail.com

References

[1] Branney MJ, Kokelaar P. Pyroclastic density currents and the sedimentation of ignimbrites. Geological Society Memoir. 2002;**27**:1-143

[2] Navarro-Ochoa C, Gavilanes-Ruíz JC, Cotés-Cortés A. Movement and emplacement of lava flows at Volcán de Colima, México: November 1998–February 1999. Journal of Volcanology and Geothermal Research. 2002;**117**:155-167

[3] Harris AJL, Flynn LP, Matias O, Rose WI, Cornejo J. The evolution of an active silicic lava flow field: An ETM+ perspective. Journal of Volcanology and Geothermal Research. 2004;**135**:147-168

[4] Pallister JS, Diefenbach AK, Burton WC, Muñoz J, Griswold JP, Lara LE, et al. The Chaitén rhyolite lava dome: Eruption sequence, lava dome volumes, rapid effusion rates and source of the rhyolite magma. Andean Geology. 2013;**40**:277-294. DOI: 10.5027/andgeoV40n2-a06

[5] Tuffen H, James MR, Castro JM, Schipper CI. Exceptional mobility of an advancing rhyolitic obsidian flow at cordon Caulle volcano in Chile. Nature Communications. 2013;**4**:2709. DOI: 10.1038/ncomms3709

[6] Farquharson JI, James MR, Tuffen H. Examining rhyolite lava flow dynamics through photo-based 3D reconstructions of the 2011–2012 lava flow field at Cordón-Caulle, Chile. Journal of Volcanology and Geothermal Research. 2015;**304**:336-348

[7] Magnall N, James MR, Tuffen H, Vye-Brown C. Emplacing a cooling-limited rhyolite lava flow: Similarities with basaltic lava flows. Frontiers Earth Science. 2017;**5**:44. DOI: 10.3389/feart.2017.00044

[8] Fink JH, Anderson SW. Emplacement of Holocene silicic lava flows and domes at Newberry, South Sister, and Medicine Lake Volcanoes, California and Oregon. U.S. Geological Survey, Scientific Investigations. Report. 2017;**5022**(I)

[9] Fink JH. Structure and emplacement of a rhyolite obsidian flow: Little Glass Mountain, Medicine Lake Highland, northern California. Geological Society of America Bulletin. 1983;**94**:362-380

[10] de Silva SL, Self S, Francis PW, Drake RE, Ramirez CR. Effusive silicic volcanism in the Central Andes: The chao dacite and other young lavas of the Altiplano-Puna volcanic complex. Journal of Geophysical Research. 1994;**99**:17805-17825

[11] Gibbon DL. Origin and development of the Star Mountain Rhyolite. Bulletin of Volcanology. 1969;**33**:438-474

[12] Bonnichsen B, Kauffman DF. Physical features of rhyolite lava flows in the Snake River Plain Volcanic Province, southwestern Idaho. Geological Society of America Special Paper. 1987;**212**:119-145

[13] Henry CD, Price JG, Rubin JN, Laubach SE. Case study of an extensive silicic lava: The Bracks rhyolite, trans-Pecos Texas. Journal of Volcanology and Geothermal Research. 1990;**43**:113-132

[14] Henry CD, Wolff JA. Distinguishing strongly rheomorphic tuffs from extensive silicic lavas. Bulletin of Volcanology. 1992;**54**:171-186

[15] Manley CR. Physical volcanology of a voluminous rhyolite lava flow: The Badlands lava, Owyhee plateau, southwestern Idaho. Journal of

Volcanology and Geothermal Research. 1996;**71**:129-153

[16] Allen SR, McPhie J. The Eucarro rhyolite, Gawler range volcanics, South Australia: A 675 km^3 compositionally zoned felsic lava of Mesoproterozoic age. Geological Society of America Bulletin. 2002;**114**:1592-1609

[17] Allen SR, Simpson CJ, McPhie J, Daly SJ. Stratigraphy, distribution and geochemistry of widespread felsic volcanic units in the Mesoproterozoic Gawler Range Volcanics, South Australia. Australian Journal of Earth Science. 2003;**50**:97-112

[18] Loewen MW, Bindeman IN, Melnik OE. Eruption mechanisms and short duration of large rhyolitic lava flows of Yellowstone. Earth Planetary Science Letters. 2017;**458**:80-91

[19] Polo LA, Giordano D, Janasi V, Freitas-Guiaraes L. Effusive silicic volcanism in in the Paraná Magmatic Province, South Brazil: Physico-chemical conditions of storage and eruption and considerations on the rheological behaviour during emplacement. Journal of Volcanology and Geothermal Research. 2018;**355**:115-135

[20] Polo LA, Janasi V, Giordano D, Canon Tapia E, Lima E, Roverato M. Effusive silicic volcanism in the Paraná Magmatic Province, South Brazil: Evidence for local fed lava flows and domes from detailed field work. Journal of Volcanology and Geothermal Research. 2018;**355**:204-218

[21] Giordano D, Vona A, Gonzalez-Garcia D, Allabar A, Kolzenburg S, Polo LA, et al. Viscosity of Palmas-type magmas of the Paraná Magmatic Province (Rio Grande do Sul State, Brazil): Role on eruption dynamics of high-temperature silicic volcanism. Chemical Geology. 2021;**560**:119981

[22] Agangi A, Kamenetsky VS, McPhie J. Evolution and emplacement of high fluorine rhyolites in the Mesoproterozoic Gawler silicic large igneous province, South Australia. Precambrian Research. 2012;**208-211**:124-144

[23] Besser ML, Gouvea Vasconcellos EM, Ranalli Nardy AJ. Morphology and stratigraphy of Serra Geral silicic lava flows in the northern segment of the Torres trough, Paraná Igneous Province. Brazilian Journal of Geology. 2018;**48**:201-219

[24] Leggett TN, Befus KS, Kenderes SM. Rhyolite lava emplacement dynamics inferred from surface morphology. Journal of Volcanology and Geothermal Research. 2020;**395**:106850. DOI: 10.1016/j.jvolgeores.2020;106850

[25] Ayalew D, Pyle D, Ferguson D. Effusive Badi Silicic Volcano (Central Afar, Ethiopian Rift); Sparse Evidence for Pyroclastic Rocks. In: Németh K, editor. Updates in Volcanology. London, UK: Intechopen; 2021. p. 16. DOI: 10.5772/intechopen.98558

[26] Peccerillo A. The Tuscany Province. In: Peccerillo A, editor. Cenozoic Volcanism in the Tyrrhenian Sea Region. 2nd ed. Cham: Springer International Publishing AG; 2017. pp. 19-60

[27] Vezzoli L, Principe C. Monte Amiata volcano (Tuscany, Italy) in the history of volcanology: 1—Its role in the debates on extinct volcanoes, source of magma, and eruptive mechanisms (AD 1733-1935). Earth Science History. 2020;**39**:28-63

[28] Sabatini V. Analogie tra Monte Amiata e Monte Cimino. Atti Reale Accademia Lincei Rendiconti. 1910;**5-19**: 284-290

[29] Sabatini V. Lave che sembrano tufi e tufi che sembrano lave. Bollettino Società Geologica Italiana. 1911;**30**: 913-921

[30] Rittmann A. Cenni sulle colate di ignimbriti. Bollettino Accademia Gioenia Scienze Naturali di Catania. 1958;**4-10**: 524-533

[31] Rutten MG. Acid lava flow structure, as compared to ignimbrites. Bulletin Volcanologique. 1963;**25**:111-121

[32] Wolff JA, Wright JV. Rheomorphism of welded tuffs. Journal of Volcanology and Geothermal Research. 1981;**10**:13-34

[33] Principe C, Vezzoli L. Monte Amiata volcano (Tuscany, Italy) in the history of volcanology: 2—Its role in the definition of "ignimbrite" concepts and in the development of the "rheoignimbrite" model of Alfred Rittmann. Rendiconti Accademia dei Lincei Scienze Fisiche e Naturali. 2020;**31**:539-561

[34] White DA. Report on the International Association of Volcanology (IAV) Symposium on Ignimbrites and Hyaloclastites, Italy, 1 September-1 October 1961. Commonwealth of Australia, Department of National Development, Bureau of Mineral Resources Geology and Geophysics, Records. 1962;**101**:1-44

[35] Andrews GDM, Branney MJ. Emplacement and rheomorphic deformation of a large, lava-like rhyolitic ignimbrite: Grey's landing, southern Idaho. Geological Society of America Bulletin. 2011;**123**:725-743

[36] Brown DJ, Bell BR. The emplacement of a large, chemically zoned, rheomorphic, lava-like ignimbrite: The Sgurr of Eigg pitchstone, NW Scotland. Journal of the Geological Society. 2013;**170**:753-767

[37] Marinelli G. Genesi e classificazione delle vulcaniti recenti toscane. Atti Società Toscana di Scienze Naturali in Pisa, Memorie Serie A. 1961;**68**:63-116

[38] Rittmann A. Volcanoes and their Activity. New York-London: Interscience Wiley; 1962

[39] Mazzuoli R, Pratesi M. Rilevamento e studio chimico petrografico delle rocce vulcaniche del Monte Amiata. Atti Società Toscana di Scienze Naturali in Pisa, Memorie Serie A. 1963;**70**:355-429

[40] Ferrari L, Conticelli S, Burlamacchi L, Manetti P. Volcanological evolution of the Monte Amiata southern Tuscany: New geological and petrochemical data. Acta Vulcanologica. 1996;**8**:41-56

[41] Cristiani C, Mazzuoli R. Monte Amiata volcanic products and their inclusions. Periodico di Mineralogia. 2003;**72**:169-181

[42] Cadoux A, Pinti DL. Hybrid character and pre-eruptive events of Mt. Amiata volcano (Italy) inferred from geochronological, petro-geochemical and isotopic data. Journal of Volcanology and Geothermal Research. 2009;**179**: 169-190

[43] Marroni M, Moratti G, Costantini A, Conticelli S, Benvenuti MG, Pandolfi L, et al. Geology of the Monte Amiata region, Southern Tuscany, Central Italy. Italian Journal of Geosciences. 2015;**134**: 171-199

[44] Conticelli S, Boari E, Burlamacchi L, Cifelli F, Moscardi F, Laurenzi MA, et al. Geochemistry and Sr-Nd-Pb isotopes of Monte Amiata volcano, Central Italy: Evidence for magma mixing between high-K calc-alkaline and leucititic mantle-derived magmas. Italian Journal of Geosciences. 2015;**134**:268-292

[45] Vezzoli L, Principe C. Building a completely effusive silicic composite volcano: Geologic history, architecture, and volcanic-tectonic interactions of Monte Amiata (Middle Pleistocene, Italy). Submitted to. Journal of Volcanology and Geothermal Research. 2022

[46] Scrocca D, Doglioni C, Innocenti F. Constraints for an interpretation of the Italian geodynamics: A review. Memorie Descrittive della Carta Geologica d'Italia. 2003;**62**:15-46

[47] Molli G. Northern Apennine Corsica orogenic system: An updated overview. Geological Society of London Special Publication. 2003;**298**:413-442

[48] Calcagnile G, Panza G. The main characteristics of the lithosphere-asthenosphere system in Italy and surrounding regions. Pure and Applied Geophysics. 1981;**199**:865-870

[49] Gianelli G, Manzella A, Puxeddu M. Crustal models of southern Tuscany (Italy). Tectonophysics. 1997;**281**: 221-239

[50] Carmignani L, Decandia FA, Fantozzi PL, Lazzarotto A, Liotta D, Meccheri M. Tertiary extensional tectonics in Tuscany (northern Apennines, Italy). Tectonophysics. 1994; **238**:295-315

[51] Brunet C, Monié P, Jolivet L, Cadet JP. Migration of compression and extension in the Tyrrhenian Sea, insights from 40Ar/39Ar ages on micas along a transect from Corsica to Tuscany. Tectonophysics. 2000;**321**:127-155

[52] Pandeli E, Bertini G, Castellucci P, Morelli M, Monechi S. The sub-Ligurian and Ligurian units of the Monte Amiata geothermal region (South-Eastern Tuscany): New stratigraphic and tectonic data and insight into their relationships with the Tuscan nappe. Bollettino della Società Geologica Italiana Special Volume. 2005;**2005**(3):55-71

[53] Laurenzi MA, Braschi E, Casalini M, Conticelli S. New 40Ar-39Ar dating and revision of the geochronology of the Monte Amiata Volcano, Central Italy. Italian Journal of Geosciences. 2015;**134**: 255-265

[54] Laurenzi MA, La Felice S. New geochronological data on a core sample from David Lazzaretti well. In: Principe C, Lavorini G, Vezzoli L, editors. Il vulcano di Monte Amiata. Nola: Edizioni Scientifiche e Artistiche; 2017. pp. 233-241. ISBN: 978-88-99742-32-4

[55] Brogi A, Liotta D, Meccheri M, Fabbrini L. Transtensional shear zones controlling volcanic eruptions: The middle Pleistocene Monte Amiata volcano (inner northern Apennines, Italy). Terra Nova. 2010;**22**:137-146

[56] Landi P, La Felice S, Petrelli M, Vezzoli L, Principe C. Deciphering textural and chemical zoning of K-feldspar megacrysts from Mt. Amiata volcano (southern Tuscany, Italy): Insights into the petrogenesis and abnormal crystal growth. Lithos. 2019; **324–325**:569-583

[57] La Felice S, Abebe AT, Principe C, Vezzoli L. Petrochemical characters of Monte Amiata volcanics vs stratigraphy. In: Principe C, Lavorini G, Vezzoli L, editors. Il vulcano di Monte Amiata. Nola: Edizioni Scientifiche e Artistiche; 2017. pp. 145-170. ISBN: 978-88-99742-32-4

[58] Rombai C, Trua T, Matteini M. Metamorphic xenoliths and magmatic inclusions in the quaternary lavas of Mt. Amiata (Tuscany, Central Italy):

Inferences for P-T conditions of magma chamber. Atti Società Toscana di Scienze Naturali in Pisa Memorie Serie A. 1995; **102**:21-38

[59] Principe C, Vezzoli L, La Felice S. Stratigraphy and geological evolution of the Monte Amiata volcano. In: Principe C, Lavorini G, Vezzoli L, editors. Il vulcano di Monte Amiata. Nola: Edizioni Scientifiche e Artistiche; 2017. pp. 85-101. ISBN: 978-88-99742-32-4

[60] Principe C, Vezzoli L, La Felice S. Geology of Monte Amiata volcano (Southern Tuscany). Alpine and Mediterranean Quaternary, Special Issue: Quaternary: Past, Present, Future —AIQUA Conference 2018. 2018;**31**: 235-238. ISSN: 2279-7335

[61] Vezzoli L, Principe C. Volcanic facies and emplacement mechanism at Monte Amiata Volcano. In: Principe C, Lavorini G, Vezzoli L, editors. Il vulcano di Monte Amiata. Nola: Edizioni Scientifiche e Artistiche; 2017. pp. 195-213. ISBN: 978-88-99742-32-4)

[62] Principe C, Vezzoli L. Characteristics and significance of intravolcanic saprolite paleoweathering and associate paleosurface in a silicic effusive volcano: The case study of Monte Amiata (middle Pleistocene, Tuscany, Italy). Geomorphology. 2021;**392**:107922. DOI: 10.1016/j.geomorph.2021.107922

[63] Salvador A, editor. International Stratigraphic Guide: A Guide to Stratigraphic Classification, Terminology, and Procedure. 2nd ed. Boulder: Geological Society of America; 1994. p. 214

[64] Cas RAF, Wright JV. Volcanic Successions, Modern and Ancient: A Geological Approach to Processes, Products, and Successions. London: Allen & Unwin; 1987. p. 528

[65] McPhie J, Doyle M, Allen R. Volcanic Textures. Centre for Ore Deposit and Exploration Studies: University of Tasmania; 1993. p. 197

[66] Walker GPL. Lengths of lava flows. Philosophical Transactions of the Royal Society of London A. 1973;**274**: 107-118

[67] La Felice S, Montanari D, Battaglia S, Bertini G, Gianelli G. Fracture permeability and water-rock interaction in a volcanic groundwater reservoir and the concern of its interaction with the geothermal reservoir of Mt. Amiata, Italy. Journal of Volcanology and Geothermal Research. 2014;**284**:95-105

[68] La Felice S, Bertini G, Principe C. Stratigraphy and characterization of the volcanics inside David Lazzaretti well. In: Principe C, Lavorini G, Vezzoli L, editors. Il vulcano di Monte Amiata. Nola: Edizioni Scientifiche e Artistiche; 2017. pp. 213-220. ISBN: 978-88-99742-32-4

[69] Montanari D, La Felice S, Bertini G. Fractures characterisation within recent exploratory wells at Monte Amiata. In: Principe C, Lavorini G, Vezzoli L, editors. Il vulcano di Monte Amiata. Nola: Edizioni Scientifiche e Artistiche; 2017. pp. 221-231. ISBN: 978-88-99742-32-4

[70] Giordano D, Nichols ARL, Dingwell DB. Glass transition temperatures of natural hydrous melts: A relationship with shear viscosity and implications for the welding process. Journal of Volcanology and Geothermal Research. 2005;**142**:105-118

[71] Sparks RSJ, Stasiuk MV, Gardeweg M, Swanson DA. Welded breccias in andesite lavas. Journal of the Geological Society. 1993;**150**:897-902

[72] Rust AC, Manga M, Cashman KV. Determining flow type, shear rate and shear stress in magmas from bubble shapes and orientations. Journal of Volcanology and Geothermal Research. 2003;**122**:111-132

[73] Walker GPL. Pipe vesicles in Hawaiian basaltic lavas: Their origin and potential as paleoslope indicator. Geology. 1987;**15**:84-87

[74] Manga M. Deformation of flow bands by bubbles and crystals. Geological Society of America Special Papers. 2005;**396**:47-54

[75] Morrow N, McPhie J. Mingled silicic lavas in the Mesoproterozoic Gawler Range Volcanics. South Australia: Journal of Volcanology and Geothermal Research. 2000;**96**:1-13

[76] Seaman SJ. Multi-stage magma mixing and mingling and the origin of flow banding in the Aliso Lava Dome, Tumacacori Mountains, southern Arizona. Journal of Geophysical Researches. 1995;**100**:8381-8398

[77] Perugini D, Ventura G, Petrelli M, Poli G. Kinematic significance of morphological structures generated by mixing of magmas: A case study from Salina Island (southern Italy). Earth Planetary Scences Letters. 2004;**222**(3–4):1051-1066

[78] Stevenson RJ, Briggs RM, Hodder APW. Emplacement history of a low-viscosity, fountain-fed pantelleritic lava flow. Journal of Volcanology and Geothermal Research. 1993;**57**:39-56

[79] Gonnermann HM, Manga M. Flow banding in obsidian: A record of evolving textural heterogeneity during magma deformation. Earth Planetary Science Letters. 2005;**236**:135-147

[80] Tuffen H, Dingwell DB, Pinkerton H. Repeated fracture and healing of silicic magma generate flow banding and earthquakes? Geology. 2003;**31**:1089-1092

[81] Anderson SW, Fink JH. Crease structures: Indicators of emplacement rates and surface stress regimes of lava flows. Geological Society of America Bulletin. 1992;**104**:615-625

[82] Lescinsky DT, Merle O. Extensional and compressional strain in lava flows and the formation of fractures in surface crust. In: Manga M, Ventura G, editors. Kinematics and Dynamics of Lava Flows, Geological Society of America Special Paper. Vol. 396. Boulder: Geological Society of America; 2005. pp. 163-179

[83] Farrell J, Karson J, Soldati A, Wysocki R. Multiple-generation folding and non-coaxial strain of lava crusts. Bulletin of Volcanology. 2018;**80**:84. DOI: 10.1007/s00445-018-1258-5

[84] Macdonald GA. Volcanoes. Englewood Cliffs: Prentice Hall Inc.; 1972. p. 501

[85] Bullock LA, Gertisser R, O'Driscoll B. Emplacement of the Rocche Rosse rhyolite lava flow (Lipari, Aeolian Islands). Bulletin of Volcanology. 2018; **80**:48. DOI: 10.1007/s00445-018-1222-4

[86] Fink JH. Gravity instability in the Holocene big and little Glass Mountain rhyolitic obsidian flows, northern California. Tectonophysics. 1980;**66**: 147-166

[87] Baum BA, Krantz WB, Fink JH, Dickinson RE. Taylor instability in rhyolite lava flows. Journal of Geophysical Research. 1989;**94**:5815-5828

[88] Andrews GDM, Kenderes SM, Whittington AG, Isom SL, Brown SR,

Pettus HD, et al. The fold illusion: The origins and implications of ogives on silicic lavas. Earth and Planetary Science Letters. 2021;**553**:116643

[89] Fink JH. Surface folding and viscosity of rhyolite flows. Geology. 1980;**8**:250-254

[90] Finch RH. Block lava. Journal of Geology. 1933;**41**:769-770

[91] Harris AJL, Rowland SK, Villeneuve N, Thordarson T. Pāhoehoe, ʻaʻā, and block lava: An illustrated history of the nomenclature. Bullettin of Volcanology. 2017;**79**:7

[92] Christiansen RL, Lipman PW. Emplacement and thermal history of a rhyolite lava flow near Fortymile canyon, South Nevada. Geological Society of America Bullettin. 1966;**77**:671-684

[93] Schneider JL, Fisher RV. Transport and emplacement mechanisms of large volcanic debris avalanches: Evidence from the northwest sector of cantal volcano (France). Journal of Volcanology and Geothermal Research. 1998;**83**:141-165

[94] Bowman ET, Take WA, Rait KL, Hann C. Physical models of rock avalanche spreading behaviour with dynamic fragmentation. Canadian Geotechnical Journal. 2012;**49**:460-476

[95] Gottsmann J, Dingwell DB. The cooling of frontal flow ramps: A calorimetric study on the Rocche Rosse rhyolite flow, Lipari, Aeolian Islands, Italy. Terra Nova. 2001;**13**:157-164

[96] Latutrie B, Harris A, Médard E, Gurioli L. Eruption and emplacement dynamics of a thick trachytic lava flow of the Sancy volcano (France). Bulletin of Volcanology. 2017;**79**:4. DOI: 10.1007/s00445-016-1084-6

[97] Manley CR, Fink JH. Internal textures of rhyolite flows as revealed by research drilling. Geology. 1987;**15**:549-552

[98] Merle O. Internal strain within lava flows from analogue modelling. Journal of Volcanology and Geothermal Research. 1998;**81**:189-206

[99] Henry CD, Price GJ, Parker DF, Wolff JA. Mid-tertiary silicic alkalic magmatism of trans-Pecos Texas: Rheomorphic tufts and extensive silicic lavas. In: Chapin CE, Zidek J, editors. Field Excursions to Volcanic Terranes in the Western United States, Volume 1: Southern Rocky Mountain Region, New Mexico Bureau of Mines and Mineral Resources Memoir. Vol. 46. Socorro (NM): New Mexico Bureau of Mines and Mineral Resources; 1989. pp. 231-272

[100] Poli G, Frederick A, Ferrara G. Geochemical characteristics of the South Tuscany (Italy) volcanic province. Constraints on lava petrogenesis. Chemical Geology. 1984;**43**:203-221

[101] Le Maitre RW, editor. Igneous rocks. A classification and glossary of terms. Recommendations of the International Union of Geological Sciences Subcommission on the Systematics of Igneous Rocks. 2nd ed. Cambridge: Cambridge University Press; 2002. p. 236

[102] Giordano D, La Felice S, Arzilli F, De Cristofaro SP, Masotta M, Polo L. Effusive acidic volcanism of Monte Amiata: Estimates of pre- and syn-eruptive conditions and volcanological implications. In: Principe C, Lavorini G, Vezzoli L, editors. Il vulcano di Monte Amiata. Nola: Edizioni Scientifiche e Artistiche; 2017. pp. 171-193

[103] Putirka KD. Igneous thermometers and barometers based on plagioclase +

liquid equilibria: Tests of some existing models and new calibrations. American Mineralogist. 2005;**90**:336-346

[104] Putirka KD. Thermometers and barometers for volcanic systems. Review Mineralogy and Geochemistry. 2008;**69**: 61-120

[105] Putirka K, Johnson M, Kinzler R, Walker D. Thermobarometry of mafic igneous rocks based on clinopyroxene-liquid equilibria, 0–30 kbar. Contributions to Mineralogy and Petrology. 1996;**123**:92-108

[106] Masotta M, Mollo M, Freda C, Gaeta M, Moore G. Clinopyroxene–liquid thermometers and barometers specific to alkaline differentiated magmas. Contributions to Mineralogy and Petrology. 2013;**166**:1545-1561

[107] Harrison TM, Watson EB. The behavior of apatite during crustal anatexis: Equilibrium and kinetic considerations. Geochimica et Cosmochimica Acta. 1984;**48**:1467-1477

[108] Ghiorso MS, Gualda GAR. An H_2O - CO_2 mixed fluid saturation model compatible with rhyolite-MELTS. Contributions to Mineralogy and Petrology. 2015;**169**:53. DOI: 10.1007/s00410-015-1141-8

[109] Batini F, Brogi A, Lazzarotto A, Liotta D, Pandeli E. Geological features of the Larderello–Travale and Monte Amiata geothermal areas (southern Tuscany, Italy). Episodes 2003;**26**: 239-244

[110] Marini L, Manzella A. Possible seismic signature of the quartz transition in the lithosphere of Southern Tuscany (Italy). Journal of Volcanology and Geothermal Research. 2005;**148**:81-97

[111] Frondini F, Caliro S, Cardellini C, Chiodini G, Morgantini N. Carbon dioxide degassing and thermal energy release in the Monte Amiata volcanic-geothermal area (Italy). Applied Geochemistry. 2009;**24**:860-875

[112] Sbrana A, Marianelli P, Belgiorno M, Sbrana M, Ciani V. Natural CO_2 degassing in the mount Amiata volcanic–geothermal area. Journal of Volcanology and Geothermal Research. 2020;**397**:106852. DOI: 10.1016/j.jvolgeores.2020.106852

[113] Irsara A, Frezzotti ML, Ghezzo C. Melt and fluid inclusion study in orthopyroxene and plagioclase phenocrysts from M. Amiata Quaternary volcanic complex. Plinius. 1993;**10**: 168-169

[114] Cioni R, Marini L. A Thermodynamic Approach to Water Geothermometry. Heidelberg: Springer; 2020. pp. 415

[115] Giordano D, Russell JK, Dingwell DB. Viscosity of magmatic liquids: A model. Earth Planetary Science Letters. 2008;**271**:123-134

[116] Costa A, Caricchi L, Bagdassarov N. A model for the rheology of particle-bearing suspensions and partially molten rocks. Geochemistry Geophysics Geosystems. 2009;**10**:Q03010. DOI: 10.1029/2008GC002138

[117] Ryan AG, Russell JK, Nichols ARL, Hess KU, Porritt LA. Experiments and models on H2O retrograde solubility in volcanic systems. American Mineralogist. 2015;**100**:774-786. DOI: 10.2138/am-2015-5030

[118] Martin RC. Some field and petrographic features of American and New Zealand ignimbrites. New Zealand

Journal of Geology and Geophysics. 1959;**2**:394-411

[119] Smith RL. Zones and zonal variations in welded ash-flows. In: Shorter Contributions to General Geology 1959, U.S. Geological Survey Professional Paper. Vol. 354-F. Denver (CO): U.S. Geological Survey; 1960. pp. 149-159

[120] Lipman PW, Christiansen RL. Zonal features of an ash-flow sheet in the Piapi canyon formation, southern Nevada. U.S. Geological Survey Professional Paper. Denver (CO): U.S. Geological Survey; 1964;**501-B**:74-78

[121] Allen SR, McPhie J. Phenocryst fragments in rhyolitic lavas and lava domes. Journal of Volcanology and Geothermal Research. 2003;**126**: 263-283

[122] Bertini G, Cappetti G, Dini I, Lovari F. Deep drilling results and updating of geothermal knowledge on the Monte Amiata area. In: Proceedings of the World Geothermal Congress; Florence, Italy. Vol. 2. Den Haag (NL): International Geothermal Association; 1995. pp. 1283-1286

[123] Cashman K. Volatile controls on magma ascent and eruption. In: Sparks RSJ, Hawkesworth CJ, editors. The State of the Planet: Frontiers and Challenges in Geophysics. Washington: American Geophysical Union; 2004. pp. 109-124. DOI: 10.1029/150GM10

[124] Heiken G, Wohletz K. Tephra deposits associated with silicic domes and lava flows. Geological Society of America, Special Paper. 1987;**212**:55-76

[125] Zellmer GF. Some first-order observations on magma transfer from mantle wedge to upper crust at volcanic arcs. The Geological Society of London Special Publication. 2008;**304**:15-31

[126] Castro JM, Dingwell DB, Nichols ARL, Gardner JE. New insights on the origin of flow bands in obsidian. Geological Society of America Special Paper. 2005;**396**:55-66. DOI: 10.1130/0-8137-2396-5.55

[127] Sparks RSJ, Tait SR, Yanev Y. Dense welding caused by volatile resorption. Journal of the Geological Society. 1999; **156**:217-225

Chapter 6

Catastrophic Processes in River Valleys of Volcanic Regions: Geomorphologist's Point of View

Ekaterina V. Lebedeva

Abstract

The river valleys located in volcanic regions are prone to various catastrophic processes, including those catalyzed by eruptions. First, to be mentioned among them are volcanic mudflows known as lahars. They commonly result from melting of ice, snow on the mountaintop, and rainfalls immediately following the eruption. This sequence of catastrophic events—"eruption-volcanic mudflow"—is quite common and has been well studied. When viewed closely the mud and debris flow in the volcanic regions appears to be brought on by various causes, with many factors and agents involved. Quite commonly, an eruption triggers not a single endo- or exogenic event, but a sequence of interrelated catastrophes following one after another. The studied cases allow identifying and describing up to two tens of probable scenarios—successions of catastrophic events in river valleys of the volcanic regions. The specific chain in any particular case depends on volcanic activities and accompanying events, such as seismic shocks, changes in local topography, hydrothermal activity, and erosion. The river valleys and adjoining areas are the most hazardous and vulnerable areas within as much as a few kilometers from the eruption center as the erupted material tends to accumulate in valleys and rapidly transported downstream.

Keywords: lava flow, pyroclastic material, gas-hydrothermal manifestations, valley infilling, dammed lake, mudflow, river network restructuring

1. Introduction

Catastrophic geomorphic processes in river valleys of volcanic regions (as well as in nonvolcanic ones) may result from various natural events, such as floods due to high-intensity rains, fast snow melting, or a water breakthrough from lake dammed by landslide or rockfall bodies. The areas of the present-day volcanicity are distinct for yet another catastrophe catalyst in river valleys: endogenic factor, primarily volcanic eruptions. The latter are often responsible for the descent of volcanic mudflows—lahars—related to melting of glaciers, snow caps on the volcanic

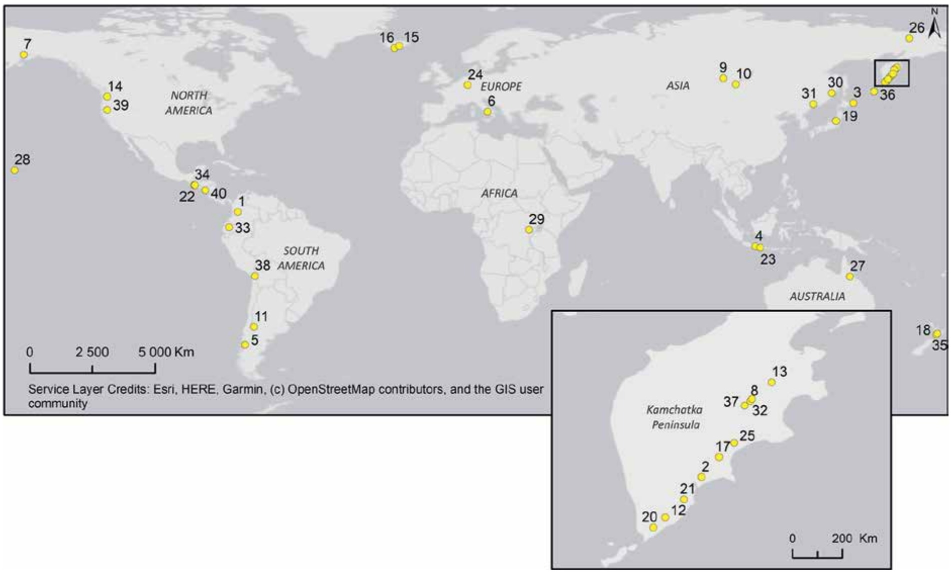

Figure 1.
Location of the volcanoes, mountains, and other objects described in this paper (yellow circles; numbering corresponds to the mentioned order in the text): 1 - Nevado del Ruiz volcano (vlc.), Columbia; 2 - Avachinsky vlc., Kamchatka, Russia; 3 - Mendeleev vlc., Kunashir Isl., Russia; 4 - Merapi vlc., Indonesia; 5 - Chaiten vlc., Chile; 6 - Vesuvius vlc., Italy; 7 - Spurr vlc., Alaska, USA; 8 - Bezymyanny vlc., Kamchatka, Russia; 9 - Eastern Sayan Mountains (Mnts.), East Siberia, Russia; 10 - Khamar-Daban Mnts., East Siberia, Russia; 11 - Pampas Onduladas lava flow, Mendoza, Argentina; 12 - Ksudach caldera, Kamchatka, Russia; 13 - Shiveluch vlc., Kamchatka, Russia; 14 - St. Helens vlc., Washington, USA; 15 - Grimsvötn vlc., Iceland; 16 - Katla vlc., Iceland; 17 - Akademia Nauk caldera, Kamchatka, Russia; 18 - Ruapehu vlc., New Zealand; 19 – Numazawa vlc., Japan; 20 - Kuril Lake caldera, Kamchatka, Russia; 21 - Mutnovsky vlc., Kamchatka, Russia; 22 - Agua vlc., Guatemala; 23 - Kelud vlc., Indonesia; 24 – Laachen see vlc., Germany; 25 - Uson-Geysernaya caldera, Kamchatka, Russia; 26 - Anyuyskiy vlc., Chukotka, Russia; 27 - Undara lava flow, Queensland, Australia; 28 - Hawaiian islands, USA; 29 - east African rift zone (Nyiragongo vlc., Congo); 30 - Sikhote-Alin' Mnts., Far East, Russia; 31 - East Manchurian Mnts., Far East, Russia; 32 - Klyuchevskoy vlc., Kamchatka, Russia; 33 - Cotopaxi vlc., Ecuador; 34 - Fuego vlc., Guatemala; 35 - Taupo volcanic zone, New Zealand; 36 - Sarychev peak vlc., Matua Isl., Russia; 37 - Tolbachik vlc., Kamchatka, Russia; 38 - Parinacota vlc., Chile; 39 - Shasta vlc., California, USA; 40 - Casita vlc., Nicaragua.

cones, or abundant rainfalls. Among them, there is a notorious lahar developed at the Nevado del Ruiz volcano eruption in Columbia (**Figure 1**) in 1985 and killing 23,000 people [1].

As summarized by Ref. [2], more than 200 million people are living in settlements within 200 km distance from active or potentially active volcanoes, that is, within the zones of immediate danger. Most of the towns and settlements within that zone are either confined to river valleys or located in close vicinity to them. As seen from the statistics cited by the specialist, 17% of human deaths during the eruptions result from lahars that occur typically in the river valleys, and another 27% from the pyroclastic flow, the maximum thickness of the latter being usually confined to topographic lows. So, the maps of endangered areas show as a rule river valleys and adjoining territories as the most hazardous, even in case they are at a considerable distance from volcanoes, see maps of volcanic regions Avachinsky [3] and Mendeleev [4] volcanoes (Kuril-Kamchatka region of Russia - See **Figure 1**), Merapi (Indonesia) [5], and many others (**Figure 2**). A good example is Chaiten town (Chile) partially destroyed because of the descent of the lahars along the Blanca River valley in

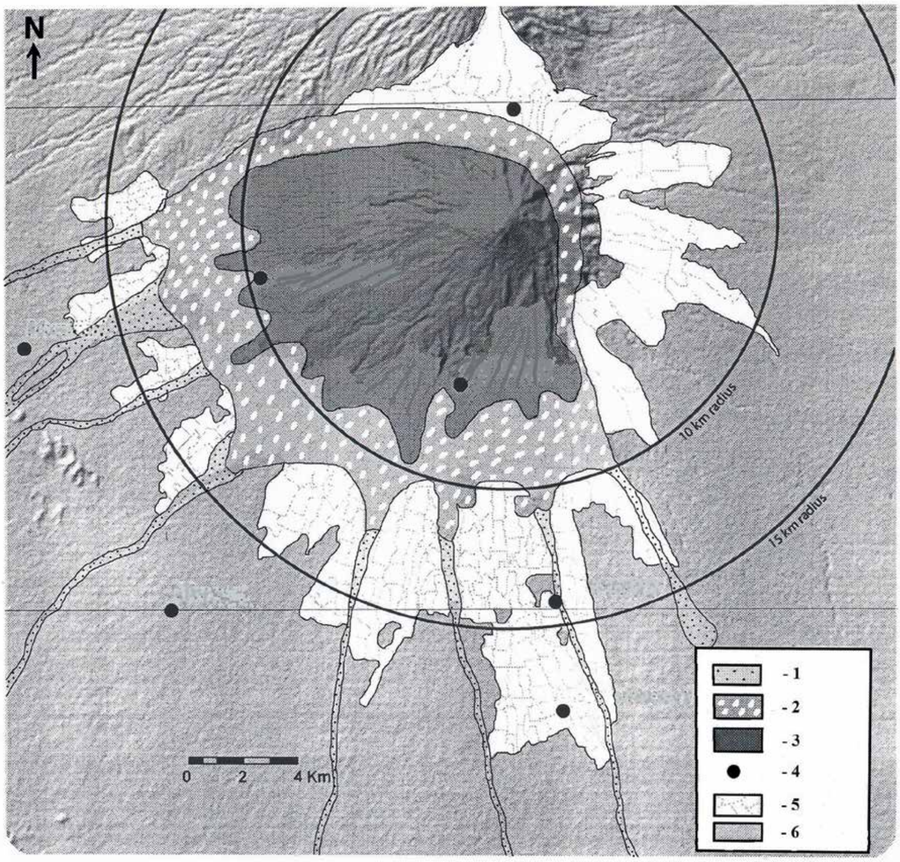

Figure 2.
Schematic map of volcanoes impact zones: 1 - river valleys originating on the volcano: Lahars, floods, and pyroclastic flow dominate; 2 - volcano foot: Pyroclastic flows, hot avalanches and lahars, lava flows, and toxic gas emissions dominate; 3 - volcano slopes: Frequent impact of pyroclastic and lava flows, rockfalls, toxic gas emissions, and formation of extrusive domes; 4 - settlements; 5 - agricultural land; and 6 - forests.

Figure 3.
*The Chaiten town (Chile) was demolished by lahars in 2008–2009 after Chaiten volcano eruption (see **Figure 1**, No 5). Buildings on the Blanco river banks: A - left bank, b - right bank. White arrow—Lahar deposits (2010, here and thereafter all photos are courtesy of the author unless stated otherwise).*

2008–2009 during the Chaiten volcano eruption. The areas of the town directly adjacent to the river suffered the most (**Figure 3**). Areas closer to the volcano but further from the river were only partially covered with ash.

The sequence of catastrophic events—“eruption-volcanic mudflow (lahar) descent” is well studied and quite common [2, 6–12], etc. To take one example, A. Neri and his colleagues [13] considered 12 scenarios of potential eruptions of Vesuvius volcano different in type and the subsequent development of catastrophic processes on its slopes; the specialists arrived at the conclusion on the probable lahar descent in eight cases. There is a commonly accepted distinction made between primary (or hot) mudflows immediately following the eruption and secondary (cold) ones that may occur a few decades after it. It should be noted that mudflows could form even on the slopes of extinct volcanoes under favorable conditions (steep slopes, loose material abundance, etc.).

When viewed more closely, the catastrophic processes in river valleys of volcanic regions display a considerable diversity of factors accountable for mudflow formation; besides, the spectrum of hazards is notably wide. Quite frequently, an endogenic event—an eruption—entails not a single catastrophic (endo- or exogenic) process, but a series of interrelated and sequentially developing catastrophes, that is, a cascade of hazardous processes.

Good examples are described in Ref. [14], where lahars associated with 1953 and 1992 eruptions of the Spurr volcanic complex descending along Crater Peak Creek (Chakachatna River tributary, Alaska, USA—— see **Figure 1**) blocked the main river with the formation of dammed lakes of quite impressive volumes (from 3.2 to 12 x 10^7 m^3). The destruction of temporary dams and the descent of lakes led to debris flows. The author concludes that the formation and failure of debris dams is a common process in this river valley and a consequence of pyroclastic eruptions of the Spurr volcanic complex.

This work is aimed at the analysis of the causes and subsequence of the hazardous phenomena in river valleys of the volcanic regions with different types of volcanic and post-volcanic activity. The methodology used is based on a thorough analysis of high and ultra-high-resolution satellite images followed by field geomorphological observations, including the study of the relief and geological structure of the territory, loose sediments, and bedrock. In key areas, a morphometric analysis of the longitudinal and transverse profiles of the valleys was carried out, and deposits of lahars and mudflows, dammed lakes, fragments of destroyed dams, and their genesis were studied. An important stage was the critical analysis of literary sources. The identification of connections and interdependencies of geological phenomena and chains of catastrophic geomorphological processes under conditions of the dominance of various types of volcanism—effusive, explosive, volcano-tectonic phenomena, and gas-hydrothermal processes—made it possible to create a classification scheme of catastrophic processes in volcanic regions river valleys. In the process of creating the scheme, the types of predominant volcanism, the nature of the volcanic material and the types of its movement, concomitant factors, and the sequence of catastrophes were identified. The cases studied by the author during her geomorphologic field survey in the volcanic regions of Russia and abroad as well as the literature analysis made it possible to identify up to two tens probable scenarios—successions of catastrophic events in river valleys (**Table 1**). In every case, the type of endogenic factor and specific features of its manifestation were taken into consideration, along with specific environmental characteristics (geology and geomorphology, hydrology, climate, and glaciation). The results may be important for the purpose of forecasting dangerous event, and for protecting people against endogenic natural disasters.

DOI: http://dx.doi.org/10.5772/intechopen.108141

Endogenic factors	Additional factors	Succession of catastrophic events			Specific case
		1	2	3	
Effusive or explosive eruption	Presence of (a) glaciers, (b) snow cover, or (c) abundant rainfall	Volcanic mudflows (lahars) in the main valley	—	—	a) Nevado del Ruiz vlc. (1985), Columbia b) Bezymyanny vlc.(1956), Kamchatka, Russia c) Chaiten vlc. (2008–2009), Chile
		Lahar flow along the tributary	The main valley is dammed by lahar, lake develop	Dammed lake outburst—mudflow descent	Spurr vlc. (1953, 1992), Alaska (Crater Peak Creek - Chakachatna R.)
Effusive eruption	Lava flow movement along the valley	The valley is filled with lava	The upstream part of the main valley and those of tributaries are flooded	Dam breach or spillover of dammed lake—mudflow descent	Maly Yenisey R., Jom-Bolok R., Eastern Sayan, Russia; Hvítá R., Iceland
	Lava flow movement across the valley	The valley is dammed by lava	Flooding of the valley upstream from the dam	Dam failure — mudflow descent	Dzhida R., Khamar-Daban, Oka R., Eastern Sayan, Russia; Colorado R., Mendoza, Argentina

Endogenic factors	Additional factors	Succession of catastrophic events			Specific case
		1	2	3	
Explosive eruption	Breakdown of the uppermost part of the volcanic cone	The valley is dammed by large fragments of the cone	The upstream part of the valley is flooded, the dammed lake level rises	Dam failure—mudflow descent	Teplaya R., Shtyubel cone (1907), Ksudach caldera, Kamchatka, Russia
	Breakdown of one side of the cone-sector collapse	Debris avalanche formed	Pyroclasts build up and fill valleys	Erosion of pyroclasts and mudflows formation	Bezymyanny vlc. (1956), Shiveluch vlc. (1964), Kamchatka, Russia
			Dams are built and dammed lakes develop upstream	Dammed lake outburst—mudflow descent	Chakachatna R., Spurr vlc. Complex, Alaska; St. Helens vlc. (1980), USA
	Pyroclastic flow descent	Valley is filled with pyroclastic material	Erosion of pyroclast contributes to mudflow development.	—	Kabeku R., Shiveluch vlc. (2010), Kamchatka, Russia
			Tributary mouths are dammed, and lakes develop	Dammed lake outburst—mudflow descent	Bekesh R., Shiveluch vlc. (2010), Kamchatka, Russia
	Pyroclastic mantle formation	Pyroclasts more than 1 m thick accumulates in the region of eruption	Pyroclasts move downslope to the valley floor	Mudflows result from rainfall and snow melting	Shtyubel cone (1907), Ksudach caldera, Kamchatka, Russia
Subglacial eruption	The ice sheets or well-developed alpine glaciers	Subglacial lake formation, the ice surface subsidence	Glacial outburst flood (jökulhlaup)	—	Grimsvötn vlc. (1996), Katla vlc. (1918), Iceland
Underwater / above water eruption	Lake in the immediate vicinity of the eruption center	The rise of tsunami or ejected water	The lake expulsion and the mudflows descent down the river flowing out of the lake	—	Karymsky R., Karymsky Lake (1996), Academia Nauk caldera, Kamchatka, Russia; Crater Lake, Ruapehu vlc., New Zealand

Endogenic factors	Additional factors	Succession of catastrophic events			Specific case
		1	2	3	
Volcano-tectonic activities	Collapse caldera formation	Partial destruction of the river valley filled with pyroclasts	Enhanced downcutting upstream, mudflow descent	—	Streams in the Ksudach caldera, Kamchatka, Russia
		The valleys are filled with pyroclasts, including ignimbrites	River damming and lake formation	Dammed lake expulsion—mudflow descent	Tadami R., Numazawa vlc., Japan
	Change in the surface slope: a dome growth in the river basin, local subsidence, and fissures.	Changes in the river's long profile—partial inundation of the valley	Water overflow from the lake—mudflow descent	—	Lagernyi creek, Shtyubel cone, Ksudach caldera, Kamchatka, Russia
	Rapid extrusion growth	Huge rockfall or debris avalanche	River damming and lake formation	Dammed lake expulsion—mudflow descent	Ozernaya R., Dikyi Greben' extrusion, Kuril Lake caldera, Kamchatka, Russia
Seismic events	Densely fissured zone, hydrothermal alteration, loose deposits, and heavy rains	The mass movement downslope (landslide, slump) blocks the valley	Descent of mudflow (removal of material brought downslope)	Partial inundation of valley, dammed lake formation; mudflow at the lake expulsion	Fal'shivaya R. tributaries, Mutnovsky vlc., Kamchatka, Russia
		Crater wall breakdown, and overspill	Mudflow descent	—	Agua vlc. (1541), Guatemala; Kelud vlc. (1875), Indonesia
		Dam failure	Mudflow descent		Laacher See vlc., Germany
Gas-hydrothermal manifestations	Steep river valley slopes, sometime rainfall or weak earthquake impact	Landslide or rockfall	Mudflow descent	—	Geysernaya R. (1982), Uzon-Geysernaya caldera, Kamchatka, Russia
		Landslide or rockfall blocking the valley	Mudflow descent, dammed lake formation	Mudflow at the lake expulsion	Geysernaya R. (2007, 2014), Uzon-Geysernaya caldera, Kamchatka, Russia

Table 1.
Catastrophic processes in river valleys of volcanic regions.

2. Chains of catastrophic events in river valleys of volcanic regions

The river valleys in volcanic regions often originate on slopes of volcanic cones. In their uppermost reaches, they have a look of erosional hollows ("barrancos" in Spanish). If a river flows in a fault zone with eruption centers of its own (moderate-size shield volcanoes), the latter appears to be within the valley itself. Such phenomena may be seen, for example, in the upper reaches of the Bolshoy and Maly Yenisey, in the Jom-Bolok (Zhom-Bolok) river valley in the Eastern Sayan mountains (Southern Baikal volcanic region, Russia) [15–17], in the Bolshoy Anyuy river valley in Chukotka (the Northeast of Russia—see **Figure 1**) [18].

In either case, an *effusive eruption* may result in the river valley being filled with lava flow, sometimes over a length of tens and even more than one hundred kilometers. The basalt flows of the Middle Pleistocene age—among them Undara (Queensland, Australia) and Pampas Onduladas (Mendoza, Argentina), both up to 160–170 km long are recognized as the longest-**Figure 1**) [19, 20]. There is a lava flow which is greater in size in the Maly Yenisey river valley (Eastern Sayan mountains, Russia)—it is 175 km long, up to 1.5 km wide, and its volume is estimated at 40–50 km^3 [16]. The youngest basalt flow comparable to the above-named in length (~140 km) is Thjorsa (Þjorsa, Iceland) [21] dated to the Holocene. Another lava flow of young age (about 13 ka BP) is the Jom-Bolok (Eastern Sayan mountains, Russia—see **Figure 1**) [22, 23]: it is 70 km long, up to 2 km wide, and as much as 150 m thick. The formation of flows of such a length is possible during the outpouring of liquid basaltic lavas and at significant flow rates. It is known that, for example, in the recent eruptions on the Hawaiian islands and in the east African zift Zone (Congo) the lava flows moved at a rate of 40 and up to 100 km per hour [2].

Under conditions of a heavily dissected topography, lava flows tend to fill river valleys. In case the land surface is relatively flattened, the lava flow may be inconsistent with valley direction, as we can see with Undara (Queensland, Australia) and Thjorsa (Iceland) basalt flows [19, 21]. Lavas may flow across flat-bottomed shallow linear hollows, cover low watersheds, and form dams of a kind; as a result, the river appears completely dammed or its flow is forced aside. A phenomenon of that type has been described in the Colorado river valley (Mendoza province, Argentina), where El Corcovo lava flow blocked the river ~840 ka BP; later the stream formed a new incision about 1 km south of its former position [24].

As to morphologically distinct valleys, they may be completely or partially filled with lava, with both mainstream and its tributaries dammed. Because of the main river displacement and tributary valleys partly flooded, dammed lakes develop as we can see in the Bolshoy Anyuy river valley in Chukotka (the Northeast of Russia) [18]. They may be considerably deep (up to tens of meters), depending on the initial topographic dissection and the lava thickness. For example, dammed lakes 50–70 m deep existed in the lower parts of the Maly Yenisey tributaries (Eastern Sayan mountains, Russia—see **Figure 1**). Sedimentary sequences, including lava series, studied in the Maly Yenisey valley, provided evidence of dammed lakes having been common enough in the main valley and its tributaries; the subaqueous outflow of lava resulted in pillow lava and hyaloclastite formation [16].

The lakes of the Jom-Bolok drainage basin (the largest of them—Khara-Nur—is approximately 9 km^2 in area) are drained under the lava at present (**Figure 4**) [25, 26]. In case such drainage is impossible, or it is less than the volume of water entering the lake, there may be several scenarios of further events. For example, the dammed lake may overflow into an adjacent valley, or even into another drainage basin [27].

Figure 4.
*Jom-Bolok lava flow (light gray), volcanoes (red), and dammed lakes (blue): 1 - existing lake Khara-Nur, 2 - drained paleolake Zun-Ukhergei. White dotted line—Watershed between the Oka and the Bolshoy Yenisey rivers basins (Eastern Sayan mountains, Russia—See **Figure 1**, No 9).*

Figure 5.
*Destroyed lava dams: A - the Hvita river, Iceland (2014); b - the Oka river, Eastern Sayan mountains, Russia (**Figure 1**, No 9). White arrow—The place of destroyed dam (2019, UVA photo courtesy by V. Pellinen).*

A similar situation periodically occurs in the upper reaches of the Jom-Bolok river, where the Khara-Nur Lake flows into the neighboring Bolshoy Yenisey river basin during periods of increased moisture. Examples of such river network restructuring are described also in Ref. [28] for the Sikhote-Alin' and the East Manchurian mountains (Russia-see **Figure 1**).

The lava dam may be also eroded completely or partly by the stream [27, 29, 30]. The remains of lava dams and traces of drained reservoirs have been preserved in the valleys of the river Oka, Dzhida, and many others. Jom-Bolok lava flow dammed Oka river with Zun-Ukhergei paleo-lake formation (**Figure 5**). In any case, an active erosion (downcutting) would initiate a mud- or debris flow descent in due course in the valley.

Explosive eruptions are more diversified in their consequences. Practically each of them is accompanied by an ejection of considerable volumes of *pyroclasts*. The ejecta volume at colossal explosive eruptions (VEI-6) exceeds 10 km^3 and may be more than 1000 km^3 during mega-colossal ones (VEI-8); the latter are relatively rare (about once in 50 thousand years). They usually result in development of ignimbrite mantles covering the pre-eruption surface and forming plains over an area of hundreds and thousands of square kilometers. More common are relatively small eruptions, though they also can produce practically instantaneous changes in local topography. During the Shtyubel cone (Ksudach caldera, Kamchatka, Russia) eruption in 1907, for example, the volume of ejected pyroclastics is estimated at 1.5 to 2 km^3; the tephra thickness varied from 0.5 to 3 m (**Figure 6a**) both in the immediate vicinity of the eruption center in the Ksudach caldera and at a distance of a few tens of kilometers from it (in the direction the wind was blowing during the eruption) [31].

In the late 1950s, Bezymyanny volcano (Kamchatka, Russia) ejected as much as 3 km^3 of tephra; the deposits formed a cover up to 40 m thick over an area of 70 km^2 and as thick as 40 cm over almost 500 km^2 [32, 33]. In explosions, blocks weighing as much as a few tons may be ejected as far as up to 300 m from the vent of ejection, those weighing a few kilograms—over a distance of 3–6 km [2], and the smaller-size ones may be thrown as far as 20 km [34]. The ash layer more than 30–40 cm thick would cause drying up or loss of vegetation [35], that is, in turn, has an effect on the erosion and slope processes [36, 37]. Ashfalls introduce noticeable changes into the local topography, reducing slope steepness and changing soil characteristics. The pyroclastic layers deposited over river valleys and watersheds may result in essential changes in the valley network pattern, as the new erosional landforms would develop in accordance with the new relief (**Figure 6b**) and may disagree with former valleys.

The *pyroclasts* ejected during an eruption are noted for high porosity and, consequently, for lightness, so that the material may be easily transported by wind and water and *concentrates gradually* in topographic lows (primarily *in river valleys*). Abundant rainfall or snow melting bring about the descent of mudflows (with solid ingredient proportion of more than 60%) or hyper-concentrated flows, with proportion of solid ingredient between 20 and 60%, which gradually transport pyroclastic material downstream (**Figure 6c**). That is best illustrated by a concrete example of Bezymyanny volcano (Kamchatka, Russia) eruption on March 30, 1956: the ejected pyroclastic induced an active snow melt that resulted in mudflows up to 75–85 km long formed in the Sukhaya Khapitsa valley on slope of the Klyuchevskoy volcano (Kamchatka, Russia) [38].

Lahar deposits are usually accumulated at the base of the volcano slopes; the length of the flows may be considerable, up to 185 km (Kelud volcano, Indonesia, 1919) and even as great as 300 km (Cotopaxi volcano, Ecuador, 1877). Traces of lahars have been recorded on most of the active volcanoes of the world having typically the explosive type of eruptions (**Figure 7a**): to take a few examples, there are 22 events of that kind recorded on Cotopaxi slopes in sixteenth-nineteenth centuries [39]; 20 glacial-volcanic

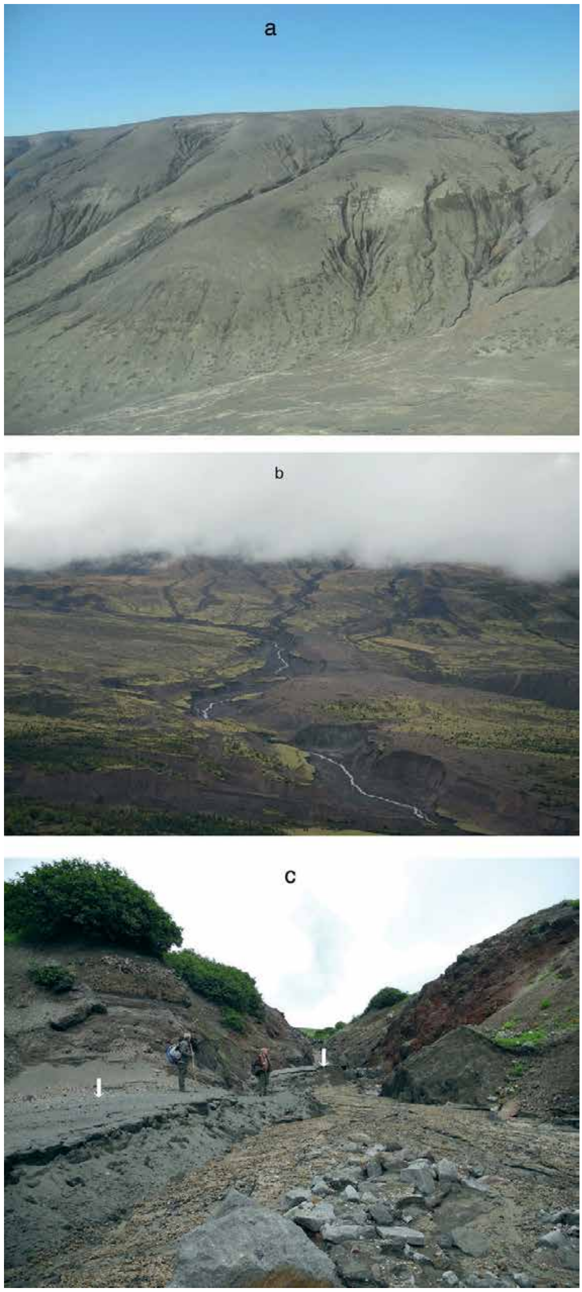

Figure 6.
Water redeposition of pyroclastic material: A - slopes with gullies in pyroclastic cover (Ksudach caldera, Kamchatka, Russia, 2016—See ***Figure 1****, No 12).); b - St. Helens volcano slopes with newly formed valleys in pyroclastic flow deposits (USA, 2018—See* ***Figure 1****, No 14); and c - modern lahars deposits in the Lagernyi creek valley (Ksudach caldera, Kamchatka, Russia, 2016).*

mudflows are known to occur on the Klyuchevskoy slopes (Kamchatka) in 1737 to 2008 time interval; there are 11 stages of large mudflows composed of melted snow and volcanic materials, which descend by the valleys on Shiveluch volcano (Kamchatka, Russia) southern slopes (the Kabeku, Bekesh, Baydarnaya, Kamenskaya, and other rivers) from 1854 to 2009 (**Figure 7b**) [11]. An eruption of the small Chaiten volcano (Chile) in 2008–2009 was responsible for three lahars; one of them (May 2009) inflicted damage on the city of Chaiten (**Figure 3**). Observations performed in valleys around volcanoes [2] proved that the valley bottom may be hazardous for a considerable length of time (several decades) after the eruption because of a lot of the unconsolidated sediments within and the expected subsequent lahar events in the valleys.

Quite often explosions occur not only with the ejection of pyroclasts but also with partial demolition of the volcanic cone. Even in the case of a small-size volcano, when its top is blown off, large blocks are scattered, and adjoining valleys may be dammed with coarse material. That often results in a dammed lake formation or in rising of the preexisting lake level. Such a case was recorded, for example, in 1907 in the uppermost reaches of the Teplaya river (Ksudach caldera, Kamchatka, Russia). Later, when the dam is broken (**Figure 8**), a mudflow descent occurs inevitably, which is confirmed by the presence of a large fan at the river mouth. Intracaldera lake breakout floods have been identified in the Taupo volcanic zone (New Zealand) also [40].

One-sided destruction of the volcanic cone during eruption—the so-called directed blast (or more neutral term - sector collapse)—is often accompanied by a debris avalanche development (see **Table 1**). As a result, non-sorted debris is deposited on the part of slope the explosion had been directed at. As noted by Ref. [34], the rock fragments may be thrown off over a distance of 29–30 km. A large debris avalanche goes as far as 85 km from the cone failure and covers an area of 100 to 1000 km^2 [2]. The resurgent material may either infill river valleys completely over a considerable length or build up dams there. The case of a valley infilling was recorded during the Bezymyanny volcano eruption (Kamchatka, Russia) in 1956 when valleys on the eastern slope of the mountain were filled with debris and ejecta over a length of a few kilometers [32]. When streams resumed their activity, a series of copious mudflows developed and brought the material onto the right side of the Kamchatka river valley [38]. Debris avalanches in the Chakachatna river valley (Alaska, USA) resulted in the formation of long dams and dammed lakes with depth up to 150 m [14]. Not-so-huge lakes were formed in valleys around St. Helens volcano after 1980 eruption (**Figure 9a**). The avalanches descent during the Holocene Shiveluch volcano eruptions (Kamchatka, Russia) brought about a radical restructuring of the valley network: the Kabeku river captured a parallel water stream blocked with large blocks of the avalanche (**Figure 9b**) [41].

Figure 7.
*Lahars: A - on the Fuego volcano slope (Guatemala, 2013—See **Figure 1**, No 34); b - in the Kabeku river valley (Shiveluch volcano foot, Kamchatka, Russia, 2013—See **Figure 1**, No 13).*

Figure 8.
*A fragment of a destroyed debris dam (white arrow) at the source of the Teplaya river cause a rise in the level of Ksudach caldera's lakes by 15 m (white dotted line) after the eruption of 1907. The black dotted line shows the top of the Shtyubel cone destroyed by the 1907 explosion (Kamchatka, Russia, 2016—See **Figure 1**, No 12).*

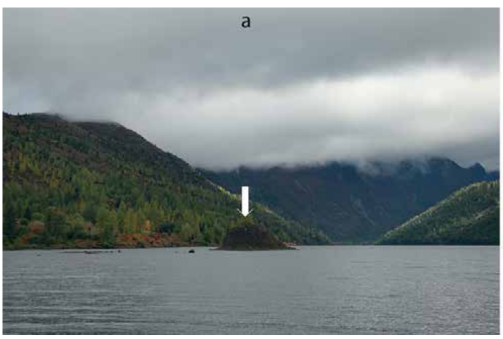

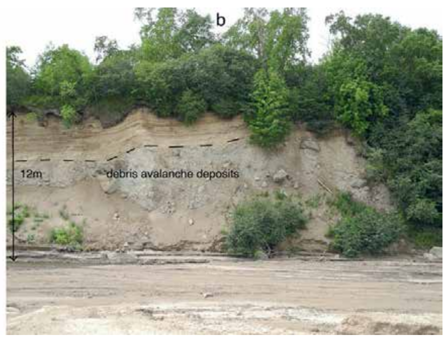

Figure 9.
*Debris avalanches impact: A - dammed Coldwater lake in the Coldwater Creek valley with hummocky relief remnants (white arrow) as islands (St. Helens volcano, USA, 2018—See **Figure 1**, No 14); b - a debris avalanche deposits with soil-pyroclastic cover in Kabeku river valley (Shiveluch volcano, Kamchatka, Russia, 2013—See **Figure 1**, No 13).*

In explosive eruptions, a heavier part of the eruptive column may form pyroclastic flows—a mixture of burning hot (often above 600–700°C) blocks, ash, and volcanic gases. They descend from the eruptive vent downslope at a rate of 100 m/s or more [2] mostly following valleys of streams dissecting the slopes. There are known occasions when pyroclastic flows rose upstream valleys passing over the mountain ranges enclosing caldera; such a case was reconstructed [42] to have occurred during the latest caldera-forming eruption of Ksudach volcano (Kamchatka, Russia) 1725 yr. BP (**Figure 10a**). As a result, the valleys turn out to be filled with pyroclasts; later the loose pyroclastic mantle was eroded, and mudflows arose. The pyroclastic flows affect great areas, up to ten and hundreds of square kilometers. After Shiveluch volcano eruption (Kamchatka, Russia) in 1964, the affected area was 45.5 km^2 [43]. In the succeeding years, the flows repeatedly descended by the stream valleys of the southern slope, and their length varied between 8 and 28 km [44]. Pyroclastic flows are known, however, to be as long as 100 km [1, 34].

On entering a valley, a pyroclastic flow covers its floor completely and, in common with lava flows, forms a convex transversal profile. On the Shiveluch volcano, the pyroclastic flow deposits (**Figure 10b**) vary between 2 and 5 m and 40 and 50 m [43–45]. The deposits may be loose or welded (as pumice and ignimbrites). Accordingly, the former is more easily destroyed by erosion and mudflow formation. Pumice and ignimbrite flow during *caldera collapse* often form plains over pre-existing landforms. However, they are seldom marked by considerable durability and their surface is often dissected by erosion to a stage of badland (**Figure 10c**).

In common with lava flows, the pyroclastic ones may block the tributaries at their entering the main valley and form dammed lakes (**Figure 11a**). The pyroclastic dams, however, are not very strong and may be broken by erosion and mudflows within a few years after the eruption. Such was the case of the southern slope of Shiveluch volcano (Kamchatka, Russia) [45]. As the streams are usually overloaded with loose pyroclasts, the deposition rate in the lakes is rather high; to take but one example, a series of horizontally stratified sands more than 6–7 m thick accumulated in the dammed lake at the Sukhoy Bekesh river per 3 years (**Figure 11b**). The lakes dammed by ignimbrites are long-lived and large, and their depth may be as great as 100 m like in Tadamy river-dammed lake (Japan). But this ignimbrite dam also was destroyed with debris (mud) flow formation along a river valley 150 km long [46]. Similar situations with ignimbrite dams were also reconstructed by [40] for Tarawera lake in Taupo volcanic zone (New Zealand).

During the observation period of the Shiveluch volcano activities (1964–2013), the lahar descent was always preceded by the pyroclastic flow eruption. This fact led I.B. Seinova and her colleagues [47] to the conclusion that the pyroclastic flows is a trigger mechanism in the lahar initiation. In 2009, the eruption of Sarychev peak volcano (Matua Isl., the Kuriles, Russia—see **Figure 1**, No 36) produced eight pyroclastic flows, which subsequently gave rise to seven mudflows (lahars) [48]. A regular lahar formation has been recorded after Merapi volcano (Indonesia) eruptions usually accompanied by pyroclastic flows. Ten out of 18 largest streams originated on the volcano became repeatedly the ways of lahar descent [5]. The studies of the pyroclastic flow deposits on St. Helens volcano showed that the pyroclastic flows (or pyroclastic density currents–PDC) exert a noticeable erosive effect on the substrate [49], particularly in case they move downward by linear hollows on steep volcanic slopes. Avulsions, riverbank erosion, and riverbed downcutting were presented as lahars geomorphic impacts at Merapi volcano river valleys after the 2010 explosion [5, 50].

After a large eruption accompanied by pyroclastic ejection, the solid runoff of rivers in volcanic regions may be several orders of magnitude greater than before the eruption, that is distinctly seen in the graphs constructed for Kamchatka and Tolbachik rivers (Kamchatka, Russia) [51]. According to Ref. [2], after St. Helens eruption in 1980, the annual solid runoff of rivers in the vicinities increased by a factor of 500, and even 20 years after the event the annual suspended load increased ~100 times as compared with the value before the eruption. The streams flowing from volcanoes are usually overloaded with rock debris varying in size, and great volumes of pyroclasts (including that redeposited by lahars) are to be transported by the rivers [52].

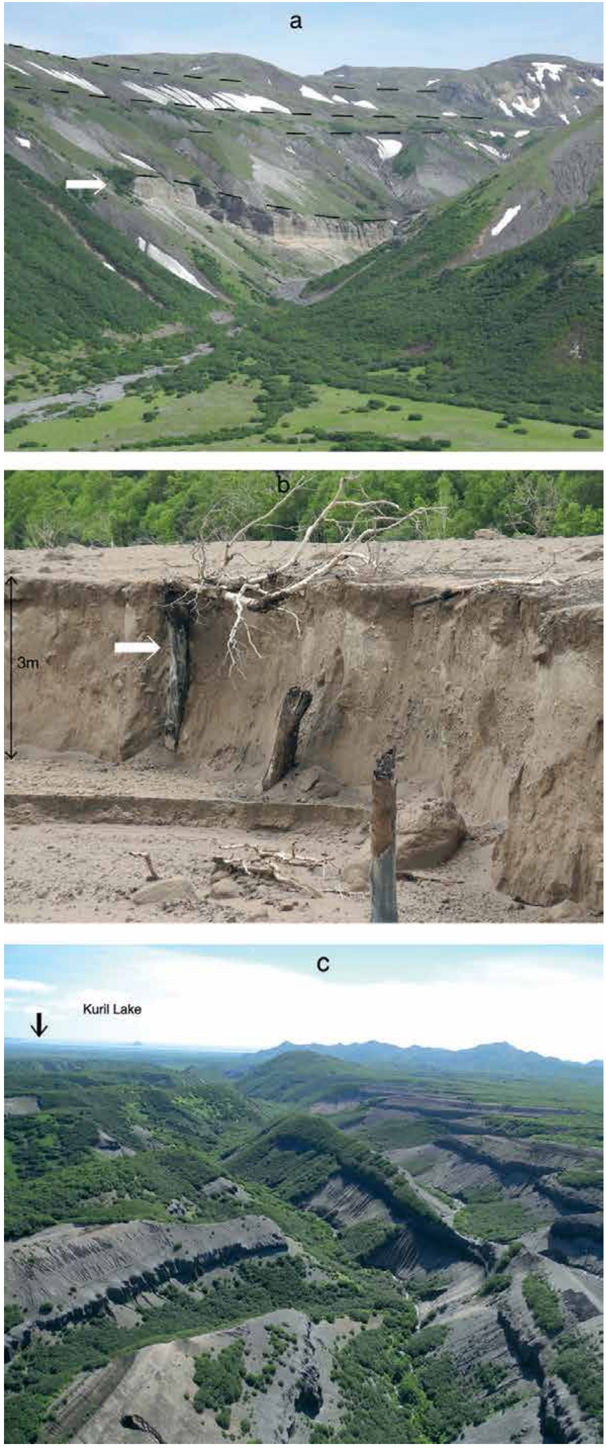

Figure 10.
*Pyroclastic flow (PF) deposits: A - traces PFs (black dotted lines) expand upstream (upslope) passing over the mountain ranges enclosing Ksudach caldera (2016); b - burnt birch trunks in a pyroclastic flow in Kabeku river valley, Shiveluch volcano (2013); and c - dissected Holocene pyroclastic plain near Kuril lake caldera (2016); all photos—Kamchatka, Russia (see **Figure 1**, No 12, 13, 20).*

Figure 11.
*Dammed lake between two pyroclastic flows (a - the Kabeku river valley) and destroyed dammed lake deposits (b - the Bekesh river valley), Shiveluch volcano slopes, Kamchatka, Russia (2013—See **Figure 1**, No 13).*

Observations in the valleys of the Kabeku and Bekesh rivers (the Shiveluch volcano slopes, Kamchatka, Russia) allow us to conclude that the frequent descent of lahars causes many changes not only in the nature of the runoff but also in the morphology of the valleys in the areas of their deposition.

In case the eruption occurs in a lake (within caldera or in a dammed water body in a valley), or in its immediate vicinity, no matter if it is underwater or above, it results in the water expulsion from the lake and a mudflow descent from the slopes or along the valley. According to Refs. [6, 7, 9, 12, 40], the generation of eruption-triggered lahars by the ejection of water from lakes is widespread in New Zealand and in other regions of the world. Since 1861 a lot of lahars have been generated from the Crater lake on Ruapehu volcano. The evidence of such phenomena is traceable in the Teplaya river valley (Ksudach caldera, Kamchatka, Russia) and in valleys of other rivers flowing out of volcanic lakes [53]. A subaqueous explosive eruption was observed in 1996 in Karymsky lake (the Akademia Nauk caldera, Kamchatka) with a series of tsunami to 15 m high and breakthrough floods from lake along Karymskaya river valley [54]. Then, at the source of the river, a dam of pyroclastic material arose, which after a few months was broken through with the descent of the lahar.

In the regions of the continental ice sheet, the eruption taking place under a thick ice cover may create giant outburst floods of meltwater known under the name of *jökulhlaup*. At present, they are known to occur in Iceland [55, 56]; during the Quaternary cold intervals, they seem to have happened in Kamchatka [57], as well as on the east Tuvinian lava upland (Eastern Sayan mountains, Russia—see **Figure 1**) [58] and in other volcanic regions of midlatitudes. When an eruption takes place under glacier, the meltwater forms a subglacial water body under considerable pressure; subsequently, the ice may subside and an outburst flood occurs accompanied by the abrupt release of great volumes of water, ice fragments, and stone debris being transported over a large distance, particularly along river valleys. Enormous volumes of water involved in the process account for the great scale of the phenomenon. For example, the length of the flows, their rate, and the transported material volume exceed the characteristics of lahars by orders of the value. For example, the Katla volcano eruption under Myrdalsjökull glacier in 1918 induced a jökulhlaup of 8 km^3 volume and a flooded area of 600–800 km^2. Those flows maybe 20 to 70 m deep and 8–9 km wide. No river channel can hold a great volume of water. Quite often, the passage of the flood causes changes in topography and a large-scale restructuring of river network. That may be illustrated by a case of a subglacial eruption of Grimsvötn volcano in 1861 when the Skeidara river channel was displaced westward by 13 km [56, 59, 60].

Quite often volcanic eruptions are accompanied by *volcanic-tectonic manifestations*, such as appearance of *fissures* and *deformations of the land surface* (uplift or subsidence of the land surface by a few meters); less common are *collapse calderas*. We mentioned above that during the formation of calderas, not only the river valleys are filled with pyroclasts, but also the formation of flat areas around the calderas, where pyroclastic flows overlap the original relief (**Figure 12**). The abundance of pyroclastic material favors the descent of lahars along the newly formed river network (see **Figure 10**); however, the influence of caldera formation on valleys is not limited to this.

The changes in topography may lead to deformations of valleys' long profiles, to displacement or restructuring of the river network. Earlier we described such changes observed in the Ksudach caldera complex (Kamchatka, Russia); among them are reconfigurations of the valleys' lowermost reaches after the caldera collapse in 1725 (the date is given after [61]), and the stream network restructuring induced by Shtyubel cone growth [29, 30]. The changes in the river network structure accompanying volcanic activities or resulting from them are also catastrophes of various scales; they are often accompanied by outbursts or spillover of dammed lakes and the subsequent descent of mudflows. So, the growth of the Shtyubel cone led to a change in the longitudinal profile of the Lagernyi creek with the formation of a lake, when overflowing and discharging water, a mudflow was formed.

The rapid extrusion growth can also provoke catastrophic processes in the valleys. So, about 1600 years ago [41] because of the giant blocks collapse of the actively grown extrusion Dikiy Greben' (Kuril Lake caldera, Kamchatka, Russia),

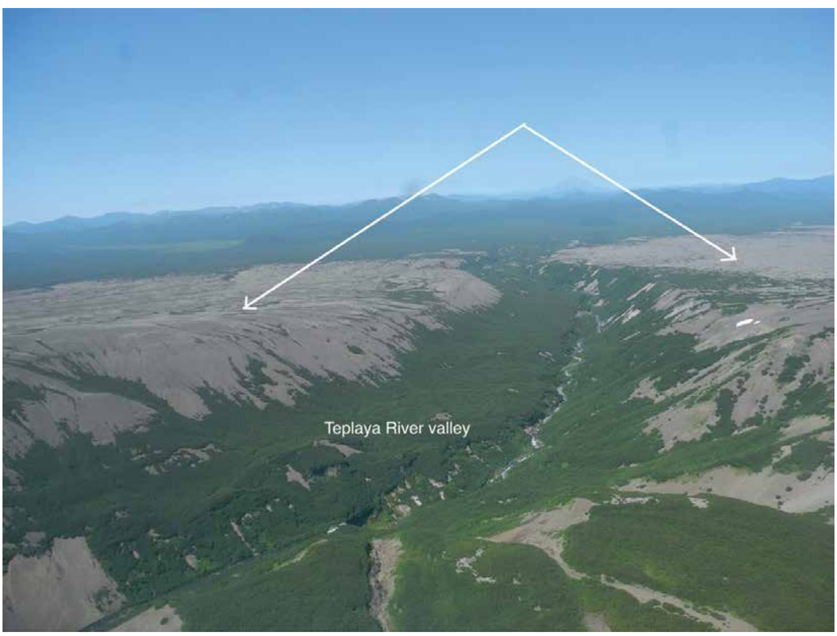

Figure 12.
The fragments of the pyroclastic plain around Ksudach caldera (white arrows) with Teplaya river valley (Kamchatka, Russia, 2016—See ***Figure 1,*** *No 12).*

the Ozernaya river valley flowing from the Kuril lake was blocked (**Figure 13**). Lavas large blocks can be traced on the left side of the valley and in the riverbed in its upper reaches. The wreckage is characterized by numerous cracks that arose because of their

Figure 13.
*Dikyi Greben' extrusion (a - black arrow) and giant blocks (white dotted lines)—Traces of it collapse; b - destroyed dam (white dash line) in the Ozernaya river valley (Kuril Lake caldera, Kamchatka, Russia, 2020—See **Figure 1**, No 20).*

Figure 14.
*New dammed lake in the Vulkannaya river upper reaches after the collapse of the Mutnovsky volcano crater wall: Thin white arrow—Direction of rock fragments displacement, thick arrow—The new dam (Kamchatka, Russia, 2021—See **Figure 1**, No 21).*

fall at more than 2 km. According to our estimates, the dam height reached 20 m and its destruction was inevitably accompanied by a debris flow.

Among the factors contributing to the hazardous processes in river valleys are the presence of unstable rocks (fissured, loose, or altered by hydrothermal processes), seismic shocks (even weak), or extremely heavy rainfall. There are well-known facts of debris avalanches, rockfalls, and other kinds of active mass wasting not only during the eruptions (as in the case of Shiveluch and St. Helens), but also long after them (as on volcanoes Parinacota in Chile, Shasta in California, Casita in Nicaragua, and others) [2]. Obviously, seismic events, both accompanying volcanism and directly independent of it, can cause the destruction of *the crater lake walls* or the body of a volcanic dam of various origins [53, 62]. In any case, these will lead to lake outbursts and mudflow descent. On the other hand, if an earthquake triggers a landslide, a new dammed lake may appear in the valley. In August 2021, we observed the consequences of a collapse on the northern wall of the crater of the Mutnovsky volcano (Kamchatka), where 19.08 another dammed lake appeared and mudflow descended (**Figure 14**).

Large-scale geomorphic catastrophes may occur in valleys within the zones of hydrothermal activities. In those zones, rocks in the valley sides are densely fissured, essentially altered, and often turned into clay by the chemical weathering processes and water encroaching. The rocks' hydrothermal weathering and moistening processes stimulate a wide range of slope processes—rockfalls, landslides, slumps, flow slides. The hydrothermal clays distribution and the presence of the steam and thermal water outlets on the valley slopes favor the numerous displacements, resulting in the formation of the local multilevel landslide and block-slide terraces. In some cases, several tiers of similar terraces can be observed (**Figure 15**).

In such areas, there is a significant widening of the valleys due to active slopes flattening. At the same time, in the bottoms, there is an accumulation of the slope material, displaced because of landslides and collapses with the periodic blocking of the valleys and the formation of the temporary dams and the dammed reservoirs, in which the river sediments accumulate. The dams' length can reach 500–700 m along the valley. The further slope and alluvial material transportation and redeposition occur mainly due to the debris flows, which are formed either directly during the gravity collapse, or during the dams' destruction and the descent of temporarily dammed reservoirs. This is well confirmed by the observations carried out in the

Figure 15.
*Landslide terraces (white arrows and dashed lines): A - on the Geysernaya river valley sides (Uzon-Geysernaya caldera, Kamchatka, Russia—See **Figure 1**, No 25), periodically blocking the river with subsequent debris flows originating (2013), b - in Kislyi Creek, Mendeleev volcano, Kunashir Isl. (Russia, 2018 - see **Figure 1**, No 3).*

Figure 16.
The Geyzernaya river valley (Uzon-Geysernaya caldera, Kamchatka, Russia, 2021—See ***Figure 1,*** *No 25): A - partly destroyed dam 2007 (1) with drained lake (2), b - dam 2014 (white arrow). Black arrows—River flow direction, white dashed lines—Dam borders.*

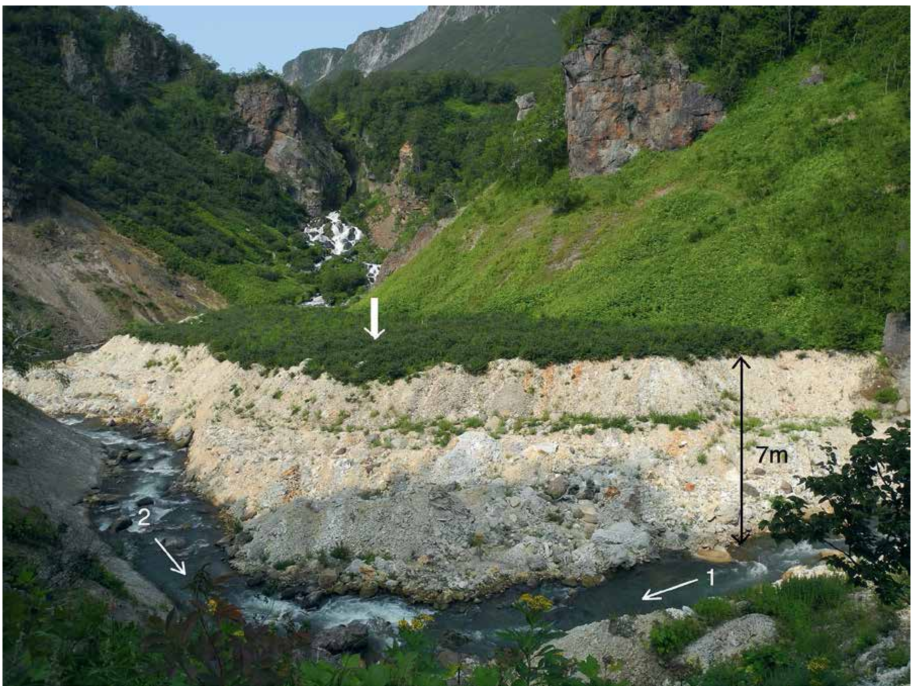

Figure 17.
The debris flow deposits formed the accumulative terrace (white arrow) in the Geysernaya river mouth (Uzon-Geysernaya caldera, Kamchatka, Russia, 2021—See ***Figure 1,*** *No 25): 1 - Geysernaya river, 2 - Shumnaya river.*

Geysernaya river valley (Uzon-Geysernaya caldera, Kamchatka, Russia) [63–67], where currently there are two similar dams—one (2007) is already cut by the river, and the other (2014) is in the early stages of erosion (**Figure 16**).

The debris flow deposits form the accumulative terraces (**Figure 17**); in the valleys of some watercourses, the debris flow embankments with a length of a few hundred meters remain, which sometimes undergo cementation. During mudflow material splashes, the recorded heights of which can reach 40 m [68], the mudflow material covers with a thickness of 0.5–1.0 m to 3–5 m remain on the valley sides and its terraces. Similar debris and mudflow traces are typical for other watercourses of the high hydrothermal activity territories in the Kuril-Kamchatka region [69, 70].

3. Conclusion

River valleys in volcanic regions become occasionally zones of rapid deposition of juvenile and resurgent material. The latter comes from volcanic eruptions of effusive or explosive type, volcanic-tectonic or hydrothermal processes (lava outflow, pyroclast ejection, volcanic cone breakdown, or explosion, sliding of rock mass weakened because of hydrothermal activity). That results in the river valleys being filled with volcanic material diversified in composition and properties, with the deposition proceeding from the upper links of the river network downstream. At the same time, the valleys serve as routes of active, and mostly intermittent (steplike), displacement of the material by various agents. Most often it takes place as a result of volcanic mudflow descent immediately after eruption due to ice or snow melting or resulting from abundant rainfalls. In some cases, however, a series of 2–3 catastrophic events occurring in a valley ends with a mudflow descent; the mudflows may occur repeatedly and are known as secondary lahars. As follows from long-term observations, the series of such events may continue through a few decades, or even centuries [2].

When considering geomorphic hazards controlled by volcanic activities, we recognized a lot of kinds of event chains of that type. An analysis of the chains permitted to identify the main geomorphic factors responsible for catastrophic events in river valleys are as follows: quick depositions of volcanic products; displacement of loose rock masses; slope angle changes; and accelerated erosion. Mudflows moving loose material downstream "in the pulse mode" occur when the loose deposits brought into valleys are actively eroded by the streams arising not only from abundant rainfall, or snow and ice melting but also resulting from an abrupt release of water from dammed lakes in case of the dam breakthrough. We agree with S. Chernomorets and I. Seinova [11] in that the mudflows are "usually the final stage in the chain of catastrophic events in the course of eruptions" (p. 57). There are also many other exogenic—fluvial, eolian, cryogenic processes taking part in the processing and transportation of the volcanic deposits, but it is much rarer that they assume the form of catastrophes [45].

It may be concluded from the above that the rivers in volcanic areas are particularly vulnerable and endangered because of several factors: large volumes of the material supplied and transported; high rates of endo- and exogenic processes on the adjoining territories; and highly energetic activity of the streams themselves, which induces a wide assortment of hazardous events and exerts a notable effect on the relief-forming processes.

Acknowledgements

The author is grateful to her colleagues who took part in organizing and conducting field works on volcanic regions in different parts of the world, at first D.V. Mikhalev without whom most trips would not be possible, and also D.V. Mishurinsky, V.A. Pellinen, T.M. Skovitina, S.S. Chernomorets, A.V. Kopanina, as well as employees of the Kuril and Kronotsky Reserves. Field works in the Geysernaya river valley were supported by the Russian Science Foundation Grant No. 21-17-00216.

Author details

Ekaterina V. Lebedeva
Institute of Geography Russian Academy of Science, Moscow, Russia

*Address all correspondence to: ekaterina.lebedeva@gmail.com

References

[1] Witham CS. Volcanic disasters and incidents: A new database. Journal of Volcanology and Geothermal Research. 2005;**148**(3-4):191-233. DOI: 10.1016/j.jvolgeores.2005.04.017

[2] Thouret J-C. Volcanic hazards and risks: A perspective. In: Alcantara-Ayala I, Gouidie AS, editors. Geomorphological Hazards and Disaster Prevention. N.-Y.: Cambridge University Press; 2010. pp. 13-32

[3] Razumov VV, Pritvorov AP, editors. Hazardous Natural Processes of the Russian Far East. Moscow: Design. Informatsiya. Kartografiya; 2008. p. 342

[4] Komedchikov NN, editor. The Atlas of Kuril Islands. Moscow: Design. Informatsiya. Kartografiya; 2009. p. 486

[5] Lavigne F, Morin J, Surono M, editors. The Atlas of Merapi Volcano. 1st ed. Paris: Laboratoire de Geographie Physique de Meudon; 2015. p. 64

[6] Neall VE. Lahars as major geological hazards. Bulletin. International Association of Engineering Geologists. 1976;**14**:233-240

[7] Major JJ, Newhall CG. Snow and ice perturbation during historical volcanic eruptions and the formation of lahars and floods. Bulletin of Volcanology. 1989;**52**:1-27

[8] Pierson TC. Flow characteristics of large eruption-triggered debris flows at snow-clad volcanoes: Constraints for debris-flow models. Journal of Volcanology and Geothermal Research. 1995;**66**:283-294

[9] Manville V, Hodgson HA, Houghton BF, Keys JR, White JDL. Tephra, snow and water: Complex sedimentary responses at an active snow-capped stratovolcano, Ruapehu, New Zealand. Bulletin of Volcanology. 2000;**62**(4):278-293. DOI: 10.1007/s004450000096

[10] Manville V, Németh K, Kano K. Source to sink: A review of three decades of progress in the understanding of volcaniclastic processes, deposits, and hazards. Sedimentary Geology. 2009;**220**:136-161. DOI: 10.1016/j.sedgeo.2009.04.022

[11] Chernomorets SS, Seinova IB. Debris Flows on Volcanoes. A Tutorial. Moscow: ESC PHSE; 2010. p. 72

[12] Procter J, Zernack A, Mead S, Morgan M, Cronin S. A review of lahars: Past deposits, historic events and present-day simulations from Mt. Ruapehu and Mt. Taranaki, New Zealand. New Zealand Journal of Geology and Geophysics. 2021;**64**(2-3):479-503. DOI: 10.1080/00288306.2020.1824999

[13] Neri A, Aspinall WP, Cioni R, Bertagnini A, Baxter PJ, Zuccaro G, et al. Developing an event tree for probabilistic hazard and risk assessment at Vesuvius. Journal of Volcanology and Geothermal Research. 2008;**178**(3):397-415. DOI: 10.1016/j.jvolgeores.2008.05.014

[14] Waythomas SF. Formation and failure of volcanic debris dams in the Chakachatna River valley associated with eruptions of the Spurr volcanic complex, Alaska. Geomorphology. 2001;**39**(3-4):111-129. DOI: 10.1016/S0169-555X(00)00097-0

[15] Yarmolyuk VV, Lebedev VI, Sugorakova AM, Bragin VY, Litasov YD,

Prudnikov ST, et al. The eastern Tuva region of recent volcanoes in Central Asia: Periods, products and types of volcanic activity. Vulkanologiya i seismologiya. 2001;**3**:3-32

[16] Yarmolyuk VV, Kozlovskiy AM, Kudryashova EA, Lebedev VI, Sugorakova AM. Major valley lava flows in Asia during Cenosoic time: Structure, composition, and the environment of the “lava river” forming in the lesser Enisey R. valley. Vulkanologiya i seismologiya. 2004;**4**:3-20

[17] Lebedeva EV, Mishurinsky DV, Pellinen VA, Skovitina TM, Mikhalev DV. Debris cones in Zhom-Bolok river valley (Eastern Sayan): Structure, formation features and impact on the development of the watercourse. Geomorfologiya (Geomorphology RAS). 2021;**52**(2):63-78. DOI: 10.31857/S0435428121020061

[18] Pevzner MM, Gertsev DO, Fedorov PI, Romanenko FA, Kusheva YV. Anyuisky volcano in Chukotka: Age, structure, rock composition and eruption. Litologiya i poleznyye iskopayemye. 2017;**1**:25-59. DOI: 10.7868/S0024497X17010050

[19] Atkinson A, Griffin TJ, Stephenson PJ. A major lava tube system from Undara volcano. North Queensland. Bulletin Volcanologique. 1975;**39**(2):1-28

[20] Espanon VR, Chivas AR, Phillips D, Matchan EL, Dosseto A. Geochronological, morphometric and geochemical constraits on the Pampas Onduladas long basaltic flow (Payun Matru volcanic field, Mendoza, Argentina). Journal of Volcanology and Geothermal Research. 2014;**289**:114-129. DOI: 10.1016/j.jvolgeores.2014.10.018

[21] Hjartarson A. Environmental changes in Iceland following the great Þjórsá lava eruption 7800 ^{14}C years BP. In: Stötter J, Wilhelm F, editors. Environmental Change in Iceland. Munchen: Münchener Geographische Abhandlungen; 1994. pp. 147-155

[22] Ivanov AV, Arzhannikov SG, Demonterova EI, Arzhannikova AV, Orlova LA. Jom-Bolok Holocene volcanic field in the East Sayan Mts., Siberia, Russia: Structure, style of eruptions, magma compositions, and radiocarbon dating. Bulletin of Volcanology. 2011;**73**:1279-1294. DOI: 10.1007/s00445-011-0485-9

[23] Arzhannikov SG, Ivanov AV, Arzhannikova AV, Demonterova EI. Valley of volcanoes in the East Sayan Mts. Planeta. 2014;**5**(6):67-83

[24] Bernardi MI, Bertotto GW, Jalowitzki TLR, Orihashi Y, Ponce AD. Emplacement history and inflation evidence of a long basaltic lava flow located in Southern Payenia Volcanic Province, Argentina. Journal of Volcanology and Geothermal Research. 2015;**293**:46-56. DOI: 10.1016/j.jvolgeores.2015.02.001

[25] Skovitina TM. The barrier lakes of the Sayan-Baikal Mountain region. Geomorfologiya (Geomorphology RAS). 2002;**3**:79-88

[26] Schetnikov AA. The lakes of the Okinsk tableland. Geomorfologiya (Geomorphology RAS). 2002;**3**:88-95

[27] Lebedeva EV. Impact of the lava flows on the structure of valleys and development of the river network. Geomorfologiya (Geomorphology RAS). 2016a;**3**:78-91. DOI: 10.15356/0435-4281-2016-3-78-91

[28] Korotkiy AM. Reconfiguration of the river system in the Primorye: Causes, mechanisms, influence on geomorphologic processes.

Geomorfologiya (Geomorphology RAS). 2010;**2**:78-91

[29] Bazarov DB, Antoshchenko-Olenev IV. The Selenga middle mountains and the Djindinsky mountain region. In: Highlands of Baikal and Transbaikalia. Moscow: Nauka; 1974. pp. 163-209

[30] Shchetnikov AA, Bezrukova EV, Filinov IA, Ivanov EV, Kerber EV. Lake morpholitogenesis in the valley of volcanoes (Eastern Sayan). Geography and Natural Resources. 2016;**3**:37-48. DOI: 10.21782/GiPR0206-1619-2016-3(37-48)

[31] Melekestsev IV, Sulerzhitskiy LD. Ksudach volcano (Kamchatka) during last 10 000 yr. Vulkanologiya i seismologiya. 1987;**4**:28-39

[32] Vinogradov VN. On the influence of volcanism on snowpack and glaciers. Issues of Kamchatka Geography. 1967;**5**:88-94

[33] Melekestsev IV. The features some of the relief-forming processes of young volcanic areas (Kamchatka as an example). Issues of Kamchatka Geography. 1967;**5**:80-87

[34] Ponomareva VV. The Largest Explosive Volcanic Eruptions and the Use of their Tephra for Dating and Correlation of Relief Forms and Sediments [thesis]. Moscow: IG RAS; 2010

[35] Grishin SY. The largest volcanic eruption of the twentieth century, in Kamchatka and the Kuril Islands, and their impact on vegetation. Izvestiya RGO. 2003;**135**(3):19-28

[36] Lebedeva EV. Caldera Ksudach (Kamchatka): Modern relief formation processes and features of the river network structure. Geomorfologiya (Geomorphology RAS). 2017a;**3**:60-75. DOI: 10.7868/S0435428117030063

[37] Lebedeva EV. Lakes of the Ksudach caldera complex (Kamchatka): Coastal processes and the level of fluctuation. Geomorfologiya (Geomorphology RAS). 2017b;**4**:35-49. DOI: 10.7868/S0435428117040046

[38] Gorshkov GS. Eruption of Bezymiannyi volcano. Volcanology Bulletin of AS USSR. 1956;**26**:1-41

[39] Tilling RI. Volcanism and associated hazards: The Andean perspective. Advances in Geosciences. 2009;**22**:125-137

[40] Manville V, Hodgson KA, Nairn IA. A review of break-out floods from volcanogenic lakes in New Zealand. New Zealand Journal of Geology and Geophysics. 2007;**50**(2):131-150. DOI: 10.1080/00288300709509826

[41] Ponomareva VV, Melekestsev IV, Dirksen OV. Sector collapses and large landslides on late Pleistocene–Holocene volcanoes in Kamchatka, Russia. Journal of Volcanology and Geothermal Research. 2006;**158**:117-138. DOI: 10.1016/j.jvolgeores.2006.04.016

[42] Braitseva OA, Melekestsev IV, Ponomareva VV, Kirianov VY. The caldera-forming eruption of Ksudach volcano about 1700-1800 ^{14}C-yr. BP - the greatest explosive event of our era in Kamchatka. Vulkanologiya i seismologiya. 1995;**2**:30-49

[43] Belousov A, Belousova M, Voight B. Multiple edifice failures, debris avalanches and associated eruptions in the Holocene history of Shiveluch volcano, Kamchatka, Russia. Bulletin of Volcanology. 1999;**61**:324-342

[44] Melekestsev IV, Volynets ON, Yermakov VA, Kirsanova TP, Masurenkov YP. Shiveluch volcano. In: Active Volcanoes of Kamchatka. Moscow: Nauka; 1991. p. 1 p. 84-105

[45] Lebedeva EV. Influence of pyroclastic emission on valley morphology and river network development: The case study of the northern group volcanoes, Kamchatka. Geomorfologiya (Geomorphology RAS). 2016b;**4**:56-69. DOI: 10.15356/0435-4281-2016-4-56-69

[46] Kataoka KS, Urabe A, Manville V, Kajiyama A. Breakout flood from an ignimbrite-dammed valley after the 5 Ka Numazawako eruption, Northeast Japan. Geological Society of America Bulletin. 2008;**120**(9/10):1233-1247. DOI: 10.1130/B26159.1

[47] Seinova IB, Chernomorets SS, Demyanchuk YV. Endogenic mechanism of lahar formation on andesitic volcanoes (by the example of the Shiveluch volcano, Kamchatka). GeoRisk. 2014;**4**:44-54

[48] Rybin AV, Degterev AV, Razjigaeva NG, Ganzey KS, Chibisova MV. Active Volcanoes of the Kuril Islands: Sarychev Peak Volcano. Yuzhno-Sakhalinsk: IMGIG DVO RAS; 2012. p. 80

[49] Brand BD, Bendaña S, Self S, Pollock N. Topographic controls on pyroclastic density current dynamics: Insight from 18 may 1980 deposits at Mount St. Helens, Washington (USA). Journal of Volcanology and Geothermal Research. 2016;**321**:1-17. DOI: 10.1016/j.jvolgeores.2016.04.018

[50] De Bélizal E, Lavigne F, Hadmoko DS, Degeai J-P, Dipayana GA, Mutaqin BW, et al. Rain-triggered lahars following the 2010 eruption of Merapi volcano, Indonesia: A major risk. Journal of Volcanology and Geothermal Research. 2013;**261**:330-347. DOI: 10.1016/j.jvolgeores.2013.01.010

[51] Kuksina LV, Chalov SR. The suspended sediment discharge of the rivers running along territories of contemporary volcanism in Kamchatka. Geography and Natural Resources. 2012;**33**:67-73. DOI: 10.1134/S1875372812010118

[52] Melekestsev IV. Volcanism and relief. In: Problems of Endogenous Relief Formation. Moscow: Nauka; 1976. pp. 350-398

[53] Manville V. Volcano-hydrologic hazards from volcanic lakes. In: Rouwet D, Christenson B, Tassi F, Vandeenlebrouck J, editors. Volcanic lakes. Berlin: Springer; 2015. pp. 21-72. DOI: 10.1007/978-3-642-36833-2

[54] Muravyev YAD, Fedotov SA, Budnikov VA, Ozerov AY, Maguskin MA, Dvigalo VN, et al. Volcanic activity in the Karymsky center in 1996: A summit eruption of Karymsky volcano and a phreatomagmatic eruption in the Akademia Nauk caldera. Vulkanologiya i seismologiya. 1997;**5**:38-71

[55] Björnsson H. Jökulhlaups in Iceland: Sources, release and drainage. In: Owens F, Slaymaker O, editors. Mountains Geomorphology. London: Arnold Publishers; 2004. pp. 164-184

[56] Gudmundsson AT. Living Earth – Outline of the Geology of Iceland. Reykjavik: Forlagid; 2013. p. 408

[57] Melekestsev IV, Braitseva OA, Erlich EN, Kozhemyaka NN. Volcanic mountains and plains. In: Kamchatka, Kurile and Commander Islands. Moscow: Nauka; 1974. pp. 162-234

[58] Arzhannikov SG, Braucher R, Jolivet M, Arzhannikova AV,

Vassallo R, Chauvet A, et al. History of late Pleistocene glaciations in the central Sayan-Tuva upland (southern Siberia). Quaternary Science Reviews. 2012;**2012**(49):16-32. DOI: 10.1016/j.quascirev.2012.06.005

[59] Zabotkin PP. Subglacial eruptions. Uchenye zapiski MOPI. 1951;**XVII**(5):182-192

[60] Galeczka I, Eiriksdottir ES, Hardardottir J, Oelkers EH, Torssander P, Gislason SR. The effect of the 2002 glacial flood on dissolved and suspended chemical fluxes in the Skaftariver, Iceland. Journal of Volcanology and Geothermal Research. 2015;**301**:253-276. DOI: 10.1016/j.jvolgeores.2015.05.008

[61] Pendea IF, Ponomareva VV, Bourgeois J, Zubrow EB, Portnyagin MV, Ponkratova I, et al. Late glacial to Holocene paleoenvironmental change on the northwestern Pacific seaboard, Kamchatka peninsula (Russia). Quaternary Science Reviews. 2017;**157**:14-28. DOI: 10.1016/j.quascirev.2016.11.035

[62] Baales M, Jöris O, Street M, Bittman F, Wninger B, Wiethold J. Impact of the late glacial eruption of the Laacher see volcano, central Rhineland, Germany. Quaternary Research. 2002;**58**:273-288. DOI: 10.1006/qres.2002.2379

[63] Kugayenko YA, Saltykov VA, Sinitsyn VI. Seismic observations in the Valley of geysers. Vestnik KRAUNTS. Nauki o Zemle. 2007;**2**(10):171-172

[64] Leonov VL. Geological preconditions and the possibility of forecasting a landslide that took place on June 3, 2007, in the valley of geysers, Kamchatka. In: Problems of Complex Geophysical Monitoring of the Far East of Russia. The 1st Regional Scientific and Technical Conference. Petropavlovsk-Kamchatskyi: Institute of Volcanology and Seismology; 2007. pp. 19-27

[65] Pinegina TK, Delemen' IF, Droznin VA, Kalacheva EG, Chirkov SA, Melekestsev IV, et al. Kamchatka Valley of geysers after the catastrophe on 3 June. Vestnik DVO RAN. 2008;**1**:33-44

[66] Dvigalo VN, Melekestsev IV. The geological and geomorphic impact of catastrophic landslides in the Geyzer Valley of Kamchatka: Aerial photogrammetry. Journal of Volcanology and Seismology. 2009;**3**(5):314-325. DOI: 10.1134/S0742046309050029

[67] Lebedeva EV, Sugrobov VM, Chizhova VP, Zavadskaya AV. The valley of the river Geysernaya (Kamchatka): Hydrothermal activity and features of relief forming. Geomorfologiya (Geomorphology RAS). 2020;**2**:60-73. DOI: 10.31857/S0435428120020066

[68] Zavadskaya AV, editor. Atlas of the Valley of the Geysernaya River in Kronotsky Reserve. Moscow: KRASAND; 2015. p. 88

[69] Lebedeva EV. Sequences of catastrophic geomorphic processes in the river valleys of volcanic regions. Geomorfologiya (Geomorphology RAS). 2018;**4**:38-55. DOI: 10.7868/S0435428118040041

[70] Lebedeva EV. Kinds of impacts of volcanic and post volcanic activity on fluvial relief. Geomorfologiya (Geomorphology RAS). 2019;**4**:49-66. DOI: 10.31857/S0435-42812019449-66

Edited by Károly Németh

Volcanic geology is a rapidly growing research field within earth sciences. It is a research field that provides the fundamental basic data to be able to reconstruct volcanism that generated eruptive products and the sedimentary processes acted upon to redeposit and rework volcanic pyroclasts. Due to the broad time and spatial scales over which volcanism takes place, it is difficult to determine the correct link between the preserved rocks and the type of volcanism responsible for their formation. Volcanic rocks represent geological processes that occur in a distinct and rapid pattern compared to other geological processes. This book provides insight into the problem of determining the scale of volcanism and linking it to the volcanic rock record. It includes comprehensive reviews and case studies representative of volcanism in diverse geological environments. This book provides a broad overview of the problems, complexity, and usefulness of the active volcanism-based volcanic geology approach to interpreting volcanic rocks in the geological record.

Published in London, UK

IntechOpen

ISBN 978-1-83768-106-8
9 781837 681068